Institut für Erd- und Umweltwissenschaften
Hydrologie / Klimatologie

Modelling of Environmental Change Impacts on Water Resources and Hydrological Extremes in Germany

Dissertation
zur Erlangung des akademischen Grades
"doctor rerum naturalium"
(Dr. rer. nat.)
in der Wissenschaftsdisziplin "Hydrologie"

kumulativ eingereicht an der
Mathematisch-Naturwissenschaftlichen Fakultät
der Universität Potsdam

von
Shaochun Huang

Potsdam, November 2011

Published online at the
Institutional Repository of the University of Potsdam:
URL http://opus.kobv.de/ubp/volltexte/2012/5974/
URN urn:nbn:de:kobv:517-opus-59748
http://nbn-resolving.de/urn:nbn:de:kobv:517-opus-59748

Acknowledgement

In the first place, I would like to heartily thank my day-to-day supervisors Dr. Valentina Krysanova and Dr. Fred. F. Hattermann at Potsdam Institute for Climate Impact Research. This thesis would not have been possible without their kind supervision, patient guidance and helpful advices throughout the whole research. In addition, their rigorous scientific attitude and rich experience inspired and nourished my growth as a student and a young researcher.

I want to express my great appreciations to Prof. Axel Bronstert for his crucial advice and valuable supervision. His involvement with his professional comments made a great improvement of the thesis and exceptionally enriched my scientific experience that I will benefit from for a long time to come.

I should also gratefully acknowledge Prof. Zbyszek Kundzewicz, who provided me steadfast encouragement and support in various ways. I am indebted to him for his constructive comments and rich scientific experience which helped me smooth my research life.

I am indebted to many of my colleagues at Potsdam Institute for Climate Impact Research. Many thanks go to Prof. Friedrich-Wilhelm Gerstengarbe, Prof. Peter C. Werner and Dr. Hermann Österle, who made the homogenized climate data and various climate scenarios available for direct application. I am grateful to Dr. Frank Wechsung for the financial support in the last two years. I should particularly thank Tobias Vetter as well as Tobias Conradt and Cornelia Hesse, who taught me SWIM at the early stage of my study. To Julia Reinhardt, thank for your hard work on the low flow simulations. To Michel Wortmann, I appreciate your nice work on the English checking. To Judith Walter, thank for helping me with the formatting of this dissertation.

My special thanks go to Dr. Alexander Gelfan and Dr. Markus Weber, who helped me develop the snow and glacier module in this research, although I didn't have chance to talk to either of them face by face. To Dr. Gelfan, thank you very much for your support on the snow code. To Dr. Weber, many thanks for your patient explanation and helpful literatures on glaciers.

I owe my deepest gratitude to my parents and husband for their wholehearted love and unflagging support during my whole study in Germany.

At last, I offer my regards and blessings to all of those who supported me in any respect during my PhD study. Please extend my thanks once again for your continued support, to all of you!

Summary

Water resources, in terms of quantity and quality, are significantly influenced by environmental changes, especially by climate and land use changes. Germany has experienced notable climate change during the last century, with an increase in the annual average temperature of ca. 1°C and a moderate increase in annual precipitation of 9% between 1901 and 2000. The scenarios of climate change for Germany suggest an increase in the long-term average annual temperature and winter precipitation, whereas summer precipitation is likely to decrease. Regarding land use change, the implementation of the European Water Framework Directive requires predicting water quality characteristics resulting from planned land use changes at the scale of large regional river basins. This requirement is particularly crucial for the Elbe River in Germany, which was one of the most heavily polluted rivers in Europe by 1990 and experienced significant socio-economical changes from the early 1990s. Accordingly, in the context of the potential climate and land use changes in Germany and their intimate link to water resources, the main objectives of the present study are

1. to project climate change impacts on the seasonal dynamics of water fluxes and spatial changes in water balance components, as well as the future flood and low flow conditions for the five largest river basins (upper Danube, Ems, Elbe, Rhine and Weser) in Germany
2. to evaluate impacts of potential land use changes on water quality in terms of NO_3-N load in selected sub-regions of the Elbe basin; and
3. to investigate various sources of uncertainty in the projections.

In this study, the process-based eco-hydrological model SWIM (Soil and Water Integrated Model) was applied to simulate water fluxes, floods, low flows and nitrogen dynamics for meso- to macro-scale basins in Germany. SWIM was intensively calibrated and validated in advance using observed climate data and it could satisfactorily reproduce river discharge and nitrogen load in most of the studied gauges. For example, 26 out of 29 selected gauges in Germany have NSE (Nash-Sutcliffe efficiency) higher than 0.7, and 22 gauges have LNSE (Logarithmic Nash-Sutcliffe efficiency) higher than 0.7 for the period 1961 – 2000. The NO_3-N load was also reasonably simulated by SWIM with the NSE ranging from 0.52 to 0.7 for eight selected gauges in the Elbe region.

The climate scenarios generated by different Regional Climate Models (RCMs) were carefully selected for the study. The SWIM outputs driven by STAR (STAtistical Regional model) realizations were used for evaluating changes in the mean seasonal runoff and annual water balance components by the mid of 21st century. The projected daily discharges driven by scenarios produced by other models (CCLM, Cosmo-Climate Local Model, REMO, REgional Model, and WettReg, Wetterlagenbasierte Regionalisierungsmethode) were particularly used for the flood and low flow analysis. The land use scenarios were introduced based on the political incentives at the regional level.

In addition, the long-term trends of observed temperature extremes at the climate station Potsdam were analysed as a complimentary study to climate impact assessment. An important finding of this study shows that “cold” extremes have become less frequent and less severe than in the past and “warm” extremes have become more frequent and more severe. However, many changes are rather weak and not statistically significant, as the variability of temperature indices at the Potsdam station has been very strong.

In the context of climate change, the actual evapotransipration is likely to increase in most parts of Germany, while total runoff generation may decrease in south and east regions in the scenario period 2051-2060. Water discharge in all six studied large rivers (Ems, Weser, Saale, Danube, Main and Neckar) would be 8 – 30% lower in summer and autumn compared to the reference period (1961 – 1990), and the strongest decline is expected for the Saale, Danube and Neckar. Higher winter flow is expected in all of these rivers, and the increase is most significant for the Ems (about 18%).

No general pattern of changes in flood directions can be concluded according to the results driven by different RCMs, emission scenarios and multi-realizations. The results driven by the statistical-empirical model WettReg show a declining trend in the 50-year flood level for most rivers (especially in the northern Germany) under all climate scenarios. The simulations driven by dynamic models (CCLM and REMO) give various change directions depending on region, scenario and time period. The 50-year low flow is likely to occur more frequently in western, southern and central Germany after 2061 as suggested by more than 80% of the model runs. The current low flow period (from August to September) may be extended until the late autumn at the end of this century.

Land use and land management scenarios were applied to two meso-scale sub-basins in the Elbe basin (the sub-basin Weiße Elster and Unstrut). The modelling results show that increasing areas under winter rape, higher fertilizer rates, excluding cover crops and converting pasture to agriculture land would lead to higher NO_3-N loads, whereas lower fertilizer rates, set-aside of agricultural land and planting more maize instead of winter rape would reduce the NO_3-N load. Mineral fertilizers have a much stronger effect on the NO_3-N load than organic fertilizers. Cover crops, which play an important role in the reduction of nitrate losses from fields, should be maintained on cropland. The planting area of winter rape should not be increased significantly in areas, where environmental targets are important. As another energy plant, maize has a moderate effect on the water environment.

The uncertainty in estimating future high flows and, in particular, extreme floods remain high due to different RCM structures, emission scenarios and multi-realizations. In contrast, the projection of low flows under warmer climate conditions appears to be more pronounced and consistent. The largest source of uncertainty related to NO_3-N modelling originates from the input data on the agricultural management. However, the calibration of retention parameters can compensate the uncertainty in the input data to a certain extent.

The robust conclusion of this study is that most part of Germany is likely to experience lower water availability in summer and autumn under a warmer climate. The low flow season may extend to late autumn with more severe low flow conditions in western, southern and parts of central Germany at the end of this century. The NO_3-N load in rivers is significantly influenced by the agriculture management, especially crop types and mineral fertilizers applications. Hence, an optimal agricultural management is essential for the improvement of water quality in the context of the regional development plans for future.

Zusammenfassung

Wasserressourcen werden in Quantität und Qualität von Veränderungen in der Umwelt, insbesondere von Änderungen des Klimas und der Landnutzung, in signifikantem Maße beeinflusst. In dieser Arbeit wurden die Auswirkungen von Klimavariabilität und Klimawandel auf die Wasserressourcen und Extremereignisse wie Hoch- und Niedrigwasser in Deutschland untersucht. Die Analyse erfolgte auf der einen Seite modellgestützt, wobei die Ergebnisse aus verschiedenen regionalen Klimamodellen durch ein ökohydrologisches Modell in Änderungen in den hydrologischen Prozessen transformiert wurden, zum anderen aber auch datengestützt, z.B. durch die statistische Interpretation von beobachteten und simulierten Zeitreihen. Zusätzlich wurden die Auswirkungen von Landnutzungsänderungen auf Umsatz von Stickstoff in der Landschaft und im Wasser untersucht, wobei dasselbe ökohydrologische Modell zum Einsatz kam.

Im Rahmen des Klimawandels wird zur Mitte dieses Jahrhunderts die aktuelle Evapotranspiration in den meisten Teilen Deutschlands mit großer Wahrscheinlichkeit zunehmen. Die täglichen Abflussmengen der fünf größten Flussgebiete in Deutschland (Ems, Weser, Elbe, Obere Donau und Rhein) werden dieser Untersuchung zur Folge im Sommer und Herbst um 8%-30% geringer sein als in der Referenzperiode (1961-1990). 80% der Szenariensimulationen stimmen darin überein, dass die 50-jährigen Niedrigwasserereignisse zum Ende dieses Jahrhunderts mit großer Wahrscheinlichkeit häufiger in den westlichen, den südlichen und den zentralen Teilen Deutschlands auftreten werden. Die gegenwärtige Niedrigwasserperiode (August-September) könnte sich zudem dann bis in den späten Herbst ausweiten. Für alle Flüsse werden höhere Winterabflüsse erwartet, wobei diese Zunahme für die Ems am stärksten ausfällt (ca. 18%). Mit größerer Unsicherheit sind dagegen die Aussagen zur Entwicklung der Hochwasser behaftet. Aus den Ergebnissen, die durch unterschiedliche regionale Klimamodelle und Szenarien getrieben wurden, kann jedoch kein allgemeingültiges Muster für die Änderungen der 50-jährigen Hochwässer ausgemacht werden.

Eine optimierte Landnutzung und ein optimiertes Landmanagement sind für die Reduzierung der NO_3-Einträge in die Oberflächengewässer essentiell. In den Einzusgebieten der Weißen Elster und der Unstrut (Elbe) kann eine Zunahme von 10% in der Anbaufläche von Winterraps zu einer 12-19% höheren NO_3 Fracht führen. Mais, eine weitere Energiepflanze, hat hingegen einen mäßigeren Effekt auf die Oberflächengewässer. Die Höhe der Gabe von mineralischen Düngern beeinflußt zudem in starkem Maße die Nitratbelastung von Flüssen. Zwischenfrüchte können den NO_3-Austrag im Sommer zusätzlich erheblich verringern.

Insgesamt bleibt die Unsicherheit in der Vorhersage von Spitzenabflüssen und im Besonderen von Extrem-Hochwässern als Folge unterschiedlicher regionaler Klimamodelle, Emissionsszenarien und Realisationen sehr hoch. Im Gegensatz dazu erscheinen die Projektionen zu den Niedrigwasserereignissen unter wärmeren Bedingungen sehr viel deutlicher und einheitlicher. Die größte Unsicherheit in der Modellierung von NO_3 dagegen sind die Eingangsdaten z.B. für das lokale landwirtschaftliche Management.

Contents

1. Introduction

Water resources, both in terms of quantity and quality, are significantly influenced by environmental changes, such as climate, land use, river engineering, construction of reservoirs and mining activities. Among the influences, climate change and land use change are two essential factors controlling the hydrological behaviour of catchments such as river discharge and water quality (Bronstert *et al.*, 2002; Hörmann *et al.*, 2005).

According to the Fourth Assessment Report (AR4) of the International Panel for Climate Change (IPCC, 2007b), the global surface temperature increased by 0.74±0.18°C from 1906 to 2005. Intimately linked to changes in atmospheric temperature and radiation balance, a number of components of the hydrological cycle can be affected, such as changing precipitation patterns (Dore, 2005), intensity and extremes (Easterling *et al.*, 2000); widespread melting of snow and ice (Dyurgerov and Meier, 2005); increasing atmospheric water vapour (Rangwala *et al.*, 2010); increasing evaporation and changes in soil moisture and runoff (Porporato *et al.*, 2004; Bates *et al.*, 2008). As a consequence, there is growing evidence worldwide of changing characteristics of stream flows (McCarthy *et al.*, 2001). For example, the stream flow has increased in the period 1944 – 1993 in many parts of the United States, especially for the low flows (Lins and Slack, 1999). In California, the winter stream flow increased due to decreased snow formation in winter and earlier snowmelt (Dettinger and Cayan, 1995). In northwest China, an increase in spring runoff since 1980 was observed caused by more glacier melt (Ye *et al.*, 1999). In large part of Eastern Europe, European Russia and central Canada, a subtle shift in stream flow from spring to winter was also reported by various studies (Georgiyevsky and Shiklomanov, 2003; Bergstrom and Carlsson, 1993; Tarend, 1998 and Westmacott and Burn, 1997). Since the 1970s, both an increasing and decreasing trends in stream flow was detected in different parts of South America (Waylen *et al.*, 2000) and a decreasing trend was found in some large rivers in Africa and Australia (Sircoulon, 1990 and Thomas and Bates, 1997).

Germany, located in central Europe, has also experienced changes in climate and water resources. During the period 1901 – 2000, an increase of approximate 1°C in annual average temperature and an increase of 9% in annual precipitation were recorded (Schönwiese *et al.*, 2006). However, the increase in annual precipitation is not evenly distributed over the four seasons, but shows a remarkable shift from summer (-16%) to winter (19%) particularly from 1951 to 2000 (Schönwiese *et al.*, 2006). Along with climate change, the changes in the hydrological regimes as well as the extreme events were also observed during the last century. Bormann *et al.* (2010) analysed the Pardé coefficients (Pardé, 1933) for 57 gauges with a minimum series of 60 years in large German rivers. They found that the hydrological regimes of German rivers have started to change mainly due to climate change. For almost all the gauges they analysed, Pardé coefficients increased in winter and decreased in summer since the middle of the 20th century. For nival runoff regimes, the seasonal variability in runoff decrease due to increasing rainfall in winter instead of snow. In contrast, for pluvial runoff regimes, the seasonal variability increased with higher winter maxima in runoff and lower summer minima, which is attributed to the shift of precipitation from summer to winter and increasing evapotranspiration in summer. Regarding extreme events, the significant increasing trend in flood behaviour was found in western, southern and central Germany. These trends were assumed to be climate driven (Petrow and Merz, 2009). The low flow trends (without considering the significance of the trends) were analysed by Stahl *et al.* (2010) for the period 1962 – 2004 in 137 near-natural catchments in Germany. They found that

the low flows tend to decrease in most of the small catchments in Germany (average area 292 km^2), where the lowest mean monthly flow occurs in summer.

In addition to the current climate change, an increase in temperature of 1.6 – 3.8 °C and a shift of precipitation from summer to winter in Germany by the year 2080 were projected by the downscaled climate scenarios from four General Circulation Models (GCMs) driven by four different emission scenarios (Zebisch *et al.*, 2005). These potential changes of climate could continue to affect the water fluxes and extremes in the long-term. Generally, more evapotranspiration is expected due to the increased temperature. However, constrained by the actual water availability in soil, higher temperature could result in lower actual evapotranspiration if water availability is low. More severe floods can be triggered by more intensive rainfall. High temperatures combined with low precipitation in summer could directly influence the pluvial-river low flows especially in catchments with limited groundwater storage.

Besides climate change, global land use has undergone significant changes over the last 300 years with more than six fold increase of crop and grass land (Goldewijk, 2001). Land-use and water resources are unequivocally linked by the processes evaporation, transpiration, interception, surface runoff as well as human activities (Baker, 2003; Bronstert *et al.*, 2002). Changes in land use can have either positive or negative impacts on water quality. For example, the increase in nitrogen loading was reported due to the combined effect of an increase in the area of arable land and increased fertilizer (Mattikalli and Richards, 1996; Ierodiaconou *et al.*, 2005), whereas the shift from intensive to sustainable land use practices can effectively help reduce the nutrient loads in groundwater and surface water (Honisch *et al.*, 2002). An overview of impact studies from and to forest on water resources is given by Whitehead and Robinson (1993).

In Germany, the Elbe River basin experienced the strongest land use change in the 1990s and the river itself was classified as one of most heavily polluted rivers in 1989 (UBA, 2001, p25). Nutrient pollution (nitrogen and phosphorus) of surface and groundwater in the basin was caused by the high intensity of water use, excessive application of fertilizers and pesticides in agriculture and discharge of domestic and industrial wastes. Although emissions from point sources were significantly reduced in the basin since the 1990s due to the reduction of industrial sources and introduction of new and better sewage treatment facilities, the diffuse sources of pollution represented mainly by agriculture are still not sufficiently controlled (Krysanova *et al.*, 2005). There are several studies focusing on the water quality problems for some meso-scale catchments in the Elbe basin (Krysanova *et al.*, 1998, Hattermann *et al.*, 2006 and Hesse *et al.*, 2008, Voss, 2007). However, further studies on the water quality situations are required to evaluate the land use impacts at the scale of large regional river basins by the implementation of European Water Framework Directive. Hence, particular interest is placed in the Elbe basin investigating the impacts of the policy-triggered land use changes.

Accordingly, in the context of the environmental changes in Germany and their intimate link to the water resources, the main objectives of this study are

1. to project impacts of climate changes on:
    a. the seasonal dynamics of water fluxes and spatial changes in water balance components;
    b. the future flood and low flow conditions

    in Germany using the eco-hydrological model SWIM (Soil and Water Integrated Model);
2. to evaluate impacts of potential land use change on NO_3-N load in selected sub-regions of the Elbe basin based on the SWIM model results; and finally,

3. to investigate various sources of uncertainty of the environmental projections.

To achieve these objectives, the applicability of the process-based eco-hydrological model SWIM was intensively tested for simulating water fluxes, floods, low flows and nitrogen dynamics in both meso- and macro-scale basins. The snow and glacier modules in SWIM were extended to better describe the snow and glacier processes in the Swiss and Austrian alpine regions. The long-term trend of observed temperature extremes in Potsdam was assessed, as a complement of large-scale climate studies and an additional motivation of climate impact studies in Germany. The climate scenarios from different RCMs were carefully analysed and selected for each specific purpose. Therefore, five chapters studying different topics are structured in the following way: first of all, the observed seasonal temperature extremes in Potsdam were analysed providing further evidence of climate change in Germany (Chapter 2). Then, three chapters focusing on the projection of water fluxes, floods and low flows are presented subsequently, giving an overview of the potential changes in hydrological responses caused by climate change (Chapter 3, 4 and 5). After the chapters on climate impact studies, SWIM was applied to model the river NO_3-N load in both the macro- and meso-scale basins. The impacts of the land use changes were assessed in selected sub-regions of the Elbe basin (Chapter 6). The general results in the Chapter 2 – 6 are summarized in Chapter 7 based on different topics. The final conclusion of the thesis is presented and future work on environmental impact researches is discussed (Chapter 8).

1.1. Study area

Germany is located in Central Europe with a total area of 357,021 km^2. It is bordered by the North Sea, Denmark and the Baltic Sea in the north, by the Netherlands, Belgium, Luxembourg and France in the west, Poland and the Czech Republic in the east, and Austria and Switzerland in the south (**Fig. 1-1**). Generally, the German territory is divided into five geographical regions (Statistisches Bundesamt Deutschland, 2008):

- North German Lowlands: a flat region including the coastal regions,
- Central German Uplands: a mountainous region with their extensive forests, rifts and valleys,
- The Southwest German Central Upland Scarps embracing the upper Rhine valley,
- The Alpine Foreland in southern Germany with its rolling green hills and stunning glacial lakes,
- The German Alps: located in the very south of Germany with peaks above 2000 meters.

From the Northwest to the East and Southeast, the maritime climate gradually changes into a more continental climate. The country's average annual temperature is about +9 °C. The mountainous regions are characterized by lower temperatures due to their higher altitudes (**Fig. 1-2(a)**). The precipitation occurs in all seasons with substantial regional differences (**Fig. 1-2(b)**). In the North German Lowlands, annual rainfall varies between less than 500 (continental) to about 700 mm (maritime). Notice that the northeast of Germany is the driest region where the Elbe basin is located. The Upland mountainous areas receive from between 700 to more than 1500 mm of precipitation per year, whereas the Alps more than 2000 mm per year caused by the orographic effect. (Statistisches Bundesamt Deutschland, 2008).

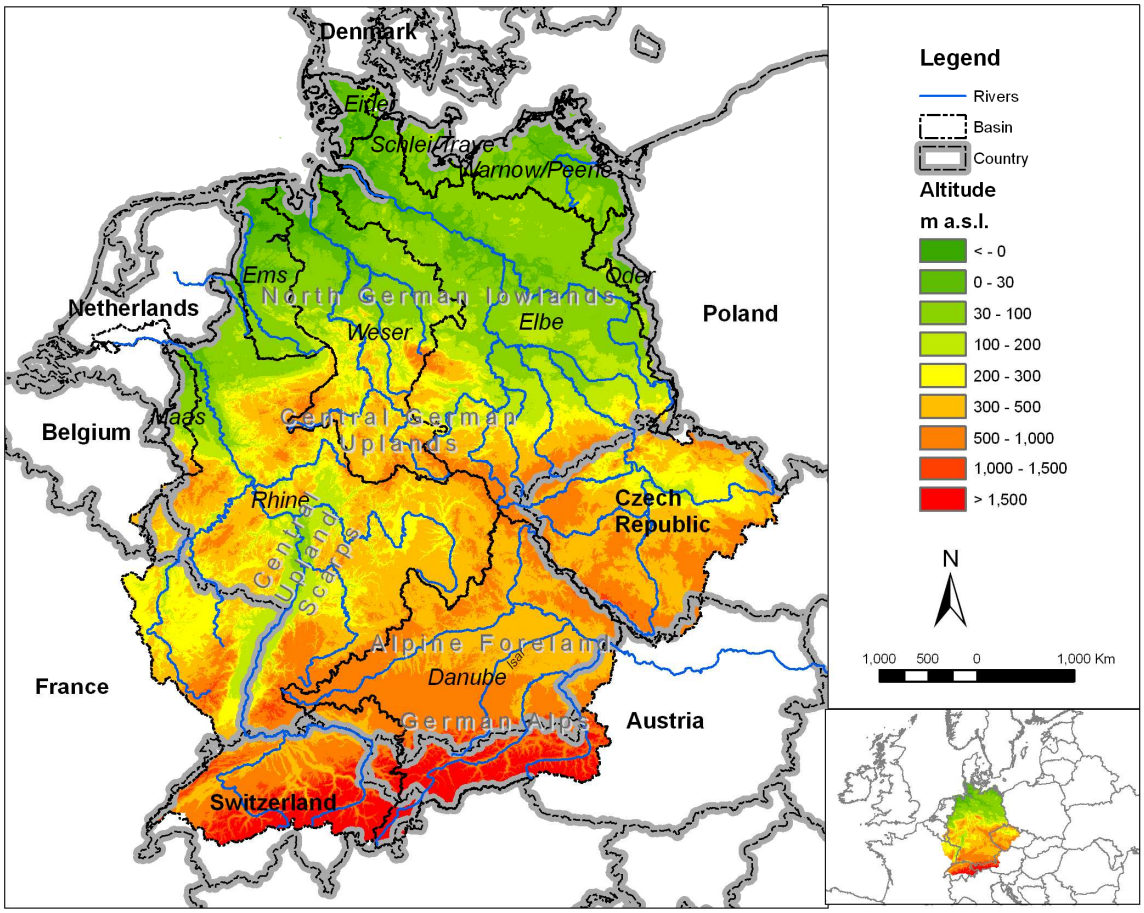

Figure 1-1: Location of Germany and the studied river basins.

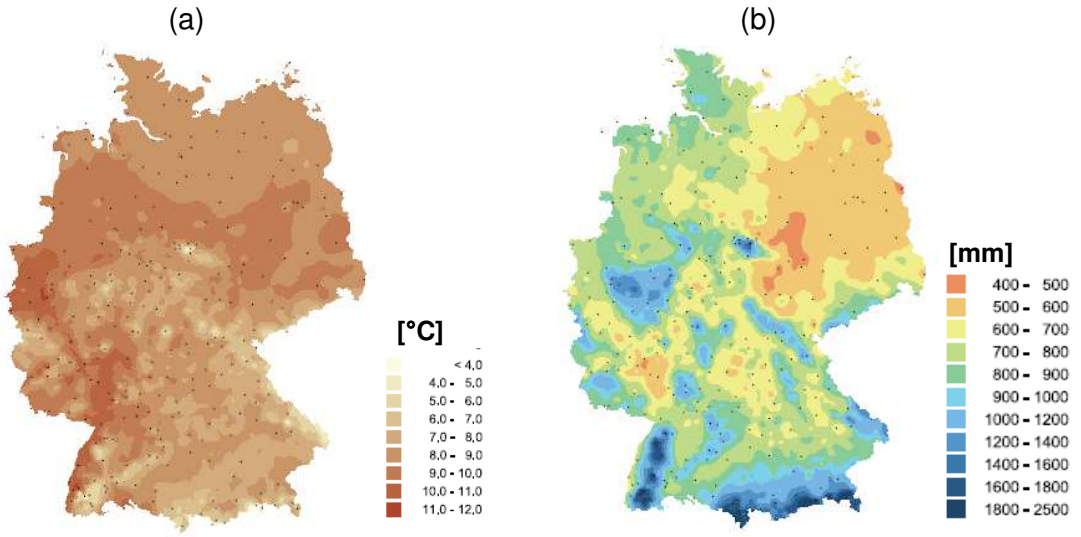

Figure 1-2: (a) Mean annual temperature (left) and (b) mean annual precipitation (right) for the period 1951 – 2006. Climate stations are represented as black dots. Source: Wodinski, Gerstengarbe and Werner, PIK Potsdam, 2010.

Hydrologically, the German territory is comprised of five large river basins (the Elbe, upper Danube, Rhine, Weser and Ems), three medium-scale basins in the coastal area (Elder, Schlei/Trave and Warnow/Peene), and small parts of the Oder and Maas basins (see **Fig. 1-1**). These five large basins were selected as the major study areas. Only the Weser basin is entirely located in Germany while the others partly extend into neighbouring countries. Altogether, the German part of the five basins covers about 90% of the whole German territory and has different geographical, climatological characteristics, which influence the river regimes (**Table 1-1**). In general, sandy soils are dominant in the north-western lowland region, while loess, rocks and sandstone prevail in the south (**Fig. 1-3(b)**). Most of German rivers correspond to the pluvial type (with local nival influences) with smooth transitions between the regions (HAD, 2000). In addition, Annex I shows a more detailed river network map for the studied area as well as the location of selected discharge gauges. It also shows the monthly Pardé coefficients at three selected gauges in each river basin, which demonstrate the river regimes at different stretches of the rivers.

Table 1-1: The characteristics of the five studied basins.

River basin		Ems (German part)	Weser	Upper Danube (till gauge Achleiten)	Rhine (till gauge Rees)	Elbe
Area (km^2)		13000	45725	77107	160000	147423
Percent area in Germany (%)		100	100	73	64	65
Mean slope (degree)		0.5	2.4	7.4	5.4	2
Altitude (m a.s.l.)		0-406	0-1127	301-3838	15-4275	0-1547
Land use shares (%)	Cropland	66	49	32	38	51
	Forest	10	30	37	36	30
	Grassland	15	14	20	13	10
Annual average precipitation (mm)*		839	807	1196	1045	721
Major river regime		pluvial	pluvial	nival-pluvial	nival-pluvial	pluvial

*the precipitation data was interpolated from the measured data in the basins for the period 1961-2000

The Ems, which is the smallest river basin among the five, is located in the flat lowland region of NW-Germany and NE-Netherlands. Only the German part of the basin is included in this study (**Fig. 1-1**). The entire basin has a low relief terrain and the river flows through the North German Lowlands to the North Sea. This basin belongs to one of the most intensively used agricultural regions in Europe. Arable land covers approximately 66% of the area. The other major land covers are grassland (15%) and forest (10%) (see **Table 1-1** and **Fig. 1-3(a)**). The Ems has a unimodal pluvial runoff regime (HAD, 2000; Bormann, 2010 and Annex I) with an amplitude significantly larger compared to other rivers in Northern Germany (*e.g.* The Elbe, Saale and Weser). The sandy sediments in this basin induce a dominant contribution of base flow to river discharge.

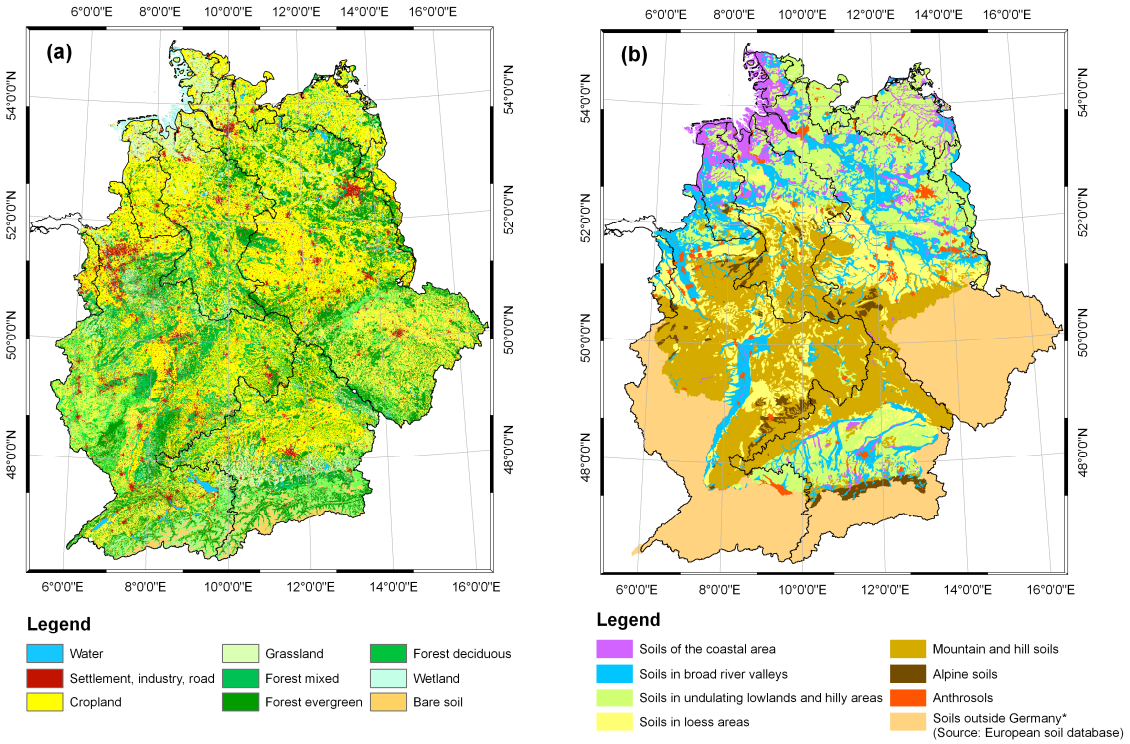

Figure 1-3: (a) Land use and (b) soils in the studied areas.

The Weser basin (**Fig. 1-1**) is located in north-western Germany and is the only basin which lies entirely within the national territory of Germany. Formed by the rivers Fulda and Werra, the Weser River flows through the North German Lowlands, and reaches the North Sea. About half of the drainage basin area is used as arable land, 30% is covered by forest, and 14% by grassland (**Table 1-1** and **Fig. 1-3(a)**). The headwaters of the Weser River located in the lower mountain range are characterized by pluvio-nival runoff regimes (Bormann, 2010). The maximum discharge of the Weser occurs in late winter (March) and the minimum discharge is observed in late summer (September) (HAD, 2000).

The Elbe River (**Fig. 1-1**) originates in the Czech Republic, drains across north-eastern Germany and flows into the North Sea. About two thirds of the whole Elbe drainage basin (approximately 100 000 km^2) is located in Germany, one third in the Czech Republic, and the negligible parts belong to Austria and Poland. The Elbe basin is also an intensively agricultural region with about 50% of the total area used as arable land. About 30% of the drainage area is forested and only 10% grassland (**Table 1-1** and **Fig. 1-3(a)**). The headwater of Elbe and the largest tributary in Czech Republic Vltava has a runoff regime dominated by snow melt as compared to rainfall. The tributaries flowing from the lower mountain range into the Elbe show a pluvio-nival regime as well (*e.g.* Mulde and Schwarze Elster). The largest tributary in Germany in terms of river length and river discharge (Saale) has a pluvial runoff regime (HAD, 2000; Bormann, 2010 and Annex I).

The total Rhine river basin (**Fig. 1-1**) is spread over nine countries with altitudes ranging from 0 (Rotterdam) to 4275m. a.s.l. (Finsteraarhorn/Swiss Alps). Beginning in the Swiss Alps, the Rhine River flows through Germany to the Netherlands with tributaries coming from France, Austria, Italy, Liechtenstein, Luxembourg and Belgium. The rivers Main, Neckar and Moselle are the

three main tributaries in Germany, and the Moselle receives drainage from France, Luxembourg and Belgium. Two thirds of the Rhine drainage basin area is situated in Germany. The Alpine countries, of which Switzerland is the largest, form about 20% of the drainage area. The arable land (40%) and forest (38%) are the two major land cover types in the German part of the Rhine basin. Maximum discharge of the Rhine in alpine regions is observed during summer due to the snow melt. Water is temporarily stored in the alpine border lakes which smooth the Rhine discharge. Downstream of Basel, a pluvial regime of the Rhine gradually becomes dominant. Rainfall dominated tributaries (the national rivers in Germany, such as Neckar and Main) contribute to a second maximum discharge of Rhine in winter. In the middle and lower Rhine, the winter peak dominates the summer one, changing the runoff regime into a pluvio-nival type (HAD, 2000; Bormann, 2010 and Annex I).

The upper part of the Danube basin (**Fig. 1-1**) is formed by Brigach and Breg rivers located in south-west Germany and several tributaries from the Alps and the Bavarian forest. The main tributary, the River Inn flows from the Swiss Alps through Austria to Germany and receives a large amount of cold melting water from snow and glaciers. About 73% of the drainage area is located within the German territory. The main land cover types in this basin are forest (37%) and arable land (32%). The upper Danube has the highest grassland cover (20%) compared to other basins. The runoff regime of the Danube considerably changes along the German river reach depending on the runoff regimes of the large tributaries from southern (nival) or northern (pluvial) directions. For example, the southern tributaries Iller and Lech contribute to a nival regime at gauge Ingoldstadt. Rainfall dominated tributaries such as Altmühl, Naab and Regen from the north modulate the nival into a nivo-pluvial runoff regime. Downstream of the tributary Inn (at the gauge Achleiten), the regime changes back to a nival type (HAD, 2000; Bormann, 2010 and Annex I).

1.2. Historical changes in climate, land use and water discharge in Germany

An extensive analysis on temperature and precipitation trends as well as the extreme events indicates that Germany has already experienced remarkable climate change during the last century (Schönwiese *et al.*, 2006). The annual average temperature has increased by ca. 1°C between 1901 and 2000 and the winters of 1980s and 1990s were observed as the warmest in Germany during the 20th century with an increase of 2.3°C (Schönwiese *et al.*, 2006). In the period 1901 – 2000, annual average precipitation in Germany experienced a moderate increase (9%), and winter precipitation showed a significant increasing trend (19%), while summer precipitation did not change significantly (-3%). However, a remarkable shift from summer (-16%) to winter (19%) precipitation was observed from 1951 to 2000 (Schönwiese *et al.*, 2006).

The recent trends in temperature and precipitation in Germany also show substantial regional differences (**Fig. 1-4**). The trend analysis was applied to the annual temperature series at 180 climate stations and the annual precipitation series at 1218 precipitation stations for the period 1951 – 2006. The 2-sided p-value was calculated by Mann-Kendall test indicating the level of significance. In general, the warming trend prevailed at the significance level of 0.05 all over Germany (**Fig. 1-4(a)**). In several southern regions the trend of temperature is larger than 1.6°C. Changes of annual precipitation in Germany show a distinct spatial pattern: reductions over large areas in the east and an increasing trend in the other regions (**Fig. 1-4(b)**). The eastern region, that it is already the driest region in Germany, experienced a decreasing trend of precipitation during the last half century. However, it should be noticed that most of the trends for precipitation are not statistically significant, indicating the strong natural variability of precipitation.

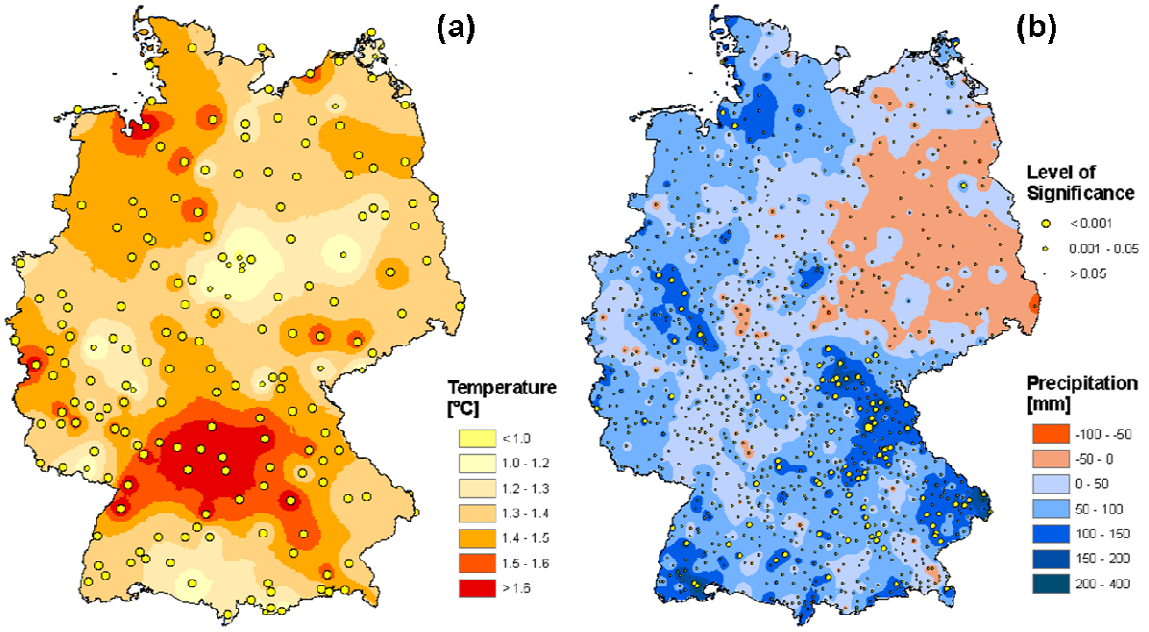

Figure 1-4: (a) The trend in annual temperature at 180 climate stations and (b) the trend in annual precipitation at 1218 precipitation stations for the period 1951 – 2006. The p-value calculated by Mann-Kendall test demonstrates the level of significance.

The land use has remarkably changed in Germany since 1945. Data from the Federal Statistical Office show that from 1951 to 1989 the agricultural area decreased from 57.8% to 53.7%, while forest area remained almost constant and impervious areas increased from 7.4% to 12.3% (Bormann, 2010). From 1992 to 2008, the settlement area increased by 17%, forest areas increased by 2.7% and agricultural area decreased by 3.8% corresponding to their land use areas in 1992 respectively (DESTATIS, Teil 4, pp 49, 2010). Moreover, East Germany has experienced significant socio-economical changes, specifically after the reunification of Germany in 1990 (Krysanova *et al.*, 2005). The comparison of CORINE 1990 and CORINE 2000 land cover data set of the European Environment Agency shows that there was about 1.6% – 4% of area in the five largest river basins experiencing land use changes during the 10 years (Annex II). Among them, the German Elbe basin experienced the largest change (about 4% of its total area) and more than half of the changes related to agriculture and forests. The most important drivers of land use change in the Elbe basin, which can be anticipated for the next 10 to 20 years, are policies of the Commission of the European Communities (CEC), regional policies, environmental standards and social development. Among the CEC policies the Common Agricultural Policy (CAP), the Agri-environmental Regulation and the Nitrate Directive have the highest impact on land use intensity and land use patterns by altering the economic competitiveness of the agricultural sector. For example, the rapid extension of set-aside of arable land in the early 1990s and the major shift from potatoes to rape and sunflowers have been observed in the Elbe basin. In addition to land use change, all large German rivers have been affected by river engineering (*e.g.* deepened rivers, weirs and reservoirs) for navigation, energy generation and floods protection (*e.g.*, Buck *et al.*, 1993; Busch *et al.*, 1989; Wechsung *et al.*, 2006).

Along with notable environmental changes in the last decades, changes in water discharges have also been observed in Germany. The long-term spatial trends in Germany are represented by the 117 observational gauges (see Annex III). For 108 gauges runoff data from 1951 to 2006 was

available. The 9 gauges, which have shorter runoff series but more than 30 years, were still selected as they are located at some large tributaries or main rivers. For each of these gauges, the trends of the annual mean discharge (**Fig. 1-5(a)**), the annual maximum discharge (**Fig. 1-5(b)**) and the annual minimum 7-day mean flow (**Fig. 1-5(c)**) were analyzed by the Mann-Kendall test. They were separated into upwards and downwards significant trend groups (at 0.05 level), and non-significant trends (more detailed results including 2-sided p-value and the relative changes for each gauge are given in Annex III). Generally, more than 77% of the studied gauges show no significant changes for these three indicators and among the remaining gauges with significant changes the positive trend is usually dominant. Regarding the annual average discharges, significant increasing trends were detected at only 5 gauges in southern Germany, whereas only 2 gauges showed a significant decrease in the north. This pattern complies with the changes in annual precipitation during the same period (**Fig. 1-4(b)**). The annual maximum discharge, as an indicator of flood behaviours, tends to increase significantly at 15% of studied gauges located in the southern, western and central parts of Germany. The low flow levels show increasing tendencies at 23 gauges in southern Germany (parts of the Rhine and Danube basins). There are also a few scattered examples of decreasing trends of the low flow in the northeastern region in the Elbe basin.

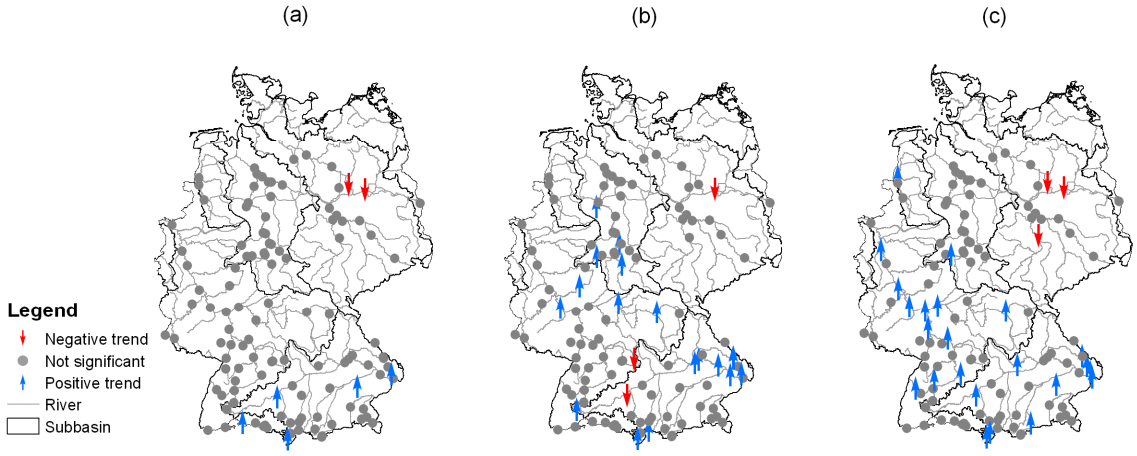

Figure 1-5: Significant trends of (a) annual average discharge, (b) annual maximum discharge and (c) annual minimum 7-day mean flow for the period 1951 – 2006 at the 0.05 significance level.

1.3. The modelling strategy

In order to reasonably project the impact of environmental changes on water resources, both the climate and hydrological models need to be selected carefully according to the study purposes. General Circulation Models (GCMs) are an important tool in the assessment of climate change and 24 GCMs are available providing various runs under different emission scenarios and spatial resolutions (IPCC, 2007b). However, due to their insufficient spatial scale (grid-cell resolutions of approximately 100 – 250 km), no detailed regional information can be derived directly from GCMs (IPCC, 2007a), and direct use of GCM results for regional hydrological impact analysis is not recommended.

To bridge the gap between the resolution of GCMs and regional scale processes, various downscaling techniques were developed in recent years. A comprehensive review paper on downscaling techniques for hydrological modelling is given by Fowler *et al.* (2007). In general,

there are two fundamental approaches for the downscaling of large-scale GCM output to finer spatial resolutions. The first is so-called dynamic Regional Climate Models (RCMs) and the other one is based on statistical relationships between large-scale climate information and regional variables. The advantages and limitations of these two downscaling approaches have been discussed by Wilby and Wigley (1997), and their ability to downscale precipitation was also assessed by Haylock *et al.* (2006) and Schmidli *et al.* (2006). Only the major characteristics of these two approaches are discussed here. The dynamic RCMs produce responses based on physically consistent processes in finer resolution from the GCM-scale output. These models are usually computationally intensive with limited number of scenario ensembles available. In addition, they are strongly dependent on GCM boundary forcing, hence inherit also the biases from the driving GCMs. In contrast, most statistical-empirical regional models are based on standard and accepted statistical procedures and more computationally efficient. They can provide point-scale climate variables from GCM-scale output and easily transferable to other regions. However, statistical-empirical models require long-term and reliable observed data series and they could not include the feedbacks in the climate system. Furthermore, they tend to underestimate variance and poorly represent extreme events.

There are different sets of regional climate projections for Germany, including those from both dynamical downscaling models, such as REMO (Jacob, 2001) and CCLM (Böhm *et al.*, 2008) and those from statistical downscaling techniques such as WettReg (Enke *et al.*, 2005a, 2005b), and STAR (Orlowsky *et al.*, 2008). Among these four models, REMO and WettReg were officially commissioned by the German Environmental Agency (UBA, 2007). Both of them used the results from the GCM ECHAM5 for the emission scenarios A1B, A2 and B1 as large-scale forcing.

Gerstengarbe *et al.* (2009) compared the simulated historical results from all four models (CCLM, REMO, STAR and WettReg) with the observed climate data in the period from 1970s to 2000. The evaluation results show that each model has its strengths and weaknesses. Reproduction of precipitation is a common problem of all models, partly caused by their relatively low resolution and partly due to the inherent difficulties to reproduce precipitation dynamics. The dynamical models REMO and CCLM generate large deviations between the observed and simulated precipitation. There are also significant problems to reproduce trends by the models REMO, CCLM and WettReg. In contrast, the simulated outputs from the model STAR have better agreement with the observed statistics, especially for temperature and air pressure. The trends of the climate variables are well reproduced by STAR as the trend is prescribed in the model and the characteristics of events are closer to the reality.

The projections generated by STAR, REMO and WettReg were also evaluated by Bronstert *et al.* (2007b) regarding their usefulness for hydrological impact simulations for southern Germany. In general, they found that all models have a rather limited value for climate impact simulations. Keeping this general shortcoming in mind, they summarized that WettReg performs marginally better than the other two downscaling methods in the overall aspects of the hydrological cycle, *e.g.* seasonal hydrological dynamics, low flow conditions and moderate flooding conditions. The dynamic model REMO has a slight advantage in modelling flood and drought conditions and the STAR method is better suited for quantifying mean catchment runoff.

These evaluations provide a general guideline to select appropriate downscaling models for hydrological impact studies with specific purposes. For example, when mean seasonal catchment runoff and some hydrological processes (*e.g.* evaportranspiration) are the projection focuses, the STAR model can be applied due to its better performance in reproducing the climate variables

which drive evapotranspiration. In contrast, if the extreme conditions are considered, the other models except STAR should be applied as the climate forcing.

A robust hydrological model is also required to capture the characteristics of different hydrological processes and regional conditions. Bronstert *et al.* (2002) propose five basic requirements for hydrological models when used for flood projections in land-use and climate impact studies. Since the flood projection is one of the important objectives of this study, these requirements are also valid to select the appropriate hydrological model here. The five requirements are:

(a) Representation of the soil zone.
(b) Spatial distribution in representing the climatic and catchment conditions.
(c) Temporal resolution of both the meteorological data and the modelling time step for the relevant processes.
(d) Dynamics of the landscape especially for long-term projections.
(e) Scale for which the model was designed.

Besides these requirements, nutrient processes need to be integrated in the hydrological modelling, as one of the objectives in this study requires a comprehensive impact research on water quality.

There are various hydrological and water quality models for the basin scale developed and tested in the last decades (Arheimer & Brandt, 1998, Whitehead *et al.*, 1998, Bicknell *et al.*, 1997, Arnold *et al.*, 1998, Krysanova *et al.*, 1998). These models vary in the level of complexity from statistical and conceptual models based on statistical and empirical relationships to process-based and physically-based models derived from physical and physicochemical laws and including also some equations based on empirical knowledge. Due to the lack of description of important physical processes, the simplified conceptual models have limited applicability and are not appropriate for the simulation of some essential spatially distributed processes. The physically-based models are by definition fully distributed accounting for spatial variations in all variables. However, these models are often considered too complex and are without a guarantee of better performance (Beven, 1989; Beven, 1996). The requirement of large amounts of input data and computational resources for such models is also a particulate concern, especially for large basins (Lunn *et al.*, 1996). As the main study areas are the large river basins in Germany, the so called hydrological models of intermediate complexity (Bronstert, 2003), which combine both physically based formulations and some empirical approaches, are more promising.

Among the numerous process-based models, *e.g.* models SWAT (Arnold *et al.*, 1998), HSPF (Bicknell *et al.*, 1997), SWIM (Krysanova *et al.*, 1998) and DWSM (Borah *et al.*, 2004), SWIM (Soil and Water Integrated Model) was intensively calibrated and validated in terms of river discharges, water components and water quality for German river basins in previous studies (Hattermann *et al.*, 2005; Krysanova *et al.*, 2007; Hesse *et al.*, 2008; Voss, 2007). It was developed for climate and land use change impact assessment on the basis of the models SWAT (Arnold *et al.*, 1993) and MATSALU (Krysanova *et al.*, 1989). SWIM is a continuous-time semi-distributed watershed model, which integrates hydrological processes, vegetation, erosion and nutrient dynamics for the meso- and macro-scale river basins (see **Fig. 1-6**). It considers the spatial heterogeneity of the landscape and possible feedbacks between vegetation, hydrological processes and nutrient transport and retentions on a daily time step.

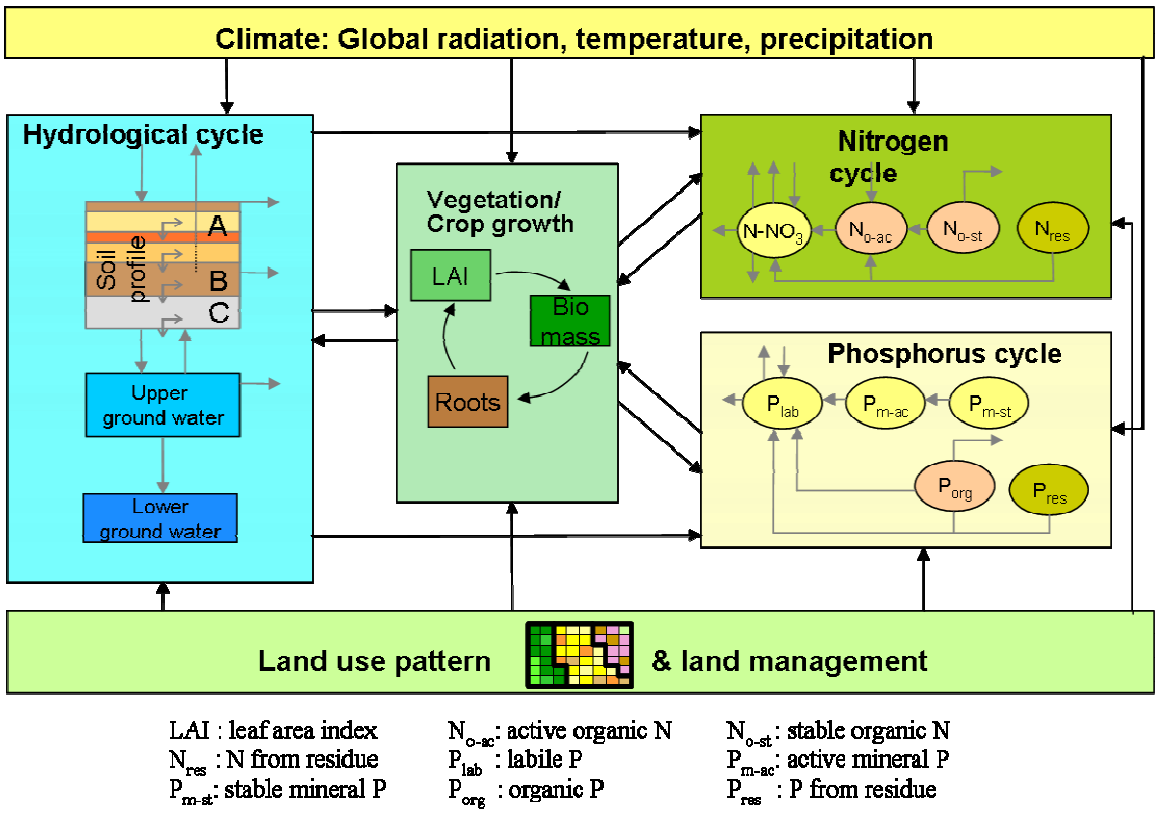

Figure 1-6: The modelling flow chart in SWIM at hydrotope level.

The SWIM model was chosen for this study for the following reasons 1) its integration of hydrological, plant growth and nutrients processes for a comprehensive investigation of environmental impacts, 2) its spatial disaggregation scheme allowing the analysis of different land use and water management strategies and 3) its successful applications in German river basins especially on the macro-scale (Hattermann *et al.*, 2005; Krysanova *et al.*, 2007). However, there are also some limitations to the model, which were addressed and overcome in this study:

- The SWIM model was not designed to investigate flood events, because some important flood generation processes (*e.g.* surface flow generation) are represented by conceptual formulations on a daily time step. This shortcoming especially restricts modelling of the flash floods in small or meso-scale basins in a short duration. However, the present study is focused on the extensive long-lasting flood events in large catchments, for which the daily discharge was taken into account. In fact, the modelling results proved that SWIM could reproduce the peak discharges satisfactorily in a daily time step for large rivers (Chapter 4).
- The basic version of SWIM does not include any glacial processes and it only uses the degree-day method to describe the snow melting process. The original version can sufficiently model the discharge generation in the Elbe basin (Hattermann *et al.*, 2005; Krysanova *et al.*, 2007), where the pluvial river regime is dominant. However, it is not sufficient for modelling the Danube and Rhine rivers in Switzerland and Austria, where the snow and glaciers play a significant role in the contribution of river discharges. To

overcome this limitation, a simple glacier module was developed along with a more sophisticated description of snow melting processes (explained in Chapter 1.3.3).

- The last requirement by Bronstert *et al.* (2002) suggests that the landscape dynamics should be taken into account especially for long-term projections. In this study, the variation of the crop rotation schedule was implemented in the model, aiming to represent the landscape dynamics under a changing climate in a certain extent (explained in Chapter 1.3.3).

The model system of this study is illustrated in **Fig. 1-7** with the selected models. For climate impact studies, the climatic and hydrological models were one-way coupled from the global to regional scales. The GCM ECHAM5 provides the boundary condition for the four RCMs, which down-scaled the global climate scenarios to the national level. Then SWIM was driven by various regional scenarios to project the daily discharges and annual water components for each studied basin. Taking into account the performance of different RCMs on hydrological impact studies (Bronstert *et al.*, 2007b), the SWIM outputs driven by STAR realizations were used for evaluating the mean seasonal runoff and annual hydrological components. The projected daily discharges driven by other RCM scenarios were particularly used for flood and low flow analysis. The land use scenarios were introduced based on the political incentives at a local level. The changes in NO_3-N load were analysed for the selected meso-scale catchments in the Elbe region. A detailed description of these selected models is provided in the Chapter 1.3.1 – 1.3.3.

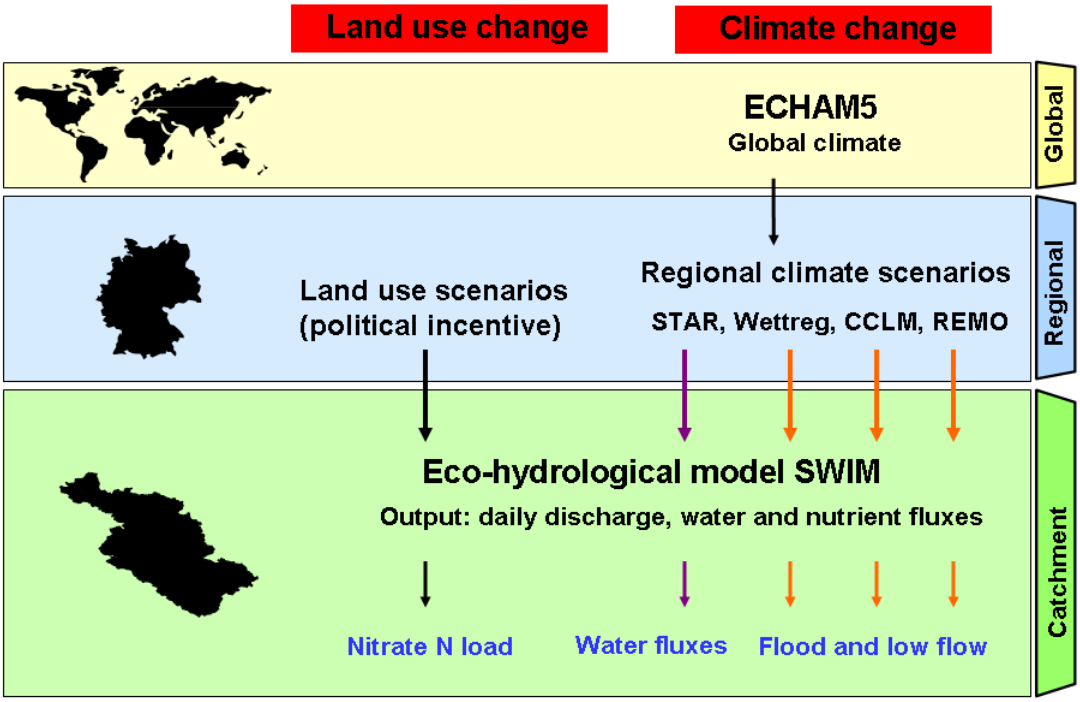

Figure 1-7: Sketch of the model system.

1.3.1. ECHAM5

The atmospheric GCM ECHAM5 is the fifth-generation climate model developed at the Max Planck Institute (MPI) for Meteorology in Hamburg, Germany. It is evolved from the model of the European Centre for Medium-Range Weather Forecasts (ECMWF) (Woods, 2006). ECHAM5

solves prognostic equations for vorticity, divergence, surface pressure and temperature expressed in terms of spherical harmonics with a triangular truncation. Water vapour, cloud liquid water, cloud ice and trace components are transported with a flux form semi-Lagrangian transport scheme (Lin and Rood, 1996) on a Gaussian grid (Stier *et al.*, 2005). A detailed model description of ECHAM5 is given by Roeckner *et al.* (2003).

Depending on the configuration, ECHAM5 resolves the atmosphere up to 10 hPa (the tropospheric model) or up to 0.01 hPa for middle atmosphere studies. The most recent ocean general circulation model, the MPI Ocean Model (MPI-OM), is coupled to EHCAM5 and this coupled system has been used for the Intergovernmental Panel on Climate Change (IPCC) Fourth Assessment Report (AR4) simulations (Giorgetta *et al.*, 2006). The emission scenarios A1B, A2 and B1 described in the Special Report on Emissions Scenarios (SRES) by IPCC served as a basis for the calculations.

Out of various global models from different countries, ECHAM5 was evaluated as the best performing individual model, globally and Antarctica (Connolley and Bracegirdle, 2007). For central Europe, it also belongs to one of the five GCMs, which simulated both realistic pressure and circulations patterns (van Ulden and van Oldenborgh, 2006).

1.3.2. Models for regional climate scenarios

Some general characteristics of each downscaling model are listed in **Table 1-2** with details given in the following sections.

Table 1-2: Characteristics of the climate downscaling models used in this study.

Model	Model type	Simulation period	GCM based	Emission scenario	Spatial resolution	Realization per scenario
CCLM	Dynamic	1960-2100	ECHAM5	A1B, B1	0.2°	2
REMO	Dynamic	1951-2100	ECHAM5	A1B, A2, B1	0.088°	1
STAR	Statistic - empirical	2007-2060	ECHAM5	A1B	2342 climate and precipitation stations in Germany	100
Wettreg	Statistic - empirical	1961-2100	ECHAM5	A1B, A2, B1	274 climate stations and 1691 precipitation stations in Germany	20

1.3.2.1. CCLM

CCLM (Cosmo-Climate Local Model) (Rockel *et al.*, 2008) originates from the weather forecast model "Lokal-Modell" (LM), which was developed by the German Meteorological Service (Steppeler *et al.*, 2003). CCLM is a non hydrostatic climate model and it is based on the basic hydro-thermodynamical equations describing a compressible non-hydrostatic flow in a moist atmosphere without any scale approximations. Its spatial resolution (0.2°) is coarser than that of REMO and its area of application is the whole of Europe. It takes the results of the GCM ECHAM5 as boundary conditions, but only two emission scenarios were available for this study (A1B and B1). Two control runs were generated based on two realizations of the 20th century reconstruction initialized in different years of the pre-industrial control experiment from ECHAM5. These control runs provide the initial conditions for the transient simulation of the future regional climate projections A1B and B1. Hence, two realizations were generated by CCLM for each emission scenario.

1.3.2.2. REMO

REMO (REgional MOdel) was developed from the ‘‘Europamodell’’, the former numerical weather prediction model of the German Meteorological Service (Majewski, 1991), in the Max-Planck-Institute for Meteorology in Hamburg, Germany (Jacob, 2001). It is a three dimensional regional hydrostatic climate model. REMO solves the hydrostatic Euler equations with a finite difference method on a hybrid terrain following a vertical coordinate system using the leapfrog time integration on an Arakawa-C grid (Suklitsch *et al.*, 2010).

REMO calculates climate variables at a 0.088° grid for Central Europe including Germany and simulates the main weather processes including cloud dynamics, precipitation and temperature development for each grid cell. Control and scenarios of future climate conditions are constructed by using GCM ECHAM5 results as large-scale forcing. Only one realization of each scenario (A1B, A2 and B1) was generated by REMO.

1.3.2.3. STAR

STAR (STAtistical Regional model) was developed at the Potsdam Institute of Climate Impact Research, Germany (Orlowsky *et al.*, 2008). Compared to other downscaling models, which can project 100-years or longer climate scenarios for Germany, STAR was developed to generate regional climate projections for the near future (50 – 60 years). Analogue approaches such as STAR assume that observations of a given day from the training period can occur again or in a similar way in the future. Hence, simulated series are constructed by resampling segments of a daily observation series. Generating a future series can thus be seen as defining a date-to-date-mapping, by which each date of the future period is assigned a date and the concurrent meteorological observations of the training period. No trend elimination or any other modification is applied to the observational data prior to resampling. The advantage of such resampling is that the physical consistency of both the spatial fields and the simultaneous combinations of different weather parameters is guaranteed. The STAR resamples in blocks of 12-days, ensuring that the projected future time-series has realistic persistence features.

One of the most important properties of STAR is that the produced climate time series are forced only by the linear temperature trend of the future period. Once the daily mean values of a long-term observed time series are obtained, it is possible to impose the assumed trend onto the series and to create the simulated series that complies with this trend. The scenario of future climate conditions was constructed by using the temperature trend derived from climate change scenario A1B produced by ECHAM5. The time series of other climate variables, such as precipitation, radiation, humidity, *etc*. were generated by using the values recorded on the same day as the temperature measurement. Therefore, this method maintains the stability of the main statistical characteristics (variability, frequency distribution, annual cycle and persistence). For the spatially differentiated projections, climatological subregions were identified (*e.g.* by meteorological stations) and an individual temperature trend was prescribed for each sub-region, representing the spatial patterns of future climate parameters.

STAR is much faster in computation time than the dynamical climate models. It is able to generate multiple climate projections by implementing a random process (Monte Carlo simulation). An ensemble of 100 realizations of the climate change scenario was generated to estimate the uncertainty inherent in the climate scenario.

Inevitably, STAR also shows some weaknesses. For example, it fully relies on the historical climate data resampling, so it is principally not able to reproduce extreme events (*e.g.* heavy precipitation) exceeding the already observed values. As a result, all the projected extreme events

will not exceed the extreme events observed in the past. The second weakness of STAR is that it relies on large amounts of observed historical data. Hence, it cannot be applied to the data-scarce regions.

1.3.2.4. WettReg

WettReg (Wetterlagenbasierte Regionalisierungsmethode: weather-type based regionalization method) is developed by Climate & Environment Consulting Potsdam GmbH (CEC), Germany. Different from physical dynamical models, WettReg uses the statistical relationships between large-scale atmospheric conditions and local climate and the characteristics of regional climate for different weather types (Enke *et al.*, 2005a, 2005b). It classifies observed weather types into 10 classes of typical 'temperature' and 8 classes of 'precipitation regimes', for each season. Variables/features which have a relatively good representation in the global models, such as temperature and circulation patterns, are selected as driving climate variables. Variables with a relatively poor representation in global models, such as precipitation or radiation, are generated by WettReg using observed correlations between large-scale patterns, *e.g.* precipitation and radiation. Precipitation conditions are modified in a further step to better fit the 'precipitation regime'.

As WettReg needs observation data to derive the correlation matrices for the observation period, climate projections can only be calculated for locations with climate observations. Input data of the model including meteorological data from 274 climate stations and 1691 precipitation stations all over Germany are available for this study. Since it is less computationally expensive, WettReg can be applied in a multiple run mode. As a result, 20 realizations of each scenario were used to evaluate uncertainty.

1.3.3. Eco-hydrological model SWIM

SWIM (Soil and Water Integrated Model) is a process-based eco-hydrological model based on two previously developed models SWAT (Soil and Water Assessment Tool, Arnold *et al.*, 1993) and MATSALU (Krysanova *et al.*, 1989). The hydrological module and the vegetation module are basically the same as in SWAT and the nitrogen module was taken from the model MATSALU. A full description of the basic version can be found in Krysanova *et al.* (1998) and an online SWIM manual is available under http://www.pik-potsdam.de/members/valen/swim.

SWIM has a three-level scheme of spatial disaggregation: 'basin–sub-basins–hydrotopes'. In addition, the root zone can be vertically subdivided into a maximum of 10 soil layers. The hydrotopes are sets of elementary units in a subbasin with homogeneous soil and land use types. It is assumed that a hydrotope behaves uniformly regarding hydrological processes and nutrient cycling. During the simulation:

1. water, nutrients and plant biomass are initially calculated for every hydrotope/every soil layer in a hydrotope level (shown in **Fig. 1-6**),
2. the outputs from hydrotopes are then integrated to estimate the sub-basin outputs taking retention into account, and
3. the routing procedure is applied to the sub-basin lateral flows of water, nutrients and sediments.

The simulated hydrological system consists of four control volumes: the soil surface, the root zone of soil, the shallow aquifer and the deep aquifer. The soil root zone is subdivided into several layers in accordance with the soil database. The water balance for the soil surface and soil

column includes precipitation, surface runoff, evapotranspiration, subsurface runoff and percolation. The water balance for the shallow aquifer includes groundwater recharge, capillary rise to the soil profile, lateral flow and percolation to the deep aquifer.

Surface runoff is estimated as a non-linear function of precipitation and a retention coefficient, which depends on soil water content, land use and soil type (modification of the Soil Conservation Service (SCS) curve number method; Arnold *et al*., 1990). Lateral subsurface flow (or interflow) is calculated simultaneously with percolation. It occurs when the storage in any soil layer exceeds field capacity after percolation. It is especially important for soils with an impermeable or less permeable layer below several permeable ones.

Potential evapotranspiration is estimated using the method of Priestley–Taylor (Priestley and Taylor, 1972), though the method of Penman–Monteith (Monteith, 1965) can also be used. Actual evaporation from soil and actual transpiration by plants are calculated separately.

The groundwater contribution to stream flow is calculated based on the approach of Smedema and Rycroft (1983), who derived the non-steady-state response of groundwater flow to periodic recharge from Hooghoudt's (1940) steady-state formula. The percolation from the soil profile recharging the shallow aquifer is corrected by the delay time function proposed by Sangrey *et al.* (1984).

The module representing crops and natural vegetation is an important interface between hydrology and nutrients. A simplified EPIC approach (Williams *et al*., 1984) is included in SWIM for simulating arable crops (like wheat, barley, rye, maize, potatoes) and aggregated vegetation types (*e.g.* 'pasture', 'evergreen forest', 'mixed forest') using specific parameter values for each crop/vegetation type. A number of plant related parameters are specified for 74 crop/vegetation types in the database attached to the model. Vegetation in the model affects the hydrological cycle by the cover-specific retention coefficient, impacting surface runoff and indirectly influencing the amount of transpiration, which is simulated as a function of potential evapotranspiration and leaf area index (LAI). SWIM allows the application of the complicated crop rotation schemes including several crops such as wheat, barley, rye, maize, potatoes, etc., that could be made specific for different subregions or federal states, and differentiated for soil types.

Interception of photosynthetic active radiation (PAR) is estimated as a function of solar radiation and LAI. The potential increase in biomass is the product of absorbed PAR and a specific plant parameter for converting energy into biomass. The potential biomass is adjusted on daily basis if one of the four plant stress factors (water, temperature, nitrogen and phosphorus) is less than 1.0, using the product of a minimum stress factor and potential biomass. The water stress factor is defined as the ratio of actual to potential plant transpiration. The temperature stress factor is computed as a function of daily average temperature, optimal and base temperatures for plant growth. The N and P stress factors are based on the ratio of accumulated N and P to the optimal values. The LAI is simulated as a function of a heat unit index (ranging from 0 at planting to 1 at physiological maturity) and biomass.

The nitrogen and phosphorus modules include the following pools in the soil layers (**Fig. 1-6**): nitrate nitrogen (N), active ($N_{o\text{-}ac}$) and stable ($N_{o\text{-}sc}$) organic nitrogen, organic nitrogen in the plant residue (N_{res}); labile phosphorus (P_{lab}), active ($P_{m\text{-}ac}$) and stable ($P_{m\text{-}st}$) mineral phosphorus, organic phosphorus (P_{org}), phosphorus in the plant residue (P_{res}) and the following fluxes (inflows to the soil, exchanges between the pools and outflows from the soil): fertilization, input with

precipitation, mineralization, denitrification, plant uptake, leaching to groundwater, losses with surface runoff, interflow and erosion. The interaction between vegetation and nutrient supply is modelled by the plant uptake of nutrients, release of residuals entering the mineralization process, and by using nitrogen and phosphorus stress factors affecting plant growth.

Amounts of soluble nutrients (N and P) in surface runoff, lateral subsurface flow and percolation are estimated as the products of the volume of water and the average concentration. Nitrogen retention in subsurface and groundwater occurs during the subsurface transport of nitrogen from soil column to rivers and lakes, and is represented mainly by denitrification. Nitrogen retention is described in SWIM by four parameters: residence times (the time period subject to denitrification) in subsurface and groundwater (K_{sub} and K_{grw}) and the decomposition rates in subsurface and groundwater (λ_{sub} and λ_{grw}) using the equation (Hattermann *et al.*, 2006):

$$N_{t,out} = N_{t,in} \frac{1}{1+K\lambda}\left(1-e^{-(\frac{1}{K}+\lambda)\Delta t}\right) + N_{t-1,out} \cdot e^{-\left(\frac{1}{K}+\lambda\right)\Delta t} \quad , \qquad (1\text{-}1)$$

where $N_{t,out}$ is nitrogen output and $N_{t,in}$ is nitrogen input at time t, the parameter K represents the residence time in days (d), and λ (d^{-1}) the decomposition rate. The term Δt is the time step. The four retention parameters are identified within ranges specified from literature, and are subject to calibration. This approach was developed for the SWIM model and tested for modelling water quality (Hattermann *et al.*, 2006).

1.3.3.1. Snow module

In the basic version of SWIM, the climate information was unique at the sub-basin scale to simulate different processes. Climate parameters were interpolated into the centroids of sub-basins, which were treated as virtual climate stations in the basins. If air temperature in one sub-basin is below a certain degree (usually 0°C), precipitation occurs as snow and snow is accumulated. If the air temperature is above a certain degree (usually 0°C), snow is melting as a function of the daily mean temperature:

$$M_{snow} = DDF_{snow} * T \qquad (1\text{-}2)$$

$$0 \le M_{snow} \le SNO$$

where M_{snow} is the snowmelt rate in mm/day, DDF_{snow} is the degree-day factor for snow, SNO is the water content of snow in mm and T is the daily mean temperature in °C. Melted snow is treated the same as rainfall for estimating runoff volume and percolation.

However, this method could neither give the precise spatial distribution of the snow pack within one sub-basin, nor consider other snow processes that play an important role in the runoff generation from snow. In order to adequately simulate the snow accumulation and snow melt processes, the classification of hydrotopes should also take into account the elevation information within one sub-basin. The elevation bands with an interval of 100 meters are used to delineate the original hydrotopes into finer units, which are characterized by sub-basin number, soil type, land use type and the mean elevation level. The snow processes (*e.g.* snow accumulation, snow melt) are simulated for the finer hydrotopes with the temperature adjusted by altitude according to the following linear correction function:

$$T_{hydrotope} = T_{subbasin} + T_{grad} * (Elev_{hydrotope} - Elev_{centroid}) \quad (1\text{-}3)$$

where $T_{hydrotope}$ is the corrected temperature for hydrotopes, $T_{subbasin}$ is the temperature interpolated into the centroids of sub-basins, T_{grad} is the correction coefficient, $Elev_{hydrotope}$ is the mean elevation of the hydrotope and $Elev_{centroid}$ is the elevation of the centroid in the corresponding sub-basin.

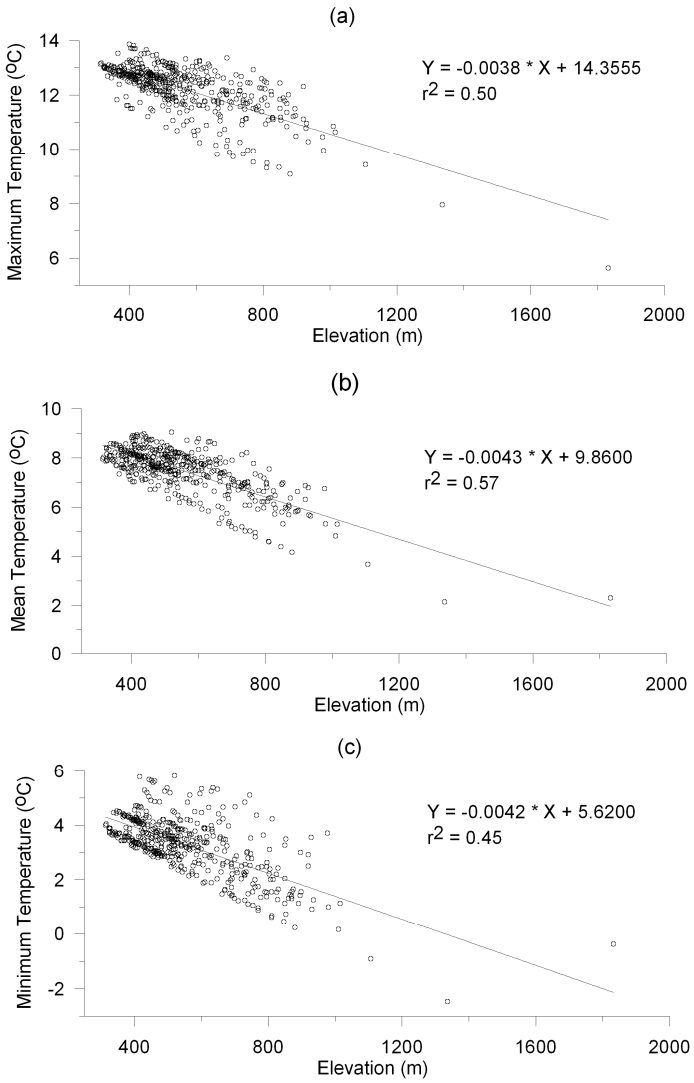

Figure 1-8: Correlations between the long-term (1951 – 2007) observed air temperatures (maximum (a), mean (b) and minimum (c)) and elevations of climate stations in the German upper Danube basin.

Figure 1-8 shows an example of the correction coefficient obtained from the regression relationships between air temperatures and the elevations of the climate stations in the upper German Danube basin. All slopes of the regression lines are approximately -0.004, indicating that the temperature decreases 0.4°C with an increase of 100 meter in elevation in this region. However, the correlation between temperature and elevation is not significantly consistent for

each station indicating by the r^2 between 0.45 and 0.57. Therefore, the correction coefficient was treated as a calibration parameter.

Besides the introduction of the elevation information for hydrotopes, the extended snow module applied the method used by Gelfan *et al.* (2004) to simulate detailed snow melting processes. Unlike the snowmelt routines that also apply degree-day method but calculate the snow water content only (*e.g.* Fontaine *et al.*, 2002), the advantage of Gelfan *et al.*'s method is a more detailed description of temporal change of the snow depth, content of ice and liquid water, snow density, refreezing melting water and snow metamorphism. With the former method, only the river discharges were normally calibrated and validated assuming the snow processes were reasonably simulated. In this study, the latter method allows us calibrating not only the river discharge at the basin outlet but also the snow accumulation and melt dynamic using the available observed snow depth at the climate stations in Switzerland and Austria. In addition, Gelfan *et al.*'s method considers the retention time of the melting water in snow, so it simulates better the temporal water discharge from the snow pack. The dynamics of snow depth according to Gelfan *et al.* (2004) is described as follows:

$$\frac{dH}{dt} = \rho_w \left[X_s \rho_0^{-1} - (S + E_s)(\rho_i i)^{-1} \right] - V \qquad (1\text{-}4)$$

where H is the snow depth in *cm*, i is the volumetric content of ice and X_s is the snowfall rate (in cm day^{-1}). S is the snowmelt rate, also calculated by the degree-day method (**Equation 1-2**). ρ_w, ρ_i and ρ_0 are the density of water (1 g cm^{-3}), ice (0.917 g cm^{-3}) and fresh fallen snow (taken as 0.08 g cm^{-3} (Hock, 2005)), respectively. E_s is the rate of snow sublimation and V is the snowpack compression rate.

The snow pack compression rate V is calculated by (in cm day^{-1}):

$$V = \frac{v_1 \rho_s}{\exp(v_2 T_s + v_3 \rho_s)} \frac{H^2}{2} \qquad (1\text{-}5)$$

where ρ_s is the density of snow pack (in g cm^{-3}), calculated as $\rho_s = \rho_i i + \rho_w w$. ($w$ is the volumetric content of liquid water), T_s is the snow pack temperature, v_1, v_2, and v_3 are the coefficients, equal to 3.4×10^{-6} cm^2 day^{-1} g^{-1}; -0.08 $^\circ$C^{-1}; 21 cm^3 g^{-1}, respectively.

The water is released based on the water content in the snow pack and the snow depth.

$$VSN = H * (w - ULMAX) \qquad (1\text{-}6)$$

where *VSN* is the water outflow from the snowpack in cm, *ULMAX* is the maximum water holding capacity of the snow pack.

1.3.3.2. Glacier module

Among the various glacier melting models from the sophisticated physically based energy balance models to the empirical methods based on one or more meteorological variables, the simplest degree-day method was chosen to simulate glacier melting in SWIM. The main reason is that this method is often sufficient for catchment scale studies employing daily time steps (Hock,

2005) and it suits the complexity of the hydrological model SWIM. On the other side, it is difficult to apply physical models in this study due to the lack of the necessary data for each glacier in the whole Danube and Rhine basins. Moreover, the degree-day method was also used for a climate change study at 37 glaciers in different parts of the world by Braithwaite and Zhang (1999).

In this module, the glacier melting occurs when the daily mean temperature T is higher than 0°C and no snow cover exists. The potential glacier melting M_{ice} (mm/d) is

$$M_{ice} = DDF_{ice} * T \tag{1-7}$$

DDF_{ice} is the degree-day factor for glacier. It was calibrated within the range of empirical values list in Braithwaite and Zhang (2000) and Hock (2003).

The annual glacier mass balance at a given glacier hydrotope b_i is calculated based on the simulated snow accumulation P_{snow} and the simulated snow and ice melt (M_{snow} and M_{ice}) over the whole year:

$$b_i = \int_{t0}^{t1} [P_{snow} - M_{snow} - M_{ice}]dt \tag{1-8}$$

Here *t0* is the 1st of October as the start date of the measurement year and *t1* is the 30th of September of the following year as the end of the measurement year (Paterson, 1994). The annual mass balance of the entire glacier in the basin is then estimated as the area-weighted sum of the mass balance of all hydrotopes.

Since it is the first attempt to include glacier module in SWIM, there are still substantial improvements needed in the future. For example, in **Equation 1-7**, the maximum daily temperature needs to be tested instead of mean temperature. Secondly, the degree-day factors for glacier melting are constant for the entire catchment and the full simulation period, so the variation of the degree day factor for different glaciers needs to considered. Thirdly, the current glacier module is not validated specifically as the glacier data is not available for the entire Danube and Rhine basins. Hence, future work should include the application of the glacier module in small catchments with sufficient data and improvement of the spatial and temporal representation of degree-day factors.

1.3.3.3. Adaptation of crop rotation in scenarios

In the basic SWIM version usually applied to reference (current) conditions, winter crop (*e.g.* winter wheat or winter barley are dominant crops in Germany) is planted and harvested according to the current practice schedule (statistical data from Voss, 2007). **Figure 1-9** illustrates an example of the LAI simulated with fixed harvest times in both reference and scenario periods at a hydrotope scale. In the reference period (black line in **Fig. 1-9**), the winter crop is planted in October and grows slowly with a slight increase in LAI until April. From April to June, the crops grow much faster and are harvest at the beginning of August, when the crops are cut and the LAI returns to zero. There is usually a cover crop growing between harvest and the next planting of winter crop, so there is a slow increase of LAI between August and October.

In warmer (*e.g.* STAR scenario) conditions, if the schedule is still fixed by the current statistical plan, the crops are cut in August even if they are actually harvested in June (blue line in **Fig. 1-9**). Hence, the crop management is not realistically simulated in the original version of SWIM as temperature rises. To overcome this shortcoming, the scheduling of agriculture crops is governed by a harvest index, so the rotation scheme can be changed when the winter crop harvests earlier than in the current condition (red dashed line in **Fig. 1-9**). In this case, SWIM would allow earlier growth of cover crop after the harvest of winter crops and let it grow until the next winter crop planting. This change can influence the runoff generation in summer as more water may be needed for the cover crop growth. Interestingly, the cover crop shown in **Fig. 1-9** could nearly reach its harvest level during the summer time, indicating the possibility of two crop rotations per year in Germany under a warmer climate.

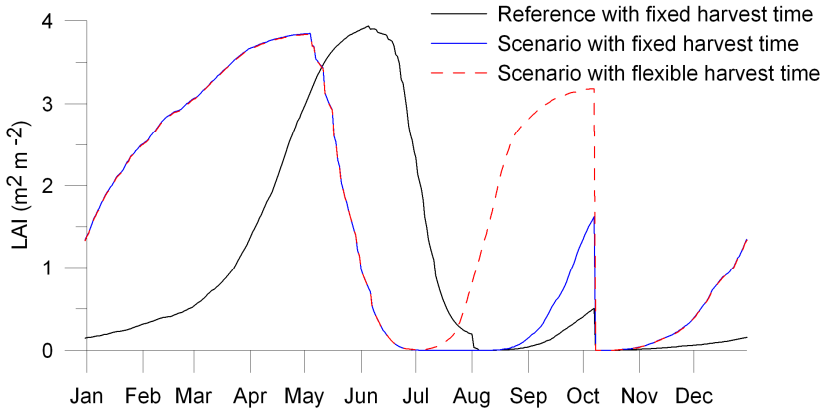

Figure 1-9: Simulated LAI in the reference period (1961 – 1990) and the STAR scenario period (2051 – 2060) with or without fixed harvest time.

1.4. Dissertation structure

The structure of the next chapters is as follows. The main part following the Introduction consists of five chapters. Chapter 2 is devoted to analysis of seasonal temperature extremes in Potsdam with the aim of providing further evidence of climate change and an additional motivation of climate impact study for Germany. Chapters 3 to 5 encompass the results of climate impact assessment for Germany, including:

1. projections of seasonal dynamics of water discharge and spatiotemporal dynamics of water flow components (Chapter 3),
2. projections of climate change on floods (Chapter 4), and
3. projections of low flow conditions impact (Chapter 5).

The climate impact assessment presented in Chapters 3-5 was done by combining different RCMs with the regional ecohydrological model SWIM. Chapter 6 is devoted to a land use change impact study, which was performed for selected sub-regions of the Saale river basin using the same model SWIM and different potential scenarios of changes in land use and land management. Finally, main results presented in Chapter 2 – 6 are summarized in Chapter 7 sequentially based on the different topics, and Chapter 8 presents the final conclusions of the thesis and discusses potential future work on environmental impact assessment.

Acta Geophysica 58(6): 1115-1133 (2010)

2. Seasonal temperature extremes in Potsdam

Zbigniew W. Kundzewicz* [1,2] & Shaochun Huang[1]

[1] *Potsdam Institute for Climate Impact Research, Telegrafenberg A62, 14412 Potsdam, Germany*

[2] *Institute for Agricultural and Forest Environment, Polish Academy of Sciences, Poznań, Poland*
* Corresponding author. Tel.: +49 331 288 2517

E-mail address: zbyszek@pik-potsdam.de

Abstract
The awareness of global warming is well covered and results from observations made on thousands of stations. This paper complements the large-scale results by examining a long time-series of high-quality temperature data from the Secular Meteorological Station in Potsdam, where observation records over the last 117 years, *i.e.* from January 1893 are available. Tendencies of change in seasonal temperature-related climate extremes are demonstrated. "Cold" extremes have to become less frequent and less severe than in the past and "warm" extremes – have become more frequent and more severe. Moreover, the interval of the occurrence of frost has been decreasing, while the interval of the occurrence of hot days has been increasing. However, many changes are weak and not statistically significant, since the variability of temperature indices at the Potsdam station has been very strong.

Key words: temperature; extremes; seasonality; climate variability; climate change; trend

2.1. Introduction

The time series of global mean air temperature, compiled by the Climatic Research Unit of the University of East Anglia, jointly with the UK Met Office Hadley Centre (cf. http://www.cru.uea.ac.uk/cru/data/temperature/ ; Brohan *et al.*, 2006) or in NASA (National Aeronautics and Space Administration) in the USA (http://data.giss.nasa.gov/gistemp/), convincingly illustrate global warming.

As noted in IPCC (2007), warming of the global climate system is unequivocal. This is now evident from observations of increases in air temperature, which show clear growing trends at a range of scales, from local, via regional, to continental, hemispheric, and global. The updated 100-year linear trend (1906 to 2005) reflects a 0.74°C [0.56°C to 0.92°C] global mean temperature increase, while global warming rates over the last 50 years and over the last 25 years were much stronger (0.128 °C/decade and 0.177 °C/decade, respectively). That is, the global warming rate over the last 25 years is over 2.4 times faster than it was over the last 100 years.

As reported by Trenberth *et al.* (2007), there has been a widespread increase in the number of warm nights between 1951 and 2003, and a decrease in the number of cold nights. Trends in the number of cold and warm days are also consistent with warming, but are less marked than at night. This is a general tendency, yet there are regional differences. Over the last half-century, nearly two-thirds of the global land area has experienced a significant decrease in the annual occurrence of cold nights; while a significant increase in the annual occurrence of warm nights also took place at nearly two-thirds of the global land area. The distributions of minimum and maximum temperatures have not only shifted to higher values, consistent with overall warming, but the cold extremes have warmed more than the warm extremes. More warm extremes imply an increased frequency of heat waves. Associated with the warming there has been a global trend towards fewer frost days.

Although global warming is unabated, one cannot claim that the values of the annual global mean temperature since 1850 are known with good accuracy. Indeed, the uncertainty range has been considerable (but not overshadowing the global warming) and has varied with time, over the time horizon of concern, being highest in the 1850s and lowest in the 1980s. Since the 1980s, the ground observation networks have been shrinking in many areas, so that recently uncertainty does not decrease with time.

The paper complements the large-scale aggregate results by demonstrating tendencies for a long time series of good-quality instrumental observation records. It examines the details of seasonal warming via analysis of temperature-related climate extremes in the unique long-term gap-free record from Potsdam, from January 1893 to February 2009.

2.2. Data

Since the accuracy and homogeneity of a long time series of records of temperature observations is often problematic, it is essential to look for data from highest-quality stations, where the time series of records are long, reliable and gap-free, and where changes of location, surrounding environment, instruments, observation principles and methods, and timing are limited. Such conditions are not easy to find, but they are fulfilled at the Secular Meteorological Station in Potsdam (Germany).

The Potsdam Station (co-ordinates: 52°23'N 13°04'E, elevation 81 m.a.s.l.) is located to the south-west of town in Potsdam, approximately 600 m away from the built-up area, so that the urban heat island effect is not present there. It is a notable station, probably the only meteorological observatory, world-wide, with uninterrupted observations of many variables carried out every day since 1st January 1893. The Secular Meteorological Station in Potsdam was established with the purpose of serving for a long time (the word saeculum means longevity in Latin). The manned observations were continued even during nearly all (except for only three) days of World War II. Since measurements from self-recording instruments were available, and incorporated into the long time series of records, there have been no gaps in the data, even in 1945.

Efforts have been made to keep the observation conditions homogeneous, by maintaining the station location (on an empty plot in Telegrafenberg in Potsdam, in a considerable distance from buildings and trees), the character of the environment (e. g. removing any tree seedlings from station's environment), and methods and principles of instrumental observation (cf. Lehmann and Kalb, 1993).

Besides air temperature (mean, minimum, maximum), many other meteorological variables are being measured at the station. These include soil temperature, air pressure, relative air moisture contents, water vapour pressure, wind, precipitation, cloudiness, snow cover, frost depth, and sunshine hours. Great efforts have been made to keep the observation conditions homogeneous, by maintaining the station location, conditions of the environment, methods and principles of instrumental observation. Measurements at the secular station have been carried out three times a day (7:08h, 14:08h, and 21:08h CET, *i.e.* UTC + 1 h). The daily mean temperature is calculated as (T7 + T14 + 2*T21)/4, where TN represents air temperature at hour N.

In the present internet era, open access to observation records on the web is very important for scientists, decision makers and the broader public alike, and contributes in a substantial way to the awareness on climate variability and change. Time series of daily meteorological records from Potsdam, extending since 1st January 1893, are freely available on the web portal: http://www.klima-potsdam.de/, together with comprehensive information about the station. The station has international reputation and its website has been frequently visited in Germany and abroad (cf. Kundzewicz *et al.*, 2007, Kundzewicz & Józefczyk, 2008).

The diagram of the mean annual temperature observed at Potsdam shows a clear increasing trend (**Fig. 2-1**), and the rate of increase grows with time. The slope of the regression line for the last 25 years (1984 – 2008) was 0.55 °C/decade, that is nearly twice stronger than during the last 50 years (1959 – 2008) (0.3 °C/decade), and five times stronger than for the last 100 years (1909 – 2008) (0.11 °C/decade). All these changes are statistically significant at the 0.01 level (or better). It should be noted that by shifting the time horizons of regressions in **Fig. 2-1** even slightly one could get different results. Selection of the last 25, 50, and 100 years follows the approach taken in IPCC (2007). The present results show that the recent acceleration of warming in Potsdam is much stronger than the global average. There have been eight calendar years on record with a mean annual temperature in excess of 10°C, five of which were in the recent 10 years (**Table 2-1**).

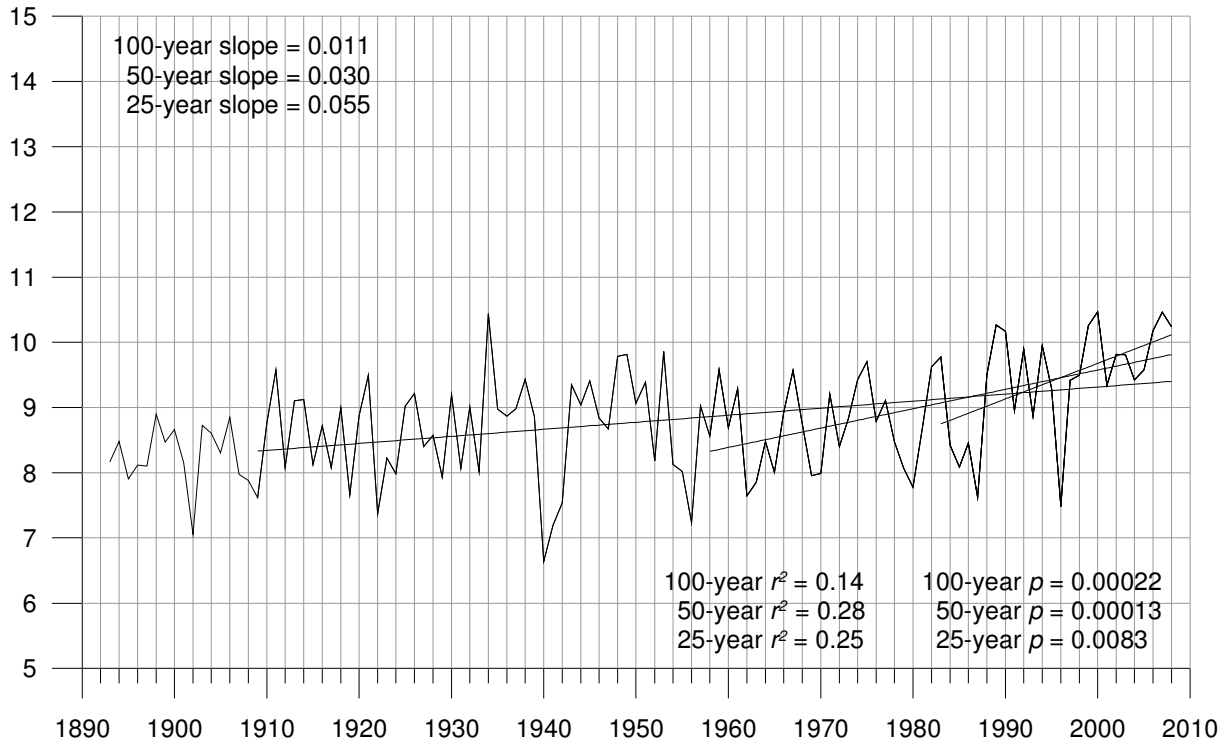

Figure 2-1: Changes in mean annual temperature in Potsdam. Notation: *r2* is the correlation coefficient; p is the significance level.

Mean annual temperature, which is presented in **Table 2-1**, is determined from 365 or 366 values of daily mean temperature (each of which, in turn, is calculated from three values measured every day with 0.1°C accuracy). Presenting of mean annual temperature with 0.01°C resolution allows, for instance, ordering of the years 2000 and 2007. Rounding up to 0.1°C resolution (matching the observation accuracy) would not make it possible to distinguish between the mean annual temperatures in these years.

The (upwards) departure from the long-term mean annual temperature in 1934, when the pre-2000 record was settled (the only excursion above 10°C until 1989) was a rare case. But annual mean temperature in excess of 10°C has become much more frequent in the last 20 years (**Table 2-1**).

Table 2-1: Mean Annual temperature of warmest years in Potsdam.

Rank	Year	Mean annual temperature, ℃
1	2000	10.47
2	2007	10.46
3	1934	10.44
4, 5	1989, 1999	10.26
6	2008	10.24
7, 8	1990, 2006	10.17

The records of mean annual temperature, presented in **Fig. 2-1**, show strong and rapid oscillations. Sudden jumps can be noted between two adjacent years, *e.g.* 1933 (8.02°C) and 1934 (10.44°C), *i.e.* the difference of 2.42 °C or between 1939 (8.86°C) and 1940 (6.64°C), *i.e.* the difference of 2.22°C, or – more recently – 1995 (9.29°C), 1996 (7.48°C) or 1997 (9.42°C), *i.e.* 1.79°C or 1.94°C, respectively. Within the seven-year interval, from 1934 to 1940, the mean annual temperature differed by 3.80 °C (from 10.44°C in 1934 down to 6.64°C in 1940). Hence, the short-term variations are much stronger than the gradual long-term trend.

Departures from the long-term trend, as illustrated by the regression lines, can be strong in individual years. Upwards excursions are a little more frequent, but less pronounced than downward excursions. Deviations of annual mean temperature from the regression line in individual years may even reach 2 °C. For instance, the downward excursions from the linear regression in 1940 and 1996 were 2.01 °C and 1.78 °C, respectively, while the strongest upward excursion in 1934 was 1.85 °C.

When looking not only at the annual temperature (in the sense of a calendar year, from 1st January to 31st December), but also at the mean air temperature of any consecutive 12-month period, that commences on the 1st of any month, one can find several recent records.

The pre-2007 record of mean 12-month temperature, 10.70 °C (July 1999 – June 2000) has been exceeded six times in 2007, reaching a very high level of 12.09 °C in the period from July 2006 to June 2007 (Kundzewicz *et al.*, 2007). In the latter record-breaking interval, there were four months with the highest monthly mean temperature ever observed in Potsdam. In July 2006, the mean temperature was 23.69°C (compared to the long-term mean 17.97 °C for 1961 – 1990), in December 2006 it was 5.17°C (long-term mean: 0.69 °C), in January 2007, 4.98 °C was observed (long-term mean: -0.80 °C), and in April 2007, the temperature was 12.02 °C (long-term mean of 8.05 °C). This last record of highest mean April temperature was broken by more than 1 °C in April 2009, to the level of 13.22 °C.

After looking at the record of a mean 12-month temperature in 2006/2007 in Potsdam, an analysis was extended to the whole of Germany, most of Europe and the Northern Hemisphere, where records were also detected (Kundzewicz *et al.*, 2008).

2.3. Changes in values of seasonal temperature extremes

The long time series of daily minimum and maximum values of temperature in Potsdam were analyzed in the context of seasonal properties for all four seasons. Seasons are defined as MAM (March, April, May) for spring, JJA (June, July, August) for summer, SON (September, October, November) for autumn, and DJF (December, January, February) for winter. Results illustrating seasonal mean of maximum and minimum temperatures for 1893 – 2008 (in case of winter – including 2009, for 1893 only January and February) are presented in **Fig. 2-2**. It shows seasonal warming for all seasons; on average about 1 °C / 100 years *i.e.* 0.1 °C / decade. The slope of regression lines for the whole 116-year period varies from 0.0074 (an increase of the maximum temperature for autumn) to 0.0121 (an increase of the minimum temperature for summer). In three seasons, the average increase of the minimum temperature is higher than the average increase of the maximum temperature, except for winter, where the maximum temperature grows slightly faster than the minimum temperature, hence the seasonal amplitude grows. In four cases (spring minimum, summer minimum, summer maximum and autumn minimum) changes are statistically significant at the 0.01 level, while in one case (spring maximum) at the 0.05 level. For three indices (autumn maximum, winter minimum, and winter maximum), changes are not

statistically significant at the 0.05 level, while one of them (winter maximum) is nearly significant (0.052).

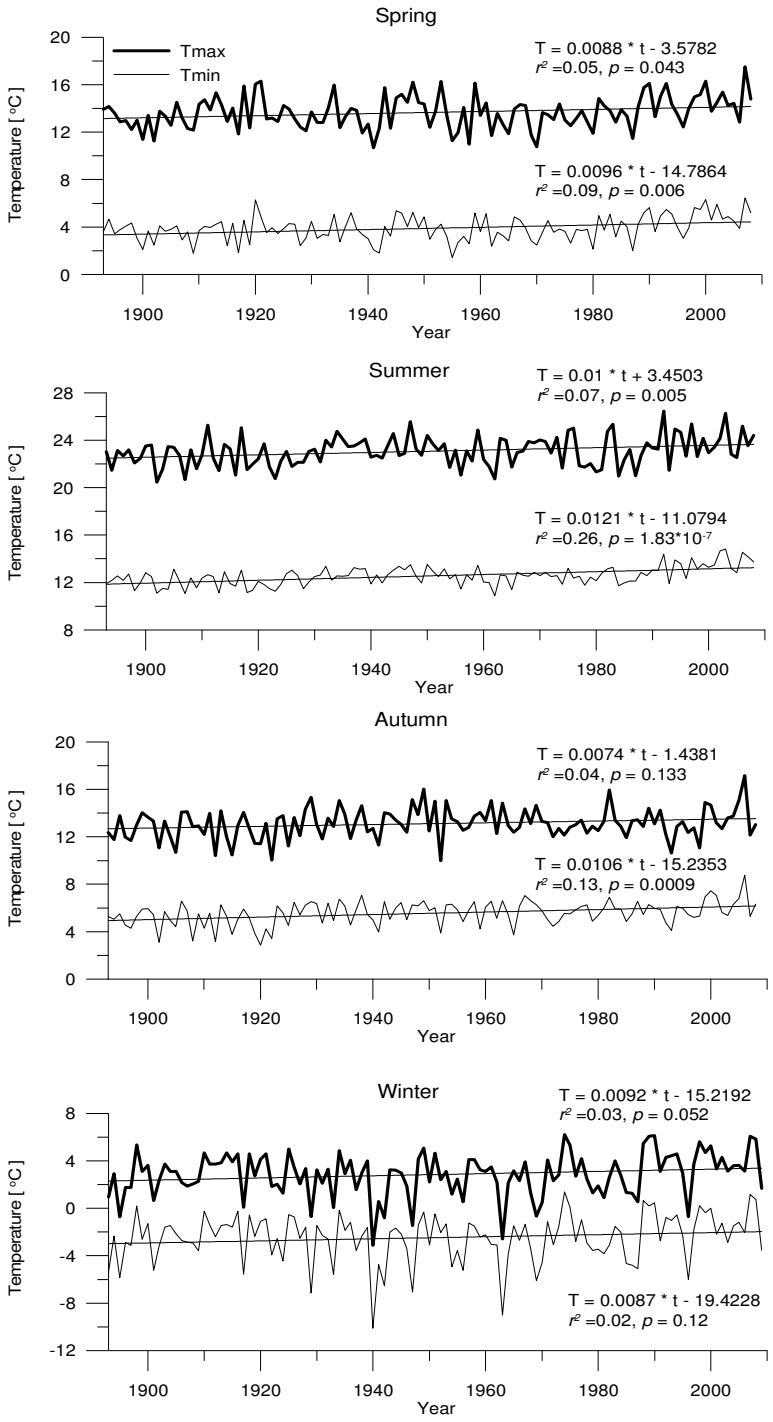

Figure 2-2: Changes in seasonal mean of daily minimum and maximum values of temperature for all seasons, in Potsdam from 1893 to 2008.

Climatic time series show strong natural variability (irregular oscillations), which is superimposed on a gradual warming trend. There is a strong random component, so that some

record-warm extremes, that occurred a long time ago, have not been exceeded to-date. Cold extremes, even if they occur now, are getting considerably less frequent and less severe. In 1917, the highest monthly mean of daily maximum temperature of June (27.15°C) was observed, even if the climate was then clearly colder than now. Only six years later, in 1923, the ever lowest monthly mean of daily maximum temperature of June (15.62°C) was observed (Kundzewicz and Józefczyk, 2008). The warmest spring day ever observed (T_{max} = 34.0°C) occurred on 24 May 1922, the warmest autumn night and day (T_{min} = 18.6°C and T_{max} = 34.0°C) occurred on 4 September 1895. All these "warm" records were set a long time ago, while one of "cold" records – the coldest autumn day observed on 21 November 1993 (T_{min} = - 6°C) – was set relatively recently.

It is clear that an occurrence of a record-high mean monthly temperature does not necessarily mean that the highest daily maximum temperature in this month is a record high. For example, July 2006 was the warmest July on record, as far as the monthly mean temperature is concerned (23.69°C). However, the highest daily maximum temperature during this month was 35.9°C, which is below the highest daily maximum temperature of 36.8°C, observed during a much less warm July 2007, when the mean monthly temperature was only 18.05°C.

Most of the intra-seasonal temperature amplitude (understood as the highest difference between daily maximum and minimum temperature in one season, cf. **Fig. 2-3(a-d)** and the difference between a seasonal maximum and minimum (**Fig. 2-3(e-h)**) have decreased. The regression slope in all but one of these diagrams is negative, yet in four cases the slope is smaller than 0.005. The steepest slope is for autumn (-0.025 for seasonal amplitude and -0.016 for maximum diurnal amplitude). Only for seasonal summer amplitude has the slope been positive.

This decreasing tendency is especially strong for the maximum diurnal amplitude for autumn (significant at 0.01 level). However, most (five out of eight) changes illustrated in **Fig. 2-3** are not statistically significant, except for maximum diurnal amplitude for summer (0.05 significance level) and autumn (0.01) and the seasonal amplitude for autumn (0.05). In the past, the temperature range was much higher. For instance, the lowest and highest autumn temperature values ever observed in 1911 – 1925 spanned the range from – 12.4 (on 29 November 1925) to +34.7°C (on 3 September 1911).

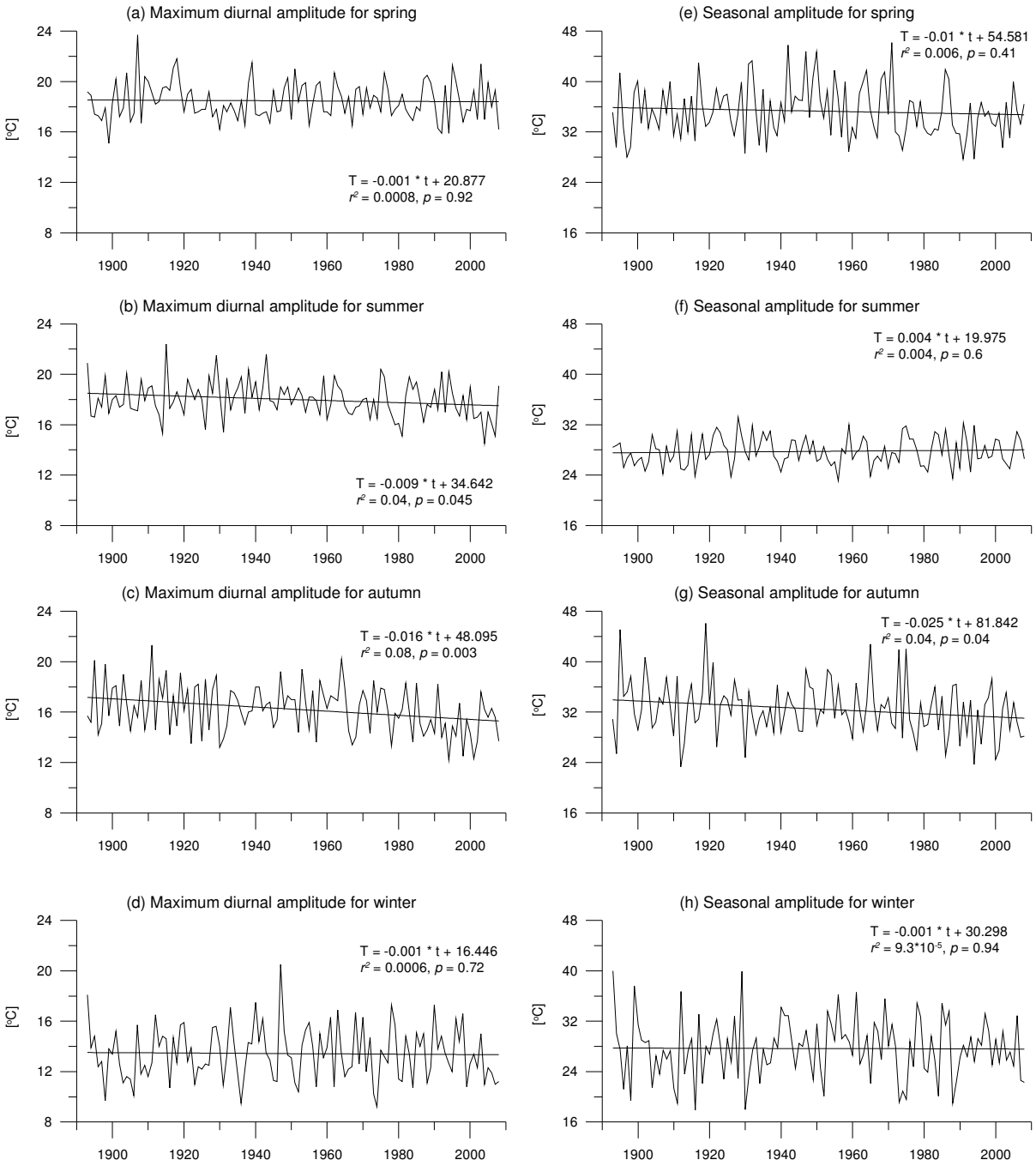

Figure 2-3: Time series of temperature amplitudes – maximum diurnal amplitude (difference between maximum and minimum temperature for the same day) for (a) spring; (b) summer; (c) autumn; (d) winter, and seasonal amplitude (difference between maximum and minimum temperature for the same season) for (e) spring; (f) summer; (g) autumn; (h) winter.

2.4. Changes in seasonal numbers of "cold" and "warm" extremes

The numbers of cold and warm days and nights were determined for each season, based on subjective definition of seasonal "cold" and "warm". Alternatively, one could use the percentile-based definitions of these notions, but here impact-based definitions are found more meaningful and easier to interpret by the readership. For instance, the number of excursions of daily minimum temperature below 0°C is far more meaningful than a percentile-based index. Also excursions under the levels: –10°C and +10°C can be intuitively expected as thresholds for a cold night in winter and summer, respectively. The impact interpretation of such thresholds is quite natural. Frosts in spring and autumn jeopardize the traffic (slippery roads), while frosts in spring cause detrimental effects to sensitive crops (*e.g.* blooming peaches and apricots, walnut, grapes). During a frosty night, some people (in particular the homeless and those under influence of alcohol) may freeze to death and sensitive plants may severely suffer. Cold summer nights adversely impact tourism (*e.g.* people camping in tents), while heat waves of longer duration adversely affect human health (hyperthermia) and crops.

Figures 2-4 – **2-7** present temporal changes in the numbers of cold nights and days for each season, for the interval 1893 – 2008 (2009 for winter). The seasonal threshold for cold nights were selected as –10°C for winter, 0°C for spring and autumn and +10°C for summer (**Fig. 2-4(a, b, c, d)**). The seasonal threshold for cold days were selected as 0°C for winter, +10°C for spring and autumn and +20°C for summer (**Fig. 2-5(a, b, c, d)**). The seasonal threshold for warm nights were selected as 0 °C for winter, +10°C for spring and autumn and +15°C for summer (**Fig. 2-6(a, b, c, d)**). The seasonal threshold for warm days were selected as +10°C for winter, +20°C for spring and autumn and the threshold for hot summer days was +30°C (**Fig. 2-7(a, b, c, d)**).

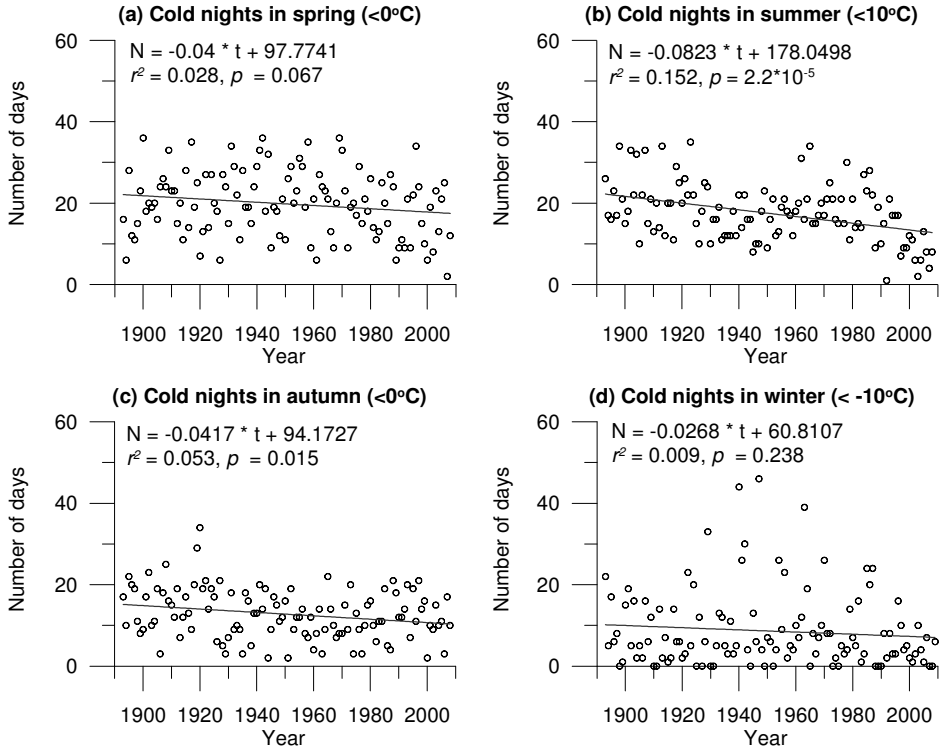

Figure 2-4: A time series of the number of cold nights for each season in Potsdam for 1893 – 2008 (2009 for winter); (a) spring; (b) summer; (c) autumn; (d) winter.

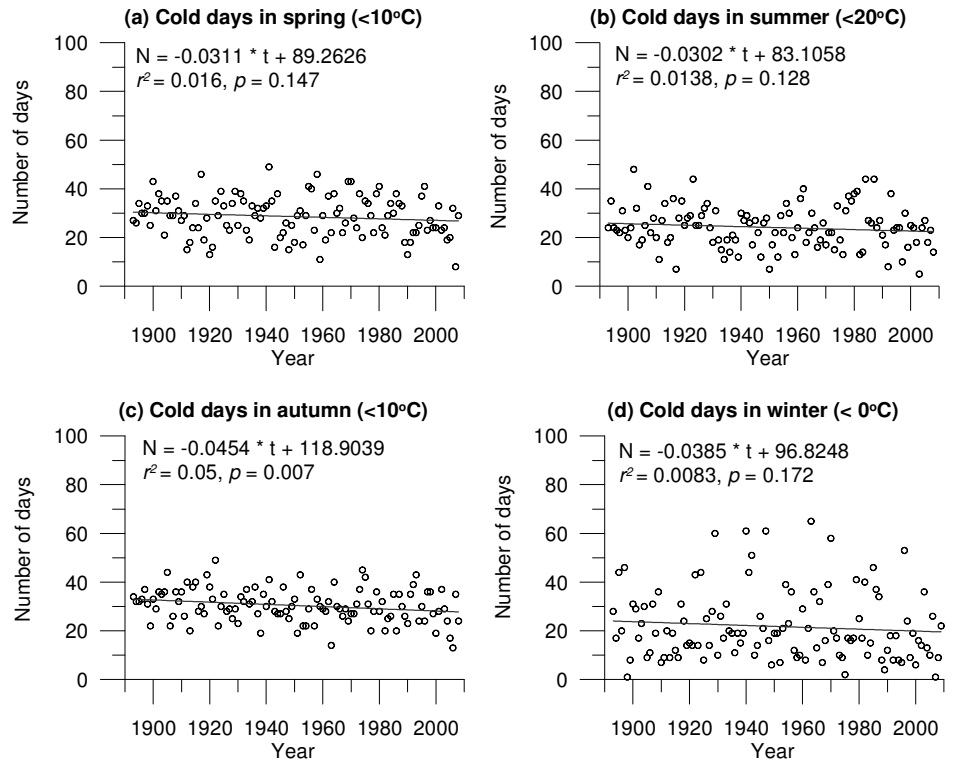

Figure 2-5: As Fig. 2-4, for cold days; (a) spring; (b) summer; (c) autumn; (d) winter.

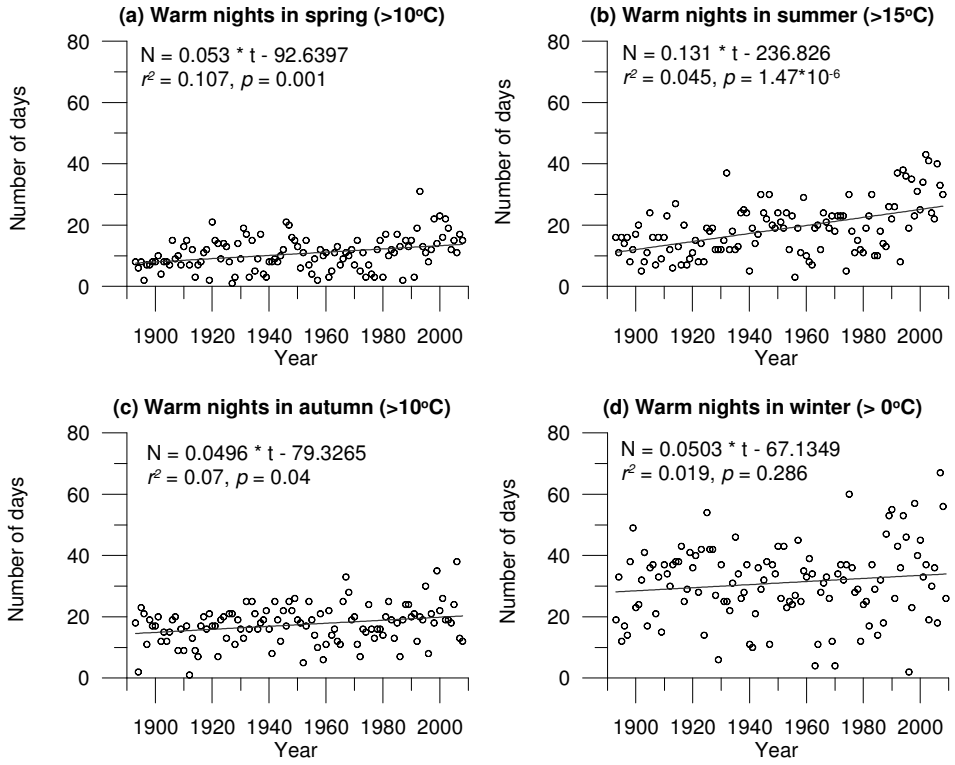

Figure 2-6: As Fig. 2-4, for warm nights; (a) spring; (b) summer; (c) autumn; (d) winter.

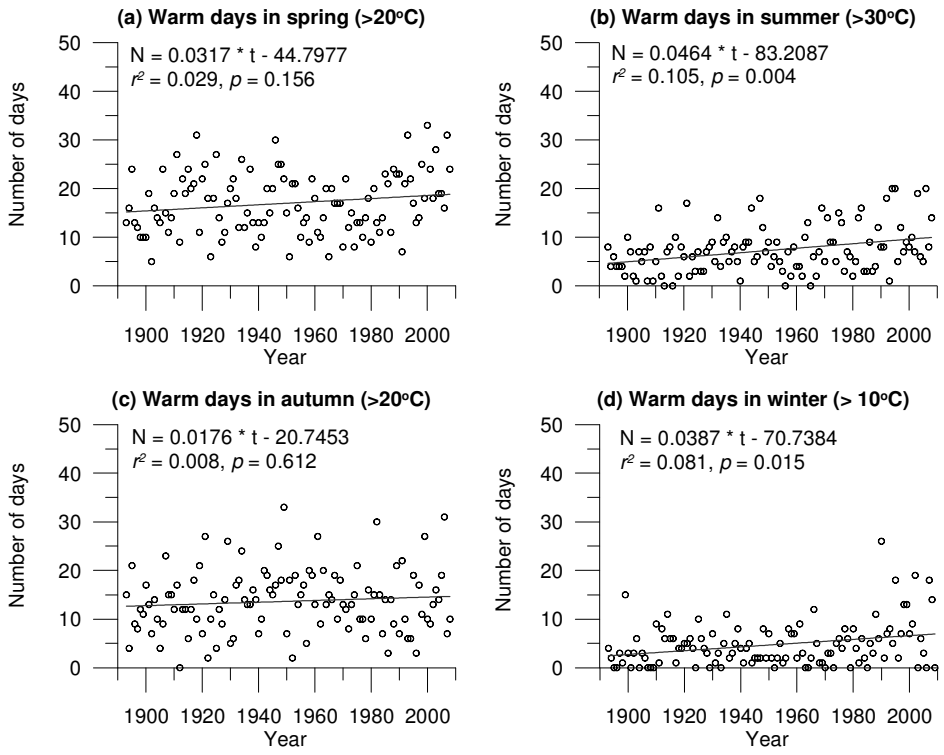

Figure 2-7: As Fig. 2-4, for; (a) warm spring days; (b) hot summer days; (c) warm autumn days; (d) warm winter days.

The warm-extreme indicators, such as the number of hot days (with maximum daily temperature exceeding 30°C) were found to increase. In agreement with the warming of winter temperatures, the cold-extreme indicators, such as the number of frost nights (assumed, for simplicity, to be equivalent to minimum daily temperature below 0°C) and of ice days (with maximum daily temperature below 0°C) have been decreasing. In 8 (out of 16) cases presented in **Figs 2-4** – **2-7**, changes are statistically significant, at either the 0.01 level or the 0.05 level. In five categories (hot summer days, cold summer nights, cold autumn days, warm summer and spring nights) that are significant at the of 0.01 level and in three categories (warm winter days, cold and warm autumn nights) at the 0.05 level. In the remaining eight categories (cold spring and winter nights, cold days in spring, summer, and winter, warm winter nights, and warm days in spring and autumn) changes are not statistically significant at 0.05 level. However, low correlation coefficient (r^2) and huge scatter illustrate strong random component (natural variability) of the data points in **Figs 2-4** – **2-7**. Seasonal values of temperature indices for a particular year may strongly depart from the mean long-term relation, such as linear regression. This is strongest in winter, and in particular for winter temperature minima, whose drop from the long-term trend in a single year can be very abrupt.

Frost in autumn occurred as early on 2 October (in 1957), while the last spring frost occurred as late on 20 May (in 1952). That is, based on the observations made so far, the absolute frost-free period extends from 21st May to 1st October (132 days). Frost has never been noted on the Potsdam Station in the months of June, July, August, and September. The first hot day, in absolute terms, *i.e.* a day with T_{max} in excess of 30°C, occurred as early on 22 April (31.8°C in 1968) and as late on 20 September (32.9°C in 1947). That is, in the light of the observations, over a couple of weeks, from 22 April (first hot day) until 20 May (last frost), air temperature in Potsdam may as well go down below 0°C (minimum) or rise above 30°C (maximum).

Indicators related to frost and hot days are also illustrated in **Fig. 2-8** – **2-10**. **Figure 2-8** presents the number of the last spring frost day (T_{min} < 0°C) and of the first autumn frost day. The regression slopes show that the last frost day has been occurring earlier than before in spring but the change is not statistically significant, while in autumn, frosts have been starting later (significance level 0.05). The increasing length of a frost-free interval also indicates a statistically significant (at 0.05 level) warming tendency (**Fig. 2-9**) – every decade the frost-free interval grows, on an average, of one day. However, in individual years, departures from the overall trends are very strong. For example, within the last 13 years (1996 – 2008) both the highest value of the annual number of frost days (133 days in 1996) and the lowest value (52 days in 2007) on record have been observed (Kundzewicz and Józefczyk, 2008).

Warming is also accompanied by the increasing tendency of the time span of occurrence of hot days (**Fig. 2-10**), but the changes are not statistically significant.

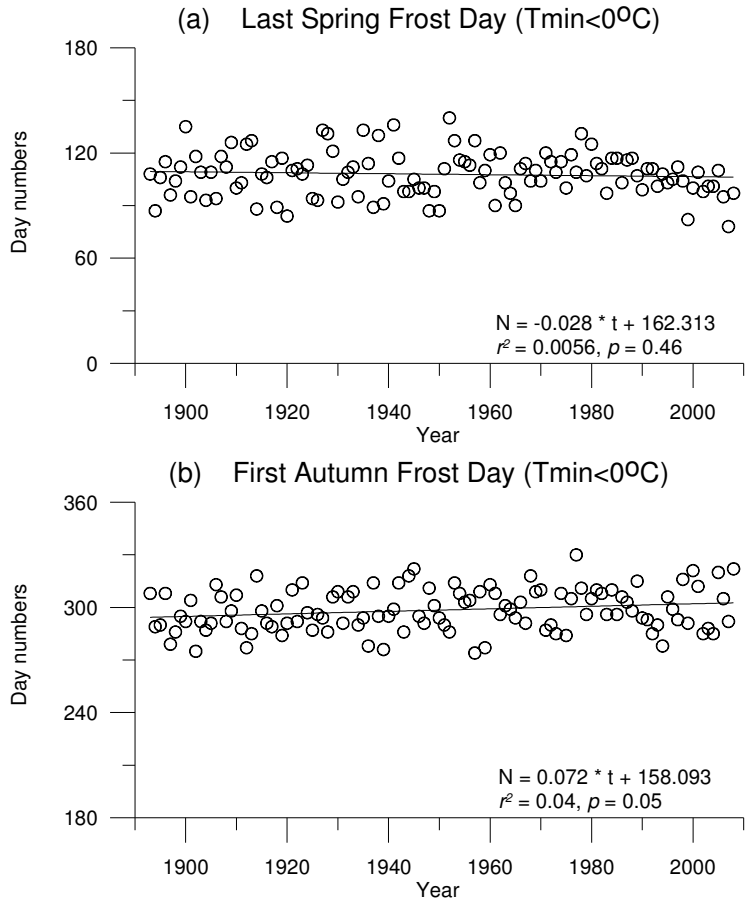

Figure 2-8: The number of the last spring frost day (T_{min} < 0°C) (a) and of the first autumn frost day (b) in individual years. New Year day is interpreted as day number 1.

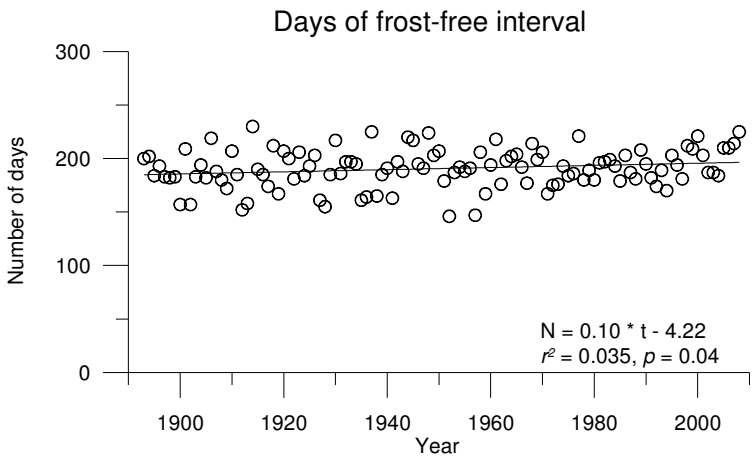

Figure 2-9: The number of days of a frost-free interval (for each year Last-Spring-Frost-Day-Number in Fig. 2-8 was subtracted from First-Autumn-Frost-Day-Number).

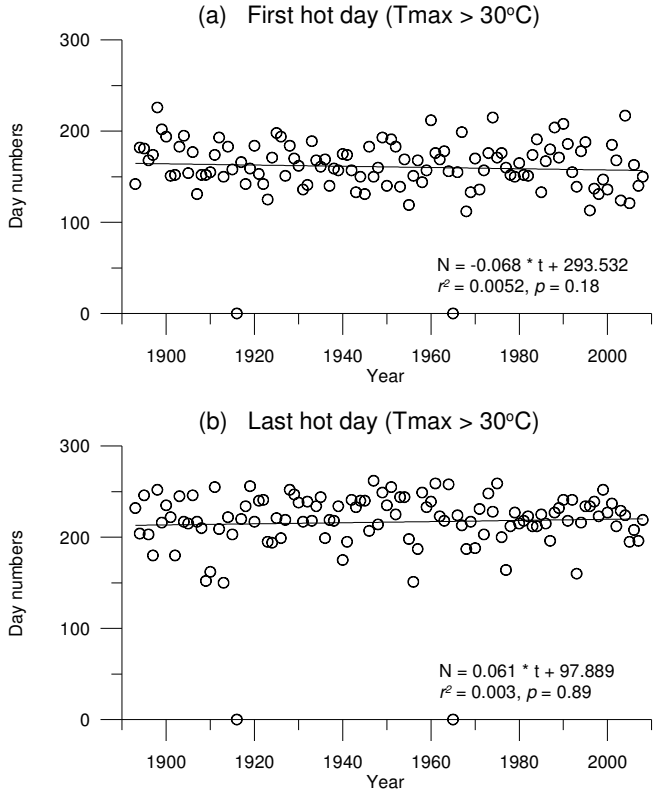

Figure 2-10: The number of the first hot day (T_{max} > 30°C) (a) and of the last hot day (b) for individual years. It should be noted that in two years, 1916 and 1965, there was not even a single day with maximum temperature above 30°C.

2.5. Interpretation of changes

This paper illustrates a high year-to-year variability of temperature indices, superimposed on a warming trend, based on an analysis of a long time series of high-quality records. One may try to explain the sources of the substantial warming in recent decades, and prior to this, the lack of warming, and even some cooling in the 1950s and 1960s. In IPCC parlance, one needs to address

a complex issue of change detection and attribution. Detection is a process of demonstrating that observed change is significantly different (in a statistical sense) from what can be explained by natural internal variability. Once a change is detected, attribution is a process of demonstration that:

- the detected change is consistent with a combination of external forcing including anthropogenic changes in the composition of the atmosphere and natural internal variability; and

- it is not consistent with alternative, physically-plausible explanations of recent climate change that exclude important elements of the given combination of forcings.

A formal process of detection and attribution cannot be carried out for records on a single station. However, the possible mechanisms of change could, and should, also be discussed.

The climate of our planet has been changing globally many times in the Earth's history – there have been many warmer and many colder intervals. Mechanisms of climate change can be divided into the following four groups: (i) changes in the solar activity (cf. sunspots number); (ii) changes in orbital parameters (in time scale of tens of millennia, irrelevant to the present climate change); (iii) changes in the composition of the Earth's atmosphere (greenhouse gases – water vapour, carbon dioxide, methane, and nitrous oxide; aerosols, dust); and (iv) changes in the properties of the Earth's surface (albedo, water storage). The first two mechanisms above are purely natural and mankind has no influence on them. The latter two mechanisms can be influenced by both natural and anthropogenic factors. The global increases of concentrations of greenhouse gases (IPCC, 2007), which are real and strong, are not sufficient to explain the details of the observed temperature change. The rapid temperature increase observed over Europe (and also at the Potsdam station) in the last three decades is considerably stronger than the mean global warming and the temperature rise expected from anthropogenic greenhouse gas increases. Variability of temperature indices can be partly explained by the oscillations in the system of ocean and atmosphere (notably North Atlantic Oscillations).

Several authors (*e.g.* Makowski *et al.*, 2008; Ruckstuhl *et al.*, 2008) found that the aerosol and cloud-induced radiative forcing could explain a portion of the recent changes in temperature indices in Europe.

Solar irradiance measurements on the Earth's surface illustrate considerable changes. An interval of global solar dimming and subsequently – an interval of global solar brightening (continuing to-date) have been noted that cannot be explained by variations of the Sun's activity. The explanation is sought in the changes of atmospheric transmittance due to increases and subsequent decreases in anthropogenic aerosol concentrations, cloud-mediated aerosol effects, and direct cloud effects. In Europe, sulphurous emissions have grown since the 1950s, then peaked in the early 1970s in Western Europe, and in the late 1980s and early 1990s in Eastern Europe, decreased since then. A reduction in anthropogenic aerosol concentrations in Western Europe, since the late 1970s and early 1980s resulted from considerable efforts undertaken in many countries to curb air pollutant emissions. The decrease in Eastern Europe can be partly associated with the economic collapse of the communist system, dominated by heavy industry, responsible for the high level of air pollution.

Aerosols affect atmospheric transmittance and hence temperature via the direct aerosol effect (scattering and absorption of sunlight by aerosol particles). There also exist, however, cloud-mediated indirect aerosol effects, such as the cloud albedo effect (enhancement of cloud albedo due to smaller droplets) or the cloud lifetime effect (extension of cloud lifetime due to smaller

droplets and less precipitation loss), cf. Ruckstuhl *et al.* (2008). Clouds simultaneously affect solar shortwave and thermal long wave radiation but with opposite sign. Hence, the total cloud effect is the sum of the negative shortwave cloud effect and the long wave cloud effect (in which water vapour functions as a greenhouse gas), that partly compensate each other.

The findings of this present paper, illustrated in **Fig. 2-3(a,b,c,d)**, show that maximum diurnal amplitude observed in Potsdam has decreased with time for all seasons, but only for summer and autumn are the changes statistically significant (at levels 0.05 and 0.01, respectively). However, there is a very strong variability around decreasing trends of seasonal maximum diurnal amplitude.

These findings can be indirectly compared to the results of Makowski *et al.* (2008), who investigated annual mean diurnal temperature range (DTR) for the period 1950 – 2005 for 23 different countries and regions in Europe as well as Europe as a whole. They demonstrated that the long-term trend of DTR has reversed from a decrease to an increase during the 1970s in Western Europe and during the 1980s in Eastern Europe. For the 16 out of 23 regions studied, as well as for the European mean, there was a statistically significant period of decrease and a subsequent increase in DTR. Of the remaining seven regions, two show a non-significant increase, three show a significant decrease and two reflect no significant trend (therein the eastern part of Germany, where Potsdam is located).

The diurnal temperature range is a suitable measure to investigate the counteracting effects of long wave and shortwave radiative forcing, because the diurnal minimum is closely related to the long wave radiative flux, while the diurnal maximum is predominantly determined by shortwave radiation. Makowski *et al.* (2008) find that the long-term trends in DTR are strongly affected by changes in incoming shortwave radiation (undergoing a dramatic change from dimming to brightening), presumably largely influenced by the direct and indirect effects of aerosol from SO_2 emissions.

2.6. Conclusion

Besides conducting the studies of change detection in mean temperature data, the research community has been carefully watching temperature extremes in different categories, such as maximum and minimum daily, monthly, seasonal, and annual temperatures. The present paper indicates that global and general findings of ubiquitous warming are in general agreement with temperature extremes in a specific, long-term, high-quality observation record. However, it shows that the natural variability at a single station is very strong and that extremes in a single year may largely differ from the dominating tendency. Absolute record values of maximum or minimum temperature do not necessarily match the trend present in the long-term time series. It can be clearly seen that high values of "warm" extremes (such temperature-related indicators as seasonal maximum and minimum temperatures, number of hot days) may have occurred for a long time in the remote past, when the level of warming (as indicated by the linear regression) was then much lower. Similarly, despite the warming, cold extremes may have occurred in recent decades, largely differing from the value corresponding to the decreasing tendency.

Hence, one has to be careful with the interpretation of warming. Rather than re-iterating the global warming statement with every exceptional warm spell and questioning it with every exceptional cold spell (*e.g.* January 2010), as often done in the media, one needs to take a more balanced view with consideration of old records and natural variability. Contrary to common interpretation, climate vagaries have always been strong. This should be remembered even if

there is a tendency for "cold" extremes to become less frequent and less severe and for "warm" extremes to become more frequent and more severe.

A formal process of change detection and attribution in temperature indices at the Potsdam station cannot be carried out. However, possible mechanisms of change were discussed, including the link between air pollution and warming. The analysis of data at a baseline station where long time series of records are available allowed the authors to contribute to a more general debate, in which the data series are typically much shorter and of lower quality.

Acknowledgements: The authors express their gratitude to Professor Peter Werner, for kind data support. The German Weather Service is commended for the continuation of observations at the baseline Potsdam station and for making data freely available on the web (online). The authors acknowledge the constructive remarks of three anonymous referees who made it possible to improve this contribution. Special thanks go to Professor Zbigniew Sorbjan, who proposed a constructive way of enriching the material.

Reference:

Brohan, P., J. J. Kennedy, I. Harris, S. F. B. Tett, and P. D. Jones (2006), Uncertainty estimates in regional and global observed temperature changes: a new dataset from 1850, *J. Geophys. Res.* **111**, 21.

IPCC (2007) *Climate Change 2007: The Physical Science Basis. Contribution of Working Group I to the Fourth Assessment Report of the Intergovernmental Panel on Climate Change*, Cambridge University Press, United Kingdom and New York, NY, USA.

Kundzewicz, Z. W., F. W. Gerstengarbe, H. Österle, P. Werner, and W. Fricke (2008), Recent anomalies of mean temperature of 12 consecutive months - Germany, Europe, Northern Hemisphere, *Theor. Appl. Climatol.* **95(3-4)**, 417-422.

Kundzewicz, Z. W., and D. Jozefczyk (2008), Temperature-related climate extremes in the Potsdam Observation Record, *Geografie (Prague)* **113(4)**, 372-382.

Kundzewicz, Z. W., D. Józefczyk , and H. Österle (2007), Warmest 12 consecutive months on record at the Potsdam meteorological station, Germany, *Weather* **62(10)**, 284-286.

Lehmann, A., and M. Kalb (1993), *100 Jahre meteorologische Beobachtungen an der Säkularstation Potsdam 1893-1992*, Selbsverlag des DeutschenWetterdienstes, Offenbach am Main.

Makowski, K., M. Wild, and A. Ohmura (2008), Diurnal temperature range over Europe between 1950 and 2005, Atmos, *Atmos. Chem. Phys. Discuss.* **8**, 7051-7084.

Ruckstuhl, C., R. Philipona, K. Behrens, M. Coen, B. Dürr, A. Heimo, C. Mätzler, S. Nyeki, A. Ohmura, L. Vuilleumier, M. Weller, C. Wehrli, and A. Zelenka (2008), Aerosol and cloud effects on solar brightening and the recent rapid warming, Geophys, *Geophys. Res. Lett.* **35(L12708)**, 6.

Trenberth, K. E., P. D. Jones, P. Ambenje, R. Bojariu, D. Easterling, A. Klein Tank, D. Parker, F. Rahimzadeh, J. Renwick, M. Rusticucci, B. Soden, and P. Zhai (2007), Observations: Surface and Atmospheric Climate Change. **In:** S. Solomon, D. Qin, M. Manning, Z. Chen, M. Marquis, K.B. Averyt, M. Tignor and H.L. Miller (eds.), *Climate Change 2007: The Physical Science Basis. Contribution of Working Group I to the Fourth Assessment Report of the Intergovernmental Panel on Climate Change*, Cambridge University Press, Cambridge, United Kingdom and New York, NY, USA.

Hydrological Processes 24: 3289-3306 (2010)

3. Simulation of spatiotemporal dynamics of water fluxes in Germany under climate change.

Shaochun Huang*, Valentina Krysanova, Hermann Österle and Fred F. Hattermann

Potsdam Institute for Climate Impact Research, P.O. Box 601203, Telegrafenberg, 14412 Potsdam, Germany
* Corresponding author. Tel.: +49 331 288 2406.
Email address: huang@pik-potsdam.de

Abstract
In most of Europe, an increase in average annual surface temperature of 0.8°C is observed, and a further increase is projected. Precipitation tends to increase in northern Europe and decrease in southern Europe, with variable trends in Central Europe. The climate scenarios for Germany suggest an increase in precipitation in Western Germany and a decrease in Eastern Germany, and a shift of precipitation from summer to winter. When investigating the effects of climate change, impacts on water resources are among the main concerns. In this study the first German-wide impact assessment of water fluxes dynamics under climate change is presented in a spatially and temporally distributed manner using the state-of-the-art regional climate model STAR and the semi-distributed process-based eco-hydrological model SWIM. All large river basins in Germany (lower Rhine, upper Danube, Elbe, Weser and Ems) are included. A special focus of the study was on data availability, homogeneity of data sets, related uncertainty propagation in the model results, and scenario-related uncertainty. After the model calibration and validation (efficiency from 0.6 to 0.9 in 80% of cases) the water flow components were simulated at the hydrotope level, and the spatial distributions compared with those in the Hydrological Atlas of Germany. The actual evapotransipration is likely to increase in most parts of Germany, while total runoff generation may decrease in south and east regions. The results for the second scenario period 2051 – 2060 show that water discharge in all six rivers would be 8% – 30% lower in summer and autumn compared to the reference period, and the strongest decline is expected for the Saale, Danube and Neckar. Higher winter flow is expected in all of these rivers, and the increase is most significant for the Ems (about 18%). However, the uncertainty of impacts, especially in winter and for extreme events, remains high.

Keywords: water fluxes, water discharge, statistical downscaling model STAR, eco-hydrological model SWIM, climate change impact, Germany

3.1. Introduction

The Fourth Assessment Report (AR4) of the International Panel for Climate Change (IPCC, 2007) summarized the knowledge of climate trends in the 20th century. In most of Europe, an increase in average annual surface temperature is observed (0.8°C over the continent on average), with stronger warming in winter than in summer. The precipitation tended to increase in northern Europe (10 to 40%) and decrease in southern Europe (up to 20% in some parts). Other wide ranging impacts have been documented as well, such as retreating glaciers, longer growing season, shifts of species distribution patterns, and impacts on human health.

Located in the central Europe, Germany has already been affected by climate change. According to Schönwiese *et al.* (2006), the annual average temperature has increased by ca. 1°C between 1901 and 2000, and the winter months became especially warmer. The winters of 1980s and 1990s were observed as the warmest in Germany during the 20th century (Schönwiese *et al.*, 2006). In 1901 – 2000, annual precipitation in Germany exhibited a moderate increase (9%), and winter precipitation showed a higher increasing trend (19%), while summer precipitation did not change significantly (Schönwiese *et al.*, 2006). The recent development of annual precipitation in Germany shows a distinct spatial pattern: an increasing trend in the western part and reductions over large areas in eastern and south-eastern areas (Menzel *et al.*, 2006). Increasing flood trends are found in the most parts of Germany during 1951 – 2002 (Petrow and Merz, 2009), with more significant changes in winter than in summer. Beside floods, other extreme events are also observed recently. For example, the extremely hot summer of 2003 in Germany is characterized by a return period of about 455 years (Schönwiese *et al.*, 2004).

Under the changing climate, it is necessary and important to study the impacts on water resources, as the water cycle in river basins is sensitive to changes in climate characteristics. The water balance components, such as evapotranspiration, runoff and groundwater recharge, which determine river discharge and the availability of water resources, will be inevitably affected. Generally, more evapotranspiration can be expected due to the increased temperature. However, the actual evapotranspiration is constrained by the actual water availability in soil, and higher temperature could result in lower actual evapotranspiration if water availability is low. The changes in river discharge are determined by changes in precipitation and temperature and the regional environmental settings, such as land use. Groundwater recharge reacts very sensitively to even small changes in precipitation and temperature, especially in lowland regions (Hattermann *et al.*, 2004). Rising temperature will result in a longer vegetation growth period and higher potential evapotranspiration. As a result, lower groundwater recharge could be expected as a consequence. In addition, the early coming of spring in the future will shorten the groundwater recharge period in winter.

Any changes in water balance components will influence the availability of regional water resources and impact economic sectors, such as water management, agriculture, forestry, tourism, hydropower production and river transport, as well as nature conservation and health. For example, drier summer could lead to water deficit in agriculture, and increase in annual river transportation costs. More money may be needed for increasing the design discharge and water level for river safety (Middelkoop and Kwadijk, 2001).

In order to indentify and investigate the effects of climate change on the water cycle, ecosystems and human being, and then to develop coping strategies for the future, numerous studies focused on the influence of climate change on water resources have been carried out around the world. The common approach is to use hydrological models driven by the projected climate scenarios for

the future. Many of these studies applied conceptual precipitation-runoff models with simple water balance components (*e.g.* Menzel & Bürger; 2002, Thodsen, 2007; Albek *et al.*, 2004; Arnell, 2003; Drogue *et al.*, 2004), and process-based hydrological models (Muttiah and Wurbs, 2002; Krysanova *et al.*, 2005; Hattermann *et al.*, 2008) at the catchment scale.

In Germany, several projects have been launched at the catchment level aiming to develop strategies that can be applied in the future to reduce the vulnerability or adapt to climate change. The projects GLOWA-Elbe (http://www.glowa-elbe.de) and GLOWA-Danube (http://www.glowa-danube.de) are two examples of comprehensive research on climate change impacts in the Elbe and Danube river basins. Several papers were published focusing on the impacts of climate change on water fluxes in different river basins of Germany (*e.g.* Hennegriff *et al.*, 2008; Mauser & Bach, 2009; Menzel & Bürger, 2002; Krysanova *et al.*, 2005). However, these catchment-scale projects do not provide an overview of the climate impacts on the water sector for the whole Germany.

The country-wide climate impact assessment using a process-based hydrological model is a challenge. It is important because it has a potential to support an overall decision making at the country scale and climate change adaptation strategies in different sub-regions, such as continental, maritime and alpine climate regions.

In this study, the main objectives were 1) to evaluate changes in the seasonal dynamics of water fluxes, and 2) to assess spatial changes in water balance components under climate change for the whole territory of Germany. The statistical regional climate downscaling model STAR (STAtistical Regional model) (Orlowsky *et al.*, 2008) was applied in the study to produce climate change scenarios, because it has better reproduction of the historical climate conditions and hence more reliable scenarios than other regional climate models (Gerstengarbe *et al.*, 2009). Besides, STAR generates multiple realizations for each scenario condition, which allows producing more robust and reliable results accounting for the inherent uncertainty of the climate scenario. The eco-hydrological process-based model SWIM (Soil and Water Integrated Model) (Krysanova *et al.*, 1998) was applied sequentially for the five river basins (Ems, Weser, Elbe, upper Danube and lower Rhine) to simulate water flow dynamics and the water flow components. An important advantage of SWIM is that the model integrates hydrological cycle with vegetation processes and takes into account interactions between water fluxes and ecosystems. Besides, it allows changing seasonal timing of plant growth stages under warmer conditions. Therefore it represents a more reliable tool for climate impact assessment compared to the pure hydrological models.

Application of a process-based river basin model for such a large regional scale as Germany is a novelty and a challenge, because the data availability and heterogeneous data sets (especially in the transboundary rivers as the Elbe, upper Danube and lower Rhine), create problems and require non-standard solutions. Hence, the experience of a large-scale model application and the problems in simulating the international river basins are presented here additionally.

3.2. Study area

Germany is located in Central Europe, bordering the North Sea and Baltic Sea, with the total area of 357,021 km^2. Generally, the German territory is divided geographically into the North German Lowlands, the Central German Upland, the Southwest German Central Upland Scarps embracing the upper Rhine River Valley, the Alpine Foreland and the German Alps (see **Fig. 3-1(a)**). From the Northwest to the East and Southeast, the maritime climate gradually changes into a more continental climate. The country's average annual temperature is about +9 °C, and the prevailing winds are westerly. The precipitation occurs in all seasons, with substantial regional differences.

In the North German Lowlands, annual rainfall varies between less than 500 (continental) to about 700 mm (maritime). The Upland mountainous areas receive from about 700 to more than 1500 mm of precipitation per year, and the Alps more than 2000 mm per year (Statistisches Bundesamt Deutschland, 2008).

The German territory is comprised of five large river basins (the Elbe, upper Danube, Rhine, Weser and Ems), three medium-scale basins in the coastal area (Elder, Schlei/Trave and Warnow/Peene), and small parts of the Oder and Maas basins (see **Fig. 3-1(b)**). Only the Weser basin lies entirely within the national German territory. The Rhine, upper Danube and Elbe drainage basins have large parts outside Germany.

In our study the five main river basins covering the territory of Germany (the Danube, Elbe, Ems, Rhine, and Weser) were selected as the major study areas for the assessment of climate change impacts. The characteristics of these five basins are listed in **Table 3-1**. Altogether, they cover about 90% of the whole German territory.

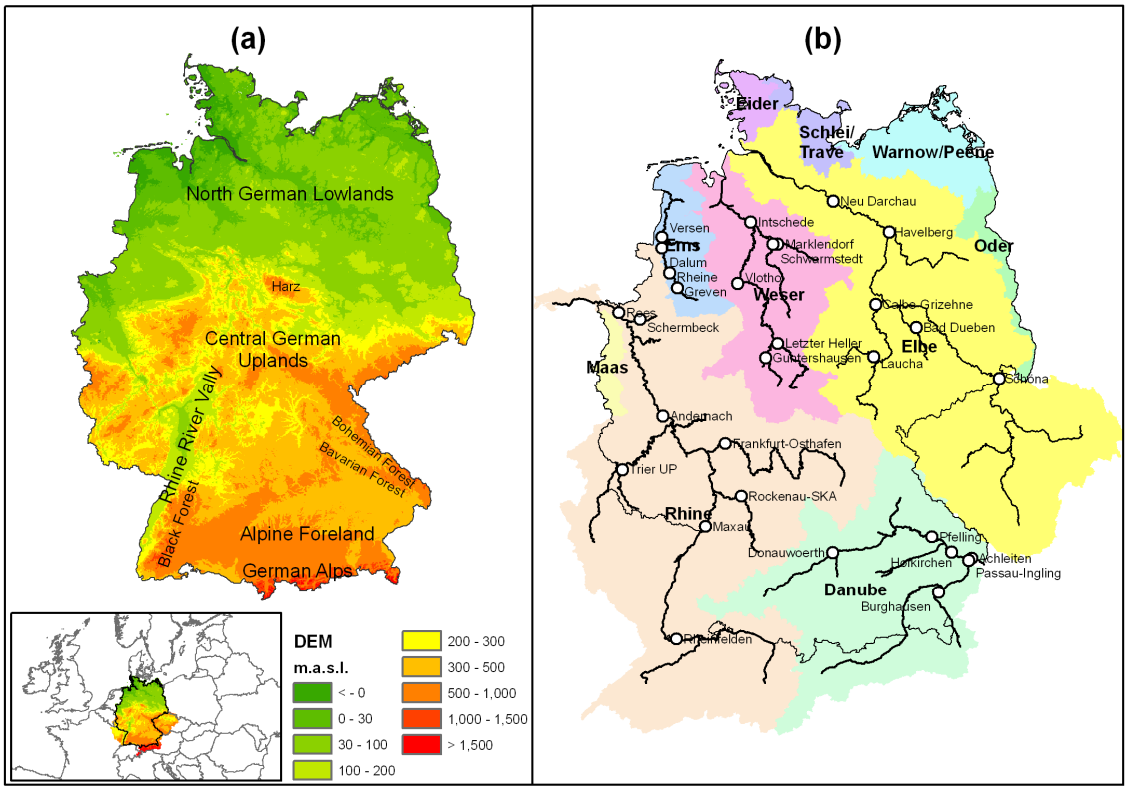

Figure 3-1: Digital Elevation Map of Germany and German sub-regions (a), and the studied river basins with locations of the gauge stations used for the model calibration and validation (b).

The smallest river basin Ems (**Fig. 3-1**) is located in the northwest of Germany and northeast of Netherland. Only the German part of the Ems basin was included in this study. The entire basin has low relief terrain and the river flows through the North German Lowlands to the North Sea. This basin belongs to one of the most intensively used agricultural regions in Europe. Arable land covers approximately 66% of the area. The other major land covers are forest (10%) and grassland (15%).

Table 3-1: Characteristics of five river basins chosen as case study areas.

River basin	Studied drainage area (km^2)	Large tributaries in Germany	First gauge on the border as input data	Other main countries included	Land use shares			Number of climate stations	
					Crop-land	Forest	Grass-land	In Germany	Outside Germany
Ems	13 000	Hase	-	no	66%	10%	15%	63	-
Weser	45 725	Werra, Fulda, Aller, Leine	-	no	49%	30%	14%	309	-
Danube	77 107	Inn, Naab, Isar, Salzach	-	Austria, Switzerland	32%	37%	20%	482	10*
Rhine	123 175	Neckar, Main, Moselle	Rheinfelden	France, Luxemburg, Belgium	40%	38%	12%	844	14*
Elbe	147 423	Havel, Saale, Schwarze Elster, Mulde	-	Czech Republic	51%	30%	10%	399	48

* These climate data were from the "Daily high-resoluation gridded climate data set for Europe"

The Weser basin (**Fig. 3-1**) is located in the north-western Germany. The Weser River is the longest solely national river in Germany. Formed by the rivers Fulda and Werra, it flows through the North German Lowlands, and reaches the North Sea. About half of the drainage basin area is used as arable land, 30% is covered by forest, and 14% by grassland.

The Elbe River (**Fig. 3-1**) originates in the Czech Republic, drains across east-northern Germany and flows into the North Sea. About two thirds of the whole Elbe drainage basin (approximately 100 000 km^2) are located in Germany, one third in the Czech Republic, and the negligible parts belong to Austria and Poland. The Elbe basin is also an intensive agricultural region with about 50% of the total area used as arable land. About 30% of the drainage area is under forest, and only 10% under grassland.

The total Rhine River basin (**Fig. 3-1**) is distributed in nine countries. Beginning in the Swiss Alps, the Rhine River flows through Germany to the Netherlands. The basin includes small parts located in France, Austria, Italy, Liechtenstein, Luxembourg and Belgium. The rivers Main, Neckar and Moselle are the three main tributaries in Germany, and the Moselle receives drainage also from France, Luxembourg and Belgium. Two thirds of the Rhine drainage basin area is situated in Germany, and the Alpine countries, of which Switzerland is the largest, form about 20% of the drainage area. The arable land (40%) and forest (38%) are the two major land cover types in the German part of the Rhine basin.

The upper part of the Danube basin upstream the gauge Achleiten (see **Fig. 3-1(b)**) is formed by Brigach and Breg rivers located in south-west Germany, and several tributaries from the Alps and the Bavarian forest. The main tributary Inn flows from the Swiss Alps through Austria to Germany and receives a large amount of cold melting water from snow and glaciers. About 73% of the drainage area above the gauge Achleiten is located within the German territory. The main land cover types in this basin are forest (37%) and arable land (32%). The upper Danube has the highest grassland cover (20%) compared to other basins.

In order to assess changes in river discharge and water flow components under climate changes scenario, hydrological processes for the whole river basins need to be simulated, and the calibration and validation should be performed first. Therefore, the model setup should include

the German areas and, in several cases, parts of other countries as well. In our study three of the five large basins: German part of the Ems, the Elbe and Weser were simulated fully. Only the upper part of the Danube, namely, the area upstream of the last gauge in Germany Achleiten (**Fig. 3-1(b)**), was considered in the study. Due to lack of land use data from Switzerland, the simulation for the Rhine basin could only be performed for the area downstream of the gauge Rheinfelden located at the Swiss-German border until the last gauge in Germany, Rees (**Fig. 3-1(b)**). For the Rheinfelden discharge data from Switzerland were used as input. The water components were also calculated for the coastal area and German parts of the Oder and Mass basins using the parameterization of the neighboring large basins.

3.3. Materials and methods

3.3.1. STAR

For projections of future changes in water flows for the whole of Germany, robust regional climate change scenarios should be applied. As the General Circulation Models (GCMs) cannot provide climate information with sufficient spatial resolution for regional studies due to their coarse horizontal resolution, several regional climate models (RCM) were developed in the recent years in Germany. There are so-called "dynamical downscaling models", such as REMO (Jacob, 2001) and CCLM (Böhm *et al.*, 2008). Besides, there are also other approaches, such as a combination of a statistical with an analogous downscaling approach, WettReg (Enke & Spekat, 1997), and a statistical downscaling technique, STAR (Orlowsky *et al.*, 2008).

Gerstengarbe *et al.* (2009) compared these four models for the historical period evaluating the agreement between the simulated and observed values. The evaluation results show that each model has its strengths and weaknesses. The dynamical models REMO and CCLM generate largest deviations between the observed and simulated precipitation. Reproduction of precipitation is a common problem of all RCMs, partly caused by their relatively low resolution and partly by their inherent difficulties to reproduce precipitation dynamics. There are also significant problems to reproduce trends with the models REMO, CCLM and WettReg. In contrast, the simulated outputs from the model STAR have better agreement with the observed statistics, especially for temperature and air pressure. The trends of climate variables are well reproduced by STAR and the characteristics of events are closer to the reality.

The model STAR has also some weaknesses. For example, STAR fully relies on the historical climate data and uses them for resampling, and it is principally not able to reproduce extreme events (*e.g.* heavy precipitation) exceeding the already observed values. So, all the projected extreme events will not exceed the extreme events observed in the past. The second weakness of STAR is that this statistical model relies on large amount of observed historical data. Hence, it cannot be applied in the poor-data regions.

Currently, the climate scenarios generated by STAR are only available for the German territory due to lack or non-availability of good historical data for other neighbouring countries. So, taking into account the main focus of this study and the characteristics of different climate models, the climate scenario produced by the statistical downscaling model STAR was applied for the assessment. In the future, other downscaling methods will also be used for cross-comparison and extreme events analysis.

Compared to other RCMs, which can project 100-years or longer climate scenarios for Germany, STAR was developed for the medium-term (about 50 – 60 years) regional climate projections due to its statistical analogue resampling technique. Analogue approaches such as STAR assume that

observations of a given day from the training period can occur again or in a similar way during the future period. Hence, simulated series are constructed by resampling from segments of observation series, consisting of daily observations. Generating a future series can thus be seen as defining a date-to-date-mapping, by which each date of the future period is assigned a date and the concurrent meteorological observations of the training period. No trend elimination or any other modification is applied to the observational data prior to resampling. The advantage of such resampling is that physical consistency of both the spatial fields and the simultaneous combinations of different weather parameters is guaranteed. The STAR resamples in blocks of 12-days, which ensures the projected future time-series with realistic persistence features.

One of the most important properties of STAR is that the produced climate time series are forced only by the linear temperature trend of the future period. Once the daily mean values of a long-term observed time series are obtained, it is possible to impose the assumed trend onto the series and to create the simulated series complying with this trend. The scenario of future climate conditions used in this study was constructed by using the trend of temperature derived from climate change scenario A1B produced by GCM ECHAM 5 (Roeckner *et al.*, 2003). It was used to generate the corresponding modified temperature series. The time series of other climate variables, such as precipitation, radiation, humidity, *etc*. were generated by using the values recorded on the same day as the temperature measurement. Therefore, the method maintains the stability of the main statistical characteristics (variability, frequency distribution, annual cycle and persistence). For the spatially differentiated projections, climatological sub-regions are identified (*e.g.* by meteorological stations), and an individual temperature trend is prescribed for each sub-region, representing spatial patterns of future climate parameters.

In addition, STAR is much faster in computation time than the dynamical climate models, so it is able to generate multiple climate projections by implementing a random process (Monte Carlo simulation). Therefore, an ensemble of 100 realizations of the climate change scenario was generated and applied in this study. This allows evaluating uncertainty of climate change impact related to the climate scenario.

3.3.2. SWIM

The dynamic process-based eco-hydrological model SWIM (Soil and Water Integrated Model) (Krysanova *et al.*, 1998) was developed for climate and land use change impact assessment on the basis of the models SWAT (Arnold *et al*., 1993) and MATSALU (Krysanova *et al.*, 1989).

SWIM simulates hydrological cycle, vegetation growth and nutrient cycling with the daily time step by disaggregating a river basin to sub-basins and hydrotopes. The hydrotopes are sets of elementary units in a subbasin with homogeneous soil and land use types. Up to ten vertical soil layers can be considered for hydrotopes. It is assumed that a hydrotope behaves uniformly regarding hydrological processes and nutrient cycling. The spatial disaggregation scheme in the model is flexible. In the regional studies climate zones, grid cells of a certain size or other areal units can be used for disaggregating a region instead of sub-basins.

Water flows, nutrient cycling and plant growth are calculated for every hydrotope. Then lateral fluxes of water and nutrients to the river network are simulated taking retention into account. After reaching the river system, water and nutrients are routed along the river network to the outlet of the simulated basin.

The simulated hydrological system consists of four control volumes: the soil surface, the root zone of soil, the shallow aquifer, and the deep aquifer. The soil root zone is subdivided into

several layers in accordance with the soil database. The water balance for the soil surface and soil column includes precipitation, surface runoff, evapotranspiration, subsurface runoff, and percolation. The water balance for the shallow aquifer includes groundwater recharge, capillary rise to the soil profile, lateral flow, and percolation to the deep aquifer.

Surface runoff is estimated as a non-linear function of precipitation and a retention coefficient, which depends on soil water content, land use and soil type (modification of the Soil Conservation Service curve number method, Arnold *et al.*, 1990). Lateral subsurface flow (or interflow) is calculated simultaneously with percolation. It appears when the storage in any soil layer exceeds field capacity after percolation and is especially important for soils having impermeable or less permeable layer(s) below several permeable ones. Potential evapotranspiration is estimated using the method of Priestley-Taylor (Priestley & Taylor, 1972), though the method of Penman-Monteith (Monteith, 1965) can also be used. Actual evaporation from soil and actual transpiration by plants are calculated separately.

The module representing crops and natural vegetation is an important interface between hydrology and nutrients. A simplified EPIC approach (Williams *et al.*, 1984) is included in SWIM for simulating arable crops (like wheat, barley, rye, maize, potatoes) and aggregated vegetation types (like pasture, evergreen forest, mixed forest), using specific parameter values for each crop/vegetation type. A number of plant-related parameters are specified for 74 crop/vegetation types in the database attached to the model. Vegetation in the model affects the hydrological cycle by the cover-specific retention coefficient, impacting surface runoff, and influencing the amount of transpiration, which is simulated as a function of potential evapotranspiration and leaf area index (LAI).

Interception of photosynthetic active radiation (PAR) is estimated as a function of solar radiation and leaf area index. The potential increase in biomass is the product of absorbed PAR and a specific plant parameter for converting energy into biomass. The potential biomass is adjusted daily if one of the four plant stress factors (water, temperature, nitrogen, N, and phosphorus, P) is less than 1.0, using the product of a minimum stress factor and the potential biomass. The water stress factor is defined as the ratio of actual to potential plant transpiration. The temperature stress factor is computed as a function of daily average, optimal and base temperatures for plant growth. The N and P stress factors are based on the ratio of accumulated N and P to the optimal values. The leaf area index is simulated as a function of a heat unit index (ranging from 0 at planting to 1 at physiological maturity) and biomass.

SWIM allows application of the complicated crop rotation schemes including several crops like wheat, barley, rye, maize, potatoes, etc., which could be made specific for different subregions or federal states, and differentiated for soil types. However, in this study a more robust though realistic enough crop rotation was applied, as the main aim was to assess the impact of climate change. In the reference (current) conditions winter crop like winter wheat or winter barley (dominant crops in Germany) is planted and harvested according to the current practice schedule. There is usually a cover crop growing between the harvest and next planting of winter crop. In warmer (scenario) conditions, the scheduling of agriculture crops is governed by harvest index, so the rotation scheme can be changed when the winter crop is harvested earlier than in the current condition. In this case, SWIM would allow earlier growth of cover crop right after the harvest of winter crop and let it grow until the next winter crop planting date.

3.3.3. Data preparation

To derive the sub-basin and hydrotope structure and the routing structure of the five basins, four spatial maps: the digital elevation model (DEM), the soil map, the land use map, and the sub-basin map were stored in a grid format with 250 m resolution. This resolution was proved to provide reliable results in previous studies for large river basins (Hattermann *et al.*, 2007a).

The DEM was provided by the NASA (National Aeronautics and Space Administration) Shuttle Radar Topographic Mission (SRTM).

The soil map of the study area was merged from the general soil map of the Federal Republic of Germany "BÜK 1000" produced by the Federal Institute for Geosciences and Natural Resources (BGR), soil map of the Czech Republic (Kosková *et al.*, 2007), and soil map from the European soil database (European Communities - DG Joint Research Centre). The data quality and their resolution were different, which could be reflected in the modelling results.

The standard sub-basin map for Germany from the Federal Environment Agency (Umweltbundesamt), and the sub-basin map for the Czech Republic (T.G.M. Water Research Institute) were available. On the basis of the DEM and the stream network, an average drainage area of 100 km^2 was chosen as a threshold to discretize the areas in the Danube and Rhine basins outside Germany into subbasins, because the standard sub-basin map for Germany had approximately the same discretization.

The land use map was obtained from the CORINE 2000 land cover data set of the European Environment Agency. Nine land cover types were considered in the study: water, urban areas, cropland, grassland, forest coniferous, forest deciduous, forest mixed, wetland, and bare soil. No changes in land use patterns were assumed for the reference and scenario periods in this study, and land use was considered to be "static". This was done on purpose, in order to investigate the "pure" impact of climate change on water fluxes, without influence of changing land use patterns.

For the subbasins in Germany and Czech Republic, climate data (temperature, precipitation, solar radiation and air humidity) were interpolated to the centroids of every sub-basin by the inverse distance method using data from 2342 climate and precipitation stations (see **Fig. 3-2**). However, climate stations with available climate data in the Czech Republic were much sparser than that in Germany.

For other areas in the five considered river basins, which are located outside of Germany (France, Austria, Luxemburg, see **Fig. 3-2**), the available observed climate data were even more poor: sparsely located virtual gridded "stations" with daily temperature and precipitation data only. So, the daily temperature and precipitation data from the "Daily high-resolution gridded climate data set for Europe" (www.ensembles-eu.org) were applied in this study for areas outside Germany and Czech Republic, and other needed climate parameters required for SWIM (solar radiation and air humidity) were interpolated using the records from the closest German climate stations. The inverse distance method was used for the interpolation. Obviously, such interpolation is very uncertain and can produce large errors in the climate input data generated for France, Austria and Luxemburg, which will definitely propagate in the modeling results.

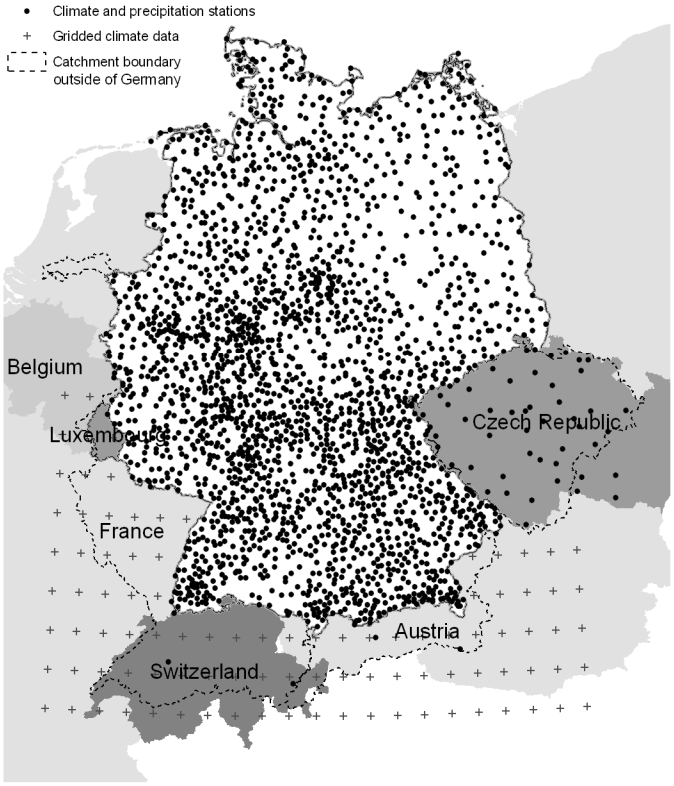

Figure 3-2: **Location of the climate and precipitation stations in Germany and Czech Republic (black), and the gridded climate data (grey cross) which were available for the study.**

In general, the problems with climate data for areas outside Germany could be solved. Necessary data of observation were not available for this study, but most probably they exist and could become available for impact assessments at the scale of international river basins in the future.

As the land use map for Switzerland is not included in the CORINE data base, and no observed climate data were available for Switzerland, the modelling setup for the Swiss part was restrained, and therefore the upper Rhine (upstream of the gauge Rheinfelden) had to be excluded from the simulation.

The climate scenario produced by STAR was available only for the meteorological stations in Germany (due to lack of historical data with similar density and completeness outside of Germany). Hence, the simulation of climate change impacts on water dynamics in the scenario periods was only possible for the German territory. Therefore, water flow components such as runoff, evapotranspiration and groundwater recharge were analyzed for the whole German territory, whereas river discharge for three largest basins: the Elbe, Rhine and Danube was analyzed in the reference and scenario periods for the selected representative gauges, whose catchments are located fully in Germany. Namely, climate change scenarios in the Elbe were analyzed for the Saale sub-basin (one of the largest and most important sub-basins in the German part of the Elbe basin), the Rhine basin was represented by the Main and Neckar subbasins, and the Danube basin was represented by the intermediate gauge Hofkirchen, whose drainage area is located mostly in Germany.

In summary, a good data base including all necessary data for modeling with SWIM and scenario analysis is available for Germany, but the data availability outside of Germany is problematic. Some of the essential data were not available so far for the international river basins, such as observed climate data and land use map for Switzerland. For some other input data the full data set was not homogeneous in terms of data quality. For example, the soil map for Germany has finer classification for soil types than that from the European data base, and the German soil parameterization is differentiated by climate zones and land use types for each soil type, whereas the European soil data is not. The gridded climate data for river basin areas in France, Austria and Luxemburg are much sparser and less complete than that in Germany. This of course will have implications on the simulation results, especially for the transboundary river basins with heterogeneous data sets. The quality of data input will directly influence the simulation results, and lead to difficulties in performing a sound evaluation of the model outputs. In our study this problem was solved by providing a part of results for the total German territory, and restricting the study area by the solely national large representative subbasins for the climate impact assessment.

3.3.4. Model calibration and validation procedure

The calibration procedure was carried out for five main discharge gauges (see **Table 3-2**) for each of the five river basins in the period from 1981 to 1990. The parameter estimation routine PEST (Doherty, 2004) was applied to calibrate the simulated discharge. The simulation period was then extended to twenty years from 1961 to 1980 to validate the simulation results at the same five gauges. In addition, 24 intermediate gauges (see **Table 3-2** and **Fig. 3-1(b)**) at the main tributaries and the main rivers (mostly with the drainage areas larger than 5 000 km^2), for which the model was not calibrated, were included in the validation procedure in order to verify the spatial performance of SWIM for the period 1981 – 1990. After calibration and validation, the whole simulation period 1961 – 1990 was considered as the reference, and the model outputs in the reference period were compared with those in two scenario periods: 2009 – 2018 and 2051 – 2060.

For the basins Ems, Weser and Elbe, where the rivers flow into the North Sea, the gauges Versen, Intschede and Neu-Darchau (see location at **Fig. 3-1(b)**) were used for the calibration, because these are the last gauges not influenced by the tidal effect.

For the Danube basin, the gauge Hofkirchen was selected as the calibration gauge, instead of the last discharge gauge Achleiten, because about 96% of the catchment of the former is located in Germany, whereas that of the latter includes also a large part of Austrian territory with quite poor available climate data (see explanation in Section 3.3). By that, the error caused by the poor climate data from Austria could be minimized.

For the Rhine basin, the gauge Frankfurt-Osthafen located at the Main River, which is one of largest tributaries of the Rhine and lies completely in Germany, was used for the calibration and validation, and the further scenario analysis. However, in the validation procedure the last gauge on the Rhine in Germany, Rees, was also included. Since the discharge at the gauge Rees could not be correctly simulated without reasonable input from Rheinfelden (border between Switzerland and Germany, **Fig. 3-1**), the observed discharge data at the Rheinfelden were used as the inflow to the River Rhine in the validation period.

Table 3-2: The gauge stations in the five river basins used for calibration and validation, and their corresponding drainage areas. (The water discharge data is from GRDC (The Global Runoff Data Centre), 56068 Koblenz, Germany, and the Ministry of the Environment and Conservation, Agriculture and Consumer Protection of the German State of North Rhine-Westphalia).

River basin	Last gauge (used for calibration and validation)	Drainage area (km^2)	Intermediate gauge (used for validation)	River	Drainage area (km^2)
			Greven	Ems	2 842
			Rheine	Ems	3 740
Ems	Versen	8 369	Dalum	Ems	4 981
			Letzter Heller	Werra	5 487
			Guntershausen	Fulda	6 366
			Schwarmstedt	Leine	6 443
			Marklendorf	Aller	7 209
Weser	Intschede	37 720	Vlotho	Weser	17 618
			Burghausen	Salzach, Inn	6 649
			Donauwoerth	Danube	15 037
			Passau Ingling	Inn	26 084
			Pfelling	Danube	37 687
Danube	Hofkirchen	47 496	Achleiten	Danube	76 653
			Schermbeck	Lippe	4 783
			Rockenau SKA	Neckar	12 710
			Trier UP	Moselle	23 857
			Maxau	Rhine	50 196
	Frankfurt-Osthafen		Andernach	Rhine	139 549
Rhine	(Main)	24 764	Rees	Rhine	159 300
			Bad Dueben	Mulde	6 171
			Laucha	Unstrut	6 218
			Calbe-Grizehne	Saale	23 719
			Havelberg	Havel	24 037
Elbe	Neu-Darchau	131 950	Schöna	Elbe	51 391

As the last step in the simulations, the coastal areas and the small areas in the Maas and Oder basins were simulated with the parameter sets from the nearest large basins, the Rhine and the Elbe. The results for water flow components in the reference and scenario periods were used to complete the water components maps for the whole Germany.

No changes in land use patterns were assumed for the calibration and validation periods. In reality, land use in Germany was definitely changing during 30 years, and taking into account land use patterns averaged at least for 3 decades could improve the results. However, such data are not available for Germany, and the validation had to be done with the "static" land use data.

In this study the non-dimensional efficiency criterion of Nash and Sutcliffe (1970) (NSE) and the relative deviation in water balance (DB) were used to evaluate the quality of simulated daily water discharge. NSE is a measure to describe the squared differences between the observed and simulated values using the following equation:

$$NSE = 1 - \frac{\sum(Q_{obs} - Q_{sim})^2}{\sum(Q_{obs} - \overline{Q}_{obs})^2} \qquad (3\text{-}1)$$

DB describes the long-term differences of the observed values against the simulated ones in percent for the whole modelling period:

$$DB = \frac{\overline{Q}_{sim} - \overline{Q}_{obs}}{\overline{Q}_{obs}} * 100 \qquad (3\text{-}2)$$

Here Qobs means the observed discharges while Qsim is the corresponding simulated value. The variables $\overline{Q}_{obs}$ and $\overline{Q}_{sim}$ are the mean values of these parameters for the whole simulation period.

The Nash and Sutcliffe efficiency can vary from minus infinity to 1. A value of 1 denotes an absolute match of predicted and measured values, while value 0 for the deviation in balance means no difference between the measured and simulated values.

3.4. Results and discussion

3.4.1. Calibration and validation

The calibration and validation results in terms of criteria of fit are presented in **Table 3-3**. In the calibration period, the NSE varies from 0.80 to 0.90 for the five main gauges (Versen, Intschede, Neu-Darchau, Frankfurt-Osthafen and Hofkirchen) and the deviation in water balance is not higher than 3%. In the validation period (20 years), the Nash-Sutcliffe efficiency and the deviation for these five gauges are within the ranges from 0.81 to 0.85 and from -8% to 6%, correspondingly. These results indicate that SWIM can reproduce water discharge in large river basins quite well.

Besides, **Table 3-3** includes the NSE and deviations in water balance for the 24 additional intermediate gauges. In general, the discharge at the most of these gauges can also be well reproduced by SWIM with the efficiency above 0.6 and deviation within ±10%, even without additional calibration. There are only a few problematic gauges whose simulated results do not comply with the observed values well enough, *e.g.* Trier UP, Havelberg and Schöna. This is mainly due to two reasons: poorer input data, or water regulation or management which was not considered in the simulation.

The discharge simulated for the gauge Havelberg at the river Havel in the Elbe basin is much lower than the measurements. The underestimation of the river discharge is mainly due to the mining activities in the catchment, especially during the 1970s and 1980s. In conjunction with the mining activities, large amounts of water were extracted from underground and discharged into the rivers causing higher than natural water level in the Havel, which cannot be reproduced by the model.

The gauges such as Trier UP, Schöna, Passau Ingling and Burghausen, which include drainage areas outside of Germany, do not show satisfactory results either. The poor results at these gauges reflect the data problems mentioned before: poor available climate data outside of Germany and heterogeneous soil data sets. As such problems could not be avoided in this study, the main focus of the climate scenario evaluation was restricted to the river discharge of several national subbasins and country-wide water components.

Table 3-3: The Nash and Sutcliffe efficiencies and deviations in water balance for the five main gauges in the calibration (1981 – 1990) and validation (1961 – 1980) periods, as well as for 24 selected intermediate gauges in the simulation period 1981 – 1990 (considered as spatial validation).

			Calibration		Validation	
Gauge	Drainage area (km^2)	% of drainage area inside Germany	Nash & Sutcliffe efficiency	Deviation in water balance	Nash & Sutcliffe efficiency	Deviation in water balance
Versen	8 369	100%	0.87	0%	0.85	-8%
Greven	2 842	100%	-	-	0.87	4%
Rheine	3 740	100%	-	-	0.78	1%
Dalum	4 981	100%	-	-	0.83	3%
Intschede	37 720	100%	0.90	0%	0.82	-2%
Letzter Heller	5 487	100%	-	-	0.71	4%
Guntershausen	6 366	100%	-	-	0.57	5%
Schwarmstedt	6 443	100%	-	-	0.68	-3%
Marklendorf	7 209	100%	-	-	0.76	9%
Vlotho	17 618	100%	-	-	0.86	0%
Hofkirchen	47 496	94%	0.83	0%	0.82	-5%
Burghausen	6 649	17%	-	-	0.56	-3%
Donauwoerth	15 037	100%	-	-	0.75	-2%
Passau Ingling	26 084	26%	-	-	0.61	12%
Pfelling	37 687	95%	-	-	0.79	1%
Achleiten	76 653	73%	-	-	0.74	6%
Frankfurt-Osthafen	24 764	100%	0.80	3%	0.81	6%
Schermbeck	4 783	100%	-	-	0.78	-5%
Rockenau SKA	12 710	100%	-	-	0.75	-8%
Trier UP	23 857	22%	-	-	0.21	57%
Maxau	50 196	23%	-	-	0.84	-4%
Andernach	139 549	59%	-	-	0.81	5%
Rees	159 300	64%	-	-	0.83	6%
Neu-Darchau	131 950	61%	0.86	2%	0.84	-3%
Bad Dueben	6 171	91%	-	-	0.59	-2%
Laucha	6 218	100%	-	-	0.60	-13%
Calbe-Grizehne	23 719	99%	-	-	0.74	-1%
Havelberg	24 037	100%	-	-	0.43	-31%
Schöna	51 391	0%	-	-	0.60	30%

Figure 3-3 shows the comparison between the simulated and observed river discharge at two selected gauges Intschede (Weser) and Hofkirchen (Danube) as the daily time series in the period 1984 – 1989 (**Fig. 3-3**, left), and as average daily dynamics for the whole calibration period 1981 – 1990 (**Fig. 3-3**, right). As one can see, in both cases the simulated river discharge is in a satisfactory agreement with the observed one, and the seasonal dynamics is also well reproduced.

The hydrograph pattern at the gauge Intschede (**Fig. 3-3(a)**, right) is very typical for the most parts of Germany. As precipitation is not concentrated in a "rainy season", but is distributed in all four seasons (though not evenly), there are usually higher water flows in winter due to low evapotranspiration, whereas in summer the abundant vegetation and high temperature lead to high water losses to atmosphere via evapotranspiration and lower runoff. In comparison with that, the seasonal water flow pattern at the gauge Hofkirchen (see **Fig. 3-3(b)**, right) is different, with relatively high water flows in early summer. The snow melting from the Alps contributes to additional water peaks in this period. The satisfactory reproduction of both patterns by SWIM confirms the model suitability for large regions with different hydrological conditions.

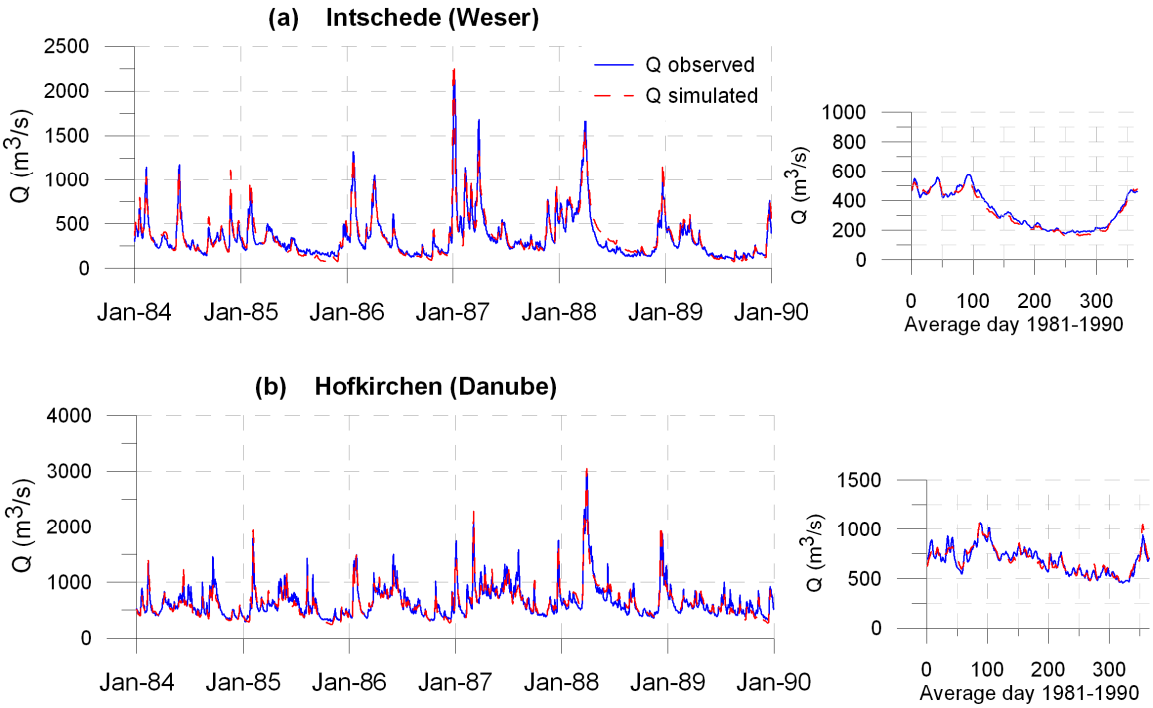

Figure 3-3: Simulated and observed water discharge (left) at the gauges Intschede (Weser) (a) and Hofkirchen (Danube) (b) in the period 1984 – 1989, and the corresponding average daily discharge (right) for the same stations for the whole calibration period (1981 – 1990).

3.4.2. Comparison of spatial patterns

The annual average evapotranspiration, total runoff (a sum of surface runoff, interflow and groundwater flow), and groundwater recharge simulated by SWIM for the reference period (1961 – 1990) were compared with those estimated for the same time period and presented in the Hydrological Atlas of Germany (HAD, 2000). Obviously, no comparison to real measurements is possible at this scale. The mean annual actual evapotranspiration depth presented in the Atlas was calculated based on the grass reference evapotranspiration (Wendling, 1995) and the BAGLUVA method developed by Glugla *et al.* (2002). The runoff map in the Atlas was obtained from the simple water balance subtracting estimated actual evapotranspiration from precipitation. The groundwater recharge was estimated from a regression model using an empirical equation of Kille (1970) to determine the base flow index (a measure of the ratio of base flow to the total runoff). In contrast to SWIM, estimates for three water flow components for the Atlas were not balanced at the catchment scale.

The spatial patterns of the water flow components simulated by SWIM (**Fig. 3-4(a, b, c)**) and estimated for the Hydrological Atlas (**Fig. 3-4(d, e, and f)**) are similar, especially for the total runoff and groundwater recharge. The maps demonstrate substantial regional differences in all three water flow components in Germany. In most of the central and northern German areas evapotranspiration is ranging from 400 mm to 600 mm, and it is lower than in the Black Forests, Rhine Valley, and in the Alpine areas (> 600 mm). The higher temperature in summer, higher precipitation in mountainous areas, and high density of forests are the main drivers of the higher evapotranspiration in southern Germany.

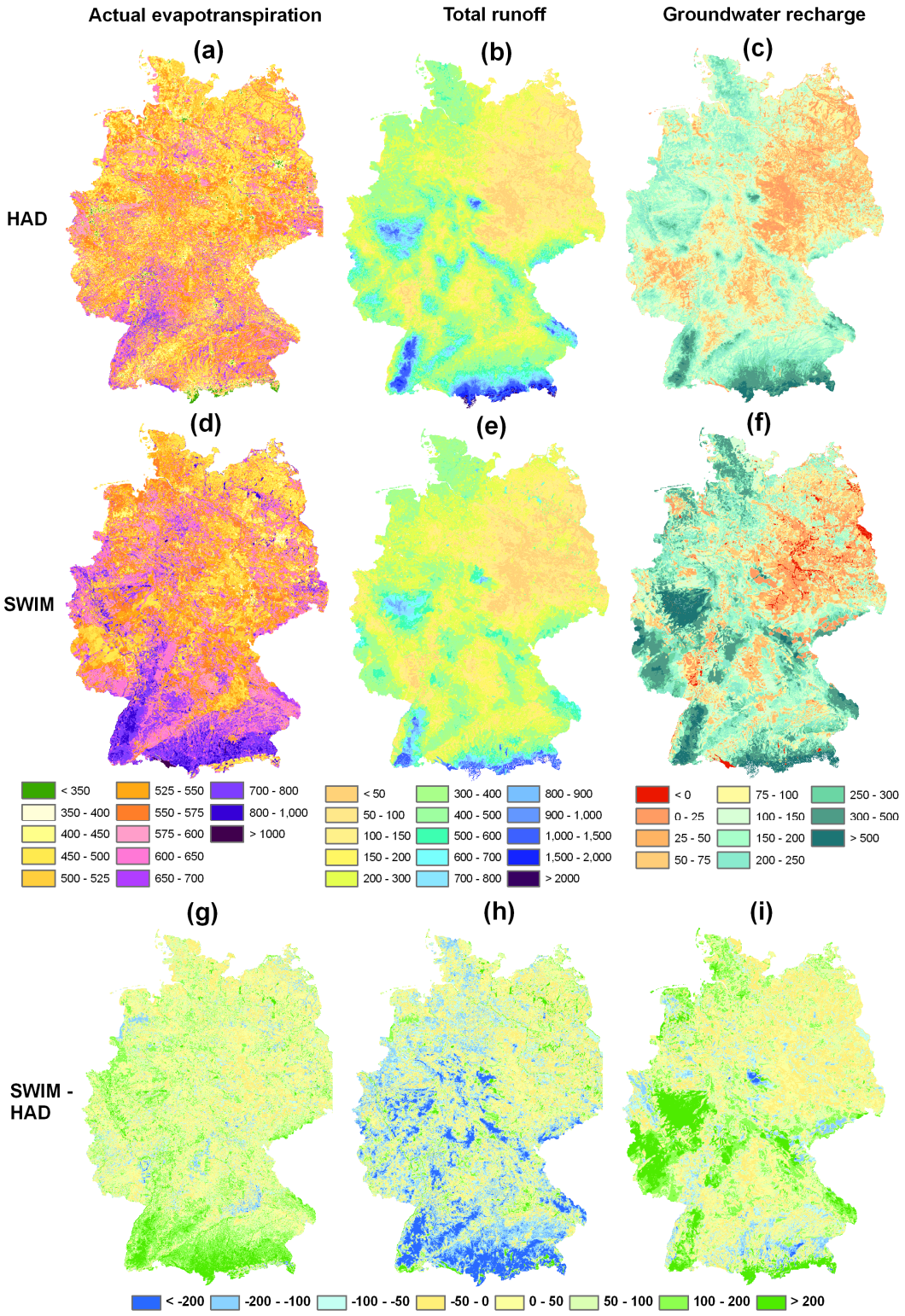

Figure 3-4: The annual average water flow components in the period 1961 – 1990 estimated for the Hydrological Atlas of Germany (a – c), simulated by SWIM for the same period (d – f), and the difference maps (SWIM - HAD) (g – i). Maps for actual evapotranspiration: (a), (d), (g), total runoff: (b), (e), (h), and groundwater recharge: (c), (f), (i) (units: mm/year).

The distribution pattern of total runoff is closely related to the geographic characteristics. The Black Forest region, the Alpine Foreland and the mountainous areas with high reliefs (as compared with the DEM map) produce larger amounts of total runoff (> 700 mm). The Elbe, the Warnow/Peene and the Oder basins have the lowest runoff production (about 178 mm, 150 mm and 90 mm on average, respectively) among all the basins mainly due to the smallest amount of precipitation.

The patterns of annual average groundwater recharge are affected by the amount of seepage water and soil properties. Apart from the similarity of positive groundwater recharge distribution, the negative groundwater recharge was also simulated in SWIM in the wetland areas and riparian zones, where groundwater is shallow and plants can satisfy their water needs also from water flowing from upper parts of the catchments into wetland areas. As a result, the total plant water uptake from groundwater in spring and summer can be higher than the amount of groundwater recharge for the same plot during the winter season, and the net groundwater recharge is negative.

In addition, **Fig. 3-4(g, h, i)** shows the difference in the absolute values between the Atlas and SWIM simulation results. The yellow color shows the difference less than ±50 mm. The dark blue and dark green highlight the hotspots of major differences. In southern and in some locations in western Germany, the evapotranspiration simulated by SWIM is up to over 200 mm higher than that in the Atlas, and the total runoff in these regions is correspondingly lower. The highest difference in groundwater recharge is in western Germany, where consolidated rocks impede the seepage water to reach groundwater (Bogena *et al.*, 2005) (feature not represented in SWIM).

Table 3-4: Comparison of the annual average precipitation and water flow components (evapotranspiration, total runoff, and groundwater recharge) simulated by SWIM in the reference period 1961 – 1990 with those estimated for the Hydrological Atlas of Germany (HAD, 2000), and the measured runoff.

	Precipitation (mm/year)		Evapotranspiration (mm/year)		Runoff (mm/year)			Groundwater recharge (mm/year)	
Catchment	HAD[1]	SWIM	HAD[1]	SWIM	HAD[1]	SWIM	Measured	HAD[1]	SWIM
Ems (Versen)	842	845	521	547	321	298	307	152	163
Weser (Intschede)	832	831	530	568	302	263	277	125	157
Danube (Hofkirchen)	1025	1052	535	633	490	419	436	201	263
Main (Frankfurt-Osthafen)	851	844	552	588	299	256	243	107	158
Saale (Calbe-Grizehne)	687	691	516	526	171	165	167	67	86

[1] HAD: Hydrological Atlas of Germany

Table 3-4 allows further comparison of average annual water components from both methods (and also with the actual measured runoff depth) in the five main basins under study. The precipitation depths used in SWIM have no more than 3% deviation to these in the Atlas, as the input data for both methods is from the same data bank (DWD, National Meteorological Service of Germany). The deviation of 1-3% could be due to different interpolation methods and precipitation correction functions. The actual evapotranspiration and groundwater recharge simulated by SWIM are higher than those estimated for the Atlas, and the difference between them is especially substantial in the upper Danube basin. In contrast, the total runoff obtained from SWIM simulation is lower than that in the Atlas, but the SWIM results are closer to the measured water discharge values (see columns 6 and 7 in **Table 3-4**) as they were validated for the large catchments.

In general, the comparison of spatial patterns of water flow components simulated by SWIM with that in the Hydrological Atlas of Germany shows a good agreement. The runoff data has also a

good agreement with the measured values. The results presented in Sections 4.4.1 and 4.4.2 confirm that the model SWIM is appropriate for conducting climate impact assessment for Germany, and evaluating changes in spatial variability of water components.

3.4.3. Climate scenarios

Firstly, the average annual precipitation and temperature for the scenario period 2051 – 2060 were calculated from one selected realization which stands for the medium climatic-water balance condition (Wechsung, *et al.*, 2008) of the 100 realizations generated by STAR, and compared with those for the reference period 1961 – 1990 estimated from the observed records for the whole Germany (see **Fig. 3-5**). The annual precipitation is expected to decrease in eastern and southeastern Germany significantly, while in the northwestern and western Germany an increase in precipitation is prevailed. The annual temperature is expected to rise by 2 to more than 3 °C in the country. The central range and the Harz region will retain a cooler climate as compared to other parts of Germany. According to the scenario, in the southern areas climate change will manifest in particular by a substantial increase in temperature. Hence, it is an important hotspot to analyze the impact on water resources.

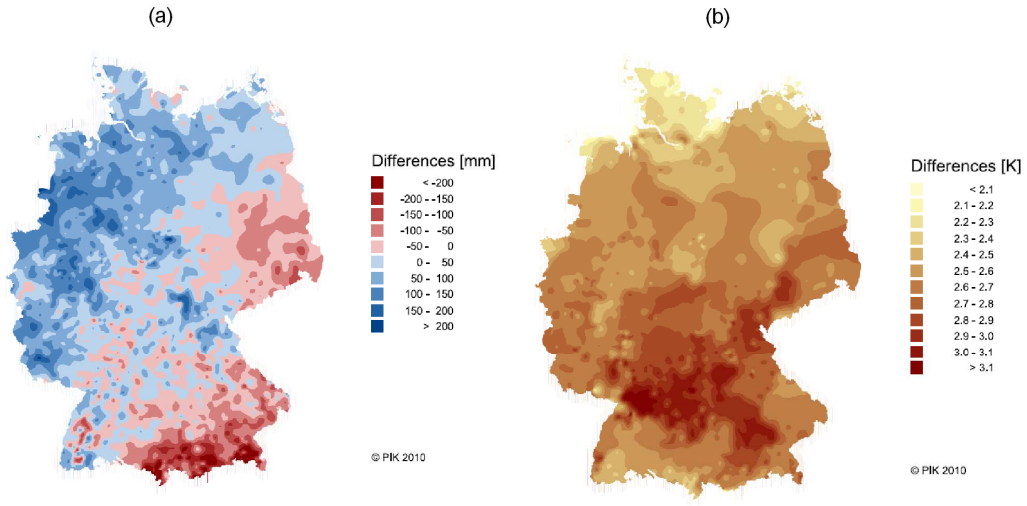

Figure 3-5: Changes in annual precipitation (a) and average annual temperature (b) in Germany in the period 2051 – 2060 (projected by STAR, medium realization) compared to 1961 – 1990 (observed). (Source: National Meteorological Service of Germany; Potsdam Institute for Climate Impact Research (PIK), base scenarios, 2010)

To demonstrate the performance of STAR in different climate regions, **Figure 3-6** shows the observed and projected annual dynamics of precipitation, and differences in average monthly values of precipitation between the generated by STAR and observed in the reference period for the basins Ems (**Fig. 3-6(a)**), Saale (**Fig. 3-6(b)**) and the upper Danube (**Fig. 3-6(c)**). These three basins belong to different climatic zones: a maritime climate (Ems), a drier and more continental climate (Saale), and an Alpine climate (upper Danube). The annual precipitation observed and simulated by STAR and averaged over the basins is shown in **Fig. 3-6** (left). The grey and dark grey boundaries include the simulated precipitation from 100 and 80 realizations, and represent the uncertainty of precipitation projections. The dashed line represents the medium realization of the 100 in terms of precipitation amount. It shows that STAR is able to project the annual variability reasonably. In addition, there are slight downward trends in the Saale and Danube

basins. In **Fig. 3-6** (right), the seasonal changes in precipitation are presented. For all the three rivers, an increase in winter precipitation (strongest for the Ems) and decrease in summer precipitation (strongest for the Danube) are projected.

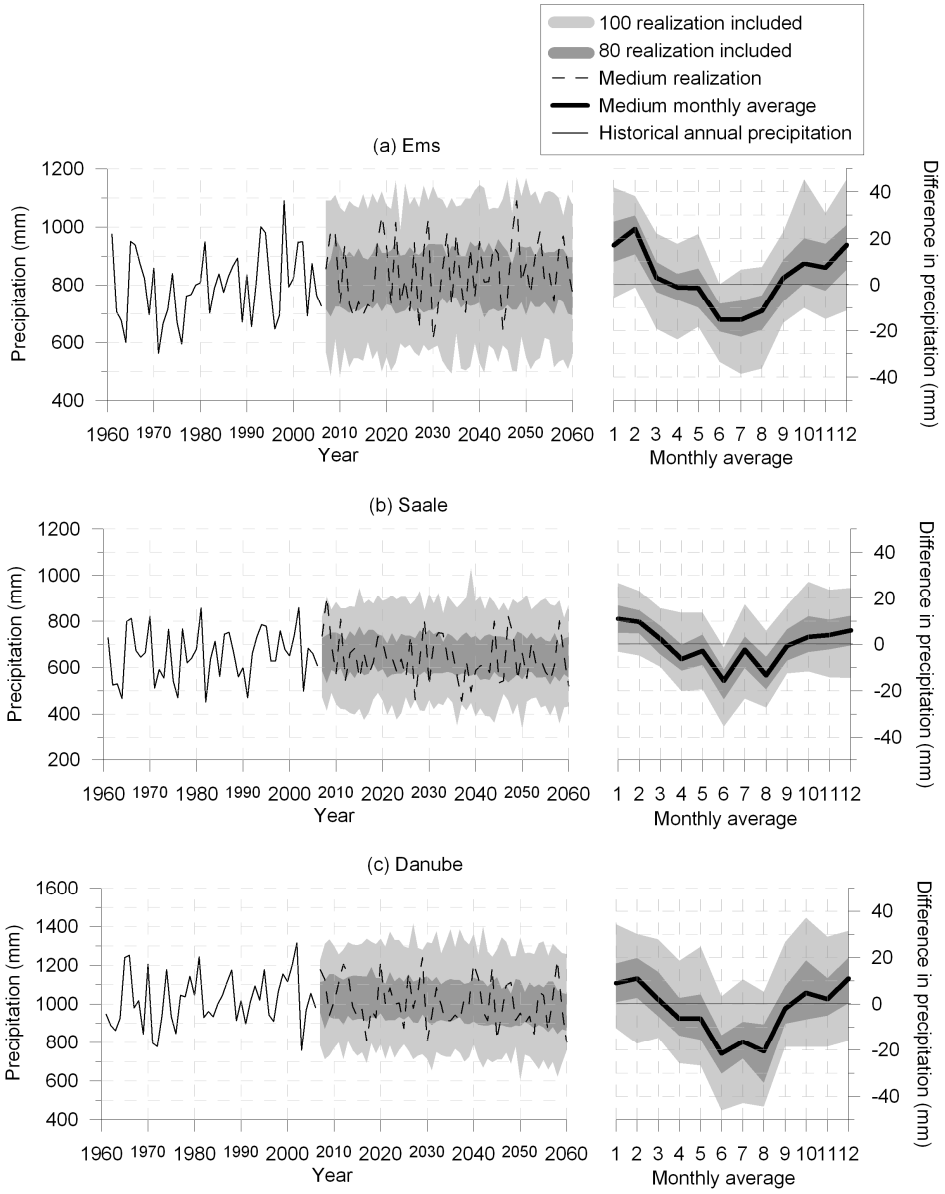

Figure 3-6: Observed annual precipitation (1961 – 2006) and generated by STAR annual precipitation (2007 – 2060) in the Ems (a), Saale (b) and the upper Danube (c) basins (left); and the difference in monthly average precipitation between the projected realizations (2051 – 2060) and the historical data (1961 – 1990) for the same basins (right).

3.4.3.1. Climate impacts on seasonal river discharge

Climate change impact on river discharge was analyzed for the gauge stations: Versen (Ems), Intschede (Weser), Calbe-Grizehne (Saale), Hofkirchen (Danube), Frankfurt-Osthafen (Main), and Rockenau SKA (Neckar), as described above in the data preparation section. Two scenario periods were evaluated: 10 years from 2009 to 2018 (to test reliability of the hydrological

response using the STAR realizations), and the last 10 years (from 2051 to 2060) as the main scenario period to evaluate the climate impacts on water resources.

Figure 3-7 shows the simulated average seasonal water discharge in two scenario periods together with the simulated average seasonal water discharge for the reference period 1961 – 1990 for six selected gauges. The light grey bounds include all simulated results from 100 realizations, and the dark grey bounds cover the 80 percentile of 100 runs. The dashed line is the medium average daily discharge simulated with the 100 realizations. And the solid lines represent the average daily water discharge during the reference period. The upper graph of each sub-figure shows changes in the next ten years (2009 – 2018), and the lower graphs show changes in the mid of the century 2051 – 2060.

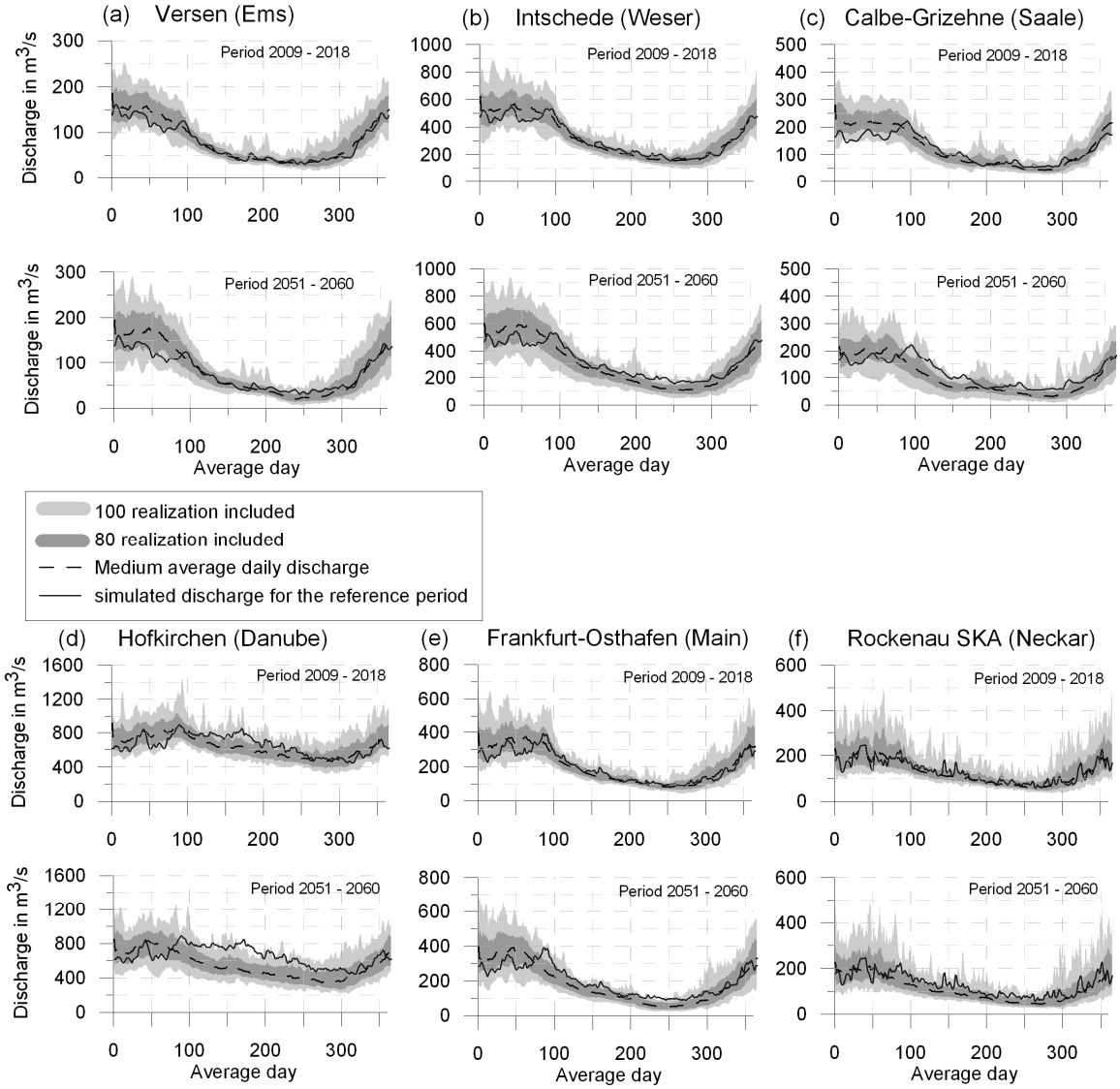

Figure 3-7: Seasonal water discharge in two scenario periods (2009 – 2018 and 2051 – 2060) including 80 and 100 realization and the medium of 100 realizations compared to the simulated discharge for the reference period 1961 – 1990 for six basins: a) the Ems basin (gauge Versen); b) the Weser basin (gauge Intschede); c) the Saale basin (gauge Calbe-Grizehne); d) the Danube (gauge Hofkirchen); e) the Main basin (gauge Frankfurt-Osthafen) and f) the Neckar basin (gauge Rockenau SKA).

In all six cases in **Fig. 3-7** the water discharge simulated in the first scenario period 2009 – 2018 has a similar seasonal dynamics compared to the observed one; only in winter water discharge is higher practically in all basins. Since the climate is changing gradually, the hydrological dynamics is not likely to vary suddenly and significantly in a short term. In the second scenario period (2051 – 2060) the changes in seasonal water discharge become obvious and differentiated among the basins and seasons, and some of them are considerably strong. In the winter time of the second scenario period river discharge is likely to increase in all rivers, especially in the Ems and Weser. A robust trend seems to be that the recession of the winter flow starts earlier in spring and lasts longer into late summer. In summer and autumn all the rivers tend to have lower water discharge, especially from July to September. The main reasons are higher evapotranspiration due to higher temperature, and lower or practically the same precipitation in summer. The earlier harvest of winter crops and the following faster growth of cover crop aggravate the loss of soil water and decrease of runoff in these months. Among the six river basins, water discharge decreases in summer most dramatically in the Danube, Saale and Neckar basins (see **Table 3-5**), where almost all 100 scenario realizations show a lower level. It is also worth mentioning that in all rivers except the Danube the water discharge in summer is already very low in the current condition, and the projected river flow in the Saale in 2051 – 2060 approaches zero in autumn.

Table 3-5: Changes in seasonal river dynamics for the six rivers (medium average daily discharge simulated in the scenario period minus average daily discharge in the reference period and devide the reference daily discharge).

Catchment	Winter (Dec. - Feb.)	Spring (Mar. - May)	Summer (Jun. - Aug.)	Autumn (Sep. - Nov.)
Ems (Versen)	17.9%	11.3%	-8.2%	-8.2%
Weser (Intschede)	13.1%	-0.8%	-19.1%	-17.4%
Danube (Hofkirchen)	12.9%	-8.4%	-24.1%	-17.7%
Main (Frankfurt-Osthafen)	15.7%	-8.0%	-14.7%	-19.0%
Neckar (Rockenau SKA)	5.3%	-14.9%	-22.1%	-19.7%
Saale (Calbe-Grizehne)	13.1%	-15.5%	-24.4%	-30.1%

This means an increased risk for hydropower plants, navigation and water availability for cooling of thermal power plants. The increasing risk of low flow conditions in Germany simulated by STAR and SWIM also complies with the results of other climate impact studies. For example, Hennegriff *et al.* (2008) forecasted the impact of climate change on low water conditions in the German state Baden-Württemberg, where the river Neckar, a part of the Rhine and headwater of the Danube are located. They argued that in the months July to September, the monthly average low flow may decrease by 10% to 20% in the Neckar and Danube in the period 2021 to 2050 compared to the reference period 1971 to 2000. Another climate impact study for the Danube basin (Mauser *et al.*, 2008) has shown that the annual low flow (minimum 7-days mean discharge) could be reduced to a half of the reference value (1971 – 2003) by 2030 and to one third by 2060 under the IPCC A1B scenario.

In addition, **Fig. 3-7** also illustrates the hydrological response to the uncertainty of climate projections. The maxima and minima of the water discharge define the uncertainty boundaries. In general, the uncertainty of high water discharge is much larger than that of low flow, and the uncertainty in winter time is much larger than that in summer. The uncertainty boundaries imply the high potential of drier summers and more frequent high water levels in winter in the future.

3.4.3.2. Impacts on average annual water flow components

The differences in average actual evapotranspiration, total runoff and groundwater recharge between the scenario period (2051 – 2060, averaged over 100 realizations) and the reference period (1961 – 1990) in Germany are illustrated in **Fig. 3-8**. In general, there is an increase of evapotranspiration in most areas of Germany. One of the most important drivers is the higher temperature in the future. In this study, the temperature increase by 2°C on average by the mid of 21st century for the whole territory of Germany was accompanied by an increase in actual evapotranspiration of about 25 mm on average. In wetlands and in some mountainous areas, the increase can reach even more than 100 mm per year. In some drier areas where precipitation may be dropped down in the future, the increasing trend is moderate. There are even some negative trends in some parts of the Elbe basin, probably due to low precipitation. The higher evapotranspiration means high loss of water, which could be critical, especially for areas with negative or minor positive tendency in precipitation.

Fig. 3-8(b) shows that, according to climate scenario, runoff would be significantly reduced (up to 100 mm per year) in the southern part of the upper Danube basin and the Rhine River valley. The Black Forest and the upper Elbe catchment (German part) are also likely to have significant reduction in water runoff in the future. In contrast, the northwest areas would have more available water resources on average, mainly due to higher precipitation.

The groundwater recharge is very sensitive to climate change. As one can see in **Fig. 3-8(c)**, large areas in the Danube, Rhine and Elbe basins have lower groundwater recharge in the scenario period. In general, spatial patterns of changes in runoff and groundwater recharge are quite similar (**Fig. 3-8(b)** and **(c)**). In warmer conditions, the higher temperatures can extend the vegetation period, and more water will be taken up from underground. The groundwater recharge period could also be shorter due to the shortening of the snow cover time. The higher water uptake by plants and shortage of the groundwater recharge time would negatively influence the quantity of groundwater and the water table level.

Figure 3-8(d – f) show the standard deviation of the changes based on 100 realizations. Larger standard deviation means higher inter-annual variations. The mean changes in actual evapotranspiration are relatively certain compared to runoff and groundwater recharge. The reason is that the main driver of potential evapotranspiration is temperature whose trend is consistent in all 100 realizations. Hence, the actual evapotranspiration is increasing as long as water supply (precipitation) is sufficient. In some regions, where the water resources are very vulnerable to the changing climate, the uncertainty is more substantial. As one can see in **Fig. 3-8(d)**, both the Elbe basin and the upper Rhine valley have high uncertainty, implying the high sensitivity of evapotranspiration to climate in these areas. In contrast, these drier areas have lower uncertainty in projected runoff and groundwater recharge. The regions with high water productions have higher uncertainty in runoff and groundwater recharge.

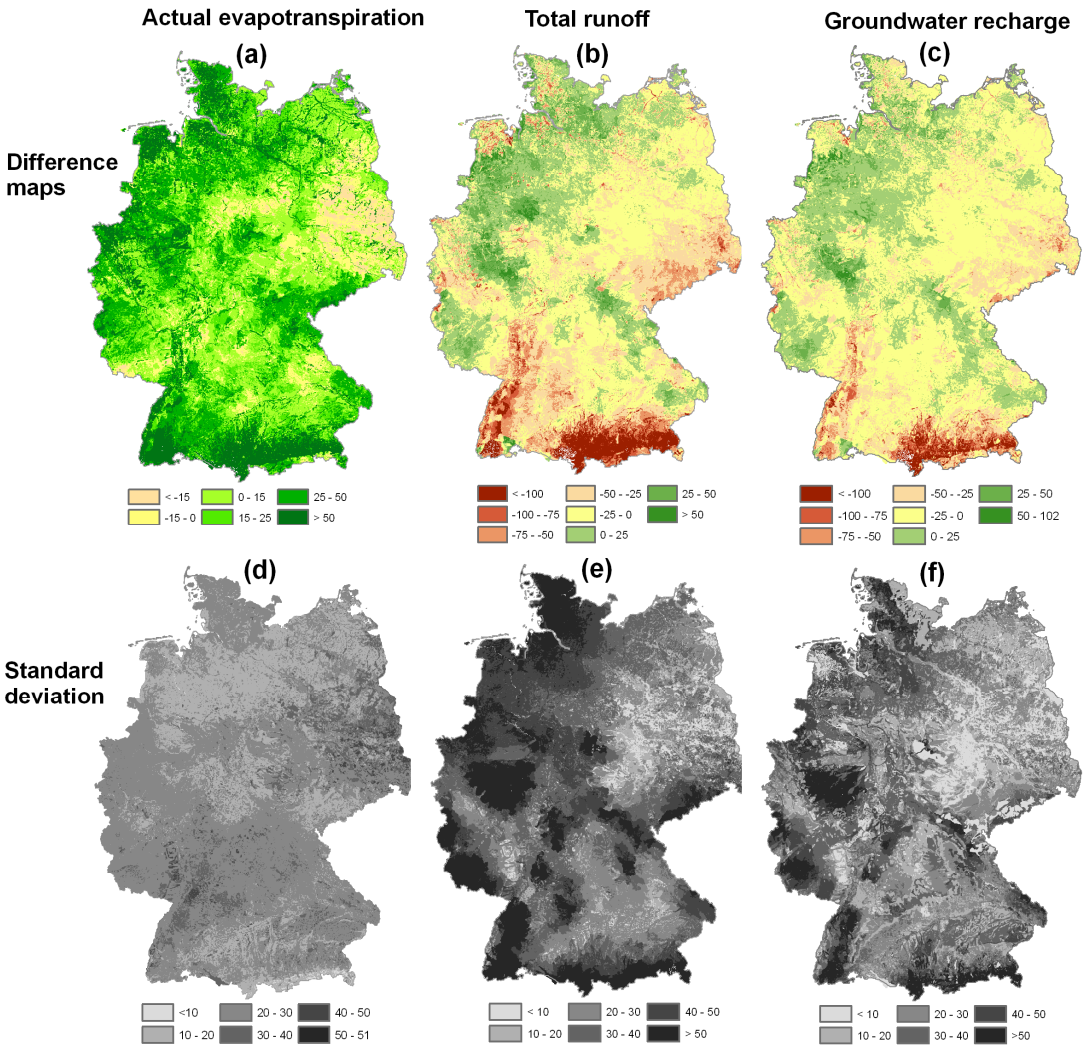

Figure 3-8: Difference maps for the simulated water flow components between the climate scenario period 2051 – 2060 (mean of 100 realizations) and the reference period 1961 – 1990 (a – c), and the standard deviations from the 100 realizations (d – f). Maps for actual evapotranspiration: (a), (d), total runoff: (b), (e), and groundwater recharge: (c), (f) (units: mm/year).

3.5. Conclusions and outlook

In this study the first German-wide impact assessment of water fluxes dynamics under climate change using a process-based river basin model is presented in a spatially and temporally distributed manner. A special focus of the study was on data availability, homogeneity of data sets, and related error and uncertainty propagation in the model results. This is especially important for transboundary river basins like the Rhine, upper Danube and Elbe. Besides, climate scenarios incorporate uncertainty, and it is necessary to analyse the related uncertainty in the results of impact assessment.

We can summarize that a good data base including all necessary data for modelling with SWIM and scenario analysis was available for Germany, but data availability outside of Germany regarding density of stations and quality of available data on land use and soil was poor. This of course had implications on the simulation results (poorer validation results for gauges

corresponding to transboundary catchments). The quality of data input directly influenced simulation results and lead to difficulties in performing a sound evaluation of the model outputs. In our study this problem was solved by doing a maximum of possible, *e.g.* providing a part of results for the total German territory (spatial patterns of water fluxes), and restricting the study area by the solely national large representative subbasins for the climate impact assessment.

The inherent uncertainty related to data availability, especially in the transboundary basins, and to climate scenarios has to be better explored in follow-up investigations. When better and homogeneous data input will be available, the validation of the model results could be improved, and the impact assessment study will cover the whole large basins, and provide sounder scenario results. Cross-comparison of climate impact results driven by several climate downscaling methods could, on one hand, extend the uncertainty bounds, and, on another hand, increase certainty of some trends.

The study was devoted to climate impact assessment, and no changes in land use patterns were considered. The same land use patterns were assumed for the reference and scenario periods in this study ("static" land use). This was done in order to investigate the "pure" impact of climate change on water fluxes, which is reasonable at this stage. Only the crop scheduling was adjusted in the warmer climate. However, the SWIM model is able to simulate complex crop rotations and changes in land use patters, as demonstrated in several previous regional studies (Wechsung *et al.*, 2000; Hattermann *et al.*, 2007b; Yu *et al.*, 2009). Therefore, possible changes in land use patterns and crop rotation could be considered in the follow-up studies to combine them with changes in climate and to explore how changes in land use could compensate for undesirable changes in water flow dynamics.

The first German-wide impact assessment of water fluxes dynamics under climate change was performed using the state-of-the-art statistical regional climate model STAR and the semi-distributed process-based eco-hydrological model SWIM. STAR provides a robust climate data set for hydrological studies and impact assessment. It reproduces not only trend in temperature, but also annual variability and trends in precipitation. In addition, STAR generates a number of realizations for one scenario, which include the uncertainty of projected climate characteristics, especially precipitation. In future, the climate impact results driven by other climate downscaling methods should be compared with those obtained with STAR.

The eco-hydrological model SWIM has proven to adequately reproduce the temporal and spatial water dynamics and river discharge in large river basins, and for such a large and heterogeneous region as Germany. The water flow components simulated by SWIM were also proved to produce comparable distribution patterns with the Hydrological Atlas of Germany. However, the lack of historical climate data and scenario data outside of Germany restricted the calibration and validation of SWIM for the largest river basins (Rhine and upper Danube), and the projection of river discharge for some other main gauges.

Besides, a particular problem was to analyze and project the flood events, especially for the Rhine and the Elbe rivers, where the large upstream drainage areas outside of Germany are important as source areas for the extreme events. This underlines the importance of availability of homogeneous data sets including climate, land use and soil parameters for Europe, which would enable improvement of the climate impact assessment for large regions and countries.

The scenario results show that, under assumption that the applied climate scenario is realistic, the reduction of water discharge in streams is likely to be a considerable problem in Germany by the middle of the century, especially in southeastern part of Germany. Summer may become the most

problematic season in the future regarding water availability in streams, as all the six rivers show a decline in water discharge (about 10% – 25%) in summer months. The projected low flow conditions also comply with the results of other regional studies in Germany. The water conflicts among different water users could become more severe in the most parts of Germany. In the winter time, all the rivers tend to have more stream flow (about 5% – 18%), especially the Ems river basin in the northwest coastal region. Regarding the major water flow components, evapotranspiration would increase by about 25 mm on average in Germany, mainly due to higher temperature. The changes in groundwater recharge and runoff generation are spatially different. The southern Germany and large parts of the Elbe basin have a negative tendency in both groundwater recharge and total runoff, while more water is expected in northwestern Germany. The climate impact assessment demonstrates potential lower water resource availability in the Elbe, upper Danube and upper part of the Rhine Valley.

The uncertainty bounds of river discharge, which are resulted from the uncertainty of the downscaling technique, show that the uncertainty of high water discharge is much larger than that of low flow, and the uncertainty in winter time is much larger than that in summer. The uncertainty boundaries imply the high potential of drier summers and more frequent high water levels in winter in the future according to the scenario. This conclusion emphasizes the higher risk of dry summers in the future. For some areas, such as the Elbe basin, even a small uncertainty of the downward trend in runoff implies a high potential of dryer condition. Hence, the adaptation to climate change in water management and other related sectors is very important, and should be highlighted for such regions.

Acknowledgements: The authors are grateful to M. Wodinski and T. Vetter for their help in data and graphs preparation, and to Prof. A. Bronstert and three anonymous reviewers for their comments, which helped to improve the presentation of simulation results and discussion of associated problems.

Reference:

Albek, M. Öğütveren, and E. Albek (2004), Hydrological modeling of Seydi Suyu watershed (Turkey) with HSPF, *J. Hydrol.* **285**, 260-271.

Arnell, N. W. (2003), Relative effects of multi-decadal climatic variability and changes in the mean and variability of climate due to global warming: future streamflows in Britain, *J. Hydrol.* **270**, 195-213.

Arnold, J. G., P. M. Allen, and G. Bernhardt (1993), A comprehensive surface-groundwater flow model, *J. Hydrol.* **142**, 47-69.

Arnold, J.G., J.R. Williams, A.D. Nicks, and N.B. Sammons (1990), *SWRRB - A Basin Scale Simulation Model for Soil and Water Resources Management*, Texas A&M University Press: College Station, Texas.

Bogena, H., R. Kunkel, T. Schöbel, H. P. Schrey, and F. Wendland (2005), Distributed modeling of groundwater recharge at the macroscale, *Ecol. Model.* **187**, 15-26.

Böhm, U., K. Keuler, H. Österle, M. Kücken, and D. Hauffe (2008), Quality of a Climate Reconstruction for the CADSES region, *MetZ special issue Regional climate modeling with COSMO-CLM (CCLM)* **17(8)**, 477-485.

Doherty, J. (2004), *PEST: Model Independent Parameter Estimation. Fifth edition of user manual*, Watermark Numerical Computing, Brisbane, Australia.

Drogue, G., L. Pfister, T. Leviandier, A. El Idrissi, J. Iffly, P. Matgen, J. Humbert, and L. Hoffmann (2004), Simulating the spatio-temporal variability of streamflow response to climate change scenarios in a mesoscale basin, *J. Hydrol.* **293**, 255-269.

Enke, W., and A. Spekat (1997), Downscaling climate model outputs into local and regional weather elements by classification and regression, *Clim. Res.* **8(3)**, 195-207.

Gerstengarbe, F., M. Kücken, and P. Werner (2009), *Modellvergleich der regionalen Klimamodelle REMO, CCLM, WETTREG und STAR II*, PIK (Potsdam Institute for Climate Impact Research) internal report, Potsdam.

Glugla, G., P. Jankiewicz, C. Rachimow, K. Lojek, K. Richter, G. Fürtig, and P. Krahe (2002), *Wasserhaushaltsverfahren BAGLUVA zur Berechnung vieljähriger Mittelwerte der tatsächlichen Verdunstung und des Gesamtabfluß*, Bundesanstalt f. Gewässerkunde, Berlin/Koblenz.

HAD (Hydrologischer Atlas von Deutschland) (2000), Bundesministerium für Umwelt, Naturschutz und Reaktorsicherheit, ISBN 3-00-005624-6.

Hattermann, F. F., V. Krysanova, F. Wechsung, and M. Wattenbach (2004), Integrating groundwater dynamics in regional hydrological modelling, *Environ. Modell. Softw.* **19(11)**, 1039-1051.

Hattermann, F.F., T. Conradt, A. Bronstert (2007a), Berechnung grosskaliger Verdunstung unter den Bedingungen des globalen Wandels. **In:** K. Miegel, Hans-B. Kleeberg (Hrsg.), *Verdunstung. Beiträge zum Seminar Verdunstung am 10./11. Oktober 2007 an der Universität Potsdam*, Forum für Hydrologie und Wasserbewirtschaftung.

Hattermann, F. F., H. Gömann, T. Conradt, M. Kaltofen, P. Kreins, and F. Wechsung (2007b), Impacts of global change on water-related sectors and society in a trans-boundary central European river basin - Part 1: project framework and impacts on agriculture, *Adv. Geosci.* **10**, 1-8.

Hattermann, F. F., J. Post, V. Krysanova, T. Conradt, and F. Wechsung (2008), Assessment of Water Availability in a Central-European River Basin (Elbe) Under Climate Change, *Adv. Clim. Change Res.* **4**, 42-50.

Hennegriff, W., J. Ihringer, and V. Kolokotronis (2008), Prognose von Auswirkungen des Klimawandels auf die Niedrigwasserverhältnisse in Baden-Württemberg, *Korrespondenz Wasserwirtschaft* **6(1)**, 309-314.

IPCC (2007), *Climate Change 2007: Impacts, Adaptation and Vulnerability - Summary for Policymakers. Working Group II Contribution to the Fourth Assessment Report of the Intergovernmental Panel on Climate Change*, Cambridge University Press.United Kingdom and New York, NY, USA.

Jacob, D. (2001), A note on the simulation of the annual and inter-annual variability of the water budget over the Baltic Sea drainige basin, *Meteorol. Atmos. Phys.* **77**, 61-73.

Kille, K. (1970), Das Verfahren MoMNQ, ein Beitrag zur Berechnung der mittleren langjährigen Grundwasserneubildung mit Hilfe der monatlichen Niedrigwasserabfüsse, *Z. Dt. Geol. Ges., Sonderh. Hydrogeol. Hydrochem.*, 89-95.

Kosková, R., S. Nemecková, C. Hesse Jakubíková, A., V. Broza, and J. Szolgay (2007), Using of the Soil Parametrisation Based on Soil Samples Databases in Rainfall-Runoff Modelling, **In:** Jakubíková, A. and Broza, V. and Szolgay, J. (eds.), *Proceedings of the Adolf Patera Workshop "Extreme hydrological events in catchments". 13.11.2007*, Bratislava.

Krysanova, V., A. Meiner, J. Roosaare, and A. Vasilyev (1989), Simulation modelling of the coastal waters pollution from agricultural watersheds, *Ecol. Model.* **49**, 7-29.

Krysanova, V., D. Möller-Wohlfeil, and A. Becker (1998), Development and test of a spatially distributed hydrological / water quality model for mesoscale watersheds, *Ecol. Model.* **106**, 261-289.

Krysanova, V., F. Hattermann, and A. Habeck (2005), Expected changes in water resources availability and water quality with respect to climate change in the Elbe river basin (Germany), *Nordic Hydrology* **36(4-5)**, 321-333.

Mauser, W., T. Marke, and S. Stoeber (2008), Climate Change and water resources: Scenarios of lowflow conditions in the Upper Danube River Basin. **In:** *XXIVth Conference of the Danubian Countries, IOP Conf. Series: Earth and Environmental Science 4*.

Mauser, W., and H. Bach (2009), PROMET - Large scale distributed hydrological modeling to study the impact of climate change on the water flows of mountain watersheds, *J. Hydrol.* **376**, 362-377.

Menzel, L., and G. Bürger (2002), Climate change scenarios and runoff response in the Mulde catchment (Southern Elbe, Germany), *J. Hydrol.* **267**, 53-64.

Menzel, L., A. Thieken, D. Schwandt, and G. Bürger (2006), Impact of climate change on the Regional hydrology - scenario-based modelling studies in the German Rhine Catchment, *Nat. Hazards* **38**, 45-61.

Middelkoop, H., and J. Kwadijk (2001), Towards integrated assessment of the implications of global change for water management - The Rhine experience, *Phys. Chem. Earth. (B)* **26(7-8)**, 553-560.

Monteith, J. L. (1965), Evaporation and the environment, *Symp. Soc. Expl. Biol.* **19**, 205-234.

Muttiah, R. S., and R. A. Wurbs (2002), Modeling the impacts of climate change on water supply reliabilities, *Int. Water Resour. Assoc.* **27(3)**, 407-419.
Nash, J. E., and J. V. Sutcliffe (1970), River flow forecasting through conceptual models. Part I: a discussion of principles, *J. Hydrol.* **10(3)**, 282-290.
Orlowsky, B., F. Gerstengarbe, and P. Werner (2008), A resampling scheme for regional climate simulations and its performance compared to a dynamical RCM, *Theor. Appl. Climatol.* **92**, 209-223.
Petrow, T., and B. Merz (2009), Trends in flood magnitude, frequency and seasonality in Germany in the period 1951 - 2002, *J. Hydrol.* **371**, 129-141.
Priestley, C. H. B., and R. J. Taylor (1972), On the assessment of surface heat flux and evaporation using large scale parameters, *Mon. Weather Rev.* **100**, 81-92.
Roeckner, E., G. Bäuml, L. Bonaventura, R. Brokopf, M. Esch, M. Giorgetta, S. Hagemann, I. Kirchner, L. Kornblueh, E. Manzini, A. Rhodin, U. Schlese, U. Schulzweida, and A. Tompkins (2003), *The atmospheric general circulation model ECHAM5. Part I: Model description*, Max Planck Institute for Meteorology, MPI for Meteorology, Bundesstr. 53, 20146 Hamburg, Germany.
Schönwiese, C., T. Staeger, and S. Trömel (2004), The hot summer 2003 in Germany. Some preliminary results of a statistical time series analysis, *Meteorol. Z.* **13**, 323-327.
Schönwiese, C., T. Staeger, and S. Trömel (2006), Klimawandel und Extremereignisse in Deutschland. **In:** *Klimawandel und Extremereignisse in Deutschland - Klimastatusbericht 2005*, Deutscher Wetterdienst, Offenbach, 7-17.
Statistisches Bundesamt Deutschland (2008), *Statistical Yearbook 2008, a*vailable in German (http://www.destatis.de/jetspeed/portal/cms/Sites/destatis/Internet/DE/Content/Publikationen/Querschnittsveroeffentlichungen/StatistischesJahrbuch/Jahrbuch2008,property=file.pdf), (last asscessed: 13.09.2011).
T.G.M. Water Research Institute, *Hydroecological Information system*, available at http://heis.vuv.cz/ (last asscessed: 10.10.2011)
Thodsen, H. (2007), The influence of climate change on stream flow in Danish rivers, *J. Hydrol.* **333**, 226-238.
Wechsung, F., V. Krysanova, M. Flechsig, and S. Schaphoff (2000), May land use change reduce the water deficiency problem caused by reduced brown coal mining in the state of Brandenburg?, *Landscape and Urban Planning* **51(2-4)**, 105-117.
Wechsung, F., F. W. Gerstengarbe, P. Lasch, and A. Lüttger (2008), Die Ertragsfähigkeit ostdeutscher Ackerflächen unter Klimawandel, *PIK Report* **112(2010)**, 62.
Wendling, U. (1995), Berechnung der Gras-Referenzverdunstung mit der FAO Penman-Monteith-Beziehung, *Wasserwirtschaft* **85(12)**, 602-604.
Williams, J., K. Renard, and P. Dyke (1984), EPIC - a new model for assessing erosion's effect on soil productivity, *J. Soil Water Conserv.* **38(5)**, 381-383.
Yu, P., V. Krysanova, Y. Wang, W. Xiong, F. Mo, Z. Shi, H. Liu, T. Vetter, and S. Huang (2009), Quantitative estimate of water yield reduction caused by forestation in a water-limited area in northwest China, *Geophy. Res. Lett.* **36(L02406)**, 5.

Climatic Change (2012)
(accepted)

4. Projections of climate change impacts on river flood conditions in Germany by combining three different RCMs with a regional eco-hydrological model

Shaochun Huang* [1], Fred F. Hattermann[1], Valentina Krysanova[1], and Axel Bronstert[1,2]

[1] *Potsdam Institute for Climate Impact Research, P.O. Box 601203, Telegrafenberg, 14412 Potsdam, Germany*

[2] *University of Potsdam, Chair for Hydrology and Climatology, Karl-Liebknecht-Str. 24-25, D-14476 Potsdam-Golm, Germany*

* Corresponding author. Tel.: +49 331 288 2406.
Email address: huang@pik-potsdam.de

Abstract

The aim of the paper is twofold: a) to project the future flood conditions in Germany accounting for various river regimes (from pluvial to nival-pluvial regimes) and under different climate scenarios (the high, A2, low, B1, and medium, A1B, emission scenarios) and b) to investigate sources of uncertainty generated by climate input data and regional climate models. Data of two dynamical Regional Climate Models (RCMs), REMO (REgional Model) and CCLM (Cosmo-Climate Local Model), and one statistical-empirical RCM, WettReg (Wetterlagenbasierte Regionalisierungsmethode: weather-type based regionalization method), were applied to drive the eco-hydrological model SWIM (Soil and Water Integrated Model), which was previously validated for 15 gauges in Germany. At most of the gauges, the 95 and 99 percentiles of the simulated discharge using SWIM with observed climate data had a good agreement with the observed discharge for 1961 – 2000 (deviation within ±10%). However, the simulated discharge had a bias when using RCM climate as input for the same period. The 50-year flood values estimated for two scenario periods (2021 – 2060, 2061 – 2100) were compared to the ones derived from the control period using the same climate models. The results driven by the statistical-empirical model show a declining trend in the flood level for most rivers, and under all climate scenarios. The simulations driven by dynamical models give various change directions depending on region, scenario and time period. The uncertainty in estimating high flows and, in particular, extreme floods remains high, due to differences in regional climate models, emission scenarios and multi-realizations generated by RCMs.

Keywords: Flood projection, SWIM, REMO, WettReg, CCLM, Germany, uncertainty

4.1. Introduction

As noted in the IPCC (Intergovernmental Panel on Climate Change) Fourth Assessment Report (IPCC, 2007), warming of the global climate system is unequivocal. The updated 100-year linear trend (1906 to 2005) shows a 0.74 °C global mean temperature increase. Higher temperatures tend to increase evaporation which can raise air humidity and result in precipitation increase. For Germany an increasing tendency has been stated; for example, an upward linear trend of about 1 °C in temperature and 9% in precipitation from 1901 to 2000 (Schönwiese *et al.*, 2006).

It has been reported that there have been more frequent floods in Germany (and in neighboring countries) during the last two decades, some of which have been among the most destructive ones ever recorded, such as the floods in 1993 and 1995 in the Rhine basin; in 1997 and 2010 in the Oder; in 1999, 2001, 2002 and 2006 in the Danube, and in 2002 and 2006 in the Elbe (Grünewald *et al*., 1998; Disse and Engel, 2001; Bronstert, 2003; Mikhailov *et al.*, 2008; Kreibich *et al.*, 2007). The observed changes in flood behaviour were analysed, and statistically significant trends were found in western, southern and central Germany; these trends were assumed to be climate driven (Petrow and Merz, 2009). In the future, the impact of climate change on flood conditions is likely to be more prominent due to the continuing rise in atmospheric temperature and changing precipitation conditions, which may result in altered hydrological regimes. Therefore, there is an increasing interest in projecting future flood conditions in Germany, which can be important information for decision makers dealing with flood risk management strategies.

Despite its high relevance, there are relatively few studies which investigated potential impacts of climate change on flood condition in Germany to date (Menzel and Bürger, 2002; Middelkoop and Kwadijk, 2001; Menzel *et al.*, 2006; Shabalova *et al.*, 2003; Lenderink *et al.*, 2007; Dankers *et al.*, 2007). These studies only focused on some individual river basins using different downscaling techniques. For example, Shabalova *et al.* (2003) and Lenderink *et al.* (2007) assessed the extreme conditions of river Rhine using two versions of climate model (HadRM2 and HadRM3H: Hadley Centre Regional Model) under different scenarios and integrated with the hydrological model RhineFlow. Dankers *et al.* (2007) simulated flood hazards in the upper Danube Basin with the high-resolution climate model HIRHAM (HIRLAM dynamics + the Hamburg physics package) under A2 and B2 scenarios and the hydrological model LISFLOOD. Not only the emission scenarios, regional climate models and hydrological models were different in these studies, but they also applied different control and scenario time slices and bias correction methods. All these differences make it difficult to aggregate these result and generate a consistent picture of the future flood conditions in Germany.

Recently, the uncertainty in projecting the future flood conditions has also been widely discussed. Kay *et al.* (2006) claimed that the modeled changes in flood frequency under one Regional climate model (RCM) run using one emission scenario should not be taken as conclusive of what will be seen in the future. Cameron (2006) highlighted the need of considering multiple climate change scenarios applying different RCMs, and accounting for model uncertainty when estimating the possible effects of climate change upon flood frequency. Kay *et al.* (2009) investigated the uncertainty sources for climate change impact especially on flood frequency and found that the largest uncertainty comes from the General Circulation Model (GCM) structures. When the uncertainty related to different GCMs is omitted, the RCMs provide higher uncertainty than other sources, such as emission scenarios and hydrological modelling. Therefore the uncertainty from the climate scenarios is one of the main focuses of our study, considering

different sources of uncertainty such as climate models, emission scenarios and the multi-realizations generated by each model.

The goals of this paper are (a) to simulate the future flood conditions in Germany, including simulations in different types of river regimes (from pluvial to nival-pluvial), and (b) to reveal the uncertainty by applying different RCMs under different climate scenarios (high (A2), low (B1), and medium (A1B) emission scenarios). To achieve this goal, three available nation-wide applications of RCMs were used to derive the required hydro-meteorological boundary conditions for a large-scale hydrological model, which was applied for the large river basins covering the whole German territory.

In this study, two dynamical RCMs, REMO (REgional MOdel) (Jacob, 2001) and CCLM (Cosmo-Climate Local Model) (Rockel *et al.*, 2008), and one statistical-empirical RCM, WettReg (Wetterlagenbasierte Regionalisierungsmethode: weather-type based regionalization method) (Enke *et al.*, 2005a, 2005b), which have been intensively tested for Germany before, were applied to derive the climatological input data. The latter was used by the hydrological model SWIM (Soil and Water Integrated Model) (Krysanova *et al.*, 1998) for simulating hydrological cycle of the river basins, with a particular focus on river discharge. For each RCM, regional climate scenarios according to various emission scenarios were generated. The five largest river basins in Germany were included and 15 gauge stations at the main rivers and large tributaries were used for calibration and validation. Based on the parameterization of the validated models, reference hydrological simulations were conducted, driven by the so-called control runs from each RCM covering a 40-year period from 1961 – 2000 as the baseline. The combined climatological-hydrological simulations were performed for the whole period 2001 – 2100, to obtain the runoff dynamics in these rivers in a transient manner. Based on these simulations, results in two selected periods (2021 – 2060 and 2061 – 2100) were compared separately with the ones in the reference period (baseline). The uncertainty in the changes of flood discharge rates and flood seasonality from all models and scenarios was analysed.

4.2. Study area

The five largest river basins in Germany (Danube, Elbe, Ems, Rhine and Weser) were selected as the study areas for the assessment of climate change impacts on flood conditions (**Fig. 4-1**). They cover about 90% of the whole German territory. About 84% of the Ems drainage area and the whole Weser basin are located in Germany, and the other three studied basins have large areas outside of Germany, *i.e.* in the Czech Republic, Austria, Switzerland, Luxemburg and France. The five basins represent different characteristics of geomorphology, climate and river regimes (**Table 4-1**).

Geomorphologically, the Ems, which is the smallest river basin among the five, is located in the flat lowland region of NW-Germany and NE-Netherlands. The other two northern basins (the Weser and the German part of the Elbe) include both the lowland part and parts of the central German mountains. The Upper Danube lies in southwestern Germany and receives its main tributaries from the Alps and the Bavarian Forest. The Rhine originates in the Swiss Alps and flows from the Austrian/Swiss border region through Germany to the Netherlands. The Rhine and Upper Danube basins have the steepest slopes and highest altitudes. Sandy soils are dominant in the northwestern lowland region while loess, rocks and sandstone prevail in the south. There are also some differences in land use composition between the northern and southern basins. In the Ems, Weser and Elbe basins about half of the basins areas are covered by agricultural crops. In the Danube and Rhine basins the share of forest is notably higher.

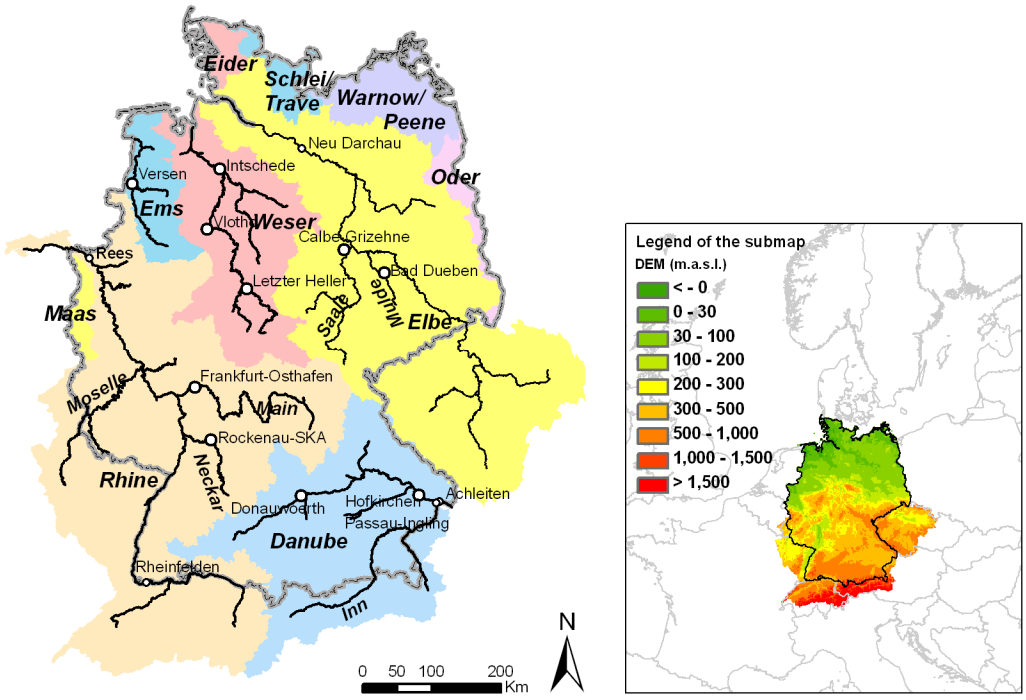

Figure 4-1: The main river basins in Germany and the location of the selected discharge gauges.

Table 4-1: The characteristics of the five basins studied.

River basin		Ems (German part)	Weser	Upper Danube (till gauge Achleiten)	Rhine (till gauge Rees)	Elbe
Area (km^2)		13000	45725	77107	160000	147423
Percent area in Germany (%)		100	100	73	64	65
Mean slope (degree)		0.5	2.4	7.4	5.4	2
Altitude (m a.s.l.)		0-406	0-1127	301-3838	15-4275	0-1547
Land use shares (%)	Cropland	66	49	32	38	51
	Forest	10	30	37	36	30
	Grassland	15	14	20	13	10
Annual average precipitation (mm)*		839	807	1196	1045	721
Major river regime		pluvial	pluvial	nival-pluvial	nival-pluvial	pluvial

*the precipitation data was interpolated from the measured data in the basins for the period 1961-2000

These five river basins also have significant differences in their climatology and hydrological regimes. From the northwest to the east and southeast, the maritime climate gradually changes into a more continental climate. The Upper Danube and Rhine river basins have the highest precipitation (more than 1000 mm per year) and the Elbe receives the lowest rainfall. At the macro-scale (national river basins), a pluvial river flow regime dominates, and most of the German large rivers have high water levels in winter and low flow in summer. However, the tributaries of Danube and upper Rhine receive a large amount of melting water from snow and

glaciers. Thus, such catchments have their main flood season in late spring or early summer, *i.e.* a nival runoff regime, the High and Upper Rhine in particular (upstream of the confluence with the Neckar at Mannheim). There are also combinations of nival and pluvial regimes (flood seasons in winter and summer, *e.g.* the German Danube or the Upper/Middle Rhine downstream from Mannheim.

Figure 4-1 also shows the location of the 15 selected gauge stations, which were used for assessing the flood conditions at the main rivers and large tributaries.

4.3. Methods

4.3.1. Regional climate models

There are different sets of regional climate projections for Germany, but only two of them were officially commissioned by (*i.e.* developed on behalf of) the German Environmental Agency. One set of regional climate projections was generated by the dynamical RCM REMO (Jacob, 2001), and another by the statistical-empirical RCM WettReg (Enke *et al.*, 2005a, 2005b). They both used the results from the GCM ECHAM5 for the emission scenarios A1B, A2 and B1 as large-scale forcing. Dynamical RCMs are very computationally intensive, while, in contrast, most statistical-empirical regional models are much less computationally demanding. The projections generated by these two models were evaluated by Bronstert *et al.* (2007b) on their usefulness for hydrological impact simulations. In general, they found that both models have a rather limited value for climate impact simulations regarding flooding conditions. Keeping this general shortcoming in mind, they conclude that the dynamical model REMO has a slight advantage in the aspect of flood simulation, while WettReg shows a relatively better performance in the overall aspects of the hydrological cycle, *e.g.* seasonal hydrological dynamics, low flow conditions and moderate flooding conditions. These findings motivated us to include another innovative dynamical model, CCLM (Rockel *et al.,* 2008), from which results for Germany are available only since recently. The more detailed information on the three RCMs used is given in the following sections, and **Table 4-2** lists some general characteristics of them.

Table 4-2: The characteristics of different RCMs (CCLM, REMO and WettReg).

RCMs	Model type	Simulation period	GCM based	Emission scenario	Spatial resolution	Realization per scenario
CCLM	Dynamic	1960-2100	ECHAM5	A1B, B1	0.2° (Ca. 1139 grids in Germany)	2
REMO	Dynamic	1951-2100	ECHAM5	A1B, A2, B1	0.088° (Ca. 3275 grids in Germany)	1
WettReg	Statistical-empirical	1961-2100	ECHAM5	A1B, A2, B1	274 climate stations and 1691 precipitation stations in Germany	20

4.3.1.1. REMO

REMO (REgional MOdel) was developed from the ‘‘Europamodell’’, the former numerical weather prediction model of the German Meteorological Service (Majewski 1991), in the Max-Planck-Institute for Meteorology in Hamburg, Germany (Jacob, 2001). It is a three dimensional regional hydrostatic climate model, and it is also available in a non-hydrostatic version. REMO solves the hydrostatic Euler equations with a finite difference method on a hybrid terrain following vertical coordinate system using the leapfrog time integration on an Arakawa-C grid (Suklitsch *et al.*, 2010).

REMO calculates climate variables at a 0.088° grid for Central Europe including Germany and simulates the main weather processes including cloud dynamics, precipitation and temperature

development for each grid cell. Control and scenarios of future climate conditions are constructed by using GCM ECHAM5 results as large-scale forcing. Only one realization of each scenario was generated by REMO.

4.3.1.2. CCLM

CCLM (Cosmo-Climate Local Model) (Rockel *et al.*, 2008) originates from the weather forecast model "Lokal-Modell" (LM), which was developed by the German Meteorological Service (Steppeler *et al.*, 2003). Compared to REMO, CCLM is a non hydrostatic climate model. It is based on the basic hydro-thermodynamical equations describing a compressible non-hydrostatic flow in a moist atmosphere without any scale approximations. It also takes the results of the GCM ECHAM5 as boundary conditions, but only two emission scenarios were available for our study (A1B and B1). There are two model outputs transformed into time series in two different grids for the whole Europe called data stream 2 and data stream 3. The data stream 2 has a finer resolution of 0.165° in a longitude-latitude rotated grid and the data stream 3 has a resolution of 0.2° in longitude-latitude regular grid. For this study, only the data stream 3 was available. Its spatial resolution (0.2°) is coarser than that of REMO, hence the spatial representation of climate variables is weaker for hydrological impact studies. However, previous studies show that the effect of spatial resolution of the rainfall data on river discharge as well as extremes is minor for the large river basins (Booij, 2002; Kleinn *et al.*, 2005), so we assume that the spatial resolution of CCLM can be accepted in this case as the case study basin area is ranging from 2842 to 159300 km^2 (see **Table 4-3**). Two control runs were generated based on two realizations of the 20^{th} century reconstruction initialized in different years of the pre-industrial control experiment from ECHAM5. These control runs provide the initial conditions for the transient simulation of the future regional climate projections A1B and B1. Hence, two realizations generated by CCLM for each scenario condition were used.

4.3.1.3. WettReg

WettReg (Wetterlagenbasierte Regionalisierungsmethode: weather-type based regionalization method) uses the statistical relationships between large-scale atmospheric conditions and local climate, and the characteristics of regional climate for different weather types (Enke *et al.*, 2005a, 2005b). It classifies observed weather types into 10 classes of typical 'temperature' and 8 classes of 'precipitation regimes', for each season. Variables/features which have a relatively good representation in the global models, such as temperature and circulation patterns, are selected as driving climate variables. Variables with a relatively poor representation in global models, such as precipitation or radiation, are generated by WettReg using observed correlations between large-scale patterns and *e.g.* precipitation and radiation. Precipitation conditions are modified in a further step to better fit the 'precipitation regime'.

As WettReg needs observation data to derive the correlation matrices for the observation period, climate projections can only be calculated for locations with climate observations. Therefore the WettReg scenarios are spatially derived for the network of the climate and precipitation stations available since 1965 in Germany, and thus can only be applied to project flood conditions in that area. However, being less computationally expensive, WettReg can be applied in a multiple run mode. Therefore, in our case, 20 realizations of each scenario were used to evaluate uncertainty.

4.3.2. Eco-hydrological model SWIM

The dynamical process-based eco-hydrological model SWIM (Soil and Water Integrated Model) (Krysanova *et al.*, 1998) was developed for climate and land use change impact assessment on the basis of the models SWAT (Arnold *et al.*, 1993) and MATSALU (Krysanova *et al.*, 1989).

SWIM simulates the hydrological cycle, vegetation growth and nutrient cycling with a daily time step by disaggregating a river basin to sub-basins and hydrotopes. The hydrotopes are sets of elementary units in a subbasin with assumed homogeneous soil and land use types. Up to ten vertical soil layers can be considered for each hydrotope. It is assumed that a hydrotope behaves uniformly regarding hydrological processes and nutrient cycling, given the same meteorological input. The spatial disaggregation scheme in the model is flexible. In the regional studies climate zones, grid cells of a certain size or other areal units can be used for disaggregating a region instead of subbasins.

Water flows, nutrient cycling and plant growth are calculated for every hydrotope. Then lateral transport of water and nutrients towards the river network are simulated on the basis of linear storage functions considering interacting hydrological compartments and nutrient retention processes. After reaching the river system, water and nutrients are routed along the river network to the outlet of the simulated basin.

The simulated hydrological system consists of four main compartments: the soil surface, the root zone of soil, the shallow aquifer, and the deep aquifer. The soil root zone is subdivided into several layers in accordance with the soil database. The water balance for the soil surface and soil column includes precipitation, surface runoff, evapotranspiration, subsurface runoff, and percolation. The water balance for the shallow aquifer includes groundwater recharge, capillary rise to the soil profile, lateral flow, and percolation to the deep aquifer.

Surface runoff is estimated as a non-linear function of precipitation and a retention coefficient, which depends on soil water content, land use and soil type (modification of the Soil Conservation Service curve number method, Arnold *et al.*, 1990). Lateral subsurface flow (or interflow) is calculated simultaneously with percolation. It appears when the storage in any soil layer exceeds field capacity after percolation and is especially important for soils having impermeable or less permeable layer(s) below several permeable ones. Potential evapotranspiration is mostly simulated using the method of Priestley-Taylor (Priestley and Taylor, 1972), though the method of Penman-Monteith (Monteith, 1965) can also be used. Actual evaporation from soil and actual transpiration by plants are calculated separately.

The module representing crops and natural vegetation is an important interface between hydrology and nutrients. Therefore, a simplified EPIC approach (Williams *et al.*, 1984) is included in SWIM for simulating arable crops (like wheat, barley, rye, maize, potatoes) and aggregated vegetation types (like pasture, evergreen forest, mixed forest), using specific parameter values for each crop/vegetation type. A number of plant-related parameters are specified for 74 crop/vegetation types in the database attached to the model. Vegetation in the model affects the hydrological cycle by the cover-specific retention coefficient, impacting surface runoff, and influencing the amount of transpiration, which is simulated as a function of potential evapotranspiration and leaf area index.

Interception of photosynthetic active radiation (PAR) is estimated as a function of solar radiation and leaf area index. The potential increase in biomass is the product of absorbed PAR and a specific plant parameter for converting energy into biomass. The potential biomass is adjusted daily if one of the four plant stress factors (water, temperature, nitrogen, N, and phosphorus, P) is less than 1.0, using the product of a minimum stress factor and the potential biomass. The water stress factor is defined as the ratio of actual to potential plant transpiration. The temperature stress factor is computed as a function of daily average, optimal and base temperatures for plant growth. The N and P stress factors are based on the ratio of accumulated N and P to the optimal values.

The leaf area index is simulated as a function of a heat unit index (ranging from 0 at planting to 1 at physiological maturity) and biomass.

Two modifications were developed in SWIM for the present study: 1) modification of the snow module, and 2) modification of the crop rotation scheme.

In order to adequately simulate snow accumulation and snow melt processes, the classification of hydrotopes for this study also takes elevation into account. The snow accumulation and snow melt are then simulated for each hydrotope with an altitude adjusted temperature. The snow module includes a description of temporal change of the snow depth, content of ice and liquid water, snow density, snowmelt sublimation, refreezing melting water and snow metamorphism according to the method introduced by Gelfan *et al.* (2004). The degree-day method was applied to simulate the snow and glacier melting, but with different degree-day factors, respectively.

SWIM allows the adaptation of crop rotation schemes under a changing climate. In warmer (scenario) conditions, the crop scheduling is governed by the harvest index, and the winter crop can be harvested earlier than in the current conditions, allowing earlier growth of cover crop until the next winter crop planting date. This modification of crop scheduling has influence on the hydrological cycle.

SWIM was calibrated/validated using the observed climate data for the five largest river basins in Germany, as observed climate is the best source to compare the simulated river discharge against observed river discharge and hence to analyze whether the model is in principle able to reproduce flood generation in the region of interest. The eco-hydrological model SWIM was previously validated and applied for another study using the same climate data and for the same area in Huang *et al.*, 2010, and more previously by Hattermann *et al.*, 2005 and Krysanova *et al.*, 2007 for the Elbe river basin.

4.3.3. Statistical methods

In this study the non-dimensional efficiency criterion of Nash-Sutcliffe (1970) efficiency (*NSE*) and relative deviation in water balance (*DB*) were used to evaluate the quality of the simulated daily water discharge.

NSE is a measure to evaluate the squared differences between the observed and simulated values using the following equation:

$$NSE = 1 - \frac{\Sigma(Q_{obs} - Q_{sim})^2}{\Sigma(Q_{obs} - \overline{Q}_{obs})^2} \qquad (4\text{-}1)$$

DB describes the long-term differences of the observed values against the simulated ones in percent for the whole modelling period:

$$DB = \frac{\overline{Q}_{sim} - \overline{Q}_{obs}}{\overline{Q}_{obs}} * 100 \qquad (4\text{-}2)$$

Here Q_{obs} means the observed discharges while Q_{sim} is the corresponding simulated value. The variables $\overline{Q}_{obs}$ and $\overline{Q}_{sim}$ are the mean values of the observed and simulated discharge for the modelling period.

The NSE can vary from minus infinity to 1. A value of 1 denotes a perfect match of predicted and measured values, and values above 0.7 usually mean satisfactory fit. A value of 0 for the deviation in balance means no difference in amount between the measured and simulated values.

In order to analyze the flood characteristics from the daily discharges, the Generalized Extreme Value (GEV) distribution (Coles, 2001) was applied to fit the annual maximum discharges and then to estimate the 10-, 30- and 50-year flood levels. This distribution combines three probability distributions (Gumbel, Fréchet and Weibull), which are commonly used in extreme value analysis.

The GEV distribution is a three-parameter distribution defined by location parameter (μ), scale parameter (σ) and shape parameter (ξ) (see **Equation 4-3**):

$$F(x;\mu,\sigma,\xi) = \exp\left\{-\left[1+\xi\left(\frac{x-\mu}{\sigma}\right)\right]^{-1/\xi}\right\} \qquad (4\text{-}3)$$

for $1+\xi(x-\mu)/\sigma > 0$, where $\mu \in \Re$ is the location parameters, $\sigma > 0$ is the scale parameter and $\xi \in \Re$ is the shape parameter.

Figure 4-2 gives an example of the GEV distribution fitted to 40 annual maxima values (see the solid line). Besides the fitting curve, the 95% confidence interval (see the dashed lines) for the return levels can be calculated using the delta method, which is generally appropriate for the short return periods (Coles, 2001). Based on the three curves, the 10-, 30- and 50-year flood levels and their corresponding confidence intervals can be estimated. The GEV method does not consider other extreme events within one year that can be considered as its major limitation. Nevertheless, this method based on annual maxima discharges was widely used in other studies of climate impact on floods (*e.g.* Leander *et al.*, 2008 and Dankers *et al.*, 2007).

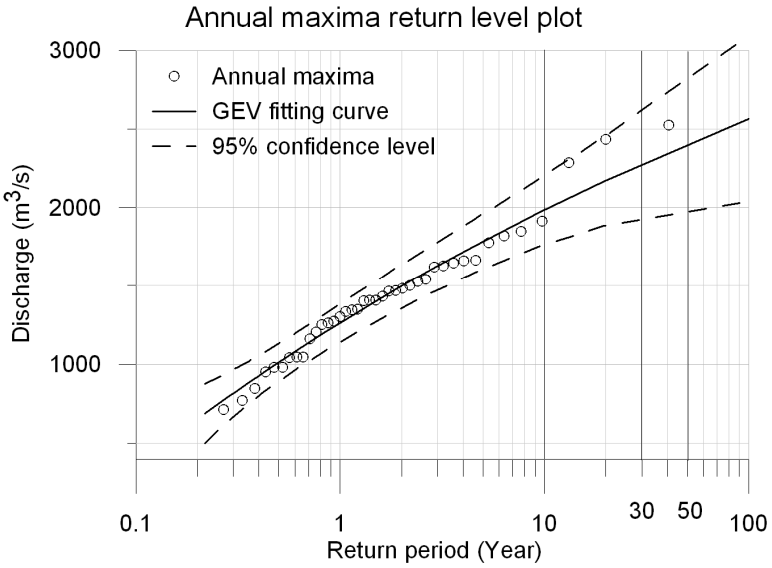

Figure 4-2: An example of Generalized Extreme Value (GEV) plots.

4.3.4. Modelling strategy

It has been reported that the GCM ECHAM5 provides simulation results with rather wet winters in central Europe (van Ulden and van Oldenborgh, 2006). This can be observed when comparing the results from the ECHAM5 control runs with the observed climatological data for that region. Thus, the downscaling conducted by the dynamical climate models REMO and CCLM on the basis of these GCM results could generate a great bias, too. Because of such systematic differences between climate simulations and observations, some authors argue for adjusting the climate model output (termed "bias correction"), and suggest different approaches to "correct" such differences (Themeßl *et al.*, 2010; Christensen *et al.*, 2008).

However, the credibility of such a "correction" is currently under extensive discussion, particularly concerning the extreme events. Graham *et al.* (2007) stated that the use of the delta approach (Hay *et al.*, 2000), which adds the change in projected climate to an observational database, offers a robust method to compare average outcomes from different climate models, but not hydrological extremes. Kay *et al.* (2006) found that direct use of the RCM data could result in relatively good estimates of flood frequency, even though there might be a systematic bias in the overall hydrological budget. Lenderink *et al.* (2007) claimed that the direct use of RCM data might be preferred if other discharge characteristics than the mean (such as extremes) are of interest. Taking into account the doubtfulness of the bias correction methods, especially for extreme events, we decided to use RCMs directly for both control and scenario periods assuming that the RCM biases in the future are approximately the same as in the control climate.

SWIM was calibrated with observed point data and then applied using RCM data. The effect of the spatial rainfall input resolution on the response of small catchments has been found to be of substantial importance, for example, for the catchment of 6.73 km^2 in the study of Lopes (1996). However, for large basins, this effect is minor as it is shown by Booij (2002), who analysed the effects of spatial resolution of rainfall on extreme river discharge for the Meuse basin (30 000 km^2). In addition, Kleinn *et al.* (2005) also stated that the climate model resolution has a limited impact upon stream flow simulation in large catchments, but may have a significant impact in small catchments. Notice that the basin area in this study is ranging from 2842 to 159300 km^2, hence the spatial effect using gridded CCLM and REMO data is assumed to be minor when considering that the mass balance is generally kept (see example in the next section) and taking into account the impact of the bias between observed and simulated climate as shown in **Fig. 4-3** and **4-4**.

In a preceding study, Huang *et al.* (2010) applied the eco-hydrological model SWIM to model the overall water balance for the same five largest river basins in Germany and obtained satisfactory results on both daily river discharge and average annual water components. In this study, SWIM model was applied with a focus on the high flows (95 and 99 percentile discharges), flood events (with 10- or 30-year return period) and extreme flood events (50-year return period). In order to better simulate the peak discharges especially for the main tributaries, the river discharge at 12 gauge stations, which are representative for the flood conditions in the main rivers and some large tributaries, were calibrated and validated based on observed climate data, and 3 additional gauges were included in the validation procedure. The validated model was then directly driven by each RCM realization to generate daily discharges at the selected gauges. The results were specifically analyzed for flood conditions by applying GEV for the annual maximum discharges, producing the changes in 30-year flood generation over the whole simulation period. In addition, to better estimate the extreme flood condition, *e.g.* 50-year flood values, three time slices of 40 years each were analyzed separately (1961 – 2000 as the control period, and 2021 – 2060 and 2061 – 2100

as the scenario periods). The 50-year flood values estimated from the scenario periods were compared to the ones from the control period to indicate changes in extreme events.

4.3.5. Data preparation

To setup the SWIM projects for the five basins, four spatial maps are needed: the digital elevation model (DEM), the soil map, the land use map and the sub-basin map. All four maps in a grid format with 250 m resolution were used.

The DEM was provided by the NASA (National Aeronautics and Space Administration) Shuttle Radar Topographic Mission (SRTM).

The soil map of the study area was merged from the general soil map of the Federal Republic of Germany "BÜK 1000" produced by the Federal Institute for Geosciences and Natural Resources (BGR), the soil map of the Czech Republic (Kosková *et al.*, 2007), and the soil map from the European soil database (European Communities - DG Joint Research Centre).

The standard sub-basin map for Germany from the Federal Environment Agency (Umweltbundesamt), and the sub-basin map for the Czech Republic (T.G.M. Water Research Institute) were available. On the basis of the DEM and the stream network, an average drainage area of 100 km^2 was chosen as a threshold to discretize the areas in the Danube and Rhine basins outside of Germany into sub-basins, because the standard sub-basin map for Germany had approximately the same discretization. There are in total 5473 sub-basins used in this study.

The land use map was obtained from the CORINE 2000 land cover data set of the European Environment Agency and the Swiss land cover data 1992 from Swiss Federal Statistical Office GEOSTAT database. Nine land cover types were considered in the study: water, urban areas, cropland, grassland, forest coniferous, forest deciduous, forest mixed, wetland, and bare soil. Land use patterns were assumed to be static in the reference and scenario periods in this study, as the study focused on climate change impacts only.

Observed climate data (temperature, precipitation, solar radiation and relative humidity) is available at 2546 climate and precipitation stations located in Germany, the Czech Republic, Austria and Switzerland. However, observed climate data for the French part of the Rhine basin were not available. So, the daily temperature and precipitation data from the "Daily high-resolution gridded climate data set for Europe" (www.ensembles-eu.org) were applied for this region. In addition, the solar radiation was estimated with a regression equation based on the correlation between the solar radiation and the differences between the daily maximum and minimum temperatures measured at German and Swiss stations, and the relative humidity was interpolated using the observed values from the two neighboring countries. With the improved climate data, the calibration and validation results are much better for the whole Rhine than those in Huang *et al.*, 2010 (see section Model calibration and validation). Also, the results for the Danube were improved compared to the previous study due to better data available for the Austrian part.

The discharge data at the 15 selected gauges, which was used to calibrate and validate the model, was obtained from GRDC (The Global Runoff Data Centre), 56068 Koblenz, Germany and from the data base of the Potsdam Institute for Climate Impact Research.

The two dynamical models CCLM and REMO offer the climate control and scenarios for Europe, so they cover the whole study area. However, as already mentioned before, the climate scenario produced by WettReg was only available for the meteorological stations in Germany. Hence, the

simulation of climate change impacts on floods in the scenario periods driven by WettReg was only possible for rivers whose basins are entirely located within German territory.

In addition, the dynamical models offer the spatial climate data which represent the climate variables averaged for each grid cell whereas the statistical-empirical model provides the station-based data considering the unique properties for each station, *e.g.* elevations and soil. Hence, the climate data at one station is incomparable with the smoothed data of the corresponding grid cell. As the homogenization of the climate data from different datasets is necessary, the climate data (both spatial and point data) were interpolated into the centroids of the sub-basins using the inverse-distance method with terrain-correction. To ensure that the total amount of areal precipitation in the RCMs (especially CCLM and REMO with smoothed data) equals the precipitation input into SWIM, the data which intercept each basin were selected for interpolation. The interpolated climate data were then compared with the original RCM data for each basin, and only small negligible differences were found. For example, in the Weser basin, the annual average precipitation interpolated from CCLM (two realizations) and REMO control runs (1961 – 2000) is 906, 904 and 895 mm and the areal precipitation in the original RCM data is 915, 910 and 873 mm respectively (0.7 – 2.5% differences). This confirms that the method applied in this study is capable of adequately representing the RCM data for large river basins.

4.4. Model calibration and validation

The parameter estimation routine PEST (Doherty, 2004) was applied to optimize the calibration procedure referring to discharge at 12 selected gauges in the period from 1981 to 1990 (**Table 4-3**). In the calibration period, all daily discharges, even for the gauges which were not specifically calibrated, were well reproduced with NSE greater than 0.8 and the deviation in water balance within ±3% (see **Table 4-3**, col. 5 and 6). In the validation period (1961 – 1980), all the efficiencies are still above 0.7 and the deviation in water balance is within ±7%. **Table 4-3** also gives the criteria values for the whole control period (1961 – 2000), which show that most of the discharge generated by SWIM is still well reproduced for a long period. It is worth mentioning that in this study SWIM was calibrated and validated as usual, *i.e.* using usual optimization criteria, which were not specifically tailored for high flow periods and flood events.

In addition, the average daily discharge for the period 1961 – 2000 simulated with observed climate data as well as with different RCM control runs is shown in **Fig. 4-3** at six selected gauges. The result confirms again the quality of the simulated daily discharge using observed climate data, and moreover reflects the different characteristics of the RCM control runs driving hydrological simulations. It is obvious that the average daily discharge can be well reproduced using WettReg at all selected gauges. The seasonal dynamics driven by REMO is reasonably well reproduced at most of the gauges except Hofkirchen in the Danube basin. The shape of the seasonal dynamics is also well simulated using the two CCLM control runs but with a significantly overestimated water discharge over the whole year.

Table 4-3: Simulation of water discharge by SWIM: statistical criteria of fit during calibration, validation and control periods at the selected gauges.

River basin	Rivers	Gauges	Area (km²)	Calibration period 1981 - 1990		Validation period 1961 - 1980		Control period 1961 - 2000	
				Nash & Sutcliffe efficiency	Deviation in water balance	Nash & Sutcliffe efficiency	Deviation in water balance	Nash & Sutcliffe efficiency	Deviation in water balance
Ems	Ems	Versen	2842	0.88	0%	0.86	-7%	0.87	-9%
Weser	Weser	Intschede	37720	0.90	1%	0.89	-5%	0.90	0%
	Werra	Letzter Heller	5487	0.85	1%	0.83	-4%	0.83	1%
	Weser	Vlotho[1]	17618	0.87	0%	0.84	-2%	0.85	0%
Danube	Danube	Hofkirchen	47496	0.87	0%	0.83	-5%	0.84	-3%
	Danube	Donauwoerth	15037	0.82	-1%	0.79	-2%	0.79	-3%
	Inn	Passau Ingling	26084	0.83	-2%	0.84	-1%	0.76	0%
	Danube	Achleiten [1]	76653	0.87	-1%	0.86	-4%	0.86	-2%
Rhine	Rhine	Rees[1]	159300	0.89	3%	0.89	-1%	0.89	1%
	Main	Frankfurt-Osthafen	24764	0.83	-1%	0.77	3%	0.82	1%
	Neckar	Rockenau SKA	12710	0.80	-1%	0.75	4%	0.78	1%
	Rhine	Rheinfelden	34550	0.83	0%	0.81	1%	0.83	1%
Elbe	Elbe	Neu-Darchau	131950	0.83	0%	0.85	-1%	0.84	2%
	Mulde	Bad Dueben	6171	0.80	-1%	0.79	1%	0.80	4%
	Saale	Calbe-Grizehne	23719	0.80	1%	0.81	-2%	0.78	3%

[1] gauges not calibrated

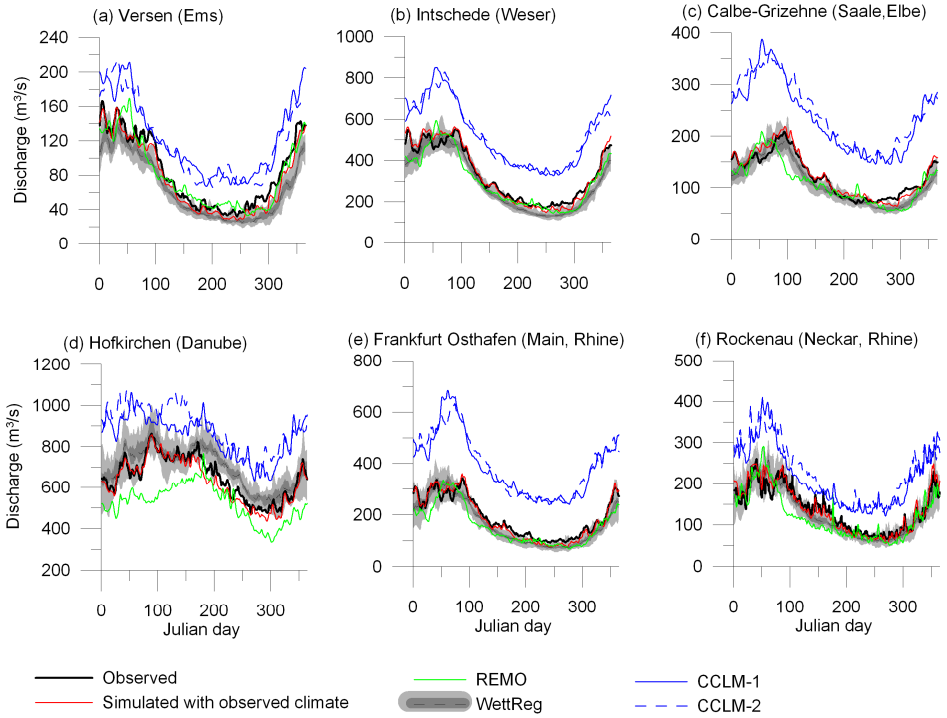

Figure 4-3: Observed and simulated average daily discharges driven by observed climate data and the three RCMs (CCLM, REMO and WettReg) control funs at the six selected gauges.

Regarding the main focus of the study, it is essential to assess the modelling performance of SWIM for flood events. In addition, a comparison of high flows observed in the control period and simulated by SWIM driven by observed data and RCMs data for the same period is of interest. **Table 4-4** lists the 95 and 99 percentile discharges of the observed discharge, and the simulated discharge by SWIM using observed climate data and climate data from three RCMs: REMO, CCLM (two realizations) and WettReg (the medium value from 20 realizations) during the control period. In **Table 4-4**, the percentiles are marked, indicating the significance of the deviation in percentiles between 1) the simulation results using the observed and RCMs-generated climate and 2) the observed discharge data. The dark grey shadowing means large absolute difference (> 50%), and the light grey shadowing indicates moderate absolute difference (21% – 50%). As climate data for WettReg was only available for Germany, simulation with WettReg data for 5 gauges having inflow from other countries was not possible (see no-data boxes in **Table 4-4** – **Table 4-8**). At most of the selected gauges, the 95 and 99 percentiles of the simulated discharge using observed climate data have a good agreement with those for the observed discharge, with the deviation within ±10%, which can be considered as a satisfactory result. However, the simulated high flows (95 and 99 percentiles) obtained by using RCM-generated climate have a generally greater bias with those for the observed high flows (see **Table 4-4**, col. 4-7 and 10-13).

For both 95 and 99 percentiles, simulated results with WettReg obviously provide the best results for most rivers in Germany compared to those with REMO and CCLM. However, WettReg-driven results always lead to underestimations in north-western regions (Ems and Weser basins). REMO can be considered as the second best climate model in reproducing high flows, as 9 – 10 of 15 simulated results driven by REMO control runs have a bias of less than 20%. The highest differences were produced by SWIM driven by CCLM climate, for which much higher flows were generated in practically all cases. Only in 3 cases of 15 are the differences within 20% for the 95 percentiles, and a slightly better performance is found for the 99 percentiles (7 cases of 15).

The comparison of high flows is insufficient to evaluate the model performance for flood conditions. Hence, the extreme values were also analyzed by estimating the 10- and 50-years return floods using the GEV method. The 10- and 50-years flood levels estimated from the simulation results could be also compared with those estimated for the observed discharge (**Table 4-5**): the differences are marked in the same way as in **Table 4-4**. Besides, **Figure 4-4** (a, c, e) shows some examples of GEV plots for the observed and simulated (using observed climate data) annual maximum daily discharge, and three GEV plots (b, d, f) comparing annual maximum observed and simulated with RCM control runs at three selected gauges (Versen (Ems), Vlotho (Weser) and Calbe-Grizehne (Saale, Elbe)).

In general, SWIM could also satisfactorily reproduce 10- and 50-years floods using observed climate data in most of the cases (see **Table 4-5**), and the GEV fitting curves for the observed values are well comparable with those for the simulated values (see **Fig. 4-4(a)** and **4-4(c)** as examples). Only for one gauge is there a pronounced overestimation of both 10-year and 50-year floods simulated with observed climate data at the gauge Calbe-Grizehen (Saale, Elbe). **Figure 4-4(e)** shows this worst simulation result.

Flood estimation based on the dynamical RCMs driven simulations (**Table 4-5**, **Fig. 4-4(b)** and **4-4(d)**) shows lower differences with observational data compared to the high flow simulations represented in **Table 4-4**. The results under the REMO control runs are closer to the observed floods than those under the CCLM control runs. Considering simulations using WettReg, we can conclude that the agreement between the simulated flood levels and observed values (see **Table**

4-5 and **Fig. 4-4(f)**) is lower than that for the high flows (**Table 4-4**), although the differences in most cases are still within 20% for both flood levels.

In summary, the mean river discharge and the extreme events in the control period are reproduced better in simulations driven by WettReg than by the dynamical RCMs. However, as claimed by Lenderink *et al.* (2007), the direct use of dynamical RCM scenarios enables to represent the complex changes in the circulation types which are strongly related to floods in Germany (cf. Petrow *et al*., 2009). Hence the dynamical RCMs in combination with an eco-hydrological model could provide valuable information on the potential extreme events in a changing climate and, as such, they are useful to account for uncertainty of the potential changes. Under the assumption of analogous systematic error of an individual RCM in both control and scenario runs, the extreme values estimated for scenario horizons were compared to the ones in the control period using the same climate models. This method emphasizes the change pattern projected in each model. Nevertheless, IPCC (2007) indicates that the direction of change can be more reliable than the absolute values. Therefore, we fairly consider all the scenario results from all the models as spanning the uncertainty range for the future changes.

Table 4-4: The 95 and 99 percentile of the observed discharge (col. 1 and 7) and simulated discharge by SWIM driven by observed climate (col. 2 and 8) and RCMs (col. 3 – 6 and col. 9 – 12) during control period (1961 – 2000) (dark grey color: large absolute difference (> 50%) of the observed discharge compared with the simulated discharges driven by observed climate data and the control runs of RCMs; light grey color: large medium absolute difference (21% – 50%); bold font: medium absolute difference (10% – 20%) and regular font: no significant difference (< 10%), (-) simulation was not possible).

	Observed 95 percentile discharge col. 1	Simulated 95 percentile discharge by SWIM with observed climate col. 2	REMO col. 3	CCLM_1 col. 4	CCLM_2 col. 5	Wettreg col. 6	Observed 99 percentile discharge col. 7	Simulated 99 percentile discharge by SWIM with observed climate col. 8	REMO col. 9	CCLM_1 col. 10	CCLM_2 col. 11	Wettreg col. 12
Versen	234	224	213	282	**278**	**189**	370	**330**	**326**	**407**	402	290
Intschede	838	838	**704**	1036	**1000**	**710**	1226	1221	**1081**	**1437**	1332	**1024**
Letzter Heller	133	145	**114**	163	161	127	232	229	**186**	230	216	**196**
Vlotho	440	451	337	**488**	**484**	**385**	744	714	535	712	**661**	589
Hofkirchen	1210	1128	945	**1429**	**1457**	1221	1759	1617	1252	**1989**	**1984**	1777
Donauwoerth	401	366	312	**449**	**459**	389	618	586	465	670	**685**	629
Passau Ingling	1460	1503	1899	2129	2195	-	2064	2052	2488	2776	2925	-
Achleiten	2580	2537	2690	3286	3317	-	3480	3344	3457	**4133**	4212	-
Rees	4740	4715	4494	5796	5811	-	6830	6284	**5930**	**7532**	7345	-
Frankfurt-Osthafen	494	536	**447**	848	827	476	868	849	**694**	1226	1114	787
Rockenau SKA	350	365	340	492	499	345	677	657	**603**	823	**778**	**606**
Rheinfelden	1880	1928	2725	2915	2935	-	2353	2394	3324	3560	3611	-
Neu-Darchau	1608	1708	1280	2574	2525	-	2164	2364	**1845**	3285	3187	-
Bad Dueben	171	**188**	**190**	250	244	184	308	295	321	391	362	294
Calbe-Grizehne	291	300	**255**	484	479	270	440	443	**395**	686	652	408

Table 4-5: The 10- and 50-year flood level observed and simulated by SWIM driven by observed climate and RCMs during control period (1961 – 2000) (color regimes: the same as in Table 4-4).

	Observed 10-year flood level col. 1	Simulated 10-year flood levels by SWIM with observed climate col. 2	REMO col. 3	CCLM_1 col. 4	CCLM_2 col. 5	Wettreg col. 6	Observed 50-year flood level col. 7	Simulated 50-year flood level by SWIM with observed climate col. 8	REMO col. 9	CCLM_1 col. 10	CCLM_2 col. 11	Wettreg col. 12
Versen	537	503	492	**615**	581	**433**	674	650	623	**758**	**794**	**599**
Intschede	1785	1747	**1429**	**1970**	1687	**1478**	2283	2123	1638	2402	**2034**	**1889**
Letzter Heller	345	343	**289**	347	**289**	**288**	417	442	412	**481**	**357**	**366**
Vlotho	1051	1114	**891**	1138	992	**928**	1209	**1365**	1173	1579	1302	1174
Hofkirchen	2586	2661	**2311**	3328	**2890**	2816	3295	3978	**3754**	4639	**3658**	3461
Donauwoerth	995	978	966	1250	1280	**1133**	1196	1279	**1400**	1689	1868	1510
Passau Ingling	3532	**3191**	3308	3724	**4149**	-	4636	4350	**4009**	4379	**5216**	-
Achleiten	5017	4757	4887	**5935**	**5826**	-	6094	6085	**7314**	8276	7453	-
Rees	9455	9157	**7765**	9978	10325	-	11378	10903	**9659**	11633	12452	-
Frankfurt-Osthafen	1459	1415	1061	**1740**	1524	**1220**	1958	1788	1320	2098	1782	**1678**
Rockenau SKA	1690	**1501**	**1497**	1567	1672	1328	2470	2282	2514	1937	2601	**2061**
Rheinfelden	3295	3276	4853	5423	5080	-	3902	4199	5840	6960	6557	-
Neu-Darchau	2865	2887	**2391**	3961	3789	-	3529	3320	**3112**	4503	5374	-
Bad Dueben	696	**589**	667	840	685	**603**	1162	782	**959**	1060	1074	**927**
Calbe-Grizehne	585	727	632	978	933	**650**	700	1055	901	1222	1288	946

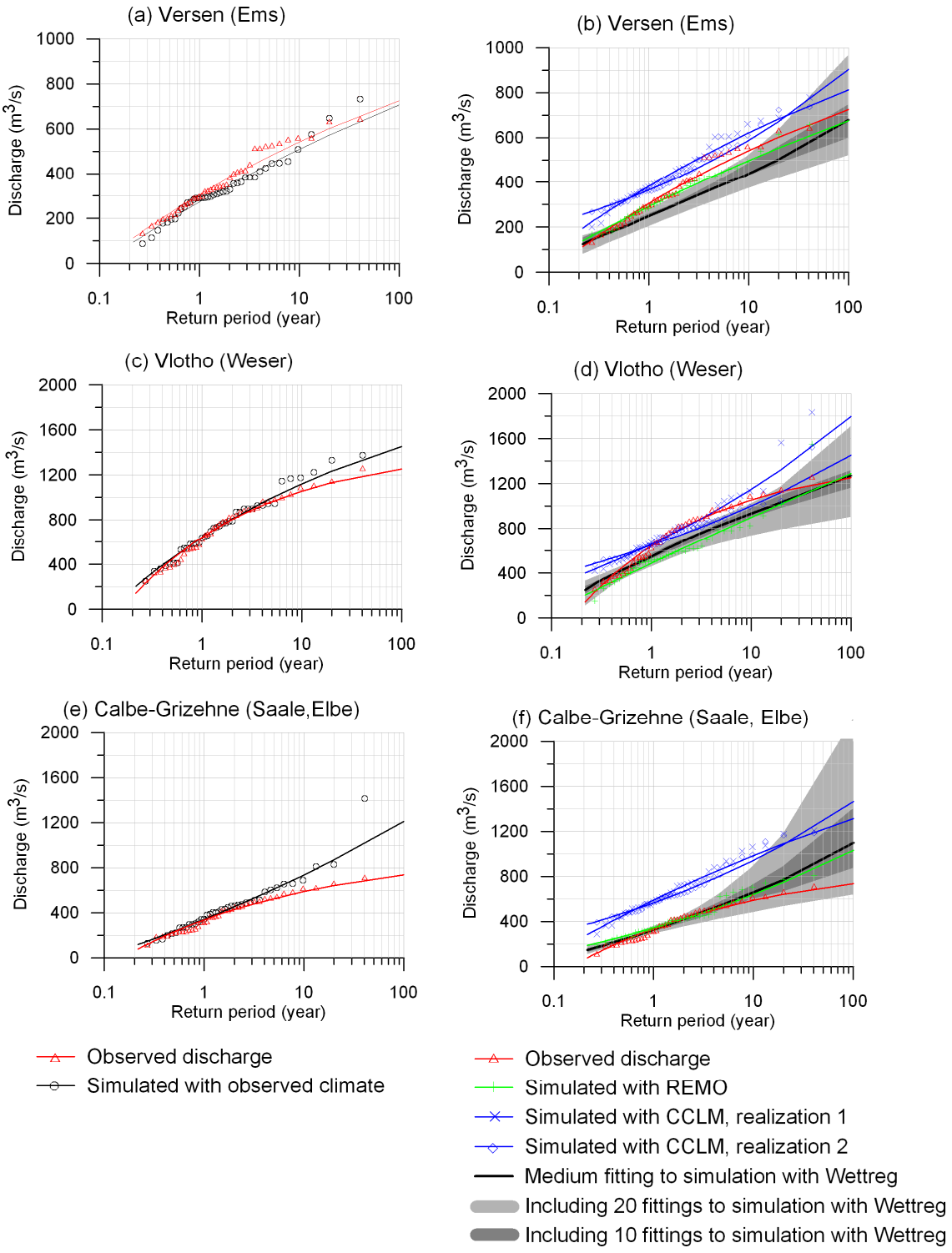

Figure 4-4: Generalized Extreme Value (GEV) plots for the annual maxima of daily discharge observed and simulated with observed climate data during control period at the gauge Versen (a), Vlotho (c) and Calbe-Grizehne (e) as well as the comparison of GEV plots of the annual maxima simulated with the three RCMs (CCLM, REMO and WettReg) and the observed discharge at the same gauges (b), (d) and (f).

4.5. Scenario results

4.5.1. Comparison of projected high discharges for future climate conditions

The 95 and 99 percentiles of the simulated discharge driven by RCMs under different emission scenarios were calculated and compared with the ones driven by the corresponding RCMs control runs. The percentage changes in the high discharges are listed in **Tables 4-6**, **4-7** and **4-8** and classified into four categories. The dark grey color highlights a strong increase (≥10%), while the light grey color marks a significant decrease (≤-10%). The numbers with normal font refer to no change or increase up to 9%, and the numbers in bold indicate decrease down to -9%.

In general, the analysis of **Tables 4-6** – **4-8** shows that the results are very diverse under different RCM scenarios for each basin. For the gauges Versen, Intschede, Letzter Heller and Vlotho located in the two northwestern basins Ems and Weser that are dominated by maritime climate, a positive change in the 95 percentile discharge is suggested by 70% of scenario results for the period 2021 – 2060. Notice that most of the negative changes are driven by WettReg. However, during the second scenario period, all the projections show an increase in the 95 percentile discharge regardless of the emission scenarios. For the 99 percentile discharges, more than 60% of all the projections indicate a decrease or no change under the A1B and B1 scenarios in both periods. In contrary, under the A2 scenario an obvious decrease is found for 2021 – 2060 with a dominant increase in 2061 – 2100. The results show that the general high flows (95 percentile) may tend to increase but not the maximum ones (99 percentile) in this region.

In the northeast region, where the Elbe basin is located and the continental climate is more dominant, the change direction in both 95 and 99 percentile discharges can be hardly agreed driven by all the RCMs for each scenario. Only the 95 percentile in the period of 2021 – 2060 under the A1B scenario and in the period of 2061 – 2100 under the B1 scenario show an increasing trend in 9 out of 11 projections. A dominant decreasing trend can only be found for the 99 percentile discharge in 2061 – 2100 under the A1B scenario. Worthy to note that most increasing changes are driven by REMO scenarios, and all the changes driven by WettReg are negative.

For the two basins in the south: the Danube and Rhine, the change in high flows is related to the hydrological regimes of the specific river reaches. For meltwater-dominated rivers (*e.g.* the Inn at the gauge Passau Ingling, Danube at the gauge Achleiten and Rhine at the gauge Rheinfelden), a strong decrease in both the 95 and 99 percentile discharges are suggested by almost all the projections in the second scenario period. For the rainfall-dominated rivers (*e.g.* at gauges Hofkirchen, Donauwoerth, Rees, Frankurt-Osthafen and Rockenau SKA), more than 60% of the projections show an increase in the 95 percentile discharges in both periods and in 99 percentile discharge in the first scenario period. However, the changes in the 99 percentile discharge for the second period are not clear with both positive and negative changes projected.

The change in the high flows, particularly the 95 percentile discharge for different rivers, can be related to the characteristics of the seasonal climate variables for each region. In general, all the RCMs project a steady increase of temperature by 2 – 3 °C over Germany by the end of this century. The changes in annual precipitation are generally within ±5% for each basin, and a distinct shift of seasonal precipitation is projected in the studied area by all models.

Table 4-6: The percentage changes in 95 and 99 percentiles of the simulated discharge driven by RCMs between the control period and two scenario periods under the emission scenario A1B (dark grey color: significant increase (≥ 10%); normal number: not significant increase (0-9%); bold number: not significant decrease (-9% - -1%) and light grey color: significant decrease (≤ -10%))

	2021 - 2060								2061 - 2100							
	% change in 95 percentile discharge (m^3/s) simulated by SWIM with				% change in 99 percentile discharge (m^3/s) simulated by SWIM with				% change in 95 percentile discharge (m^3/s) simulated by SWIM with				% change in 99 percentile discharge (m^3/s) simulated by SWIM with			
Gauges	REMO	CCLM_1	CCLM_2	Wettreg	REMO	CCLM_1	CCLM_2	Wettreg	REMO	CCLM_1	CCLM_2	Wettreg	REMO	CCLM_1	CCLM_2	Wettreg
Versen	10	10	9	0	1	0	5	**-9**	7	6	9	12	5	0	3	1
Intschede	15	7	8	**-5**	2	**-3**	7	**-8**	7	2	6	11	**-1**	**-3**	**-1**	6
Letzter Heller	12	7	5	**-9**	0	0	2	-13	8	3	2	9	**-5**	**-5**	**-5**	2
Vlotho	11	7	7	**-5**	2	**-3**	5	**-7**	7	3	4	15	**-6**	**-8**	**-2**	8
Hofkirchen	7	4	3	-13	11	1	3	-12	**-4**	1	0	-19	4	1	**-5**	-15
Donauwoerth	8	2	4	-13	13	1	1	-12	**-2**	**-2**	**-4**	-19	5	2	**-4**	-18
Passau Ingling	**-2**	**-1**	**-4**	-	**-2**	1	**-2**	-	-19	-10	-15	-	-13	**-6**	-10	-
Achleiten	0	1	0	-	0	1	5	-	-13	**-5**	**-6**	-	-10	**-1**	**-6**	-
Rees	8	8	8	-	8	4	11	-	7	6	7	-	-20	1	6	-
Frankfurt-Osthafen	11	5	6	**-9**	5	**-1**	8	**-8**	5	1	3	13	1	**-8**	1	8
Rockenau SKA	7	3	4	**-8**	3	**-4**	0	**-9**	1	**-1**	**-3**	2	**-5**	-12	**-8**	2
Rheinfelden	**-3**	**-7**	**-5**	-	1	**-5**	**-5**	-	-25	-23	-23	-	-17	-13	-20	-
Neu-Darchau	20	5	5	-	15	2	**-1**	-	4	**-1**	3	-	-6	**-3**	**-1**	-
Bad Dueben	9	4	5	-17	7	**-5**	9	-19	**-3**	**-5**	**-1**	-31	-11	**-6**	3	-30
Calbe-Grizehne	22	6	7	-21	20	**-1**	5	-19	10	2	2	-13	10	**-3**	**-3**	-19

Table 4-7: The percentage changes in 95 and 99 percentiles of the simulated discharge driven by RCMs between the control period and two scenario periods under emission scenario B1 (color regimes: the same as in Table 4-6)

	2021 - 2060								2061 - 2100							
	% change in 95 percentile discharge (m^3/s) simulated by SWIM with				% change in 99 percentile discharge (m^3/s) simulated by SWIM with				% change in 95 percentile discharge (m^3/s) simulated by SWIM with				% change in 99 percentile discharge (m^3/s) simulated by SWIM with			
Gauges	REMO	CCLM_1	CCLM_2	Wettreg	REMO	CCLM_1	CCLM_2	Wettreg	REMO	CCLM_1	CCLM_2	Wettreg	REMO	CCLM_1	CCLM_2	Wettreg
Versen	8	5	0	4	4	**-3**	**-8**	**-2**	10	6	6	7	2	0	3	0
Intschede	10	4	1	1	**-3**	**-5**	**-2**	2	14	4	8	4	**-5**	**-3**	**-1**	0
Letzter Heller	10	6	**-1**	**-1**	-4	**-4**	3	**-2**	12	4	4	1	**-6**	**-5**	**-5**	**-5**
Vlotho	10	5	**-1**	1	-2	**-2**	0	1	13	4	6	7	**-4**	**-8**	**-2**	2
Hofkirchen	7	6	0	**-4**	12	8	0	**-5**	4	1	1	-15	7	1	**-5**	-12
Donauwoerth	11	8	1	**-2**	12	10	1	**-3**	5	1	**-3**	-15	10	2	**-4**	-13
Passau Ingling	3	3	**-6**	-	6	5	**-7**	-	**-5**	**-7**	-11	-	**-4**	**-6**	-10	-
Achleiten	4	3	**-4**	-	6	7	**-5**	-	**-3**	**-4**	**-5**	-	**-5**	**-1**	**-6**	-
Rees	10	7	5	-	6	1	9	-	9	4	5	-	7	0	11	-
Frankfurt-Osthafen	8	6	0	1	6	**-3**	5	3	11	3	3	3	4	**-8**	1	1
Rockenau SKA	7	8	1	3	3	**-1**	9	3	3	3	1	**-7**	**-1**	-12	**-8**	**-6**
Rheinfelden	2	**-1**	**-9**	-	5	1	**-5**	-	-11	-17	-17	-	**-4**	-13	-20	-
Neu-Darchau	16	2	**-3**	-	6	**-3**	**-6**	-	18	4	5	-	8	**-3**	**-1**	-
Bad Dueben	6	**-1**	**-4**	**-7**	5	**-1**	1	-11	10	2	4	-21	12	**-6**	3	-25
Calbe-Grizehne	20	5	0	**-7**	15	1	1	**-3**	22	6	7	-12	17	**-3**	**-3**	-13

Table 4-8: The percentage changes in 95 and 99 percentiles of the simulated discharge driven by RCMs between the control period and two scenario periods under emission scenario A2 (color regimes: the same as in Table 4-6)

	2021 - 2060				2061 - 2100			
	% change in 95 percentile discharge (m^3/s) simulated by SWIM with		% change in 99 percentile discharge (m^3/s) simulated by		% change in 95 percentile discharge (m^3/s) simulated by		% change in 99 percentile discharge (m^3/s) simulated by	
Gauges	REMO	Wettreg	REMO	Wettreg	REMO	Wettreg	REMO	Wettreg
Versen	0	1	0	**-5**	13	8	5	1
Intschede	5	0	**-3**	**-4**	15	6	3	2
Letzter Heller	4	**-3**	**-3**	**-8**	13	2	6	**-4**
Vlotho	6	1	1	**-2**	16	9	5	5
Hofkirchen	4	-15	5	-18	8	-22	18	-15
Donauwoerth	4	-15	1	-19	9	-25	15	-19
Passau Ingling	**-1**	-	1	-	**-6**	-	**-2**	-
Achleiten	**-1**	-	0	-	**-1**	-	3	-
Rees	4	-	2	-	15	-	19	-
Frankfurt-Osthafen	1	**-5**	1	**-4**	17	4	16	0
Rockenau SKA	**-2**	**-6**	**-7**	**-8**	10	-13	5	-10
Rheinfelden	**-4**	-	**-1**	-	-14	-	**-8**	-
Neu-Darchau	7	-	8	-	13	-	6	-
Bad Dueben	0	-19	1	-21	7	-27	12	-32
Calbe-Grizehne	12	-16	9	-16	19	-15	14	-14

In the northwest area, where the high flows generally occur in cold half-year (October-April), the winter precipitation may increase in the range of 10 – 20%. The summer precipitation may decrease by 3 – 15%, especially in the second scenario period. Hence, an increase in the 95 percentile discharge is often projected.

In the Elbe region, the increasing trend of winter precipitation is not as strong as in the other basins, and therefore the change direction varies due to the combined effect of higher evapotranspiration under the warmer climate and more precipitation.

For the meltingwater-dominated rivers in the southern part of the Danube and Rhine basins, where the high flows occur in the summer season, the runoff generation is influenced by two factors. The first factor is a higher temperature which can lead to higher runoff due to stronger snow and ice melting in summer. The second factor is a remarkable decrease in precipitation in summer, especially at the end of this century, which can reduce the level of runoff. Hence, there is a mixture of change directions for the first period and a dominant decreasing trend in the second period.

At last, the results regarding high flows produced using three climate models were analyzed by the histograms built on all results presented in **Tables 4-6** – **4-8** (**Fig. 4-5**). The statistical-empirical model WettReg leads to quite a different trend direction compared to the dynamical models. REMO projects more increase in high flows, and WettReg indicates drier conditions, especially in southern and eastern regions. The two CCLM realizations generated some opposite trend directions at 99 percentile discharges especially under B1 scenario, but most of results with CCLM, about 70%, demonstrate rather minor changes, within ±10%. The two dynamical models, REMO and CCLM, show a higher frequency of agreement compared to agreement of all three RCMs.

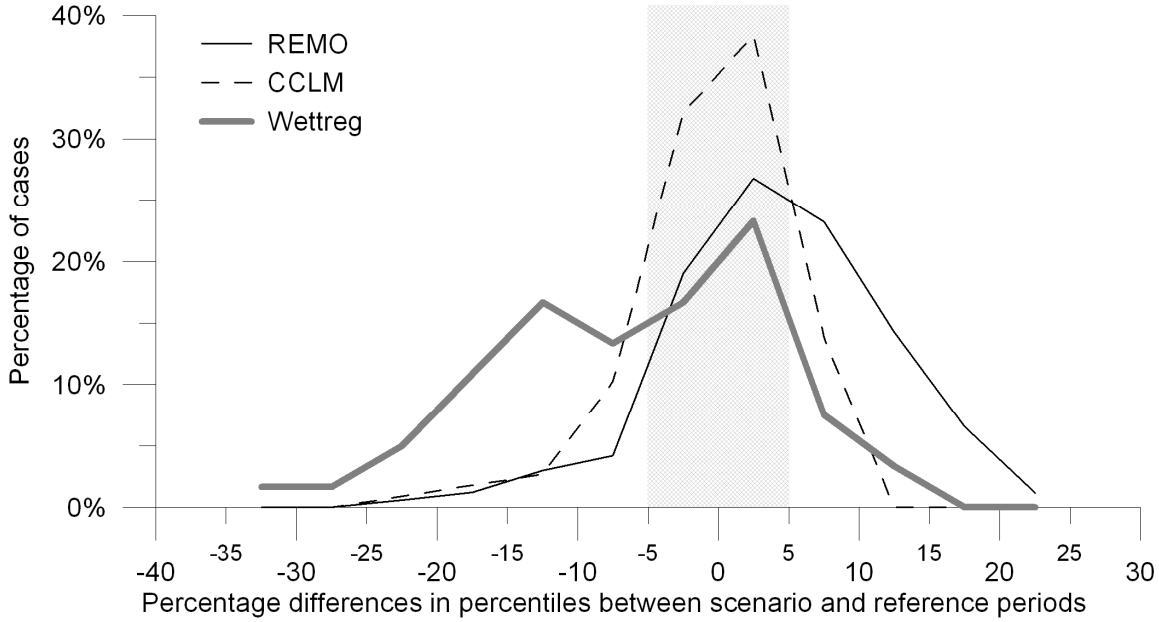

Figure 4-5: The distribution function of percentage differences in 95 and 99 percentile discharges between scenario and reference periods; dataset includes 15 stations, 2 scenario periods and 3 emission scenarios.

4.5.2. Comparison of projected floods

The flood events, namely 30-year and 50-year flood levels, were estimated using GEV distribution function fitted to annual maxima of daily discharge simulated with three climate models. At the first step, the 30-year flood was generated for some selected gauges for each RCM over the whole simulation period aiming at revealing the characteristics of temporal flood generation patterns projected by different models. Secondly, the 50-year flood levels were estimated for all 15 gauges during the control period 1961 – 2000 and two scenario periods 2021 – 2060 and 2061 – 2100 separately. The changes in the 50-year flood level between the control and scenario periods projected by three RCMs are illustrated on spatial maps for each scenario and period. The overall results were summarized and depicted as box-and-whisker plots showing the main trend directions, and separately for the dynamical models and the statistical-empirical model WettReg. Finally, the change in seasonality as projected by different models was explored.

4.5.2.1. 30-year flood level for selected gauges over the whole period

Figure 4-6 illustrates the 30-year floods generated using REMO from 1951 to 2100 at gauges Versen (Ems) and Bad Dueben (Mulde, the tributary of the Elbe) under three emission scenarios. The choice of Versen is due to good simulation results under the REMO control run (**Fig. 4-4**), and Bad Dueben was chosen due to full agreement of the increasing trend projected by all three scenarios. The 30-year flood level shown as the solid black line in **Fig. 4-6** is estimated from the annual maximum discharges of every 30 years in the simulation period using the GEV method and the moving window method. For example, the point on the black line at year 1980 is the 30-year flood estimated from the annual maximum discharges in the first 30 year period (1951 – 1980). The flood level at year 1981 is obtained from the period 1952 – 1981, and so on. The grey boundaries indicate 95% confidence level for the estimated 30-year flood levels. The red solid and dash lines stand for the 30-year flood level for the reference period 1961 – 1990, and the corresponding confidence level as the baseline for comparison of flood levels. If the black line is above the red solid line, it implies an increase in 30-year flood level. If the whole grey range is

outside the confidence corridor (the red dash lines), this is a very strong indication of statistically significant increase or decrease in 30-year flood level. As the uncertainty increases with flood level, this is not very often the case for the 30-year floods, although periods with strong changes in flood levels occur.

At the gauge Versen (**Fig. 4-6**), the pronounced increase in the flood level is projected for the last twenty years under the A1B scenario, indicating some extreme events occurring in this period. However, this does not mean that the flood level is always high during the twenty years. Based on the moving window method, one or two extreme events could result in very high flood levels estimated for the subsequent 30 years. Hence, the high flood period in these figures only illustrates the potential time frames when the extreme event can happen. Under A2 scenario, there are two high flood periods projected: around the middle and the end of the century. According to the B1 scenario, strong flood events may occur between 2050 and 2080.

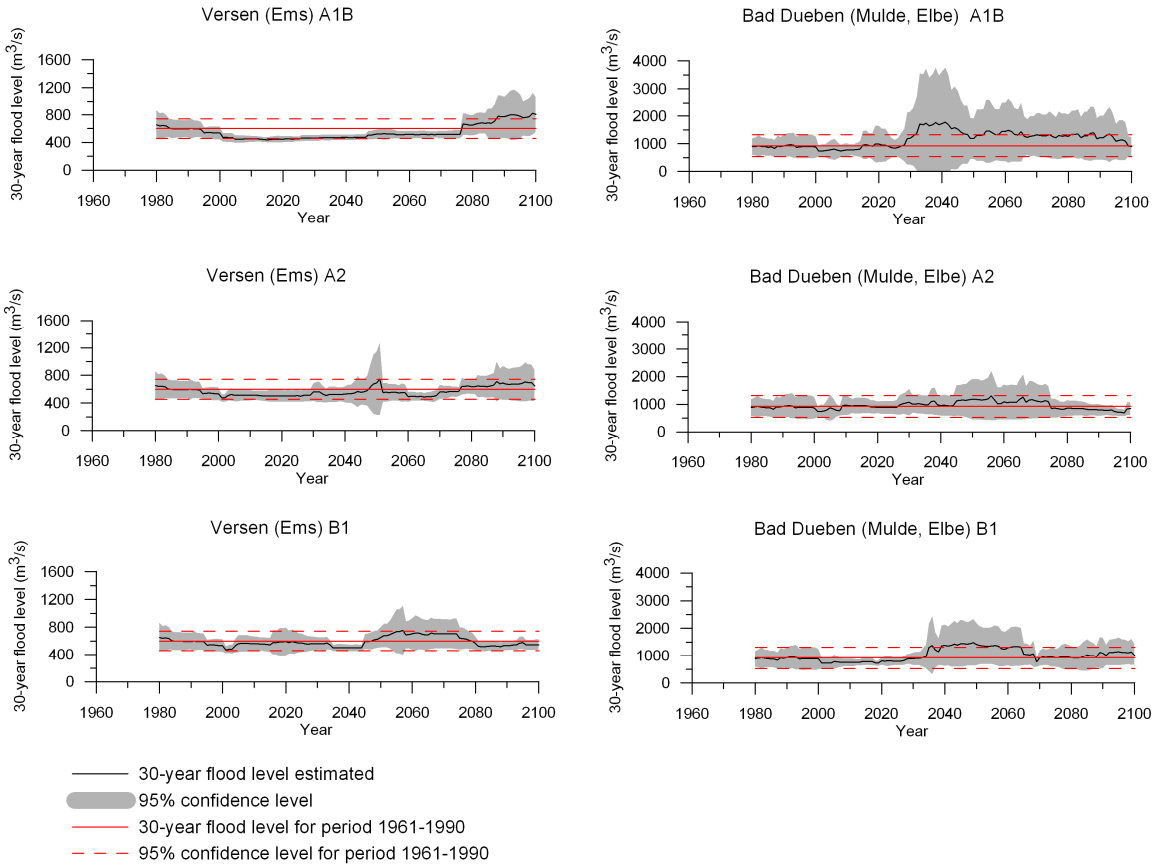

Figure 4-6: 30-year flood level and its 95% confidence level over the whole simulation time at gauge Versen (Ems) and Bad Dueben (Mulde, Elbe) under REMO scenarios.

At Bad Dueben, the projected high flood periods last longer. According to A1B scenario, the flood level exceeds the reference corridor in 2030, and remains very high until the end of the century. Also, a long period of high flood level is projected in B1 scenario: from 2035 to 2065. Under A2 scenario, there is a relatively shorter high flood period (from 2055 to 2065), and the increase in flood levels is moderate.

The flood generation curves show that the flood level does not increase linearly with time, but fluctuates irregularly. According to REMO, the high flood events exceeding the current flood level may likely happen around and after the middle of the century in these two rivers. However, the uncertainty of high flow estimation is much larger than that for the lower flows, as the confidence boundaries of high levels are much wider than those of lower ones. **Figure 4-6** also implicates that analyzing one short scenario period in the flood studies is not sufficient.

Figure 4-7 shows the 30-year flood generation from 1960 to 2100 by CCLM using the same estimation and illustration methods as described above for **Fig. 4-6**. The gauge Vlotho was chosen, because the high flows and floods driven by CCLM control runs have good agreement with the observed values at this gauge. The two realizations (A1B scenario, realization 1 and B1 scenario realization 2) project a similar flood pattern indicating extreme events at the end of the century (2080 – 2100). Other two realizations do not project stronger floods until 2100. The four realizations provided two distinct flood trends, and under each scenario the two realizations differ. It reveals again that the large uncertainties originate not only from the emission scenarios, but also from the boundary condition derived from the GCM.

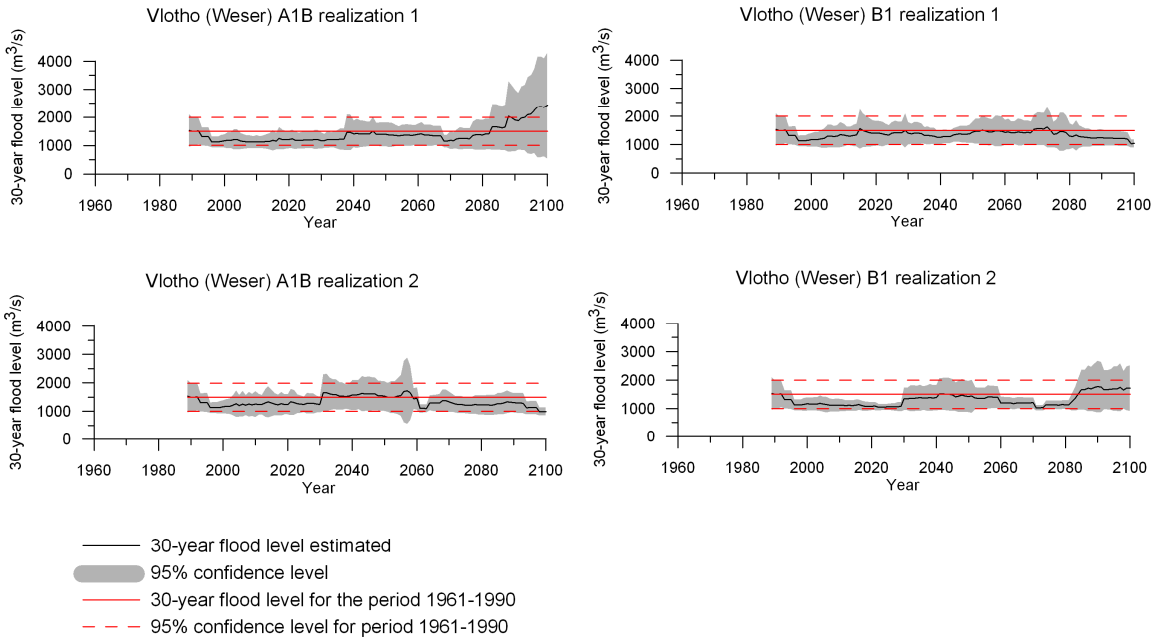

Figure 4-7: 30-year flood level and its 95% confidence level over the whole simulation time at gauge Vlotho (Weser) under CCLM scenarios.

All 20 realizations for each scenario generated from the statistical-empirical model WettReg were applied as climate input for SWIM, and the medium simulation result was considered as the major information indicating changes in flood characteristics. **Figure 4-8** shows the 30-year flood generation at the gauges Calbe-Grizehne (river Saale, a tributary of the Elbe) and Rockenau (river Neckar, a tributary of the Rhine) over the whole simulation period. The former one has downward trends in flood level in all 3 scenarios in both periods, and the latter one shows small trends in both directions. Here, the solid black line stands for the medium flood level from all 20 realizations (different from **Fig. 4-6** and **4-7**). The dark grey boundaries include all 30-year flood levels from 20 realizations, and light grey boundaries depict all confidence levels estimated from 20 realizations.

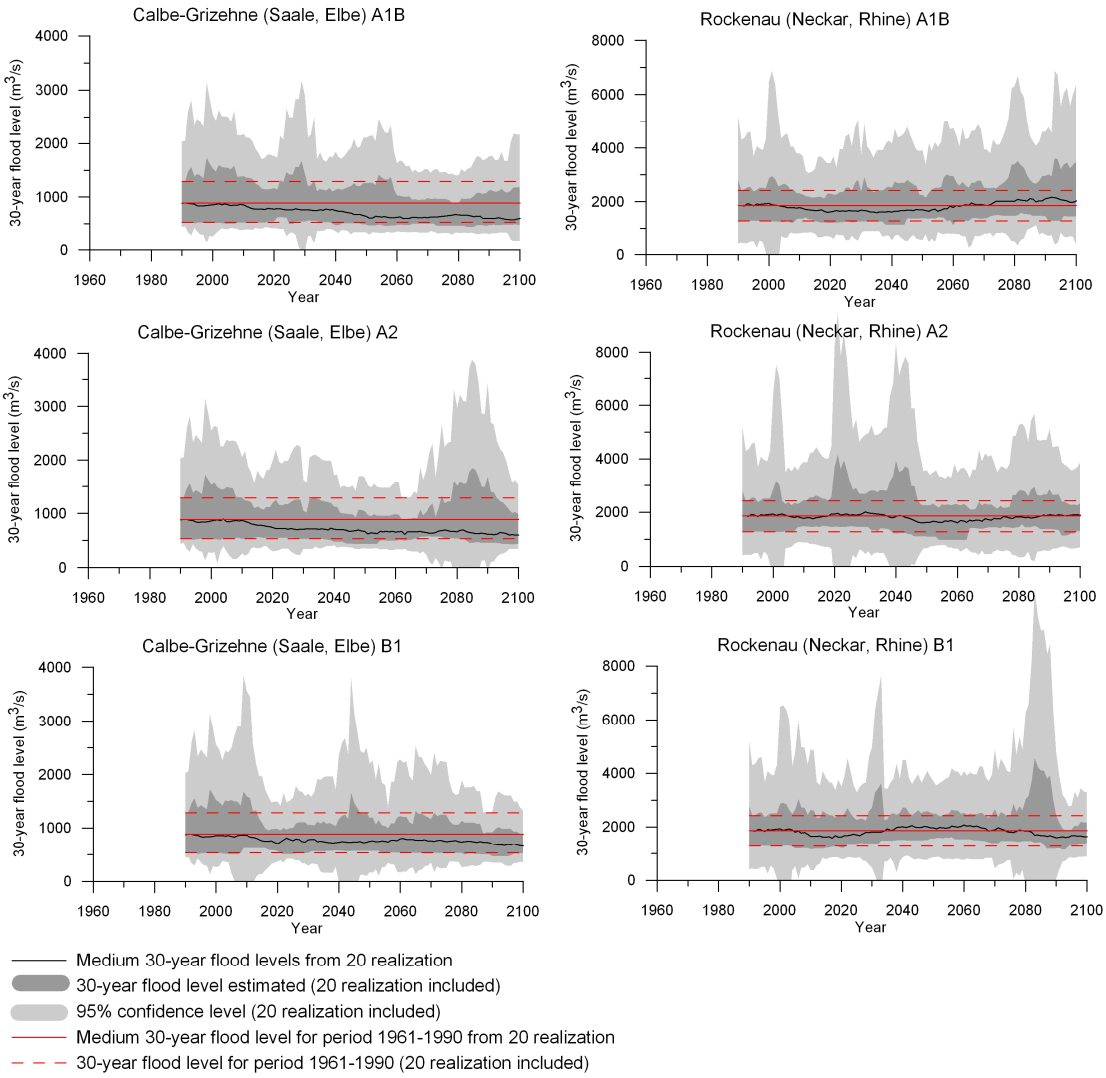

Figure 4-8: Medium 30-year flood level and its 95% confidence level over the whole simulation time at gauge Calbe-Grizehne (Saale, Elbe) and Rockenau (Neckar, Rhine) under WettReg scenarios.

Compared to the dynamical model projections presented above, which have shown more dynamic behaviour, the medium flood level derived from 20 realizations of WettReg goes steadily downward at the gauge Calbe-Grizehne under all three scenarios. This downward tendency is especially pronounced in scenarios A1B and A2, as almost all 20 simulations are below the reference line in 2040 – 2080. At the gauge Rockenau, there are small increasing and decreasing trends in A1B and B1 scenario at the end of the century. It should be noted that although the medium 30-year flood level has a smooth and graduate change pattern, the variation among 20 realizations are pronounced, particularly in some extreme events. Therefore, some peaks of the dark grey boundaries show projected extreme flood conditions, and the wide light grey boundaries also imply the high uncertainty in estimating these extreme values.

4.5.2.2. Changes in the 50-year flood level

The relative changes in the 50-year flood level were analyzed for all 15 gauges. They were subdivided into six categories: strong increase (>20%), moderate increase (11 – 20%), small increase (0 – 10%), small decrease (-10 – 0%), moderate decrease (-19– -10%) and strong

decrease (< -20%) for REMO and CCLM scenarios and two periods (**Fig. 4-9** and **4-10**). As the climate data simulated by WettReg is only available for Germany, the 50-year flood levels are only evaluated for the national rivers (**Fig. 4-11**).

In general, the three scenarios driven by REMO resulted in different changes in flood levels, but some robust regional patterns can still be found. The four realizations driven by CCLM generated various spatial patterns of changes in the 50-year flood levels. All basins show different changes, especially between the two realizations under each scenario. According to the three WettReg scenarios, the change pattern is more consistent for the whole region compared with other RCMs.

For the two northwestern basins (the Ems and Weser), a diversity of trends is projected by simulations driven by REMO in the first period, depending on the emission scenario. From 2061 to 2100, an increase in the 50-year flood level is projected under all three emission scenarios at the gauge Intschede. However, the upstream parts of the Weser River may have noticeable lower flood levels under A2 and B1 scenarios. Under CCLM scenarios, a decrease in flood levels is suggested in the Ems River in both periods by all realizations except A1B realization 1, II period. For the Weser, no clear trend can be found from all realization results, especially in the second period. Namely, a significant increase in flood levels is projected at all three gauges for the A1B realization 1 (but only small changes in realization 2), and the B1 realization 2 (but a strong decrease in realization 1). Driven by WettReg, a downward trend (lower flood level) is projected for all three emission scenarios in both scenario periods in the two northwestern basins.

Regarding the Elbe under REMO scenarios, the flood level in the Elbe basin tends to increase under all scenarios and both periods with different magnitudes of change. However, the opposite direction of change is projected under all WettReg scenarios. Driven by CCLM scenarios, similar patterns as for the Weser are projected for the Elbe in the second period, with striking differences between two realizations.

For the two southern basins (the Danube and Rhine), an increase in the 50-year flood level in the meltingwater-dominated rivers can be found in the first period, except the REMO-driven A2 scenario. No consistent significant changes were found for these rivers in the second period. Simulations for the pluvial river in these two basins, the River Neckar (a large tributary of the Rhine), show a strong decrease (< -20%) under all REMO scenarios, and a decrease in 75% of the CCLM scenarios. The results driven by WettReg for the Neckar show different directions of change in two periods for all three scenarios. In contrast, the gauge Rees at the lower Rhine shows an upward trend projected by the simulations under all CCLM and two REMO scenarios in the second period. For the other pluvial rivers in this sub-region, like Main (a tributary of the Rhine) and Danube, both upward and downward trends are projected depending on the emission scenarios.

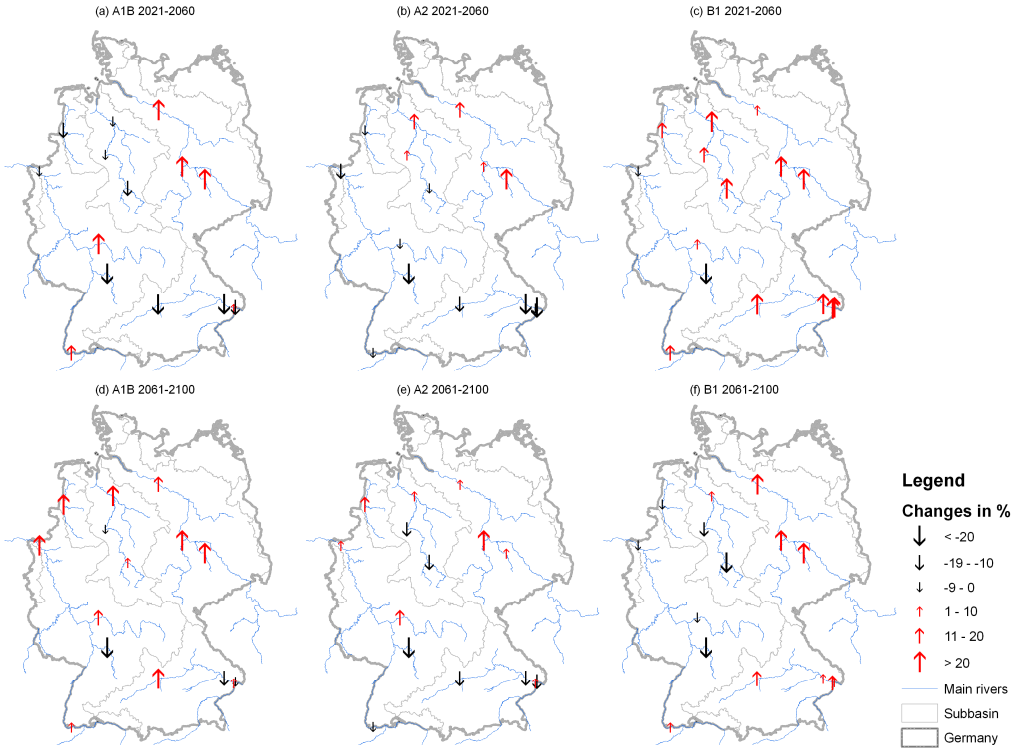

Figure 4-9: Spatial distribution of relative changes in 50-year flood level in two scenario periods with regard to the baseline series in the control period driven by REMO.

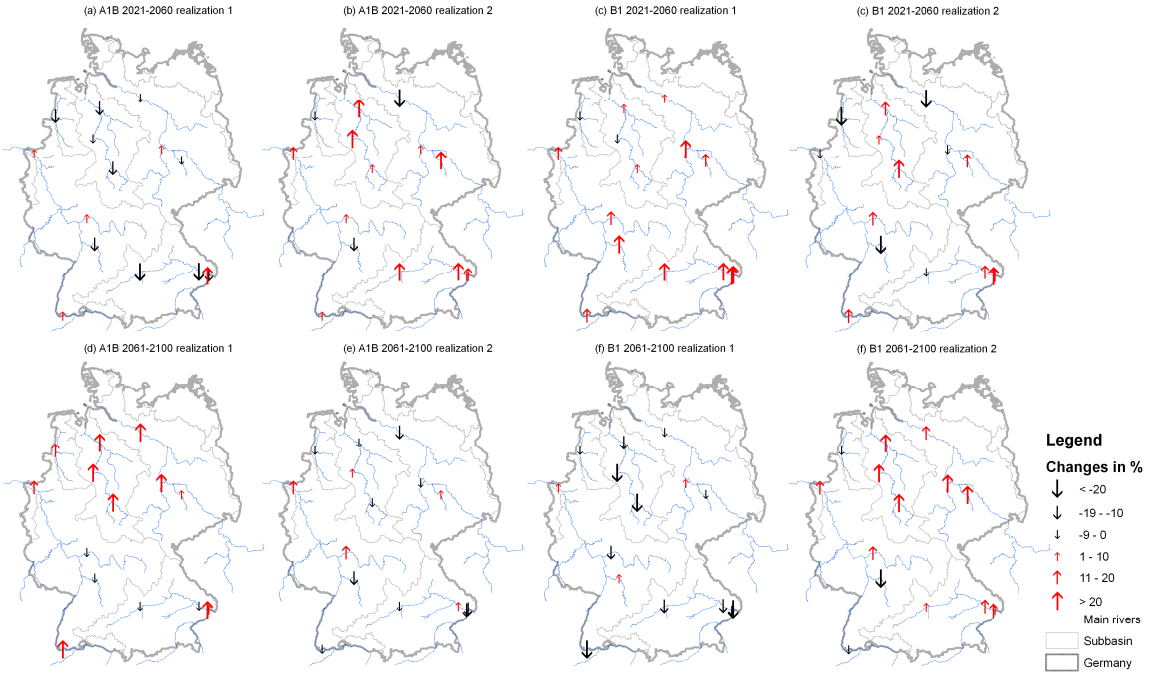

Figure 4-10: Spatial distribution of relative changes in 50-year flood level in two scenario periods with regard to the baseline series in the control period driven by CCLM.

The changes in the flood events may be partly explained by the changes in extreme precipitation events, *e.g.* the 99 percentile of the 10-day precipitation. For example, realization 2 of A1B scenario and realization 1 of B1 scenario from the CCLM project a smaller 99 percentile of the 10-day precipitation than the reference one for the most part of Germany. In contrary, the other two realizations show higher precipitation events. The change in the characteristics of extreme precipitation events coincide with the change direction of the flood levels.

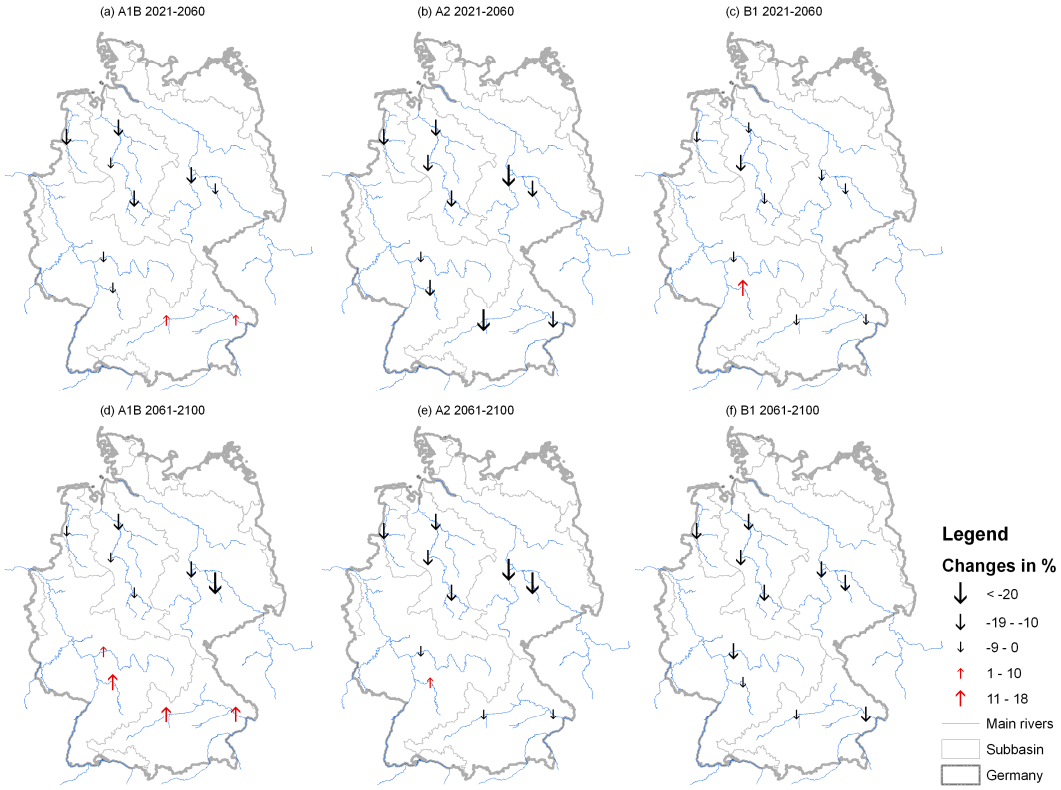

Figure 4-11: Spatial distribution of medium relative changes in 50-year flood level in two scenario periods with regard to the baseline series in the control period driven by WettReg.

It is clear that the hydrological simulation results driven by climate scenarios from the dynamical and statistical-empirical model show even more diverse performance in representing flood conditions than high flows. The relative changes in 50-year flood levels, resulting from scenarios of different climate models (**Fig. 4-9** – **4-11**) yields a rather ambiguous picture of the flood projections in Germany. Similarly, varying results between the dynamical and statistical-empirical climate models were also reported by Haylock et al., (2006) and Schmidli et al., (2007), whose results are based on the cross-comparison of the precipitation downscaling skills of six statistical models and two/three dynamical ones. Since the differences between models were found at least as large as the differences between the emission scenarios for a single model, Haylock et al. claimed that it is an advantage of including as many different types of downscaling models, global models and emission scenarios as possible to account for uncertainties. To display the different hydrological responses caused by different climate models input is also an objective of this study, as it gives evidence of the uncertainty inherent in the climatic-hydrological system.

In order to summarize the results, the probability of the upward or downward trend could be evaluated based on all scenario and realization results, as none of them can be identified as being

the most "reliable" one. However, the results from the dynamical and the statistical-empirical models should be analyzed separately, because the large number of realizations from WettReg (60 realizations in three emission scenarios) could lead to an overweight in the final evaluation compared with seven realizations from the dynamical models.

Figure 4-12 illustrates the box-and-whisker plots for changes in 50-year flood level simulated with seven realizations of dynamical models at nine selected gauges. These selected gauges include the last gauges studied in each catchment, namely Versen (Ems), Intschede (Weser), Neu-Darchau (Elbe), Achleiten (Danube) and Rees (Rhine). In addition, the gauges at some large tributaries were also considered to provide regional information, *i.e.* Calbe-Grizehne (Saale, Elbe), Frankfurt and Rockenau (Main and Neckar, two large tributaries of the Rhine). The gauge Hofkirchen at the Danube River was also included because the upstream basin of this gauge is mainly located in Germany, and the discharge at this gauge could represent the flood conditions of the river Danube within German territory.

An upward trend in floods was projected by SWIM driven by dynamical models for the rivers Weser, Saale, and Main for both scenario periods (**Fig. 4-12**). An increase only in the second scenario period can be stated for the Elbe (Neu Darchau) and Rhine (Rees). The last gauge in the upper Danube basin, Achleiten, where the flood condition is also influenced by the tributary Inn from the Austrian Alpine region, may face higher floods in 2021 – 2060, and lower flood levels in 2061 – 2100. A distinct downward trend in floods was projected for the Neckar. The future flood conditions are quite uncertain in the Ems (Versen) and in the German part of the Danube (Hofkirchen). The uncertainty of the projected change, which can be determined by the height of the boxes and the whiskers, is relatively small at the Rhine and Main and very large in the Saale River.

The direction of change in flood level derived from all 60 WettReg realizations is shown for six gauges, whose basin areas are located fully in Germany (**Fig. 4-13**). The horizontal bands in the boxes, which represent the medium changes of all realizations, clearly indicate lower flood levels for three northern basins: Ems, Weser and Saale. The medium changes in other three basins (Danube, Main and Neckar) are negligible. However, there are some realizations projecting very extreme flood levels for each basin (see the upper whiskers). The uncertainty bounds of both the change direction and magnitude are wider than those for the dynamical models, especially in the Elbe and Rhine, mainly due to a large number of realizations generated by WettReg.

In addition, it is worth mentioning that although the statistical method (GEV) estimated the changes in the 50-year flood level, it cannot fully reflect the magnitude of the most extreme flood events, which were projected. In order to fill this gap, an additional step in the analysis was done. **Table 4-9** shows the return periods of the maximum discharges during the control and the second scenario period according to the return curves for REMO and CCLM runs. Most of the maximum discharges in the control period correspond to the return period of less than 200 years. However, in 2061 – 2100, some simulated maximum discharges can be considered as over 200-year floods and even over 1000-year floods. Such high floods could be very crucial in terms of flood protection even if the rest flood events projected in the scenario periods are moderate. Finally, one should always keep in mind that the time period to analyse the flood return periods is still limited.

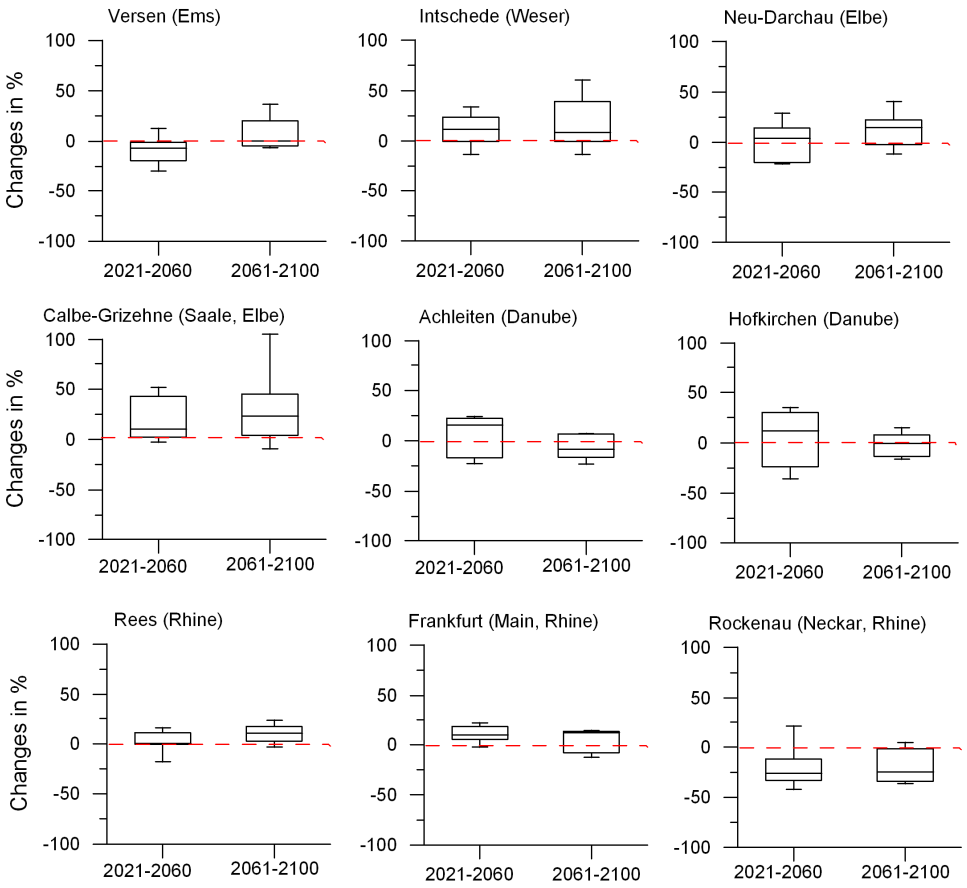

Figure 4-12: Box-and-whisker plots for changes in 50-year flood level simulated with dynamic models at the nine selected gauges.

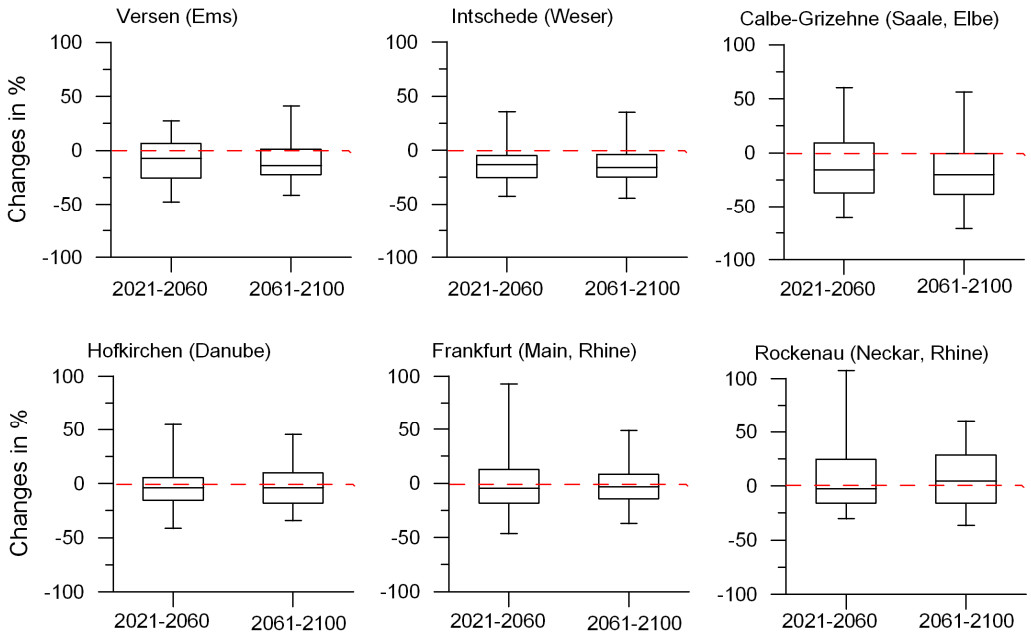

Figure 4-13: Box-and-whisker plots for changes in 50-year flood level simulated with 60 realizations from WettReg at the six selected gauges.

Table 4-9: The classes of the estimated return period for the simulated maximum discharges driven by REMO and CCLM in the control period (1961 – 2000) and the second scenario period (2061 – 2100) (the shadow highlights three categories: dark >1000; dark grey 200 – 999; light grey 100 – 199; and no shadow <100)

	Estimated return period of the simualted maximum discharge driven by									
	REMO				CCLM Realization 1			CCLM Realization 2		
Gauge	Control run	A1B	A2	B1	Control run	A1B	B1	Control run	A1B	B1
Versen	100-199	>1000	200-999	50-99	50-99	>1000	100-199	<50	50-99	50-99
Intschede	100-199	-	<50	-	50-99	200-999	<50	100-199	100-199	>1000
Letzter_Heller	200-999	100-199	<50	<50	<50	200-999	<50	100-199	100-199	>1000
Voltho	200-999	200-999	<50	<50	100-199	200-999	<50	100-199	200-999	200-999
Hofkirchen	50-99	<50	<50	50-99	100-199	<50	<50	50-99	200-999	200-999
Donauworth	100-199	100-199	50-99	100-199	100-199	<50	<50	50-99	50-99	50-99
Passau	<50	200-999	100-199	200-999	<50	>1000	50-99	200-999	<50	100-199
Achleiten	<50	50-99	<50	<50	<50	100-199	<50	100-199	<50	200-999
Rees	<50	100-199	50-99	50-99	100-199	>1000	200-999	50-99	>1000	50-99
Frankfurt	50-99	200-999	200-999	<50	50-99	<50	<50	50-99	>1000	200-999
Rockenau	100-199	<50	<50	<50	100-199	<50	100-199	<50	<50	50-99
Rheinfelden	50-99	>1000	<50	100-199	<50	>1000	<50	50-99	<50	50-99
NeuDarchau	100-199	100-199	200-999	>1000	50-99	>1000	100-199	<50	50-99	100-199
Mulde	50-99	100-199	100-199	100-199	50-99	50-99	<50	50-99	100-199	100-199
Saale	<50	200-999	200-999	200-999	<50	200-999	200-999	<50	<50	>1000

4.5.3. Change in seasonal dynamics

In addition to changes in the flood levels, changes in flood seasonality are of interest, as they could also reflect differences between models. The comparison was done in the following way. Firstly, for all the scenarios and realizations driven by one specific RCM, the 95 percentile of the monthly maxima of daily discharge for the whole simulation period (1961–2100) was calculated as a threshold to select the extreme high flows for each month. After that the number of monthly maxima over this 95 percentile discharge was accounted for each month during the control and scenario periods for each scenario/realization of the RCM. In addition, this procedure was also applied on the observed series but with the threshold for the control period 1961–2000 to show the observed distribution of high flow events in each month. **Figure 4-14** shows an example of the number of monthly discharges over the 95 percentile in the control period (1961–2000) and in the second scenario period (2061 – 2100) at the gauge Calbe-Grizehne (Saale, tributary of the Elbe). This figure displays the distribution of high flows in different months or seasonality of high flows, and the seasonal patterns in the control and scenario periods could be compared. In the control period, the observed high flows occur mainly from December to May. The similar distribution of high flows can be found in the results by REMO and WettReg (**Fig. 4-14(a)** and **4-14(b)**), while the extremely high monthly flows were projected for all seasons driven by the CCLM realizations (**Fig. 4-14(c)** and **4-14(d)**). In the scenario period, there are much more projected monthly high flows occurring not only in winter but also in spring and summer under all three emission scenarios generated by REMO. Driven by CCLM realization, the high flows frequency does not increase strongly, but the share of the spring and summer high flows becomes more significant. No changes in high flow seasonality could be found in the results driven by WettReg (**Fig. 4-14(b)**). The distribution of monthly high flows in the scenario period is similar to that in the control period, but a smaller number of high flows are projected for the future.

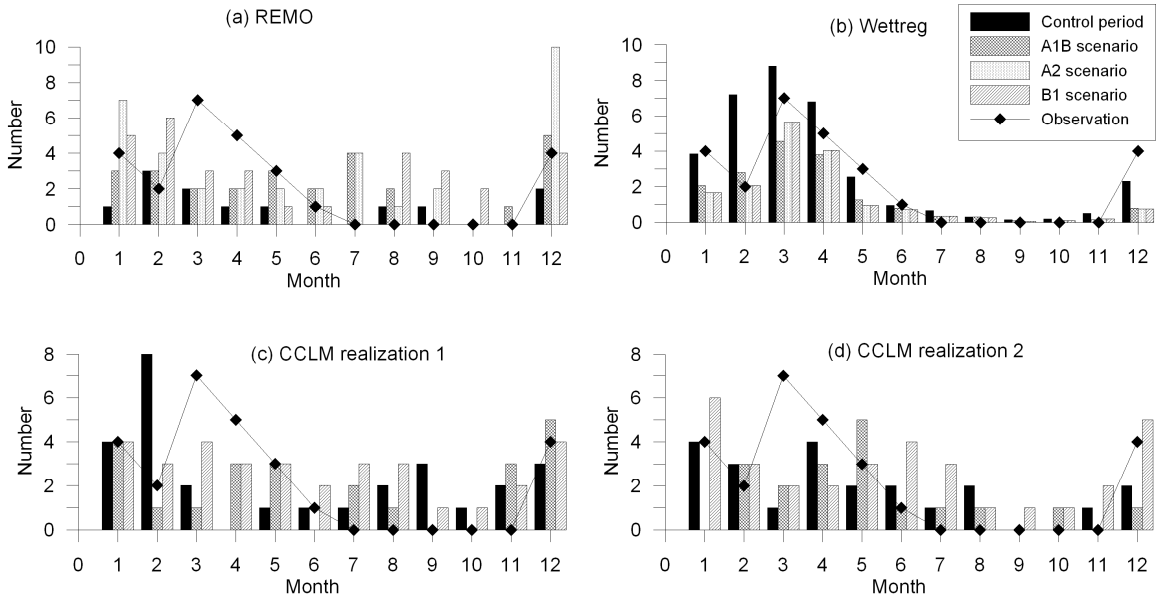

Figure 4-14: Number of monthly discharges over 95 percentile observed and simulated with the three models under A1B, A2 and B1 scenarios in both control period 1961 – 2000 and scenario period 2061 – 2100 at the gauge Calbe-Grizehne (Saale, Elbe).

Hence, this result confirms again the distinct characteristics of the flood behavior projected using different types of RCMs. Based on the projections driven by all three RCMs, no distinct information on the change in seasonality can be provided.

4.6. Discussion and conclusions

SWIM validation and comparison of RCMs. The eco-hydrological model SWIM has proven to have a capability to simulate high flows and extreme floods reasonably for large river basins in Germany with a daily time step. In the control runs, the dynamical model CCLM generated a large bias in the amount of water discharge compared with another dynamical model, REMO. The statistical-empirical model WettReg performed better for the control period, and it is not surprising, because WettReg is based on the statistics of observed climate data from the control period. The dynamical models generally have small number of realizations while the statistical-empirical model can offer plenty of realizations, which could be used to account for uncertainty. The disadvantage of the statistical-empirical model is that it highly depends on the availability of the historical records, restricting its application in large-scale assessments. Another disadvantage of WettReg is that possible alterations in physical conditions of the regional climate system can not be projected by an empirical-statistical model, because the underlying statistical relationships cannot be valid for such altered conditions.

Results. The two dynamical models (REMO and CCLM) and the statistical-empirical model (WettReg) resulted in different characteristics of the flood conditions for the future. In general, the two dynamical models projected wetter conditions and higher floods than the statistical-empirical model, and resulted in a variety of temporal and spatial changes in both directions. In contrast, the medium results obtained using WettReg normally show a steady and simple trend in temporal flood generation and rather small changes in spatial distribution. The two dynamical models suggest an increase of about 10 – 20% in the 50-year flood levels in the rivers Weser, Rhine, Main, Saale and Elbe; the Ems and the German part of the Danube do not have a clear trend, whereas there is a likelihood of 20% decrease in the flood level for the Neckar. In contrast, the model WettReg projects a downward trend for the northern basins Ems and Weser (10%), and Saale (20%), and no distinct trend could be found for the Main, Danube, and Neckar. It is quite surprising that the change directions obtained using two types of RCMs are even opposites in most of the cases. The dynamical models also imply an extension of flood seasons, so that the extreme flood events may also occur frequently in spring and summer. However, there was no shift in flood seasons in the results driven by WettReg. Summarizing the results, one can see that there are more significant increasing trends in high flow and flood levels simulated using REMO, whereas most of the changes under CCLM scenarios are quite moderate, and most of the significant decreasing trends in floods were found in simulations driven by WettReg. It is quite surprising that opposite trends were found in two CCLM realizations driven by the same emission scenario, and the two realizations from different emission scenarios often have similar spatial patterns, *e.g.* A1B realization 1 and B1 realization 2, A1B realization 2 and B1 realization 1, especially in the second period. It is possible that this result reflects the inherent uncertainty of GCMs.

Sources of uncertainty. The major uncertainty in this study should be assigned to the use of RCMs with different structures. Often two dynamical models yield different temporal and spatial patterns from the statistical-empirical one, and the unbalanced number of realizations from each model makes it difficult to summarize all the model results. Besides, there are some major uncertainty sources in the scenarios generated by each RCM. For the WettReg model, the major uncertainty source should be assigned to the multiple realizations for every emission scenario. Although only the medium result was taken into the final evaluation, the large deviations from the

medium result should not be ignored, especially for some basin like the Elbe and Rhine. In simulations driven by CCLM, the important uncertainty source is represented by two realizations, which were used as the forcing data for the control runs and the initial boundary conditions for the scenario runs. As a result, under each emission scenario, the two CCLM realizations lead to two quite opposite directions of the hydrological response. In the simulations driven by REMO, the "external" uncertainty should be assigned to different emission scenarios: only the results in some basins agree between all three scenarios.

Future strategy: how to account for uncertainty? It is clear that the future flood conditions cannot be easily projected when the uncertainty of the projections is enormous, even without including the large uncertainty due to the GCM used in this study. For example, the large difference of the two CCLM realizations for each scenario can simply reflect the inherent uncertainty of the climate system which actually exists. The essential causes of uncertainty may arise from unknown factors for all projections. Advancements in bias correction and model design are two ultimate ways to reduce the uncertainty. Hence, it may be more meaningful to use and further develop specific tools or models "specialised" in flood conditions. This means that climate change impact studies on river flood conditions should be based on regional climate scenarios which are tailored in such a manner that they perform best for flood conditions, *i.e.* reproduce satisfactorily heavy rainfall conditions and snow melt. This strategy may be adequate to reduce the particularly high uncertainties related to such problems. Such tailored scenario methods for regional flood conditions have been proposed in recent years, *e.g.* by considering observed trends and correlations of flood prone circulation patterns and flood events of specific catchments (Samaniego and Bárdossy, 2007), or by empirical-statistical downscaling optimised for flood events, *e.g.* by Bürger (2009). Of course, this work cannot be done by hydrologists alone. More integrative links between hydrologists / climate impact modellers and the RCM / climate community should be set up (Varis *et al.*, 2004). In addition, it is also important to consider how to gain valuable information from such exercises for the management of flood risk.

Future strategy: analysis of extreme values. One should also be aware that the analysis of extreme values inevitably incorporates a particular uncertainty, because only the tail of the probability distribution is taken into account. To increase the reliability of the flood analysis, additional information should also be considered in the future research. For example, changes in the whole shape of the river runoff distribution may also reveal some clue of the changing trend in flood conditions.

Future strategy: scale of the study. In this study, only the impacts of changing climate on the flood conditions were analyzed in the macro-scale basins. However, for the meso-scale basins other important environmental changes, like changes in land use, should also be considered for the regional flood risk assessment, as the influence of land use on storm runoff generation in the meso-scale is much stronger than in the macro-scale basins (Bronstert *et al.*, 2007a). Therefore, one should always analyze the relevant factors of flood generation according to the characteristics of the study areas.

Acknowledgement: The authors would like to thank the German Federal Ministry of Education and Research (BMBF) and the Berlin-based German Insurance Association (GDV), who supported this work as one part of the GDV research project (Climate impact on the damage situation in the German insurance system). Many thanks go also to the colleagues at PIK who supported the work and especially the set-up of the data bases, namely Hermann Österle and Tobias Vetter.

Reference:

Arnold, J. G., P. M. Allen, and G. Bernhardt (1993), A comprehensive surface-groundwater flow model, *J. Hydrol.* **142**, 47-69.

Arnold, J.G., J.R. Williams, A.D. Nicks, and N.B. Sammons (1990), *SWRRB - A Basin Scale Simulation Model for Soil and Water Resources Management*, Texas A&M University Press: College Station, Texas.

Booij, M.J. (2002), Modelling the effects of spatial and temporal resolution of rainfall and basin model on extreme river discharge, *Hydrol. Sci. J.* **47(2)**, 307-320.

Bronstert, A. (2003), Floods and climate change: Interactions and impacts, *Risk Anal.* **23(3)**, 545-557.

Bronstert, A., A. Bárdossy, C. Bismuth, H. Buiteveld, M. Disse, H. Engel, U. Fritsch, Y. Hundecha, R. Lammersen, D. Niehoff, and N. Ritter (2007a), Multi-scale modelling of land-use change and river training effects on floods in the Rhine basin, *River Res. Appl.* **23(10)**, 1102-1125.

Bronstert, A., V. Kolokotronis, D. Schwandt, and H. Straub (2007b), Comparison and evaluation of regional climate scenarios for hydrological impact analysis: General scheme and application example, *Int. J. Climatol.* **27**, 1579-1594.

Bürger, G. (2009), Dynamically vs. empirically downscaled medium-range precipitation forecasts, *Hydrol. Earth. Syst. Sci.* **13**, 1649-1658.

Cameron, D. (2006), An application of the UKCIP02 climate change scenarios to flood estimation by continuous simulation for a gauged catchment in the northeast of Scotland, UK (with uncertainty), *J. Hydrol.* **328**, 212-226.

Christensen, J., F. Boberg, O. Christensen, and P. Lucas-Picker (2008), On the need for bias correction of regional climate change projections of temperature and precipitation, *Geophys. Res. Lett.* **35(L20709)**, 6.

Coles, S. (2001), *An Introduction to Statistical Modeling of Extreme Values*, Springer-Verlag, London.

Dankers, R., O. Christensen, L. Feyen, M. Kalas, and A. de Roo (2007), Evaluation of very high-resolution climate model data for simulating flood hazards in the Upper Danube Basin, *J. Hydrol.* **347**, 319-331.

Disse, M., and H. Engel (2001), Flood events in the Rhine basin: genesis, influences and mitigation, *Nat. Hazards* **23(2-3)**, 271-290.

Doherty, J. (2004), *PEST: Model Independent Parameter Estimation. Fifth edition of user manual*, Watermark Numerical Computing, Brisbane, Australia.

Enke, W., T. Deutschlaender, F. Schneider, and W. Kuechler (2005a), Results of five regional climate studies applying a weather pattern based downscaling method to ECHAM4 climate simulations, *Meteorologische Zeitschrift* **14(2)**, 247-257.

Enke, W., F. Schneider, and T. Deutschlaender (2005b), A novel scheme to derive optimized circulation pattern classifications for downscaling and forecast purposes, *Theor. Appl. Climatol.* **82**, 51-63.

Gelfan, A., J. Pomeroy, and L. Kuchment (2004), Modelling Forest Cover Influences on Snow Accumulation, Sublimation, and Melt, *J. Hydrometeorology* **5(5)**, 785-803.

Graham, L., J. Andreasson, and B. Carlsson (2007), Assessing climate change impacts on hydrology from an ensemble of regional climate models, model scales and linking methods - a case study on the Lule River basin, *Clim. Change* **81**, 293-307.

Grünewald, U., M. Kaltofen, W. Rolland, S. Schümberg, R. Chmielewski, M. Ahlheim, T. Sauer, R. Wagner, W. Schluchter, H. Birkner, R. Petzold, L. Radczuk, R. Eliasiewicz, L. Paus, and G. Zahn (1998), *Ursachen, Verlauf und Folgen des Sommer-Hochwassers 1997 an der Oder sowie Aussagen zu bestehenden Risikopotentialen. Eine interdisziplinäre Studie*, Deutsches IDNDR-Komitee für Katastrophenvorbeugung e. V, Bonn.

Hattermann, F., V. Krysanova, F. Wechsung, and M. Wattenbach (2005), Runoff simulations on the macroscale with the ecohydrological model SWIM in the Elbe catchment - validation and uncertainty analysis, *Hydrol. Process.* **19**, 693-714.

Hay, L., R. Wilby, and G. Leavesley (2000), A comparison of delta change and downscaled GCM scenarios for three mountainous basins in the United States, *J. Am. Water Resour. Assoc.* **36**, 387-398.

Haylock, M. R., G. Cawley, C. Harpham, R. Wilby, and C. M. Goodess (2006), Downscaling heavy precipitation over the United Kingdom: a comparison of dynamical and statistical methods and their future scenarios, *Int. J. Clim.* **26(10)**, 1397-1415.

Huang, S., V. Krysanova, H. Österle, and F. Hattermann (2010), Simulation of spatiotemporal dynamics of water fluxes in Germany under climate change, *Hydrol. Process.* **24(23)**, 3289-3306.

IPCC (2007), *Climate Change 2007: Impacts, Adaptation and Vulnerability - Summary for Policymakers. Working Group II Contribution to the Fourth Assessment Report of the Intergovernmental Panel on Climate Change*, Cambridge University Press.United Kingdom and New York, NY, USA.

Jacob, D. (2001), A note on the simulation of the annual and inter-annual variability of the water budget over the Baltic Sea drainige basin, *Meteorol. Atmos. Phys.* **77**, 61-73.

Kay, A., H. Davies, V. Bell, and R. Jones (2009), Comparison of uncertainty sources for climate change impacts: flood frequency in England, *Climatic Change* **92**, 41-63.

Kay, A., R. Jones, and N. Reynard (2006), RCM rainfall for UK flood frequency estimation. II. Climate change results, *J. Hydrol.* **318**, 163-172.

Kleinn J, C. Frei, J. Gurtz, D. Lüthi, P. L. Vidale and C. Schär. (2005), Hydrologic simulations in the Rhine basin driven by a regional climate model, *J. Geophys. Res.,* **110(D04102)**, Doi:10.1029/2004JD005143.

Kosková, R., S. Nemecková, C. Hesse Jakubíková, A., V. Broza, and J. Szolgay (2007), Using of the Soil Parametrisation Based on Soil Samples Databases in Rainfall-Runoff Modelling, **In:** Jakubíková, A. and Broza, V. and Szolgay, J. (eds.), *Proceedings of the Adolf Patera Workshop "Extreme hydrological events in catchments". 13.11.2007*, Bratislava.

Kreibich, H., B. Merz, and U. Grünewald (2007), Lessons learned from the Elbe River floods in August 2002 - with a special focus on flood warning. Extreme Hydrological Events: New Concepts for Security, *NATO Science Series* **78(1)**, 4020-5741.

Krysanova, V., A. Meiner, J. Roosaare, and A. Vasilyev (1989), Simulation modelling of the coastal waters pollution from agricultural watersheds, *Ecol. Model.* **49**, 7-29.

Krysanova, V., D. Möller-Wohlfeil, and A. Becker (1998), Development and test of a spatially distributed hydrological / water quality model for mesoscale watersheds, *Ecol. Model.* **106**, 261-289.

Krysanova, V., F. Hattermann, and F. Wechsung (2007), Implications of complexity and uncertainty for integrated modelling and impact assessment in river basins, *Environ. Modell. Softw.* **22**, 701-709.

Leander, R., T. Buishand, B. van den Hurk, and M. de Wit (2008), Estimated changes in flood quantiles of the river Meuse from resampling of regional climate model output, *J. Hydrol.* **351(3-4)**, 331-343.

Lenderink, G., A. Buishand, and W. van Deursen (2007), Estimates of future discharges of the river Rhine using two scenario methodologies: direct versus delta approach, *Hydrol. Earth Syst. Sci.* **11(3)**, 1145-1159.

Lopes, V. L. (1996), On the effect of uncertainty in spatial distribution of rainfall on catchment modeling, *Catena* **28**, 107-119.

Majewski, D. (1991), The Europa Modell of the Deutscher Wetterdienst, *ECMWF Seminar on numerical methods in atmospheric models* **2**, 147-191.

Menzel, L., and G. Bürger (2002), Climate change scenarios and runoff response in the Mulde catchment (Southern Elbe, Germany), *J. Hydrol.* **267**, 53-64.

Menzel, L., A. Thieken, D. Schwandt, and G. Bürger (2006), Impact of climate change on the Regional hydrology - scenario-based modelling studies in the German Rhine Catchment, *Nat. Hazards* **38**, 45-61.

Middelkoop, H., and J. Kwadijk (2001), Towards integrated assessment of the implications of global change for water management - The Rhine experience, *Phys. Chem. Earth. (B)* **26(7-8)**, 553-560.

Mikhailov, V., V. Morozov, N. Cheroy, M. Mikhailova, and Y. Zavyalova (2008), Extreme flood on the Danube River in 2006, *Russian Meterol. Hydrol.* **33(1)**, 48-54.

Monteith, J. L. (1965), Evaporation and the environment, *Symp. Soc. Expl. Biol.* **19**, 205-234.

Nash, J. E., and J. V. Sutcliffe (1970), River flow forecasting through conceptual models. Part I: a discussion of principles, *J. Hydrol.* **10(3)**, 282-290.

Petrow, T., and B. Merz (2009), Trends in flood magnitude, frequency and seasonality in Germany in the period 1951 - 2002, *J. Hydrol.* **371**, 129-141.

Petrow T, J. Zimmer and B. Merz (2009), Changes in the flood hazard in Germany through changing frequency and persistence of circulation patterns, *Nat. Hazards Earth Syst. Sci.* **9**, 1409–1423.

Priestley, C. H. B., and R. J. Taylor (1972), On the assessment of surface heat flux and evaporation using large scale parameters, *Mon. Weather Rev.* **100**, 81-92.

Rockel, B., A. Will, and A. Hense (2008), The regional climate model COSMO-CLM (CCLM), *Meteorologische Zeitschrift* **17(4)**, 347-348.

Samaniego, L., and A. Bárdossy (2007), Relating macroclimatic circulation patterns with characteristics of floods and droughts at the mesoscale, *J. Hydrol.* **335**, 109-123.

Schmidli J., C. M. Goodess, C. Frei, M. R. Haylock, Y. Hundecha, J. Ribalaygua and T. Schmith (2007), Statistical and dynamical downscaling of precipitation: An evaluation and comparison of scenarios for the European Alps, *J. Geophys. Res.* **112(D04105)**, doi:10.1029/2005JD007026.

Schönwiese, C., T. Staeger, and S. Trömel (2006), Klimawandel und Extremereignisse in Deutschland. **In:** *Klimawandel und Extremereignisse in Deutschland - Klimastatusbericht 2005*, Deutscher Wetterdienst, Offenbach, 7-17.

Shabalova, M., W. van Deursen, and T. Buishand (2003), Assessing future discharge of the river Rhine using regional climate model integrations and a hydrological model, *Climate Research* **23**, 233-246.

Steppeler, J., G. Doms, U. Schaettler, H. Bitzer, A. Gassmann, U. Damrath, and G. Gregoric (2003), Meso-gamma scale forecasts using the nonhydrostatic model LM, *Meteorol. Atmos. Phys.* **82**, 75-96.

Suklitsch, M., A. Gobiet, H. Truhetz, N. Awan, H. Göttel, and D. Jacob (2010), Error characteristics of high resolution regional climate models over Alpine area, *Clim. Dyn.* **37(1-2)**, 377-390.

Themeßl, M., A. Gobiet, and A. Leuprecht (2010), Empirical-statistical downscaling and error correcton of daily precipitation from regional climate models, *Int. J. Climatol.* **31(10)**, 1530-1544.

Van Ulden, A., and G. van Oldenborgh (2006), Large-scale atmospheric circulation biases and changes in global climate model simulations and their importance for climate change in Central Europe, *Atmos. Chem. Phys.* **6**, 863-881.

Varis, O., T. Kajander, and R. Lemmelä (2004), Climate change and water: from climate models to water resources management and vice versa, *Climatic Change* **66(3)**, 321-344.

Williams, J., K. Renard, and P. Dyke (1984), EPIC - a new model for assessing erosion's effect on soil productivity, *J. Soil Water Conserv.* **38(5)**, 381-383.

5. Projection of low flow condition in Germany under climate change by combining three RCMs and a regional hydrological model

Shaochun Huang* [1], Valentina Krysanova[1], and Fred F. Hattermann[1]

[1] *Potsdam Institute for Climate Impact Research, P.O. Box 601203, Telegrafenberg, 14412 Potsdam, Germany*

* Corresponding author. Tel.: +49 331 288 2406.
Email address: huang@pik-potsdam.de

Abstract

The present study is aimed to a) project the future low flow conditions in the five largest river basins in Germany and b) to account for the uncertainty of the projections. The eco-hydrological model SWIM (Soil and Water Integrated Model) was driven by different regional climate models (REMO (REgional Model), CCLM (Cosmo-Climate Local Model) and WettReg (Wetterlagenbasierte Regionalisierungsmethode)) to simulate the daily river discharges in each of the study basins. The occurrence of the 50-year low flow during 1961 to 2000 was estimated for the two scenario periods (2021 – 2060 and 2061 – 2100) using the Generalized Extreme Value distribution. The 50-year low flow is likely to occur more frequently in western, southern and part of central Germany after 2061 as suggested by more than or equal to 80% of the model runs. The current low flow period (from August to September) may be extended until the late autumn at the end of this century. When compared with flood projections using the same models, the severer low flows projected in this study appear more pronounced and consistent.

Keywords: Low flow, RCMs, SWIM, Germany, Climate scenarios, Uncertainty

5.1. Introduction

Stream low flow is defined as the 'flow of water in a stream during prolonged dry weather' (WMO, 1974). Understanding this condition is essential for a wide range of water management applications, such as the design of water supply systems, estimation of safe surface water withdrawals, navigation, and the requirements for environmental flows, *etc*. Moreover, low flow is one of the most important characteristics of drought and is often used as an index in drought studies (Feyen and Dankers, 2009, Pfister *et al.*, 2006).

There are a number of both climatic and non-climatic drivers which influence low flow conditions in rivers and streams. Stahl et al. (2010) analyzed the low flow trends (without considering the significance of the trends) during the period 1962–2004 in 441 near-natural catchments across Europe. Due to negligible human influences in the study areas it has been assumed that climate is the dominant driver. The study found that the low flows tend to decrease in most of the small catchments in Germany (area mean 292 km2), where the lowest mean monthly flow occurs in summer. This trend partly complies with observed climate change in Germany where an increase of approximate 1°C in annual average temperature and a significant decrease of 16% in summer precipitation were recorded during the period 1951 – 2000 (Schönwiese et al., 2006). However, the trends of low flow or drought are not necessarily reflected by the seasonal average rainfall. Hisdal (2001) found that the southern part of Germany has a significant trend towards less severe drought conditions, this coinciding with an increased winter precipitation during the period 1962 – 1995. The increase in winter precipitation contributes to more groundwater recharge, by which the stream flow is fed in summer. Hence, the generation of low flow is a complex natural process influenced not only by climate, but also by various other aspects including the characteristics of soils and aquifers, vegetation type, topography and so on. In addition, the low-flow regimes in most of the larger catchments have been modified significantly, through either excessive water withdrawals, which can exacerbate the low flow conditions, or through the regulation of reservoirs, which can alleviate the severe low flow problem. Climate related trends may therefore be difficult to detect due to the influence of a wide range of both natural and anthropogenic factors. For example, Svensson et al. (2005) found that a trend towards less severe low river flows over the 20th century at several stations in Europe are consistent with an increasing number of reservoirs becoming operational in the catchments over the period of record.

According to the latest climate change scenarios described in the IPCC Fourth Assessment Report (IPCC, 2007), the temperature is likely to continue to increase with more precipitation in winter and less in summer in Germany. The combination of these patterns will probably result in higher evaporation in summer and, in consequence, more frequent and intense low flow conditions. Such changes raise the risk of extremely low flow and drought events, which are critical for water resources management in terms of meeting water demands and mitigating water conflicts. Hence, the future development of low flow conditions as a consequence of climate change is of a great interest for water managers.

There are already some published studies investigating the low flow conditions under several specific climate change scenarios in different regions in Germany and in Europe. For example, the impact of climate change on hydrological regimes in the Rhine basin has been investigated by Middelkoop *et al.* (2001) based on two General Circulation models (GCMs) (UKHI (UK Meteorological Office High Resolution model) and XCCC (Canadian Climate Centre model)). Hennegriff *et al.* (2008) projected the low flow conditions in the federal state of Baden-Württemberg applying the statistical-empirical Regional Climate Model (RCM) WettReg driven

by the GCM ECHAM4 under B2 scenario. They compared different low flow indices derived from the scenario period 2021 – 2050 and the control period 1971 – 2000. The GLOWA-Danube project (www.glowa-danube.de), which intensively studied water resources under climate change in the Upper Danube basin, simulated the annual low flow development from 1971 to 2003 and from 2011 to 2060 using realizations from RCMs MM5 (Das Mesoscale Meteorology Model 5) and REMO (REgional MOdel) under A1B scenario (Mauser *et al.*, 2008). Feyen and Dankers (2009) have recently examined the impact of global warming on stream flow drought in Europe by comparing both low flow and deficit indices using a large scale hydrological model LISFLOOD and RCM HIRHAM (HIRLAM dynamics + the Hamburg physics package) for the end of 20th and 21st centuries under A2 emission scenario. However, it is practically impossible to compare and aggregate these results in terms of the low flow conditions for the whole of Germany due to the different RCMs, emission scenarios and spatial/temporal scales which are used. Moreover, these studies usually applied only one RCM and one emission scenario without considering the uncertainty of the climate boundary conditions. Several authors have already found large uncertainty in the simulated hydrological extremes (particularly, flood) due to different emission scenarios, global climate models, and down-scaling techniques used (Kay *et al.* 2009, Huang *et al.* 2012). Hence, the uncertainty in the low flow projections should also be considered as complementary information and presented alongside the projection results.

This study is aimed to present a German wide assessment of the potential impacts of climate change on the frequency of extreme low flows in the future, based on the results of an eco-hydrological model SWIM (Soil and Water Integrated Model) driven by several RCMs for Germany, accounting for the uncertainty of climate boundary conditions. One advantage of the eco-hydrological model SWIM is that it incorporates crop/vegetation growth under a warmer climate and hence reflects the impacts of both climate and partly land use changes on the hydrological cycle. Three available nation-wide applications of RCMs were applied to generate climate realizations under different climate scenarios (high (A2), low (B1), and medium (A1B) emission scenarios). For each realization, the generated annual minimum 7-day mean flows (AM7) simulated by SWIM were fitted to a Generalized Extreme Value distribution to estimate the 50-year low flow level in the control period (1961 – 2000) and its corresponding return period in two scenario periods (2021 – 2060 and 2061 – 2100). This method facilitates the analysis of changes in the frequency of the current 50-year low flow under various climate projections, and does not require bias correction. After that, the monthly minimum 7-day discharges (MM7) under different scenarios in 2061 – 2100 were compared with the ones in the control period to reveal possible shifts in the critical season of low flow conditions in the future. The uncertainty in the changes of low flow frequency and seasonality due to the application of different RCMs, emission scenarios and realizations were accounted for in terms of the number of the projections which suggest the same change direction.

5.2. Study areas and data preparation

5.2.1. Study areas and low flow regime

The five largest river basins in Germany (Danube, Elbe, Ems, Rhine and Weser) were selected as study areas for the assessment of climate change impacts on the low flow conditions. **Figure 5-1** shows the location of these five river basins as well as selected gauge stations, which were used for calibration and validation of the model. These basins cover about 90% of the whole German territory. Three of the five studied basins have large areas outside Germany, *i.e.* the upper Elbe basin in the Czech Republic, the Alpine regions in the Danube and Rhine basins in Austria and Switzerland, and the western part of the Rhine basin in France and Luxemburg.

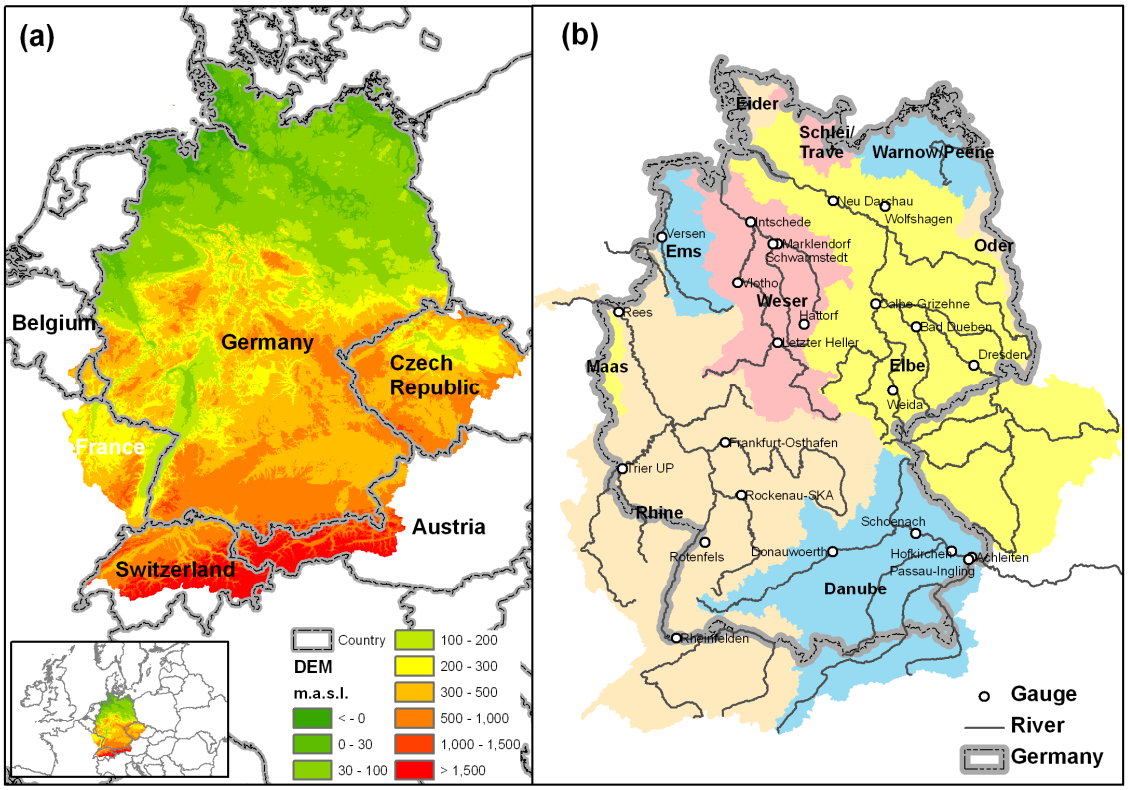

Figure 5-1: Elevation map for the five largest river basins in Germany (a) and the location of selected gauges which were used for calibration and validation (b).

Table 5-1 highlights the differences in geographical, climatological and low flow characteristics for each of the five basins. Geomorphologically, the northern three basins are located in the flat lowland region and partly in the central German mountains. The Upper Danube lies in southwestern Germany and receives its main tributaries from the Alps and the Bavarian Forest. The Rhine originates in the Swiss Alps and flows from the Austrian/Swiss border region through Germany to the Netherlands. Climatologically, the maritime climate gradually changes into a more continental climate from the northwest to the east and southeast. The Upper Danube and Rhine river basins have the highest precipitation (more than 1000 mm per year) and the Elbe receives the lowest rainfall. Regarding the low flow regimes, most national rivers, like the German part of Ems, Weser, Main and Neckar, and the international river Elbe are characterized as the rain-dominant regimes with a distinct dry season in summer (**Fig. 5-2**). August and September are two critical months of low flows in these rivers when the evapotranspiration is high and water storages are depleted. In contrast, the low flow at the last gauge Achleiten of the Upper Danube occurs during the cold season when the precipitation is stored as snow. In the German part of the Danube and in the Rhine Rivers, a mixture of gauges with rain-dominant regimes and snow-dominant regimes can be detected with no distinct dry season and a long period of high flow.

Table 5-1: General characteristics of the five largest river basins in Germany.

River basin	Ems	Weser	Danube	Rhine	Elbe
Total area (km^2)*	13000	45725	77107	160000	147423
Temperature (℃)**	9.3	8.6	6.6	9.4	12.4
Annual average precipitation (mm)**	839	807	1196	1045	721
Low flow regime	rain-dominant	rain-dominant	rain/snow-dominant	rain/snow/gleicher-dominant	rain-dominant

*the total basin area for the river Danube and Rhine before the rivers enter Austria and Netherland
**the temperature and precipitation data was interpolated from the measured data in the basins for the period 1961-2000

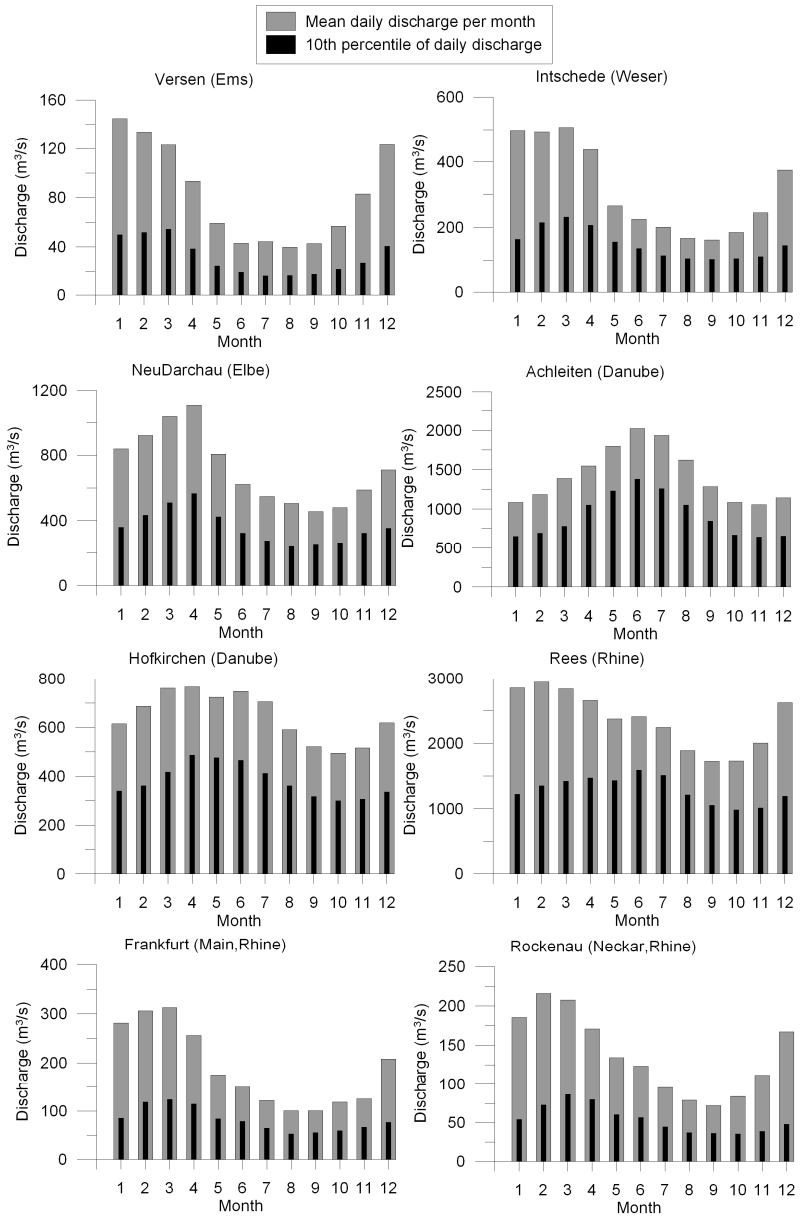

Figure 5-2: Monthly mean stream flow and the 10th percentile of daily discharge in some selected rivers.

5.2.2. Data preparation

In order to setup a SWIM model for each of the five basins, four spatial maps are needed: the digital elevation model (DEM), the soil map, the land use map and the sub-basin map. All four maps in a grid format with 250 m resolution were used.

The DEM was re-sampled using data from the NASA (National Aeronautics and Space Administration) Shuttle Radar Topographic Mission (SRTM). The soil map of the study area was merged from the general soil map of the Federal Republic of Germany "BÜK 1000" produced by the Federal Institute for Geosciences and Natural Resources (BGR), soil map of the Czech Republic (Kosková *et al.*, 2007), and soil map from the European soil database (European Communities - DG Joint Research Centre). The land use map was obtained from the CORINE 2000 land cover data set of the European Environment Agency and the Swiss land cover data 1992 from Swiss Federal Statistical Office GEOSTAT database. Land use patterns were assumed to be static in the reference and scenario periods in this study, as the study focused on climate change impacts only. The standard sub-basin map for Germany from the Federal Environment Agency (Umweltbundesamt), and the sub-basin map for the Czech Republic (T.G.M. Water Research Institute) were available. On the basis of the DEM and the stream network, an average drainage area of 100 km^2 was chosen as a threshold to discritise the areas in the Danube and Rhine basins outside Germany into sub-basins, because the standard sub-basin map for Germany had approximately the same discretisation.

There are about 270 climate stations offering observed climate data (temperature, precipitation, solar radiation and relative humidity) and more than 2000 precipitation stations located in the study area shared by Germany, the Czech Republic, Austria and Switzerland for the period of 1951–2003. However, observed climate data for the French part of the Rhine basin was not available. As such, the daily temperature and precipitation data from the "Daily high-resolution gridded climate data set for Europe" (www.ensembles-eu.org) was applied for this region. In addition, the solar radiation was estimated with a regression equation based on the correlation between the solar radiation and the differences between the daily maximum and minimum temperatures measured at German and Swiss stations, and the relative humidity was interpolated using the observed values from the two neighboring countries.

The discharge data from 145 selected gauges in Germany was used, of which 144 have long-term runoff data (1951 – 2003). The gauge Wolfshagen with the observation data from 1977 to 2003 was also added here because longer series of discharge data are usually not available in northeastern Germany. The observation data was obtained from GRDC (The Global Runoff Data Centre), UNESCO's European Water Archive (EWA) (Stahl *et al.*, 2008) and the data base of the Potsdam Institute for Climate Impact Research. 67 of the gauges are located at the large rivers with drainage area ranging from 1000 to 159300 km^2, while the other 78 gauges represent the near-natural catchments with drainage areas ranging between 100 and 1000 km^2. Among the 145 gauges, the discharge data at 24 gauges (for their location see **Fig. 5-1(b)**) was selected to calibrate and validate the model at some specific rivers. The trend of low flows at the 145 gauges gives the spatial pattern of the low flow development in the past 50 years, which can be compared with the long-term trend simulated by SWIM.

5.3. Methods

5.3.1. Regional climate models

For projections of future changes in low flows for the whole of Germany, robust regional climate change scenarios should be applied. There are several RCMs developed in the recent years which cover German territory. They are so-called "physical regional climate models", such as REMO (Jacob, 2001) and CCLM (Rockel *et al.*, 2008), and statistical-empirical regional climate models like WettReg (Enke *et al.*, 2005a, 2005b) and STAR (Orlowsky *et al.*, 2008). Among them, REMO and WettReg were officially developed on behalf of the German Environmental Agency. According to Bronstert *et al.* (2007), who evaluated the usefulness of RCMs for hydrological impact simulations, these two models are considered to better quantify the low flow conditions, although all the investigated climate models had rather limited value for climate impact assessment. They also found that the physical models have some advantages in modeling extreme events compared to the statistical-empirical ones. Therefore, beside REMO and WettReg, another physical model, CCLM, was included in this study. **Table 5-2** lists some general characteristics of these RCMs.

The physical RCMs are based on the basic physical movement and transport equations describing processes in the atmosphere and land surface. They usually take all climate variables on the border of the region from the observed climate or General Circulation Models as the boundary condition and simulate the main weather processes for the region of interest including cloud dynamics, precipitation and temperature development for each grid cell. Physical RCMs are very computationally intensive and are deterministic by definition; hence they usually have limited number of realizations (often only one) under each emission scenario.

REMO (REgional MOdel) was developed from the ''Europamodell'', the former numerical weather prediction model of the German Meteorological Service (Majewski 1991), in the Max-Planck-Institute for Meteorology in Hamburg, Germany (Jacob, 2001). It is a three dimensional regional hydrostatic climate model, calculating climate variables at a 0.088° grid for Central Europe including Germany. Control (1951 – 2000) and scenario (2001 – 2100) runs are constructed by using GCM ECHAM 5 results under three emission scenarios (A1B, A2 and B1). Only one realization of each scenario was generated by REMO.

CCLM (Cosmo-Climate Local Model) (Rockel *et al.*, 2008) originates from the weather forecast model "Lokal-Modell" (LM) developed by the German Meteorological Service (Steppeler *et al.*, 2003). Compared to REMO, CCLM is a non-hydrostatic climate model. It also takes the results of the GCM ECHAM5 as boundary conditions, but only two emission scenarios were available for our study (A1B and B1). Its spatial resolution (0.2°) is coarser than that of REMO, because its area of application covers the whole of Europe. Two control runs (from 1960 to 2000) were generated based on the two realizations of the control experiment from ECHAM5. These control runs provide the initial conditions for the transient simulation of the future regional climate projections A1B and B1. Hence, two realizations generated by CCLM for each scenario condition were used in this study.

Compared to the physical climate models, the statistical-empirical climate model WettReg (Wetterlagenbasierte Regionalisierungsmethode: weather-type based regionalization method) uses the statistical relationships between large-scale atmospheric conditions and local climate, and the characteristics of regional climate for different weather types (Enke *et al.*, 2005a, 2005b).Variables/features which have a relatively good representation in the global models, such as temperature and circulation patterns, are selected as driving climate variables. Variables with a

relatively poor representation in global models, such as precipitation or radiation, are generated by WettReg using observed correlations between large-scale patterns. As WettReg needs observation data to derive the correlation matrices for the observation period, climate projections can only be calculated for locations with climate observations; in this case, only for the stations within the German territory. This limitation restricts the hydrological simulations for some international rivers. Hence, the simulation of climate change impacts on low flow in the scenario periods driven by WettReg was only possible for rivers whose basins are entirely located within the German territory. However, the general advantage of using statistical-empirical regional models is their lower computational demand compared to the physical RCMs. In this study, 20 realizations of each scenario generated by WettReg were used, allowing accounting for the uncertainty of climate projections related to each emission scenario.

The climate change scenario of another statistical RCM, the model STAR (Orlowsky *et al.*, 2008), was used in the discussion part as additional information when analyzing the plausibility of the climate change impacts. The STAR data were used as supplementary information only because they cover merely the first scenario period until 2060.

Table 5-2: General information of RCMs.

RCMs	Model type	GCM based	Emission scenario	Spatial resolution	Number of control runs	Control period	Number of scenario runs	Scenario period
CCLM	Dynamic	ECHAM5	A1B, B1	0.2°	2 (C20_1, C20_2)	1960-2000	4 (A1B_1, A1B_2, B1_1, B1_2)	2001 - 2100
REMO	Dynamic	ECHAM5	A1B, A2, B1	0.088°	1	1951-2000	3	2001 - 2100
WettReg	Statistical-empirical	ECHAM5	A1B, A2, B1	1965 stations in Germany	20	1961-2000	60	2001 - 2100

5.3.2. Eco-hydrological model SWIM

The dynamic process-based eco-hydrological model SWIM (Soil and Water Integrated Model) (Krysanova *et al.*, 1998) was developed for climate and land use change impact assessment on the basis of the models SWAT (Arnold *et al.*, 1993) and MATSALU (Krysanova *et al.*, 1989).

SWIM simulates the hydrological cycle, vegetation growth and nutrient cycling with a daily time step by disaggregating a river basin to sub-basins and hydrotopes. The hydrotopes are sets of elementary units in a sub-basin with assumed homogeneous soil and land use types. Up to ten vertical soil layers can be considered for each hydrotope. It is assumed that a hydrotope behaves uniformly regarding hydrological processes and nutrient cycling, given the same meteorological input. The spatial disaggregation scheme in the model is flexible. In the regional studies climate zones, grid cells of a certain size, or other areal units can be used for disaggregating a region instead of sub-basins.

Water flows, nutrient cycling and plant growth are calculated for every hydrotope. Then lateral transport of water and nutrients towards the river network are simulated on the basis of linear storage functions considering interacting hydrological compartments and nutrient retention processes. After reaching the river system, water and nutrients are routed along the river network to the outlet of the simulated basin.

The simulated hydrological system consists of four main compartments: the soil surface, the root zone of soil, the shallow aquifer, and the deep aquifer. The soil root zone is subdivided into several layers in accordance with the soil database. The water balance for the soil surface and soil

column includes precipitation, surface runoff, evapotranspiration, subsurface runoff, and percolation. The water balance for the shallow aquifer includes groundwater recharge, capillary rise to the soil profile, lateral flow, and percolation to the deep aquifer.

Surface runoff is estimated as a non-linear function of precipitation and a retention coefficient, which depends on soil water content, land use and soil type (modification of the Soil Conservation Service curve number method, Arnold *et al.*, 1990). Lateral subsurface flow (or interflow) is calculated simultaneously with percolation. It appears when the storage in any soil layer exceeds field capacity after percolation and is especially important for soils having impermeable or less permeable layer(s) below several permeable ones. Potential evapotranspiration is mostly simulated using the method of Priestley-Taylor (Priestley and Taylor, 1972), though the method of Penman-Monteith (Monteith, 1965) can also be used. Actual evaporation from soil and actual transpiration by plants are calculated separately.

The groundwater contribution to stream flow is calculated based on the approach of Smedema and Rycroft (1983), who derived the non-steady-state response of groundwater flow to periodic recharge from Hooghoudt's (1940) steady-state formula. The percolation from the soil profile to recharge the shallow aquifer is corrected by the delay time function proposed by Sangrey *et al.* (1984).

A simplified EPIC approach (Williams *et al.*, 1984) is included in SWIM for simulating arable crops (like wheat, barley, rye, maize, potatoes) and aggregated vegetation types (like pasture, evergreen forest, mixed forest), using specific parameter values for each crop/vegetation type. A number of plant-related parameters are specified for 74 crop/vegetation types in the database attached to the model. Vegetation in the model affects the hydrological cycle by the cover-specific retention coefficient, impacting surface runoff, and influencing the amount of transpiration, which is simulated as a function of potential evapotranspiration and leaf area index.

SWIM allows the adaptation of crop rotation schemes under a changing climate. In warmer (scenario) conditions, the crop scheduling is governed by the harvest index, and the winter crop can be harvested earlier than in the current conditions, allowing earlier growth of cover crop until the next winter crop planting date. This modification of crop scheduling has influence on the hydrological cycle in summer.

5.3.3. Modelling strategy

SWIM was intensively calibrated/validated in terms of water components, river discharges and flood conditions for German river basins in previous studies (Hattermann *et al.*, 2005; Krysanova *et al.*, 2007; Huang *et al.*, 2010, Huang *et al.*, 2012). In this study, the simulated discharges driven by the observed climate data at 24 selected gauges (see **Fig. 5-1** for the location and **Table 5-3** for some detailed information on these gauges) were calibrated for the period of 1961 to 1980 and validated from 1981 to 2000 against the observations. These two periods together cover the whole control period (1961 – 2000), which is determined by the maximum length of all RCM control runs data available. Of these gauges 20 represent the low flow conditions in the large rivers and their main tributaries in Germany (with drainage area > 5000 km^2). The other four gauges are from the near-natural small catchments (drainage area ≤ 500 km^2), where a significant upward or downward trend in low flow conditions was observed during the last 50 years. Selection of these gauges was aimed to verify the simulation performance of low flow at different scales and for different characteristics of the catchments. In order to calibrate the low flow, a specific statistical criterion, Logarithmic Nash-Sutcliffe Efficiency (LNSE) was applied to magnify the weight of the low flows in the whole hydrograph (**Equation 5-1**).

$$LNSE = 1 - \frac{\sum(\log(Q_{obs}) - \log(Q_{sim}))^2}{\sum(\log(Q_{obs}) - \overline{\log(Q_{obs})})^2} \quad (5\text{-}1)$$

Here Q_{obs} means the observed discharges while Q_{sim} is the corresponding simulated value. The variable $\overline{\log(Q_{obs})}$ is the mean values of logarithm of the observed data for the simulation period.

After calibration and validation, the simulation period was extended to the period 1951 – 2003, the whole period with the observed climate data available. The simulated discharge was used to validate the spatial distribution of the long-term trend of low flows compared with the observations.

In order to investigate changes in the low flow frequency caused by climate change, both the control and scenario runs generated by the three RCMs including different emission scenarios and realizations were applied to drive SWIM for the periods 1961 – 2000, 2021 – 2060 and 2061 – 2100. As there is a common problem in the RCM simulation results, which generate bias compared with observations (for more details see section "Changes in meteorological forcing"), many authors suggested different approaches to adjust the climate model output (termed "bias correction") and "correct" such differences mainly for annual average values (Themeßl *et al.*, 2010; Teutschbein and Seibert, 2010). However, this methodology is much less reliable when considering extremes (Graham *et al.*, 2007), and the direct use of RCM data might be still preferred when analysis of extreme conditions is of interest (Lenderink *et al.*, 2007). In addition, the summer projections are less biased than annual means in the applied scenarios (for more details see section "Changes in meteorological forcing"). Hence, taking into account the assumption that the RCM biases in the future are approximately the same as in the control climate, we did not apply any bias correction methods on the RCM scenarios. Furthermore we do not focus on the absolute magnitudes of low flow level in the scenario periods, but consider the changes in frequency of the reference 50-year low flow in the future.

5.3.4. River low flow indices and extreme value statistics

An extensive overview of various low flow indices are given by Smakhtin (2001) and WMO (World Meteorological Organization, 2008). In this study, the low flow frequency analysis is the major method applied for the river discharge time series under each climate realization.

Namely, the series of annual minimum 7-day (*AM7*) mean flow were selected to construct the low flow frequency curve. The 7-day duration is commonly used for the low-flow analysis (Svensson *et al.*, 2005, Feyen and Dankers, 2009), as it eliminates the day-to-day variation in river flows and provides a "true" low flow value (Stahl *et al.,* 2010). The annual minimum 7-day (*AM7*) mean flow was obtained by selecting the smallest values of mean discharge computed over any 7-consecutive days for each hydrological year (from 1st November to 31st October). A probability distribution is then fitted to the annual series of 7-day minimums and the 7Q50 (the annual 7-day minimum flow with a 50-year recurrence interval) statistic can be estimated from the distribution curve. In order to minimize the error in estimating the extreme low flows, the series of AM7 ought to be as long as possible. Hence, the 40-year period, the maximum length of the control period available in all RCMs' projections, is determined with control period (1961 – 2000) and two scenario periods (2021 – 2060 and 2061 – 2100).

The Generalized Extreme Value (GEV) distribution (Coles, 2001) was applied to fit the 40 yearly minima driven by both control and scenario runs from the same RCM, because it combines three

probability distributions (Gumbel, Fréchet and Weibull), which are commonly used in extreme value analysis. The GEV distribution is a three-parameter distribution defined by location parameter (μ), scale parameter (σ) and shape parameter (ξ) (see **Equation 5-2**). The method PWM (Probability-Weighted Moments) was used to provide robust estimation of these parameters.

$$F(x;\mu,\sigma,\xi)=\exp\left\{-\left[1+\xi\left(\frac{x-\mu}{\sigma}\right)\right]^{-1/\xi}\right\} \tag{5-2}$$

for $1+\xi(x-\mu)/\sigma>0$, where $\mu\in\Re$ is the location parameters, $\sigma>0$ is the scale parameter and $\xi\in\Re$ is the shape parameter.

The change in frequency of today's 50-year low flow is analyzed in the following steps (see **Fig. 5-3**). Firstly, the GEV distribution is fitted to the annual minimum series during the control period (see the solid line) and the 50-year low flow can be estimated from this curve. Secondly, the dash line is generated by fitting another 40-year AM7 series during a scenario period. Given the 50-year low flow level, the return period can be calculated in the new distribution curve, indicating the frequency of current 50-year low flow in the future (approximately 4 years in **Fig. 5-3**).

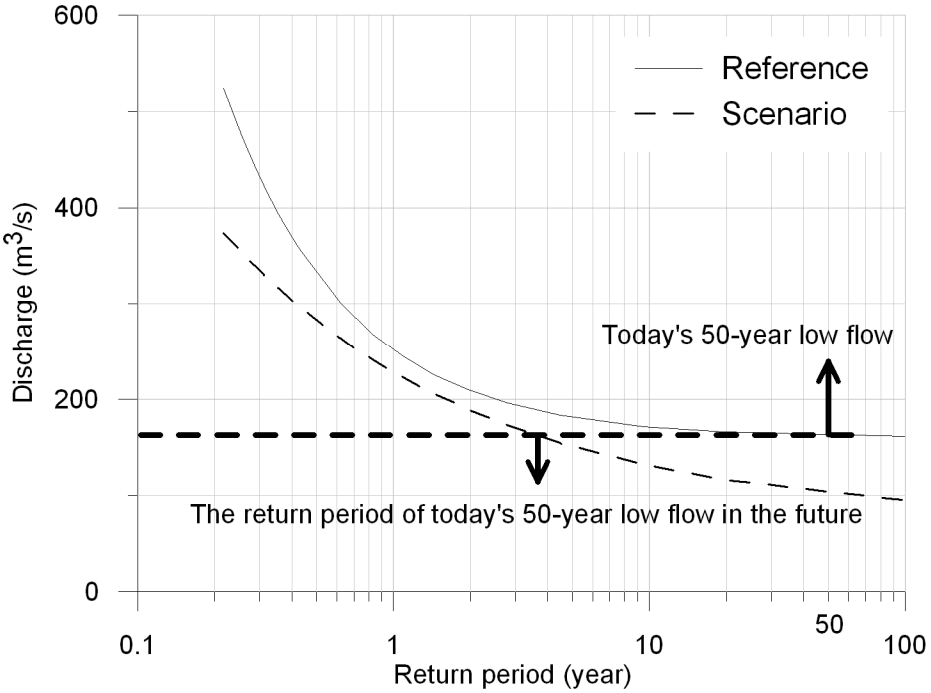

Figure 5-3: Schematic diagram for calculating the return period of today's 50-year low flow in the scenario period.

5.4. Model Calibration and Validation using observed climate data

The results in terms of the NSE (Nash-Sutcliffe Efficiency) and LNSE (Logarithmic Nash-Sutcliffe Efficiency) criteria in the calibration period (1961 – 1980) and in the validation period from 1981 to 2000 are listed in **Table 5-3**. In general, high NSE and LNSE (≥ 0.7) indicating

satisfactory results are achieved for the most rivers in both the calibration and validation periods: the NSE and LNSE values are higher than 0.7 for 16 – 17 gauges, and higher than 0.8 for 10 – 11 of the 24 gauges. The LNSE values in the calibration period are slightly higher (≥ 0.7 at 21 gauges) than in the validation period (≥ 0.59 at 21 gauges). It was more difficult to reproduce the low flow conditions in the 4 small catchments, where the LNSE values are ranging from 0.31 to 0.62 and the NSE value are from 0.01 to 0.78.

Table 5-3: Logarithmic Nash & Sutcliffe efficiency (LNSE) during calibration and validation periods for the selected gauges.

				NSE		LNSE	
River basin	Rivers	Gauges	Area (km^2)	Calibration 1961 - 1980	Validation 1981 - 2000	Calibration 1961 - 1980	Validation 1981 - 2000
Ems	Ems	Versen	2842	0.80	0.86	0.79	0.79
Weser	Weser	Intschede	37720	0.90	0.90	0.88	0.86
	Leine	Schwarmstedt	6443	0.82	0.74	0.86	0.82
	Aller	Marklendorf	7209	0.74	0.60	0.72	0.63
	Sieber	Hattorf	127	0.56	0.66	0.62	0.42
	Werra	Letzter Heller [1]	5487	0.63	0.58	0.76	0.77
	Weser	Vlotho[1]	17618	0.84	0.87	0.80	0.85
Danube	Danube	Hofkirchen	47496	0.84	0.85	0.85	0.84
	Danube	Donauwoerth [1]	15037	0.77	0.78	0.79	0.79
	Gross Laber	Schoenach	406	0.01	0.37	0.31	0.44
	Inn	Passau Ingling	26084	0.83	0.80	0.85	0.83
	Danube	Achleiten [1]	76653	0.86	0.85	0.86	0.85
Rhine	Rhine	Rees[1]	159300	0.84	0.85	0.84	0.82
	Main	Frankfurt-Osthafen	24764	0.72	0.81	0.82	0.81
	Neckar	Rockenau SKA	12710	0.78	0.80	0.84	0.83
	Murg	Rotenfels	468.8	0.72	0.73	0.76	0.77
	Moselle	Trier Up	23857	0.86	0.84	0.87	0.88
	Rhine	Rheinfelden	34550	0.68	0.71	0.71	0.71
Elbe	Elbe	Neu-Darchau	131950	0.84	0.79	0.84	0.76
	Weida	Weida	296.7	0.43	0.38	0.53	0.47
	Stepenitz	Wolfshagen[2]	571	0.78	0.47	0.75	0.59
	Mulde	Bad Dueben	6171	0.73	0.71	0.81	0.80
	Saale	Calbe-Grizehne	23719	0.78	0.57	0.78	0.66
	Elbe	Dresden[1]	53096	0.70	0.70	0.70	0.63

[1] gauges not calibrated

[2] observed discharge is only available from 1977 to 2003, so the calibraton period is the first half of the whole period.

The trends of simulated AM7 were compared with the observed ones during the period 1952 – 2003 (simulation for year 1951 was considered as the initialization of the model) (**Fig. 5-4** and **5-5**). **Figure 5-4** shows the observed and simulated AM7 at four selected gauges, two of which exhibit statistically significant upward trends and the other two show significant downward trends of the observed series. The upward trends (**Fig. 5-4(a)** and b) were well reproduced by the

simulated AM7 series and the two-sided p-values estimated by Mann-Kendall test also indicate the significance of the trends at 0.1 level. At the gauge Wolfshagen with significant downward trends (**Fig. 5-4(c)**), the simulated trend agrees with the observed one during the period of 1977–2003. However, at the gauge Hattorf (**Fig. 5-4(d)**) no trend can be found in the simulated series. The observed downward trend here is mainly caused by the zero discharges at the last 13 years. The reason is that in the east of the Weser drainage basin a karst region is located, and during the dry seasons water flows in the cracks, and does not reach the rivers. Such processes are difficult to reproduce using the SWIM model.

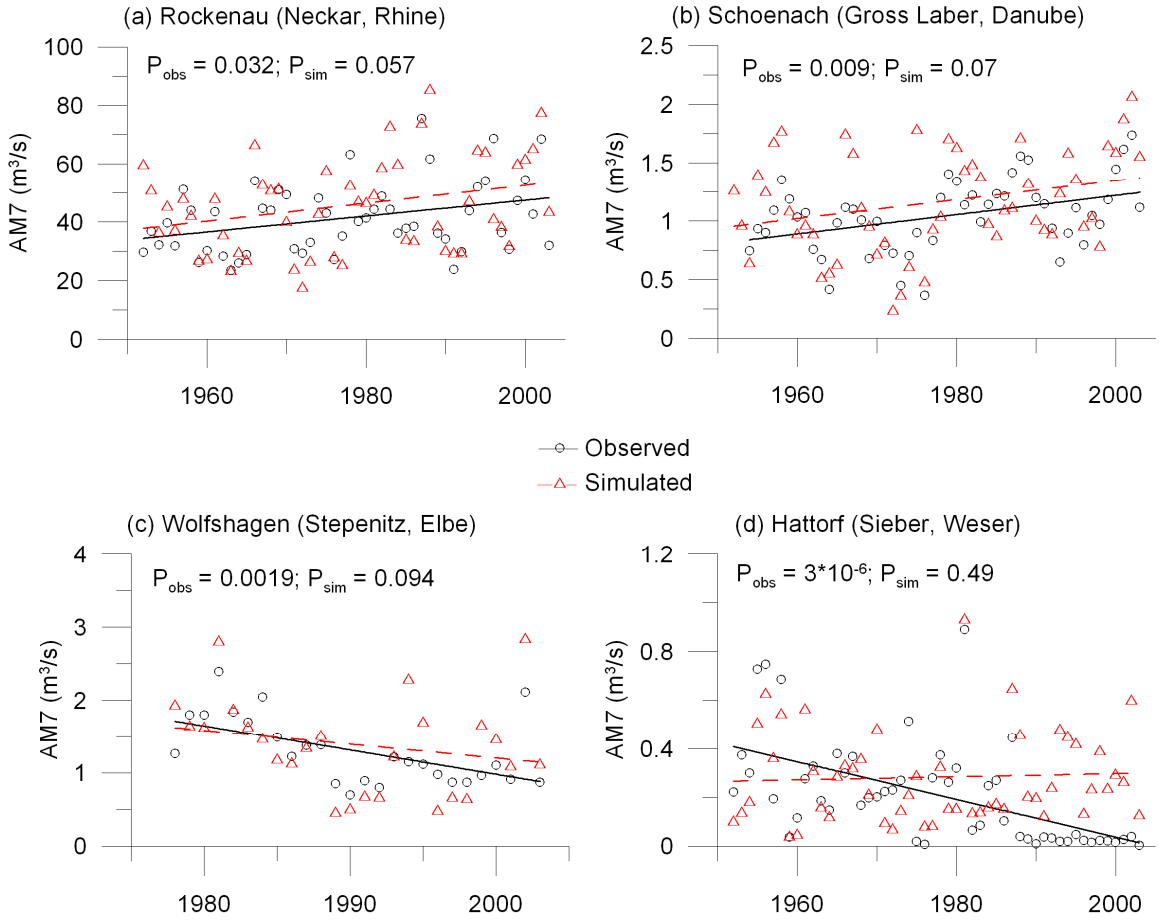

Figure 5-4: Observed and simulated AM7 at the selected gauges (Rockenau, Schoenach, Wolfshagen and Hattorf). The linear fitting curves indicate the upward or downward trend and the two-sided p-values detect the significance of the trend.

The spatial long-term trends in Germany are represented by the 144 observational gauges. For each of these gauges (**Fig. 5-5**), the trends were separated into upwards and downwards significant trend groups at the 0.1 significance level, and non-significant trends. Generally, the low flow level is increasing in southern Germany (parts of the Rhine and Danube basins). This result complies with the trend analysis by Hisdal (2001), who pointed out that the southern part of Germany has the trends towards less severe drought conditions coinciding with the increased precipitation. There are also a few scattered examples of decreasing trends of the low flow in northern Germany, particularly in the northeastern region and the karst region located in the Weser basin.

The trends of AM7 for 3768 river reaches simulated by SWIM (**Fig. 5-5**) were superimposed on the observed trends and depicted in the same categories. A distinct and similar spatial pattern in the south (toward less severe low flow) is well represented by SWIM. However, the scattered points of downward trends are hardly reproduced, especially at the small catchments (where three fourths of all downward trends are observed). The reasons why it is hard to reproduce the low flow condition in these small catchments by SWIM will be presented in the following paragraphs.

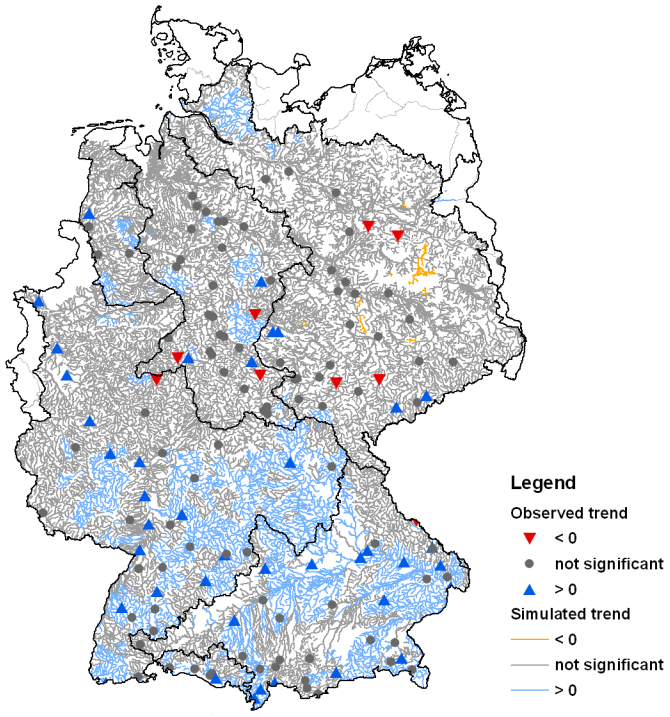

Figure 5-5: Trends of observed and simulated AM7 for the period 1952 – 2003.

As the low flow frequency curve is the key measure to analyze changes of low flow occurrences, it is also important to validate the fitted frequency curves of the simulated data against the observed ones. **Figure 5-6** with 12 examples shows that the hydrological model driven by the observed climate data reproduces the low-flow frequency curves reasonably well. It is interesting that in large rivers (**Fig. 5-6(a)** – **5-6(i)**), the low flow levels of return periods lower than 1 year are slightly overestimated while the ones of return period larger than 10 years are somewhat underestimated. These disagreements may be partly due to the man-made modifications of low-flow regimes which are not accounted for in the hydrological model. Dynesius and Nilsson (1994) classified Weser, Elbe and Danube as strongly affected river systems and Rhine as moderated affected, this may explain the differences of the extreme low flows in the former three basins are relatively larger than in the Rhine basin. In addition, the impact of land use change during the past 40 years is not considered in the simulations, and the "static" land use information may also contribute to a bias of the simulation results.

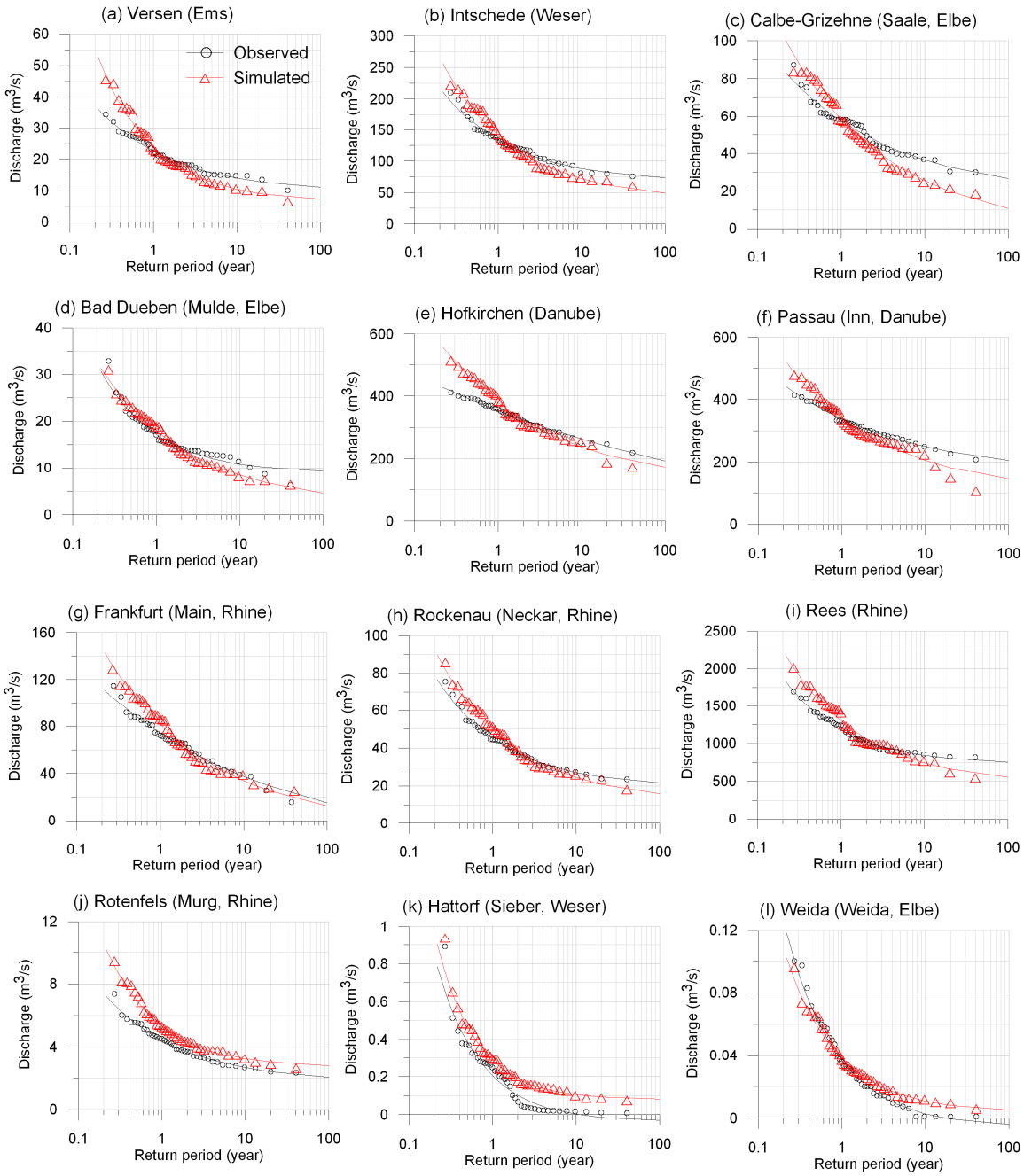

Figure 5-6: Return level plots for the observed and simulated annual minimum 7-days discharge (AM7) at selected gauges during the control period (1961 – 2000).

The fitted frequency curves for the small rivers (see **Fig. 5-6(j)** – **5-6(l)**) also reflect poorer reproduction of the low flow levels. Beside the complex water processes in the karst regions, there are also other possible reasons which add to difficulties in simulating the low flow conditions. The first reason is that the near-natural catchments are not completely natural. For example, a hydropower plant is located upstream the gauge Hattorf in the catchment Sieber (Weser) (**Fig. 5-4(d)** and **Fig. 5-6(k)**) and an increasing groundwater irrigation was reported by Wittenberg (2003) in northern Germany since 1950. Even a small interference on the natural river processes in small rivers can change the river low flow substantially. Secondly, the low flows in

the small rivers are practically beyond the precision of the calculation. The example of River Weida shows a difference between the simulated and observed extreme low flow of just 0.01 m^3/s (**Fig. 5-6(l)**). However, this small difference can influence the LNSE substantially in this case indicating poorer simulation results and mislead the trend direction. The third reason, which cannot be seen from the figures, is rather poor climate data and geological data available for the small-scale areas. There are about 270 climate stations and more than 2000 precipitation stations distributed over Germany, which provides a very good data base for the large-scale modeling. However, such a distribution is still insufficient for simulation of some small catchments if *e.g.* none precipitation station is located directly within them. In addition, other climate variables other than precipitation (*e.g.* temperature, radiation, humidity) are generally interpolated from the stations located far from the catchment, causing substantially larger errors in small-scale modeling. More detailed aquifer and soil information are also required to model the processes more accurately and the land use change during the long-term period is also influential for small catchments.

5.5. Scenario results

5.5.1. Changes in meteorological forcing

Before investigating the changes in the low flow frequency, the climate driving forces in terms of annual and summer (from April till October) average temperature and precipitation were analysed to reveal the characteristics of the changing patterns and the performance in reproducing the current climatic conditions. The simulated variables in three time slices by each RCM realization are compared with the observed values in the period of 1961 – 2000, and only the differences between them are plotted in **Fig. 5-7**. Due to the spatial restriction of the WettReg scenarios, this comparison can only be done for the climate data in the German part of the five basins.

The bias between the simulated and observed data in the control period is shown as the deviation from the dashed line across zero (see the plots for 1961 – 2000 in **Fig. 5-7**). Regarding both annual and summer temperatures, the physical RCMs project a bias in a range from -1.3 to 0.7 °C. CCLM projects obviously a cooler condition (from -1.3 to -0.9 °C) in both realizations and REMO overestimates the temperature slightly (from 0.5 to 0.7 °C). The temperature generated by the medium realization of WettReg shows a good agreement with the observed values both in summer time and the whole year.

REMO and WettReg generate reasonable results for annual and summer precipitation, with a bias of 20 – 30 mm, while CCLM has a bias of more than 100 mm in annual precipitation. CCLM projects cooler and wetter conditions with the greatest bias among the three RCMs. However, for the summer temperature and precipitation, the bias of all realizations becomes smaller compared to the annual values except the summer precipitation generated by REMO. The two realizations generated by CCLM seem to project nearly the same summer conditions, indicating a small difference between the realizations. The better performance of the summer climate scenarios implies a more robust projection of low flow conditions in Germany.

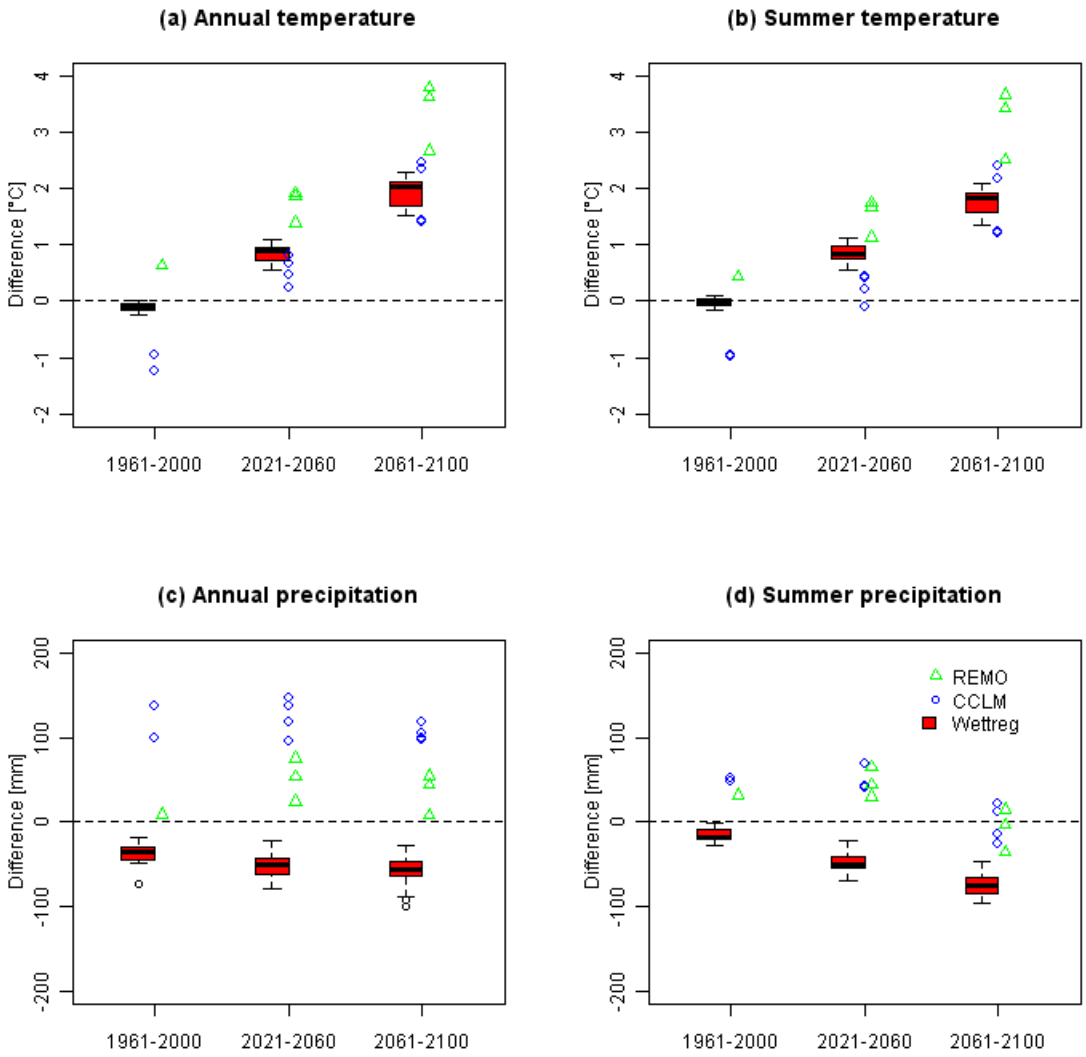

Figure 5-7: Changes between observed and simulated average temperatures and precipitation under different RCM scenarios in both control and scenario periods in the German part of the five basins.

Figure 5-7 also demonstrates the changing pattern by comparing the scenario data with their corresponding control runs. Regarding the annual and summer average temperature, all RCMs project a steady increase of 2 – 3 °C with time. However, no general trend in precipitation is agreed by all models. The 60 realizations from the empirical-statistical model WettReg show a continuously downward trend in precipitation, while the two physical models (REMO and CCLM) project more dynamic changes with an increase in precipitation in the middle of this century and a slight decrease at the end of this century. It should be noticed that all three RCMs project similar summer precipitations during the second scenario period and hence a more robust projection of summer low flow conditions could be expected due to more robust climate input. In addition, the large difference of the projected annual precipitation partly reveals the reason why it was more difficult to obtain similarity in flood (occurring mostly in winter) patterns simulated by SWIM driven by different RCMs (Huang *et al.*, 2012).

5.5.2. Changes in return period of today's 50-year low flow

5.5.2.1. REMO

The low flow frequency analysis was applied for 5473 river reaches, and the changes of 50-year low flow in the control period (1961 – 2000) at all these river reaches for three emission scenarios in the two future periods are shown in **Fig. 5-8**. In the first period 2021 – 2060, both the spatial patterns and the magnitude of the return period reflect somehow the difference between emission scenarios. Under B1 scenario, which is more environmental friendly with a relatively small increase in temperature, less severe low flow conditions are expected in most parts of Germany, and the 50-year low flow is likely to occur every 100-year or more. In contrast, the 50-year low flow may occur more frequently under A2 scenario over Germany (except some rivers flowing from the Alpine region). There is no dominant pattern of the changes in the return period projected under A1B scenario. The basin Ems and western part of Rhine may become the critical regions with more frequent extreme low flows, while in the Weser, German part of the Elbe and eastern part of the Rhine basin the 50-year low flow could recur in more than 100 years.

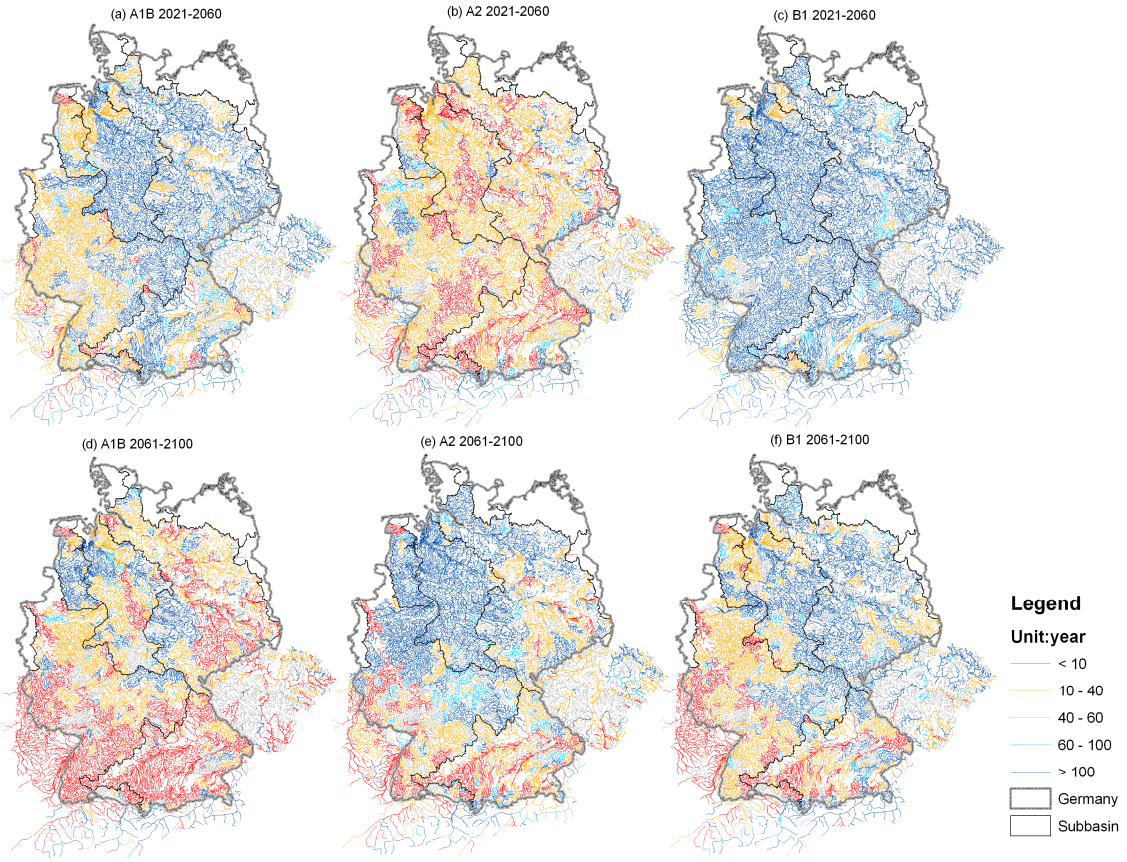

Figure 5-8: Return periods for the 50-year low flow in the reference period under REMO scenarios (unit: year).

During the second scenario period 2061 – 2100, A1B and B1 scenario results show more severe low flow conditions than in the middle of the century. The 50-year low flow may occur more often in most German rivers under A1B scenario, and in some parts of the Rhine, Danube and Ems under B1 scenario. However, the A2 scenario, which projects globally warmer and dryer conditions than A1B and B1 scenarios, has moderate increase in temperature and precipitation in

Germany simulated by REMO (MPI, 2008). Hence, the low flow problems would be partly alleviated under A2 scenario, especially in the northern Germany, compared to the middle of the century. However, there are some areas where all three scenario results agree with the change direction in this period. The western Rhine and the German part of the Danube may face extreme low flow conditions more often than before.

The Alpine regions outside Germany seem to have less frequent extreme low flows suggested by all scenarios in both periods, maybe due to changes in discharge regime with higher flows in winter.

We can conclude that the changes of low flow conditions in the first scenario period are uncertain due to the different emission scenarios. However, in the second period the projected changing pattern is more pronounced and certain suggesting more frequent 50-year low flows in the western part of the Rhine basin and in the German part of the Danube basin.

5.5.2.2. CCLM

In the first scenario period, it is obvious that the simulation with the B1_1 realization is the wettest one with less frequent extreme low flows over Germany, while the other simulations show drier conditions with shorter return periods in large regions of southern, central and eastern Germany (**Fig. 5-9(a) – (d)**). The highest uncertainty is visible in the western part of the Rhine basin and in the northern part of Germany.

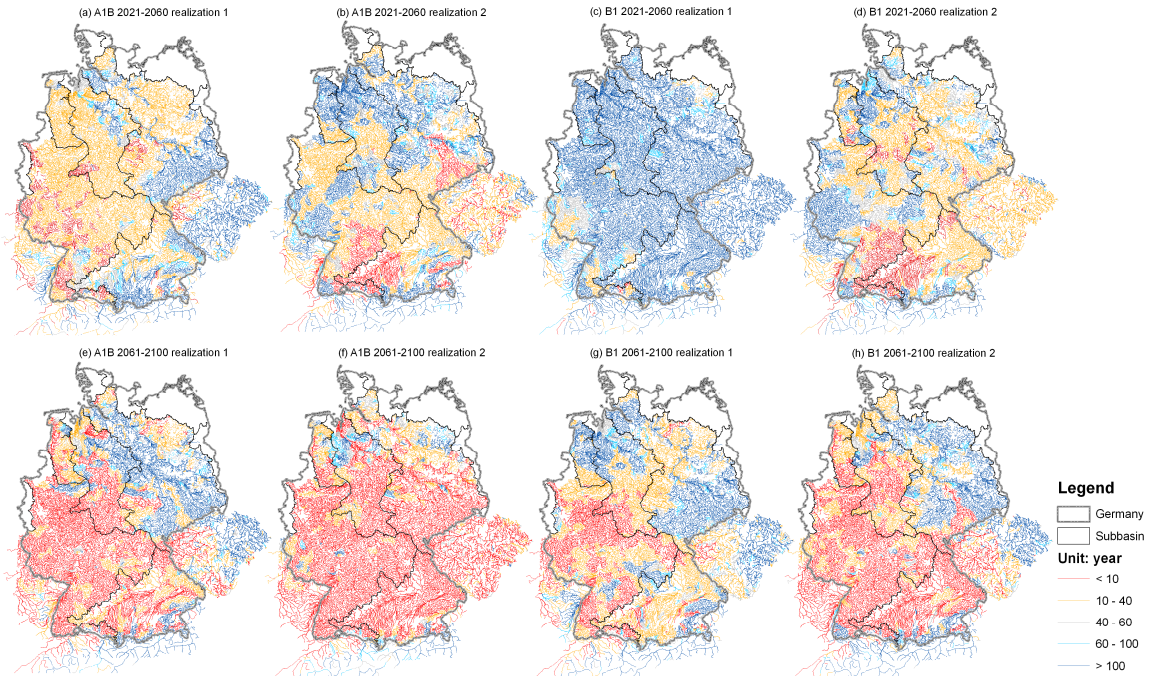

Figure 5-9: Return periods for the 50-year low flow in the reference period under CCLM scenarios (unit: year).

In the second scenario period, more similar changes of return period can be found in all realizations. The rivers in all basins except the Elbe and the northern parts of the Ems and Weser basins show significant increases in low flow frequencies. In the critical regions: German Rhine and Danube, upper Ems and Weser, the current 50-year low flow may recur every 10 years or

less. Less frequent low flow is still expected in the Alpine regions in Austria. However, there is no distinct change pattern agreed by all realizations in the Elbe basin.

5.5.2.3. WettReg

Due to the lack of WettReg scenarios outside Germany, the climate data in other countries can only be obtained from the interpolation of the German neighboring stations. This of course leads to unreliable simulation results not only in the river reaches outside Germany but also the international rivers flowing through Germany, *e.g.* the Elbe, Inn flowing from Austria, Rhine and Moselle river flowing from France (see the green lines in **Fig. 5-10**). Therefore, instead of all river reaches shown in **Fig. 5-8** and **Fig. 5-9**, only 3768 river reaches inside Germany were plotted (see **Fig. 5-10**). In addition, the international rivers (the green lines) should not be taken into account as well. The medium changes of all 20 realizations are plotted and they show a good agreement toward lower return periods among different emission scenarios for Germany. In the near future, the simulation driven by the B1 scenario shows moderate changes with return period between 10 and 40 years, while the changes under other two scenarios are more significant (partly also less than 10 years). From 2061 to 2100, the changes under all scenarios indicate that today's 50-year low flow may recur less than 10 years in southern Germany and in southern part of the Elbe basin.

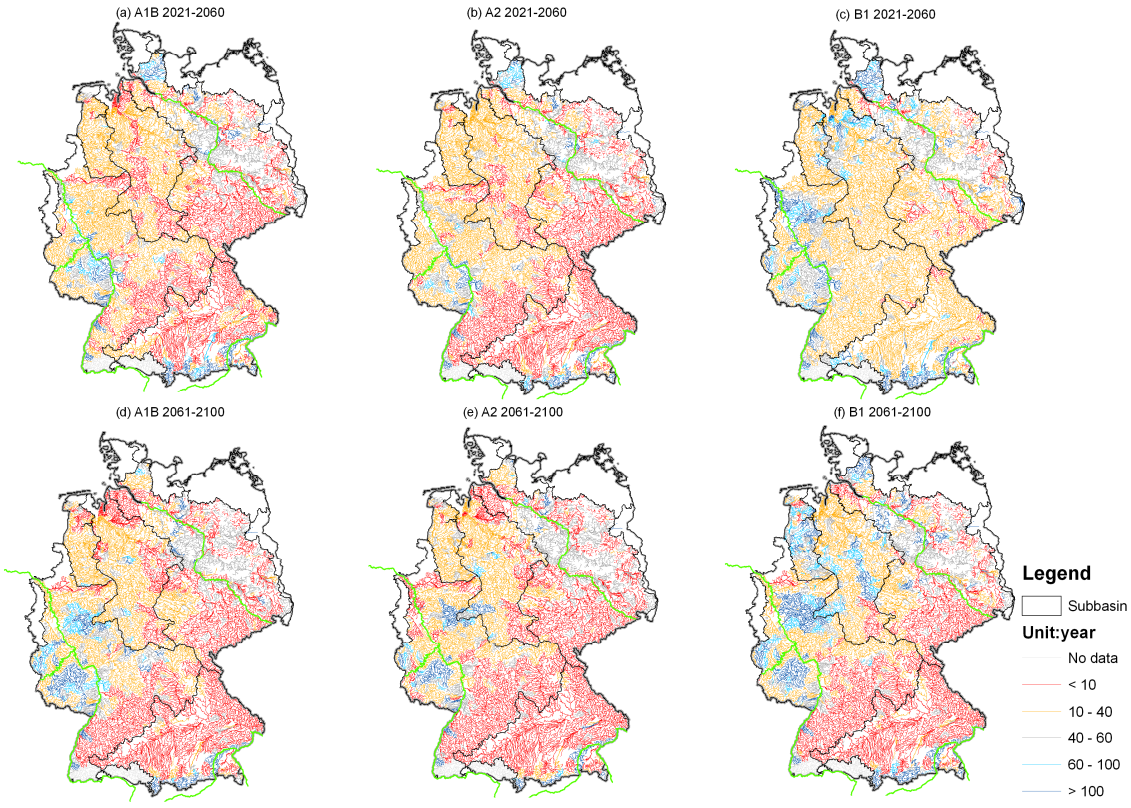

Figure 5-10: Return periods for the 50-year low flow in the reference period under WettReg scenarios (unit: year).

5.5.2.4. Summary of all scenario results

Finally, in order to get the general change pattern of the low flows in Germany and account for the uncertainty from different climate scenarios, the medium return period for each river reach was calculated from all outputs in **Fig. 5-8**, **5-9** and **5-10** and shown in **Fig. 5-11**. The medium return period is highlighted only for the river reaches where more than 6 of the 10 results agree with the return period less than 40 years or more than 60 years. The outputs are divided into two groups: high agreement (more than or equal to 8 of 10 projections (≥80%), which means low uncertainty) and moderate agreement (6 – 7 projections (60% – 70%), meaning moderate uncertainty). For the river reaches, which are colored grey in **Fig. 5-11**, the uncertainty of the projections remains high or the return period does not change significantly (40 – 60 years). It should be noticed that there are only 7 scenario results (3 REMO runs and 4 CCLM runs) available for the river reaches outside Germany. Hence, the change in return periods agreed by 6 or 7 projections means high agreement (more than 80% of the total projections) outside Germany.

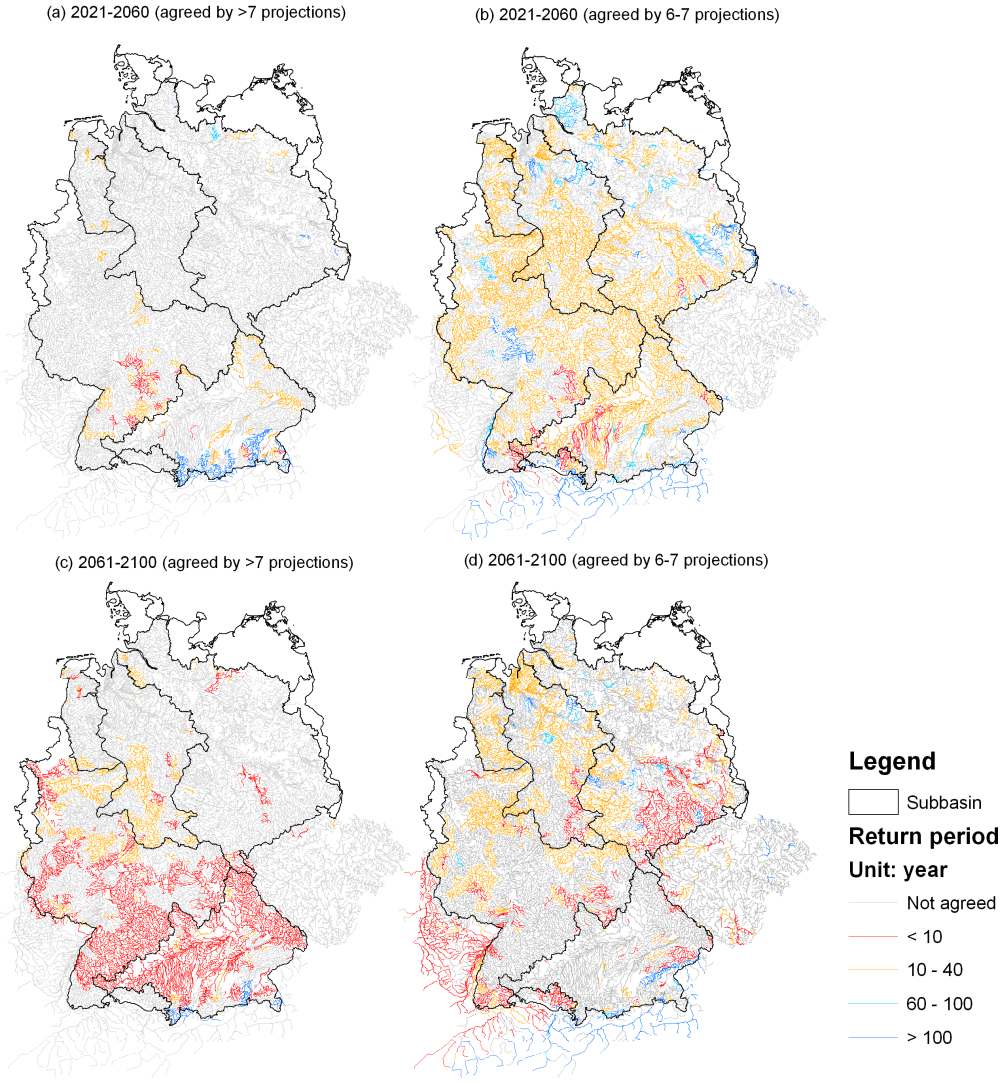

Figure 5-11: Medium return period for the 50-year low flow (the middle number of the ones driven by REMO, CCLM and WettReg scenarios and shown in Fig. 5-8, 5-9 and 5-10) with the change directions agreed by 8-10 projections (a) and 6-7 projections (b).

As it is shown in **Fig. 5-11**, in the period of 2021–2060 there may be only small changes in low flow frequencies because most of the return periods change to between 10 and 40 years and are agreed by 6 or 7 projections only. However, in the second period 2061 – 2010, more frequent low flows were projected in western, southern and central Germany, and the agreement level has increased. In **Fig. 5-11(c)**, more than or equal to 80% of all projections indicate that the current 50-year low flow may occur in less than 10 years in the southern and part of western Germany. In addition, 6 – 7 projections show more frequent low flows in the central and western Germany. There is large uncertainty of the change patterns in the northern part of Germany, especially in the Elbe basin. In both periods, the rivers in the southern Alpine region outside Germany may have less frequent low flow conditions as agreed by 6 or 7 projections. At the end of this century, severe low flow conditions may occur more frequently in the western Swiss and French part of the Rhine basin (high agreement between projections).

5.5.3. Changes in seasonal dynamics

The previous results show the changes in frequency of extreme low flows in the long-term without any clue on the changes of the critical seasons. The analysis of seasonal dynamic is aimed to investigate the low flow seasons in the second scenario period, when more severe low flow condition are likely to occur. The relative changes are represented by the average of monthly minimum 7-day (MM7) mean flows in the scenario period (2061 – 2100) divided by the average in the reference period (1961 – 2000). **Figure 5-12** shows the relative changes under all RCM realizations at six selected gauges, which represent the main large rivers in Germany. The relative changes lower than 100% (under the red dashed line) mean that lower MM7 are expected in the future, while the changes more than 100% refer to a wetter condition with higher MM7. At the selected gauges in Ems, Weser and Rhine, the winter low flow level (from December to February) tends to increase driven by all the physical RCMs realizations and more than half of the WettReg realizations. This increase complies with the projected increase in winter precipitation in central Europe (IPCC, 2007). In contrast, the low flow level is likely to decrease in late summer and autumn (from August to November) under warmer and drier climate conditions. This tendency is particularly pronounced in the Danube and the two tributaries in Rhine, with all the results driven by WettReg realizations and more than 75% realizations by the dynamic models. In other rivers, the decrease in low flow level is confirmed by more than three fourth of the WettReg realizations and part of the CCLM and REMO realizations. Compared with the current low flow regimes in August and September (see **Fig. 5-2**), the length of the low flow seasons tends to expand until late autumn. In the Danube and Rhine basins, the low flow seasons would be twice longer compared to the current situation.

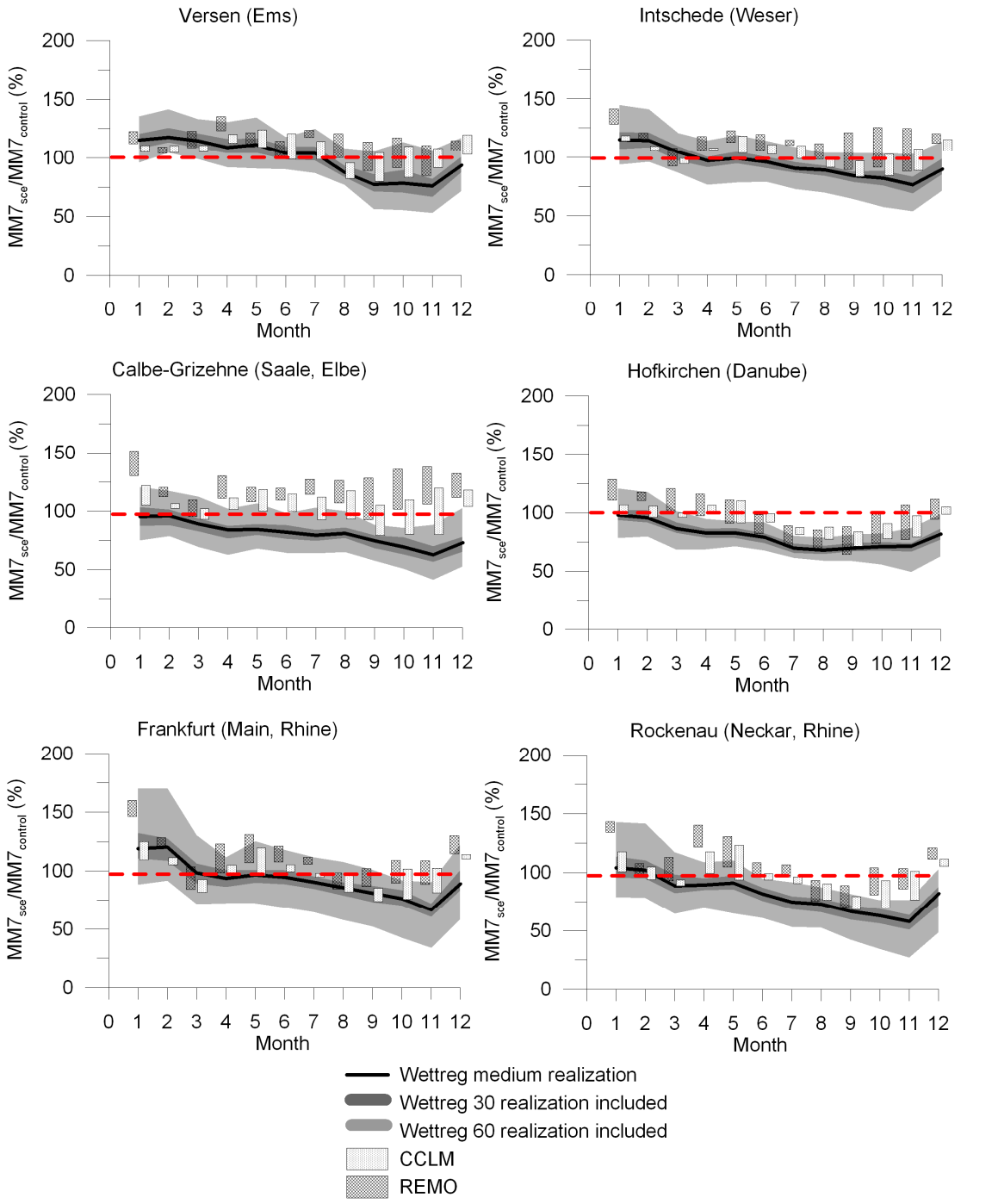

Figure 5-12: Changes in monthly minimum 7-days mean discharge between the second scenario period (MM7sce) (2061 – 2100) and the control period (MM7control) (1961 – 2000) at selected gauges.

5.6. Discussion

In general, there is a relatively large uncertainty in projecting the low flow frequency for the middle of this century. The simulations driven by B1 realizations of the physical RCMs tend to result in less frequent occurrences of extreme low flows due to higher precipitation combined

with relatively small increase in temperature. The simulations driven by A1B scenario are generally drier with more diverse spatial patterns of the low flow changes. Model WettReg always projects drier scenarios, under which the extreme low flow is likely to recur more frequently, practically everywhere in Germany. However, it doesn't mean that the empirical-statistical models only project dry scenarios.

The simulation results driven by another German RCM, the empirical-statistical model STAR (Orlowsky *et al.*, 2008) agreed with the WettReg results in the long-term trend, showing reductions of summer flows in most German rivers (Huang *et al.*, 2010). However, the extreme low flows occur less frequent in the central of Germany. The results of the STAR model are not further discussed here because they cover only the first scenario period until 2060.

A more robust result, agreed by ≥ 80% of the scenario realizations is that more frequent extreme low flow situations are likely to occur in western, southern and part of central Germany towards the end of this century. Central Germany may also become a more critical region as suggested by CCLM realizations and the medium WettReg realizations. The rivers originating from the south Alpine regions will probably have higher low flows due to a reduction of precipitation as snow in winter and spring. Higher uncertainty was found in the northeastern Germany. Both increase and decrease in the low flow frequency are projected under the realizations from REMO and CCLM depending on emission scenario. According to the simulations with WettReg, more frequent low flow could be dominant in the future, and in the southern and eastern Germany the 50-year low flow may recur every 10 year or less.

Recently, the same climate scenarios from REMO, CCLM and WettReg were applied as the input data for SWIM to analyze the flood occurrence in Germany (Huang *et al.*, 2012). Here, the uncertainty of projections was substantially higher, so that no strong change pattern agreed by 3 models and 3 emission scenarios could be detected. Compared with this uncertainty in flood projections, the signal of severer low flow is much stronger, especially at the end of the century.

The lower uncertainty in low flow projections is in agreement with climate input; especially for the summer half of the year (see climate input data in **Fig. 5-7(b)** and **5-7(d)**). The simulations driven by the statistical model WettReg always produce drier projections due to continuous reduction of precipitation and rise in temperature. The physical models with more dynamic changes in precipitation result in more diverse changes at both spatial and temporal scales. However, the consequence of the combination of higher temperature and lower precipitation becomes more apparent at the end of the century, particularly in summer and autumn seasons. The higher temperature increases the potential evapotranspiration and can lead to a reduction of river flows even when the precipitation stays at the same level. Hence, during the warmer and drier times, the deficit of precipitation accompanied by higher evapotranspiration demand is the major factor triggering the extreme low flows. August and September, which are already the critical months in most German rivers, are likely to experience more frequent low river discharges. In addition, the low flow season tends to expand until late autumn, increasing further the risk of water stress in water-related sectors.

The strong signal of severe low flow conditions has also been found in other low flow studies in Germany, though they were done only for specific rivers. For example, Hennegriff *et al.* (2008) found that in the months July to September, the monthly average low flow may decrease by 10% to 20% in the Neckar and Danube in the period 2021 to 2050 compared to the reference period 1971 to 2000 under WettReg scenarios. For the entire Rhine basin, summer low flow is expected to reduce by about 5% for the XCCC2050 scenario and by 12% under conditions of the UKHI2050 scenario (Middelkoop *et al.*, 2001). They also pointed out that the projection

reliability is higher due to the lower temporal variability of low flows (in the order of weeks), which is more in accordance with the temporal resolution of the climate scenarios. The projection results for the Danube basin (Mauser *et al.*, 2008) has shown that the AM7 could be reduced to a half of the reference value (1971 – 2003) by 2030 and to one third by 2060. These studies suggested a high potential of decrease in low flow level in some specific regions in Germany. In contrast, our study covers the whole of Germany, and it shows that not only Danube and Rhine rivers, but also large regions in western, southern and central Germany are likely to experience longer and severer low flow conditions. In addition, the demonstrated changes in low flow patterns are more robust and reliable due to use of various RCMs and including different emission scenarios. Of course, one should always keep in mind that the low flow conditions are associated with many factors, climate change being only one of them, though very important. The extreme low flow events can be alleviated by proper water resources and land-use management *e.g.* releases of imported water from dams and changes of the vegetation regime (Harboe, 1988, Walker and Thoms, 1993, Gustard and Wesselink, 1993).

5.7. Conclusion

In this paper, the changes in low flow condition due to climate change in the five largest river basins of Germany were analyzed by combining the eco-hydrological model SWIM and three regional climate models under various emission scenarios. Both the spatial distribution of the long-term trend and the low flow frequency curves derived from the SWIM simulations for the reference period show satisfactory results compared with the observed ones for large catchments. It shows that SWIM is capable of reproducing the low flow characteristics after calibration. However, it should be mentioned that some difficulties were experienced in reproducing the exact year-to-year AM7 as well as the low flows in small catchments. Human interferences and land-use conditions play significant roles in low flow generation and modification. More detailed information, *e.g.* precise climate, geological and soil data, are required to improve simulation results in the small-scale catchments.

The present study suggests that the river low flows in western, southern and part of central Germany may occur much more frequently in the last decades of this century. The rivers originating from the Alpine regions are likely to have less severe low flows. These results are agreed by more than or equal to 80% of the climate realizations used in this study. From summer to late autumn months the large German rivers may experience more severe low flow events due to the combination of high temperature, low precipitation and high evaporation demand. The potential changes in the low flow conditions imply severe water stress at the country scale for the period 2061 – 2100, which can affect various water use sectors, like river navigation, water supply, power plants and agriculture. There is still a relatively large uncertainty in projecting the low flow frequency for the middle of this century and in the northeastern Germany.

However, one should notice that all the RCM runs in this study are based on one GCM projection. Kay *et al.* (2009) found that the largest uncertainty in climate impact assessment comes from the GCM structures. This motivates us to undertake other realizations based on various GCMs to investigate whether the predictions of the low flows obtained in this study are still robust.

As mentioned above, climate change is only one factor affecting the low flow conditions in the future. In order to better quantify the potential changes in low flows, land-use change scenarios and water management practices in Germany should also be considered in the future studies for specific catchments and rivers. Sustainable water and land-use management are helpful to alleviate the water stress caused by climate factors. However, this requires engagement with

stakeholders in order to analyze potential measures and provide robust adaptive solutions. Such research and negotiation has already begun in the German federal state Saxony-Anhalt with intensive discussion on technical measures and management strategies to adapt to climate change impacts on hydrology (Hattermann *et al.*, 2010).

Acknowledgement: The authors would like to thank GRDC (The Global Runoff Data Centre, 56068 Koblenz, Germany) and UNESCO's European Water Archive (EWA) for the data support. Many thanks go also to the colleagues at PIK who supported the work and especially the set-up of the data base.

Reference:

Arnold, J. G., P. M. Allen, and G. Bernhardt (1993), A comprehensive surface-groundwater flow model, *J. Hydrol.* **142**, 47-69.

Arnold, J.G., J.R. Williams, A.D. Nicks, and N.B. Sammons (1990), *SWRRB - A Basin Scale Simulation Model for Soil and Water Resources Management*, Texas A&M University Press: College Station, Texas.

Bronstert, A., V. Kolokotronis, D. Schwandt, and H. Straub (2007), Comparison and evaluation of regional climate scenarios for hydrological impact analysis: General scheme and application example, *Int. J. Climatol.* **27**, 1579-1594.

Coles, S. (2001), *An Introduction to Statistical Modeling of Extreme Values*, Springer-Verlag, London.

Dynesius, M., and C. Nilsson (1994), Fragmentation and flow regulation of river systems in the northern third of the world, *Science* **266**, 753-762.

Enke, W., T. Deutschlaender, F. Schneider, and W. Kuechler (2005a), Results of five regional climate studies applying a weather pattern based downscaling method to ECHAM4 climate simulations, *Meteorologische Zeitschrift* **14(2)**, 247-257.

Enke, W., F. Schneider, and T. Deutschlaender (2005b), A novel scheme to derive optimized circulation pattern classifications for downscaling and forecast purposes, *Theor. Appl. Climatol.* **82**, 51-63.

Feyen, L., and R. Dankers (2009), Impact of global warming on streamflow drought in Europe, *J. Geophys.* **114(D17116)**, 17.

Graham, L., J. Andreasson, and B. Carlsson (2007), Assessing climate change impacts on hydrology from an ensemble of regional climate models, model scales and linking methods - a case study on the Lule River basin, *Clim. Change* **81**, 293-307.

Gustard, A., and A. Wesselink (1993), Impact of land use change on water resources: Balquidder catchments, *J. Hydrol.* **145**, 389-401.

Harboe, R. (1988), Including daily constraints in a monthly reservoir operation model for low-flow, *Adv. Water Resour.* **11(2)**, 54-57.

Hattermann, F., V. Krysanova, F. Wechsung, and M. Wattenbach (2005), Runoff simulations on the macroscale with the ecohydrological model SWIM in the Elbe catchment - validation and uncertainty analysis, *Hydrol. Process.* **19**, 693-714.

Hattermann, F.F., M. Weiland, S. Huang, V. Krysanova, and Z. Kundzewicz (2010), Model-supported Impact Assessment for the Water Sector in Central Germany under Climate Change - a Case Study, *Water Resour. Res.* (accepted).

Hennegriff, W., J. Ihringer, and V. Kolokotronis (2008), Prognose von Auswirkungen des Klimawandels auf die Niedrigwasserverhältnisse in Baden-Württemberg, *Korrespondenz Wasserwirtschaft* **6(1)**, 309-314.

Hisdal, H., K. Stahl, L. Tallaksen, and S. Demuth (2001), Have droughts in Europe become more severe or frequent?, *Int. J. Climatol.* **21**, 317-333.

Hooghoudt, S. (1940), Bijdrage tot de kennis van enige natuurkundige grootheden van de grond, *Versl. Landbouwkd. Onderz.* **46(14)**, 515-707.

Huang, S., F. Hattermann, V. Krysanova, and A. Bronstert (2012), Projections of climate change affected river flood conditions in Germany by combining three different RCMs with a regional hydrological model, *Climatic Change* (accepted).

Huang, S., V. Krysanova, H. Österle, and F. Hattermann (2010), Simulation of spatiotemporal dynamics of water fluxes in Germany under climate change, *Hydrol. Process.* **24(23)**, 3289-3306.

IPCC (2007), *Climate Change 2007: Impacts, Adaptation and Vulnerability - Summary for Policymakers. Working Group II Contribution to the Fourth Assessment Report of the Intergovernmental Panel on Climate Change*, Cambridge University Press.United Kingdom and New York, NY, USA.

Jacob, D. (2001), A note on the simulation of the annual and inter-annual variability of the water budget over the Baltic Sea drainige basin, *Meteorol. Atmos. Phys.* **77**, 61-73.

Kay, A., H. Davies, V. Bell, and R. Jones (2009), Comparison of uncertainty sources for climate change impacts: flood frequency in England, *Climatic Change* **92**, 41-63.

Kosková, R., S. Nemecková, C. Hesse Jakubíková, A., V. Broza, and J. Szolgay (2007), Using of the Soil Parametrisation Based on Soil Samples Databases in Rainfall-Runoff Modelling, **In:** Jakubíková, A. and Broza, V. and Szolgay, J. (eds.), *Proceedings of the Adolf Patera Workshop "Extreme hydrological events in catchments". 13.11.2007*, Bratislava.

Krysanova, V., A. Meiner, J. Roosaare, and A. Vasilyev (1989), Simulation modelling of the coastal waters pollution from agricultural watersheds, *Ecol. Model.* **49**, 7-29.

Krysanova, V., D. Möller-Wohlfeil, and A. Becker (1998), Development and test of a spatially distributed hydrological / water quality model for mesoscale watersheds, *Ecol. Model.* **106**, 261-289.

Krysanova, V., F. Hattermann, and F. Wechsung (2007), Implications of complexity and uncertainty for integrated modelling and impact assessment in river basins, *Environ. Modell. Softw.* **22**, 701-709.

Lenderink, G., A. Buishand, and W. van Deursen (2007), Estimates of future discharges of the river Rhine using two scenario methodologies: direct versus delta approach, *Hydrol. Earth Syst. Sci.* **11(3)**, 1145-1159.

Majewski, D. (1991), The Europa Modell of the Deutscher Wetterdienst, *ECMWF Seminar on numerical methods in atmospheric models* **2**, 147-191.

Mauser, W., T. Marke, and S. Stoeber (2008), Climate Change and water resources: Scenarios of lowflow conditions in the Upper Danube River Basin. **In:** *XXIVth Conference of the Danubian Countries, IOP Conf. Series: Earth and Environmental Science 4*.

Middelkoop, H., K. Daamen, D. Gelllens, W. Grabs, J. Kwadijk, H. Lang, Parmet, B.W.A.H, B. Schädler, J. Schulla, and K. Wilke (2001), Impact of climate change on hydrological regimes and water resources management in the Rhine basin, *Climatic Change* **49**, 105-128.

Monteith, J. L. (1965), Evaporation and the environment, *Symp. Soc. Expl. Biol.* **19**, 205-234.

MPI (2008), MPI (Max-Planck-Institute), available at http://www.giwep.de/fileadmin/pdf/pr%C3%A4sentation_mpi_meteorologie_2008.pdf (last asscessed: 10.10.2011).

Orlowsky, B., F. Gerstengarbe, and P. Werner (2008), A resampling scheme for regional climate simulations and its performance compared to a dynamical RCM, *Theor. Appl. Climatol.* **92**, 209-223.

Pfister, C., R. Weingartner, and J. Luterbacher (2006), Hydrological winter droughts over the last 450 years in the Upper Rhine basin: a methodological approach, *Hydrol. Sci. J.* **51(5)**, 966-985.

Priestley, C. H. B., and R. J. Taylor (1972), On the assessment of surface heat flux and evaporation using large scale parameters, *Mon. Weather Rev.* **100**, 81-92.

Rockel, B., A. Will, and A. Hense (2008), The regional climate model COSMO-CLM (CCLM), *Meteorologische Zeitschrift* **17(4)**, 347-348.

Sangrey, D., K. Harrop-Williams, and J. Kaliber (1984), Predicting ground-water response to precipitation, *ASCE J. Geotech. Eng.* **110(7)**, 957-975.

Schönwiese, C., T. Staeger, and S. Trömel (2006), Klimawandel und Extremereignisse in Deutschland. **In:** *Klimawandel und Extremereignisse in Deutschland - Klimastatusbericht 2005*, Deutscher Wetterdienst, Offenbach, 7-17.

Smakhtin, V. (2001), Low flow hydrology: A review, *J. Hydrol.* **240**, 147-186.

Smedema, L., and D. Rycroft (1983), *Land Drainage - Planning and Design of Agricultural Drainage Systems*, Cornell University Press, Ithaca, NY.

Stahl, K., H. Hisdal, J. Hannaford, L. Tallaksen, H. van Lanen, E. Sauquet, S. Demuth, M. Fendekova, and J. Jodar (2010), Streamflow trends in Europe: evidence from a dataset of near-natural catchments, *Hydrol. Earth Syst. Sci.* **14**, 2367–2382.

Stahl, K., H. Hisdal, L. Tallaksen, H. van Lanen, J. Hannaford, and E. Sauquet (2008), *Trends in low flows and streamflow droughts across Europe*, UNESCO Report, Paris.

Steppeler, J., G. Doms, U. Schaettler, H. Bitzer, A. Gassmann, U. Damrath, and G. Gregoric (2003), Meso-gamma scale forecasts using the nonhydrostatic model LM, *Meteorol. Atmos. Phys.* **82**, 75-96.

Svensson, C., W. Kundzewicz, and T. Maurer (2005), Trend detection in river flow series: 2. Flood and low-flow index series, *Hydrol. Sci. J.* **50(5)**, 881-824.

Teutschbein, C., and J. Seibert (2010), Regional climate models for hydrological impact studies at the catchment scale: A review of recent modeling strategies, *Geography Compass* **4(7)**, 834-860.

Themeßl, M., A. Gobiet, and A. Leuprecht (2010), Empirical-statistical downscaling and error correcton of daily precipitation from regional climate models, *Int. J. Climatol.* **31(10)**, 1530-1544.

Walker, K., and M. Thoms (1993), Environmental Effects of Flow Regulation on the Lower River Murray, Australia, *Regul. Rivers Res. Manag.* **8(1-2)**, 103-119.

Williams, J., K. Renard, and P. Dyke (1984), EPIC - a new model for assessing erosion's effect on soil productivity, *J. Soil Water Conserv.* **38(5)**, 381-383.

Wittenberg, H. (2003), Effects of season and man-made changes on baseflow and flow recession: case studies, *Hydrol. Process.* **17**, 2113-2123.

WMO (World Meteorological Organization) (1974), *International Glossary of Hydrology*, WMO, Geneva.

WMO (World Meteorological Organization) (2008), *Manual on low-flow estimation and prediction,* Operational hydrology report No. 50.

Ecological Modelling 220, 2543–2558 (2009)

6. From meso- to macro-scale dynamic water quality modelling for the assessment of land use change scenarios

Shaochun Huang*, Cornelia Hesse, Valentina Krysanova and Fred Hattermann

Potsdam Institute for Climate Impact Research, P.O. Box 601203, Telegrafenberg, 14412 Potsdam, Germany
* Corresponding author. Tel: +49 (331) 288-2406.
Email address: huang@pik-potsdam.de

Abstract
The implementation of the European Water Framework Directive requires reliable tools to predict the water quality situations in streams caused by planned land use changes at the scale of large regional river basins. This paper presents the results of modelling the in-stream nitrogen load and concentration within the macro-scale basin of the Saale river (24,167 km^2) using a semi-distributed processed-based ecohydrological dynamic model SWIM (Soil and Water Integrated Model). The simulated load and concentration at the last gauge of the basin show that SWIM is capable to provide a satisfactory result for a large basin. The uncertainty analysis indicates the importance of realistic input data for agricultural management, and that the calibration of parameters can compensate the uncertainty in the input data to a certain extent. A hypothesis about the distributed nutrient retention parameters for macro-scale basins was tested aimed in improvement of the simulation results at the intermediate gauges and the outlet. To verify the hypothesis, the retention parameters were firstly proved to have a reasonable representation of the denitrification conditions in six meso-scale catchments. The area of the Saale region was classified depending on denitrification conditions in soil and groundwater into three classes (poor, neutral and good), and the distributed parameters were applied. However, the hypothesis about the usefulness of distributed retention parameters for macro-scale basins was not confirmed. Since the agricultural management is different in the sub-regions of the Saale basin, land use change scenarios were evaluated for two meso-scale sub-basins of the Saale. The scenario results show that the optimal agricultural land use and management are essential for the reduction in nutrient load and improvement of water quality to meet the objectives of the European Water Framework Directive and in view of the regional development plans for future.

Keywords: Water quality modelling, SWIM, meso-scale river basin, macro-scale river basin, uncertainty analysis, retention parameters, land use change scenarios

6.1. Introduction

The increasing input of nutrients in rivers induced or caused by point sources (sewage treatment plants, industrial enterprises and municipal wastewater) and diffuse sources (agricultural land, atmosphere) often leads to pollution and degradation of water quality and can cause ecological changes in freshwater. As the discharge of polluted wastewater has been notably reduced by wastewater treatment in the recent decades, agriculture is generally perceived as the main source of nutrient input to rivers in Europe (De Wit *et al.*, 2002). In recognition of the importance of water quality problem and the need for integrated management in river basins, the European Water Framework Directive (WFD) was adopted in 2000, aiming to restore the "good ecological status" at the scale of large river systems until 2015 (EC, 2000).

Water quality models could provide an important and valuable support for the assessment and analysis of pollution loads in river basins and possible measures to improve water quality, and therefore they could be a useful instrument for fulfilling the requirements of the Water Framework Directive. Hence, various water quality models for the basin scale were developed and tested in the last decades (Arheimer & Brandt, 1998, Whitehead *et al.*, 1998, Bicknell *et al.*, 1997, Arnold *et al.*, 1998, Krysanova *et al.*, 1998). These models vary in the level of complexity, from statistical and conceptual models based on statistical and empirical relationships to process-based and physically based models derived from physical and physicochemical laws and including also some equations based on empirical knowledge. Due to the lack of description of important physical processes, the simplified conceptual models have limited applicability, and are not appropriate for simulation of some essential spatially distributed processes. The physically based models are by definition fully distributed accounting for spatial variations in all variables. However, these models are often considered too complex without a guarantee of better performance (Beven, 1989; Beven, 1996). The requirement of large amount of input data and computation resources for such models is also a particulate concern, especially for large basin simulations (Lunn *et al.*, 1996). This indicates that using the process-based models (Krysanova *et al.*, 2005a) of intermediate complexity for the basin-scale water quality assessment may be sufficient and even more promising. Numerous studies have proven that the process-based models are spatially explicit and sufficiently adequate to represent major hydrological, biogeochemical and vegetation growth processes at the catchment scale (Arnold and Allen, 1996; Chaplot *et al.*, 2004; Krysanova *et al.*, 2005b; Stewart *et al.*, 2006; Hattermann *et al.*, 2006). The models SWAT (Arnold *et al.*, 1998), HSPF (Bicknell *et al.*, 1997), SWIM (Krysanova *et al.*, 1998) and DWSM (Borah *et al.*, 2004) belong to the process-based modelling tools for river basins. However, in the most of the published studies the validation is performed using the catchment outlet data only, which provides no information on how they perform spatially (Cherry *et al.*, 2008).

Besides, most of the current catchment scale studies with dynamic process-based models focus on micro-scale and small catchments ranging from 1 to 100 km^2 (Du *et al.*, 2006, Chaplot *et al.*, 2004, Eisele *et al.*, 2001 and Bogena *et al.*, 2003) and meso-scale basins with the drainage area from 100 km^2 to 5000 km^2 (Abbaspour *et al.*, 2007, Saleh *et al.*, 2000 and Volk *et al.*, 2008). The process-based modelling at the macro-scale is very rare in literature, where the statistical and conceptual riverine load models are usually applied. One example is by Even *et al.* (2007), who simulated water quality conditions in the Seine River basin (78650 km^2) using four coupled deterministic models with satisfactory seasonal results at different stations. Since the WFD requires the assessment on large river basin scale, more efforts are needed on improving the capabilities of describing nutrient fluxes in large basins.

As all necessary input data, such as crop rotations and fertilization schedule, and parameters of the current process-based models usually cannot be precisely defined at the basin scale, there are considerable uncertainties in the water quality modelling. Moreover, the process-based water quality models often confront the problem of over-parameterization, which results in the equal or very similar model result using various parameter combinations (problem of equifinality) (Oreskes *et al.*, 1994). There are already many published studies on uncertainty in water quality modelling related to physical data such as rainfall (Bertoni, 2001), spatial data such as land use maps (Payraudeau *et al.*, 2004), and parameters (Abbaspour *et al.*, 2007, Hattermann *et al.*, 2006). The uncertainty analysis allows to find the most important factors controlling the model behaviour, and to represent the modelling results in a more reliable way.

Recent studies on land use change impacts have demonstrated that the process-based water quality models are effective tools to simulate the hypothetic land use scenarios. They are helpful to either evaluate the long-term impacts of implementation of the current management practices (Santhi *et al.*, 2005), or to investigate the optimal solutions in order to reduce the nutrients loads in rivers (Zammit *et al.*, 2005; Hesse *et al.*, 2008 and Volk *et al.*, 2008). However, these studies did not account for some new tendencies in land use, like the influence of introducing energy plants on the water quality aspect in the future. In this study the land use scenarios are based on various measures of controlling nutrient emissions, and include the potential agricultural practice changes due to the development of the energy market.

Hence, the objectives of the study were:

1. to test the applicability of the process-based ecohydrological model SWIM for simulating nitrogen dynamics in a macro-scale basin considering the outlet and intermediate gauges as validation points,
2. to investigate the uncertainties related to input data and parametrization,
3. to test the hypothesis about the usefulness of distributed retention parameters for nitrogen simulation in a macro-scale basin, and to establish ranges of retention parameters depending on the catchment characteristics, and
4. to evaluate impacts on nitrate nitrogen load under the potential land use changes.

In this study, both input data and a set of most sensitive parameters for nitrogen dynamics were included in the uncertainty analysis. The most effective factors revealed in the analysis could explain the difficulties in simulating nutrient loads simultaneously in a large basin and its subbasins, and to suggest the ways for improvement.

6.2. Method, study area and data

6.2.1. Model SWIM

The dynamic process-based ecohydrological model SWIM (Soil and Water Integrated Model) was developed on the basis of the models SWAT (Arnold *et al.*, 1993) and MATSALU (Krysanova *et al.*, 1989). Until now, SWIM was intensively tested, validated and applied for simulating water discharge in meso- to macro-scale basins, and water quality in meso-scale basins (Krysanova *et al.*, 1998, Hattermann *et al.*, 2006 and Hesse *et al.*, 2008). An overview of processes included in SWIM is shown in **Fig. 6-1**.

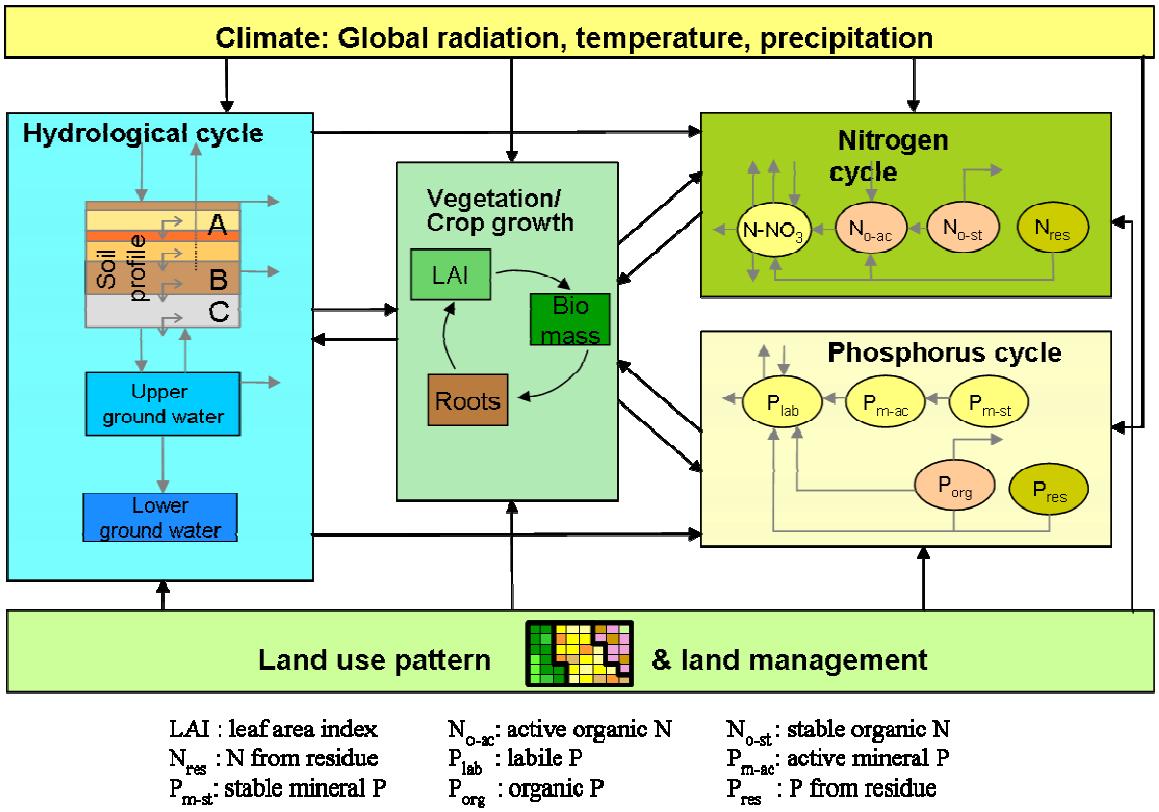

Figure 6-1: The modeling flow chart in SWIM at hydrotope level.

SWIM simulates all processes by disaggregating the basins to subbasins and hydrotopes, where the hydrotopes are sets of elementary units in a subbasin with homogeneous soil and land use types. Up to 10 vertical soil layers can be considered for hydrotopes. It is assumed that a hydrotope behaves uniformly regarding hydrological processes and nutrient cycles. Spatial disaggregation scheme in the model is flexible, *e.g.* grid cells can be considered instead of subbasins, and hydrotope units instead of sets of units.

Water flows, nutrient cycling and plant growth are calculated for every hydrotope and then lateral fluxes of water and nutrients to the river network are simulated taking into account retention. After reaching the river system, water and nutrients are routed along the river network to the outlet of the simulated basin.

The simulated hydrological system consists of three control volumes: the soil surface, the root zone of soil and the shallow aquifer. The water balance for the soil surface and soil column includes precipitation, surface runoff, evapotranspiration, subsurface runoff and percolation. The water balance for the shallow aquifer includes groundwater recharge, capillary rise to the soil profile, lateral flow, and percolation to the deep aquifer.

Surface runoff is estimated as a non-linear function of precipitation and a retention coefficient, which depends on soil water content, land use and soil type (modification of the Soil Conservation Service (SCS) curve number method, Arnold *et al.*, 1990). Lateral subsurface flow (or interflow) is calculated simultaneously with percolation. It appears when the storage in any soil layer exceeds field capacity after percolation and is especially important for soils having impermeable or less permeable layer below several permeable ones. Potential evapotranspiration

is estimated using the method of Priestley-Taylor (Priestley and Taylor, 1972), though the method of Penman-Monteith (Monteith, 1965) can also be used. Actual evaporation from soil and actual transpiration by plants are calculated separately.

The module representing crops and natural vegetation is an important interface between hydrology and nutrients. A simplified EPIC approach (Williams *et al.*, 1984) is included in SWIM for simulating arable crops (like wheat, barley, rye, maize, potatoes) and aggregated vegetation types (like 'pasture', 'evergreen forest', 'mixed forest'), using specific parameter values for each crop/vegetation type. A number of plant-related parameters are specified for 74 crop/vegetation types in the database attached to the model. Vegetation in the model affects the hydrological cycle by the cover-specific retention coefficient, influencing surface runoff, and indirectly controlling transpiration, which is simulated as a function of potential evapotranspiration and leaf area index (LAI).

The nitrogen and phosphorus modules include the following pools in the soil layers: nitrate nitrogen, active and stable organic nitrogen, organic nitrogen in the plant residue, labile phosphorus, active and stable mineral phosphorus, organic phosphorus, and phosphorus in the plant residue, and the fluxes (inflows to the soil, exchanges between the pools, and outflows from the soil): fertilization, input with precipitation, mineralization, denitrification, plant uptake, leaching to groundwater, losses with surface runoff, interflow and erosion.

Amounts of soluble nutrients (N and P) in surface runoff, lateral subsurface flow and percolation are estimated as the products of the volume of water and the average concentration. Nitrogen retention in subsurface and groundwater occurs during the subsurface transport of nitrogen from soil column to rivers and lakes, and is represented mainly by denitrification. Nitrogen retention is described in SWIM by four parameters: residence times (the time period subject to denitrification) in subsurface and groundwater (K_{sub} and K_{grw}) and the decomposition rates in subsurface and groundwater (λ_{sub} and λ_{grw}) using the equation (Hattermann *et al.*, 2006):

$$N_{t,out} = N_{t,in} \frac{1}{1+K\lambda}\left(1-e^{-(\frac{1}{K}+\lambda)\Delta t}\right) + N_{t-1,out} \cdot e^{-\left(\frac{1}{K}+\lambda\right)\Delta t} \quad , \qquad (6\text{-}1)$$

where $N_{t,out}$ is nitrogen output and $N_{t,in}$ is nitrogen input at time t, the parameter K represents the residence time in days (d), and λ (d^{-1}) the decomposition rate. The term Δt is the time step. The four retention parameters are identified within ranges specified from literature, and are subject to calibration. This approach was developed for the SWIM model and tested for modelling water quality (Hattermann *et al.*, 2006).

Four maps (Digital Elevation Model, land use map, soil map and subbasin map) are essential spatial input data for SWIM. They are used to generate the hydrotope classes, basin structure and routing structure, as well as the attributes of subbasins and rivers. The daily climate data (minimum, maximum and mean temperature, precipitation, solar radiation and air humidity) is the main driver of the simulation. The soil parameters including texture, bulk density, saturated conductivity, *etc*. are needed for each layer of each soil type represented on the soil map. The parameters for different crop types and their corresponding fertilization regimes are of importance, especially in case of water quality modelling. For more details about the model concept, input data, parameters, equations as well as the GIS interface, an online SWIM manual is available under http://www.pik-potsdam.de/members/valen/swim.

6.2.2. Evaluation of the model results

In this study the non-dimensional efficiency criterium of Nash-Sutcliffe (1970) efficiency (NS*E*) and relative deviation in water or load balance (D*B*) were used to evaluate the quality of simulated model results (daily water discharge and NO_3-N load).

NSE is a measure to describe the squared differences between the observed and simulated values using the following equation:

$$NSE = 1 - \frac{\sum(X_{obs} - X_{sim})^2}{\sum(X_{obs} - X_{obs\_av})^2} \quad (6\text{-}2)$$

DB describes the long-term differences of the observed values against the simulated ones in percent for the whole modelling period:

$$DB = \frac{X_{sim\_av} - X_{obs\_av}}{X_{obs\_av}} \times 100 \quad (6\text{-}3)$$

Here X_{obs} means the observed values while X_{sim} is the corresponding simulated value. The variables X_{obs_av} and X_{sim_av} are the mean values of these variables for the whole simulation period.

The NSE can vary from minus infinity to 1. A value of 1 denotes a perfect match of predicted and measured values. A value of 0 for the deviation in balance means no difference in amount between the measured and simulated values.

6.2.3. Study areas

The main case study area is the Saale River basin in Germany. The Saale is the second largest tributary of the Elbe River (Reimann and Seiert, 2001) with the length of 427 km, the catchment area of 24.167 km^2, and average discharge of 115 m^3/s (FGG-Elbe, 2004) (see the area marked by dots in **Fig. 6-2**). The relief as well as the precipitation is heterogeneous. The altitude is between 15 and 1100 m above the sea level, and the average annual precipitation amount varies between 450 and 1600 mm/year, strongly depending on the relief (FGG-Elbe, 2004). Wide loess areas and low mountain ranges characterize the Saale catchment. Due to very fertile loess soils more than two-thirds of the catchment area is used for agriculture. The land use in the catchment area is represented by agriculture (69%), forests and natural areas (23%), settlements (6%), industry and mining 2% (FGG-Elbe, 2004). The Saale basin covers large parts of two German federal states Thuringia and Saxony-Anhalt, and a part of Saxony.

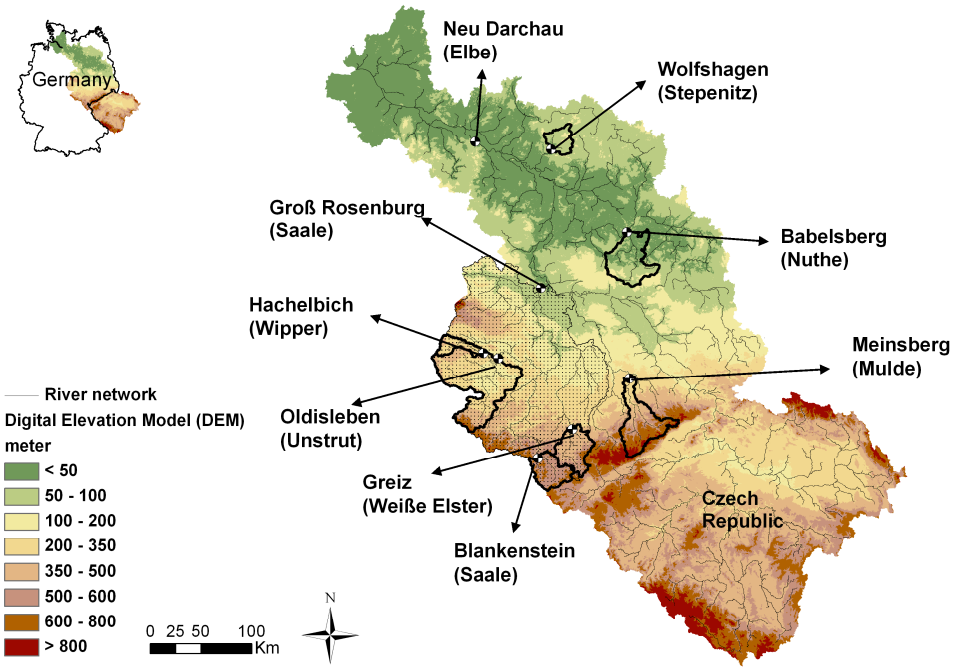

Figure 6-2: The Elbe River basin and the locations of the target catchments and their outlet gauges (The Saale basin is marked by dots).

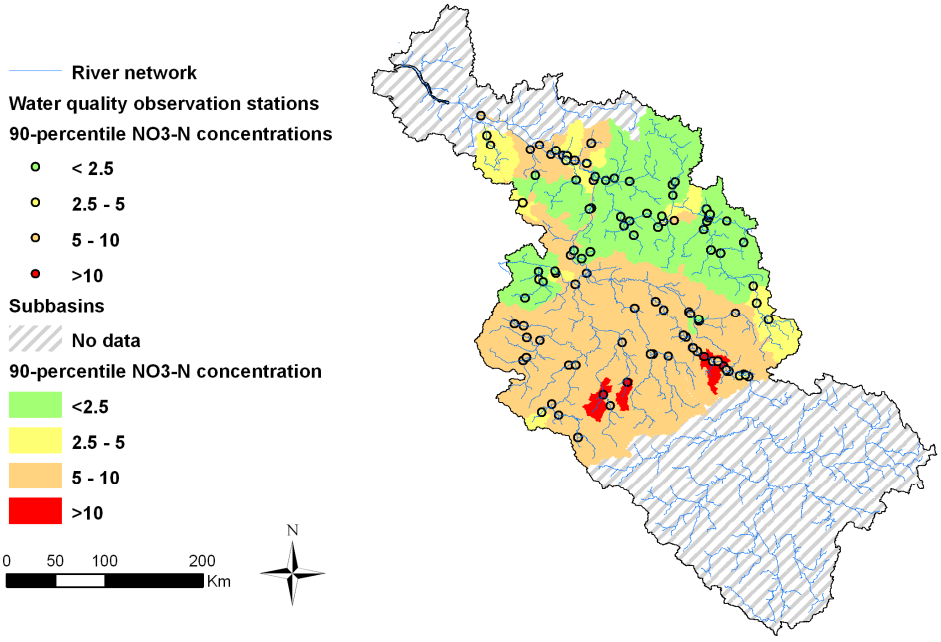

Figure 6-3: Spatial patterns of 90 percentile NO_3-N concentrations in the German part of the Elbe basin estimated from the records at water quality stations from 1990 to 2005 (The 90 percentile concentrations at the stations are assumed to represent the average NO_3-N concentrations of their corresponding catchments).

There is a distinct seasonality within the annual course of the discharge cycle. Snowmelt causes high discharges in March and April. Then the discharge steadily decreases to its lowest values in August and September. In the lower reach, weirs and locks have been constructed to store the water and to make the river navigable in the drier summer months. Additionally, the river's morphology is modified with a series of five reservoirs in the upper course for water harvest, flood protection and the salt-load control system. All these regulatory measures have a large impact on the hydrological regime of the river.

At the time of the German reunification the Saale was a very eutrophied and polluted water body. The region has been subject to rapid economic and social changes since then. Although the water quality in the Saale has been progressively improved after the reunification due to improvement of sewage treatment, closure of some industries and changes in agriculture practices, the river is still heavily loaded with nutrients mainly from diffuse sources (Behrendt *et al.*, 2001). According to the published data, the total nitrogen concentration is not expected to decrease significantly in a near future (Theile, 2001) as a result of the relative long retention time of nutrients in the catchment, and the high proportion of agricultural areas in the basin (FGG-Elbe, 2004). There is still an increasing trend in nutrient concentrations in the flow direction. This trend is attributed more to the emissions in the middle Saale, and less to the emissions in the lower course of the river (Lindenschmidt, 2005).

Figure 6-3 shows spatial patterns of 90 percentile NO_3-N concentrations in the German part of the Elbe basin, classified according to the German Regional Water Association (LAWA, 1998). The 90 percentile concentrations are estimated from the records at water quality stations from 1990s to 2005, and they are assumed to represent the average NO_3-N concentrations of their corresponding catchments. The 90 percentile concentrations below 2.5 mg/L indicate small to moderate level of NO_3-N in the rivers, and the values above 5 mg/L mean high to very high level. This figure shows how heavily the Saale basin is polluted currently. The lowland catchments are notably less polluted.

In addition, seven meso-scale catchments located in the Elbe basin were included in the modelling study, partly to investigate the model uncertainties and the physical representation of retention parameters in SWIM, and partly to simulate land use change scenarios. Their location is shown in **Fig. 6-2** and the general characteristics are listed in **Table 6-1**. They are: the Stepenitz, gauge Wolfshagen; the Nuthe, gauge Babelsberg; the Wipper, gauge Hachelbich; the Unstrut, gauge Oldisleben; the upper Saale, gauge Blankenstein; the Weiße Elster, gauge Greiz; and the Mulde, gauge Meinsberg. The Nuthe is located in the lowland part of the Elbe basin, and has the lowest average annual precipitation. The upper Saale and Mulde are located in the mountainous and loess sub-regions with the highest average annual precipitation compared to other catchments. The Stepenitz, Unstrut, Wipper and Weiße Elster have an intermediate position between mountains and loess areas, and also include lowlands, and their average annual precipitation is also at the medium level – from 620 to 763 mm/year. The land use characteristics are different in the catchments, though agriculture areas occupy significant share of drainage areas in all of them: from 36% to 67%.

Table 6-1: Characteristics of the target basins.

	Saale Blankenstein	Stepenitz Wolfshagen	Nuthe Babelsberg	Wipper Hachelbich	Weiße Elster Greiz	Mulde Meinsberg	Unstrut Oldisleben	Saale Groß-Rosenburg
Area (km^2)	994	556	1703	519	1204	1813	4174	23719
Slope range (degree)	0 - 29	0 - 9.3	0 - 12.2	0 - 28.8	0 - 24.7	0 - 35.9	0 - 32.9	0 - 41.1
Mean slope (degree)	4	1.06	1.18	4.8	4.54	5.04	3.14	3.32
Standard deviation of slope (degree)	2.54	0.95	1.08	4.24	2.77	3.53	3.38	3.68
Altitude (m a.s.l.)	415 - 855	39 - 165	26 - 179	173 - 538	257 - 811	176 - 1244	93 - 982	14 - 1139
Share of crop land (%)	51%	71%	39%	52%	44%	36%	67%	63%
Point source (kg/d)	774	9	62	136	503	542	1384	9947
Contribution of point sources to the total load (%)	12.8%	0.1%	1.0%	2.3%	8.3%	9.0%	12.2%	17.3%
Annual average precipitation (mm)**	840	620	566	737	763	923	665	630
Average water discharge* (m^3/s)	11	3.4	7.85	3.4	10.3	19.9	18.8	115
Max. water discharge* (m^3/s)	161	39	32.6	43.9	124	300	220	741
Min. water discharge* (m^3/s)	0.96	0.43	0.15	0.8	1.65	1.36	2.5	11.5
Specific water discharge* ($L/(s*km^2)$)	11.4	6.33	4.96	6.22	8.37	13.8	4.5	4.85
90 percentile of NO_3-N concentrations* (mg/L)	7.3	8.2	1.3	8.6	7	6.6	8.2	7

* only for the simulation periods.

**the precipitation data was interpolated from the measured data of climate and precipitation stations in the basins for the simulation periods

6.2.4. Study scheme and data preparation

Table 6-2 shows the sequential scheme of the study performed in both the macro-scale basin and the meso-scale catchments. First, the calibration and validation were carried out for all of the study areas. The meso-scale Weiße Elster catchment was used for uncertainty analysis since it is located in one federal state, and the agricultural management could be identified in accordance with the state's statistical data.

Table 6-2: Sequential scheme of the study.

Study procedures		Saale (macro-scale basin)	Subbasins of the Saale (intermediate gauges)	Meso-scale catchments
Calibration/Validation		done	done	done for all
Uncertainty analysis				done for the Weiße Elster catchment
Hypothesis	1) Plausibility test			done for the six selected catchments
	2) Test of hypothesis in the Saale basin	done	done	
Search for optimal parameter ranges				done for the six selected catchments
Land use change scenarios				done for the Unstrut and Weisse Elster catchments

The differences in retention parameters obtained after calibration for the six selected meso-scale catchments indicate that the physical representation of these parameters corresponds to the denitrification conditions in soils and groundwater, *i.e.* higher decomposition rates are generally found in catchments with a high share of poorly drained soils like gleysols and histosols (a plausibility test). When the plausibility of the parameters was proved, the distributed parameters were applied in the Saale basin aiming in improvement of the simulation results at the last and intermediate gauges. After that a search for optimal parameter ranges was done for the six meso-scale catchments.

Land use change scenarios were applied for the Unstrut (Oldisleben) located in the German federal state Thuringia, and the Weiße Elster (Greiz) located in the federal state Saxony. The land use change scenarios were based on the current and planned agricultural practices, which are proved to be major factor affecting nitrate input from diffuse sources to surface water (Wade *et al.*, 2002).

To setup the model, four raster maps are required. The digital elevation model (DEM) provided by the NASA (National Aeronautics and Space Administration) Shuttle Radar Topographic Mission (SRTM), the general soil map of the Federal Republic of Germany BÜK 1000 from the Federal Institute for Geosciences and Natural Resources (BGR), the land use map (Corine 2000), and the subbasin map which was generated from the DEM map were used. The Saale drainage basin includes 39 soil types among the 72 soil types classified in BÜK 1000 for Germany, and the chernozems and cambisols are the main soil types in the region.

Climate data (temperature, precipitation, solar radiation and air humidity) were provided by the German Weather Service, and interpolated to centriods of the subbasins. Fertilization data for seven major crops in the region (winter wheat, silage maize, potatoes, summer barley, winter barley, winter rape and winter rye) were identified taking into account the regional recommendations (see **Table 6-3**).

Table 6-3: Fertilization data for seven major crops used in the study (except potato and maize, all the crops have two fertilization stages in one year) (Source: Voss, 2007).

	Nitrogen fertilization	
Crop	Fertilization dates in one year (julian day)	Amount [kg N/ha]
Potato	110	120
Silage maize	180	150
Summer barley	85, 120	60,20
Winter rye	293, 95	40, 60
Winter barley	283, 95	40, 60
Winter wheat	300, 95	40, 80
Winter rape	257, 95	60, 120

The daily water discharge and fortnightly measurements of NO_3-N concentrations at the last gauge of each catchment obtained from the State Office of Flood Protection and Water Management Saxony-Anhalt, Thuringia State Office of Environment and Geology, Federal Environmental Agency of Brandenburg and Saxonian State Ministry of the Environment and Agriculture were used for the model calibration and validation.

6.3. Calibration, validation and uncertainty analysis

The model calibration and validation is a basis for its further application for environmental and water quality assessment. Usually, hydrological validation is performed first, and then the model is validated for nutrient dynamics. The simulation periods for each basin are not identical because they are based on the observed data available for the respective basins. The fortnightly measurements of nitrate nitrogen are available for several gauges in the Saale basin during the period 1997 to 2002, for the Nuthe basin between 1990 and 1994 and for the Stepenitz in the 1980s. In the Mulde basin, only monthly data is available for the period 1987 to 1992. For each basin, the period of observations was divided into two equal sub-periods, and then the first half period was used for the calibration and the second half period was used for the validation. The following parameters were used for hydrological calibration: the correction factors for evapotranspitation, curve numbers and saturated conductivity as well as the baseflow factor, alpha factor for groundwater and two routing coefficients. For nitrogen load, the residence time and the decomposition rates in subsurface and groundwater were used as calibration parameters.

6.3.1. Hydrological calibration and validation

To simulate the dynamics of nitrogen load and concentrations, a sufficiently good simulation of water discharge is a prerequisite. Therefore, calibration and validation of SWIM for all eight catchments was performed firstly for water discharge, and then for concentrations and loads of nitrogen. **Table 6-4** includes the Nash-Sutcliffe efficiencies (from 0.7 to 0.84) and the deviations in water discharge (±3%) for each of the eight basins for the validation period. **Figure 6-4** shows

the comparisons of the observed and simulated daily and average monthly discharges at the last water discharge gauges for three meso-scale catchments (the Nuthe, the Weiße Elster and the Unstrut) and the macro-scale basin of the Saale (gauge Calbe-Grizehne). All simulated results have a good agreement with the observed values. Only the hydrograph for the Nuthe was reproduced not as well as the others. This is most probably due to the extensive anthropogenic water regulation measures in this lowland catchment, which transform the natural behaviour of water fluxes. Therefore, the calibration and validation for this catchment was more difficult. Generally, the efficiencies are satisfactory and the deviations in water discharge are low for all catchments.

Table 6-4: The Nash-Sutcliffe efficiencies and deviations for water discharges and NO_3-N load in the target basins for the validation period.

		Saale	Stepenitz	Nuthe	Wipper	Weiße Elster	Mulde	Unstrut	Saale
		Blankenstein	Wolfshagen	Babelsberg	Hachelbich	Greiz	Meinsberg	Oldisleben	Groß-Rosenburg
Water discharge	Efficiency	0.84	0.78	0.70	0.78	0.82	0.80	0.79	0.84
	Deviation	3%	-3%	-2%	0%	0%	-1%	1%	3%
NO_3-N load	Efficiency	0.52	0.64	0.70	0.72	0.58	0.70	0.59	0.70
	Deviation	3%	8%	-7%	3%	1%	-6%	0%	-3%

6.3.2. Calibration and validation for nitrogen dynamics

The calibration and validation of SWIM for nitrogen dynamics was done for the Saale basin, checking also several intermediate gauges, and in addition separately for seven meso-scale catchments (for locations see **Fig. 6-2**, and for characteristics see **Table 6-1**). All the eight basins were firstly calibrated with the "global" (unique for the basin) retention parameters: residence times in subsurface and groundwater (K_{sub} and K_{grw}) and the decomposition rates in subsurface and groundwater (λ_{sub} and λ_{grw}).

As crop rotation data for the basins are not available, and only average annual crop shares can be estimated from statistical data for the federal states, winter wheat was applied for calibration and validation. It is justified by the facts that it is usually one of the dominant crops in the study areas, and it behaves similar to most other winter crops. Based on the ranges of the amount of fertilizers recommended by the local governments (Landwirtschaft und Landschaftspflege in Thüringen (Kerschberger and Franke, 2001); Ministerium für Landwirtschaft und Umwelt in Sachsen-Anhalt, 2004; Sächsische Landesanstalt für Landwirtschaft, 2007 and Ministerium für Landwirtschaft, Umweltschutz und Raumordnung des Landes Brandenburg, 2000), the mean rates of fertilizer applications were chosen as input data (**Table 6-3**). Input from point sources (waste water treatment plants and industries) was taken into account assuming constant daily rates estimated from the average annual data (source: IKSE, 2005).

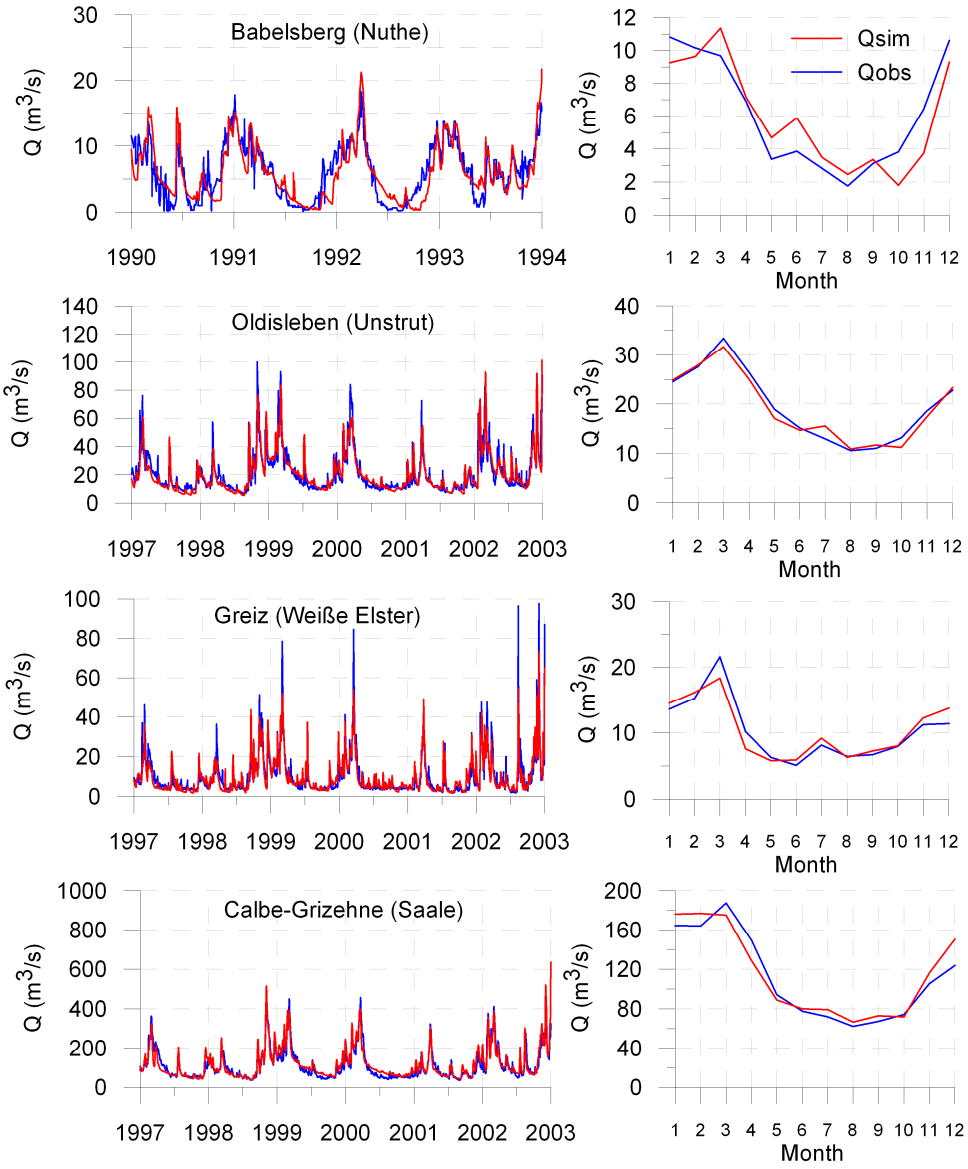

Figure 6-4: Comparison of the observed and simulated water discharges (left) at gauges Babelsberg (River Nuthe), Oldisleben (River Unstrut), Greiz (River Weiße Elster) and Calbe-Grizehne (River Saale) for calibration and validation periods, and the comparisons of the average monthly discharges for the whole period (right).

Table 6-4 includes the model validation results: the Nash-Sutcliffe efficiencies and the deviations in N load for the Saale and seven meso-scale catchments. Only the last gauge of the Saale basin was calibrated and validated, and results for several intermediate gauges (not calibrated) were also compared. The efficiencies for several intermediate subbasins of the Saale are listed in **Table 6-5**. As an example, **Figure 6-5** shows the comparison between the observed and simulated nitrate N loads and concentrations for the Saale basin and four meso-scale catchments.

One can see that the observed seasonal dynamics: higher concentrations and loads in winter season and lower in summer are reproduced by SWIM quite well. However, the high peaks in concentration are often underestimated, and in general the load dynamics is reproduced better than concentrations.

Table 6-5: Comparison of the efficiencies for the simulated NO_3-N load at the main gauge and intermediate gauges in the Saale basin using global and distributed parameters.

Rivers	Gauges	Global Parameters Efficiency	Distributed Parameters Efficiency
Saale	Groß-Rosenburg	0.7	0.68
Saale	Halle-Trotha	0.52	0.51
Saale	Naumburg	0.53	0.58
Saale	Rudolstadt	0.42	0.51
Ilm	Niedertrebra	0.32	0.24
Unstrut	Freyburg	0.67	0.63
Weiße Elster	Halle-Ammendorf	0.49	0.47
Wipper	Hachelbich	0.38	0.35
Saale	Blankenstein	0.44	0.39
Schwarza	Schwarzburg	0.24	0.33
Weiße Elster	Greiz	0.13	0.15
Unstrut	Oldisleben	0.58	0.54

The efficiency at the last gauge of the Saale basin is 0.70, indicating a good simulation result for this macro-scale basin. The simulated nitrate loads in seven meso-scale catchments (**Table 6-4**) are in a good agreement with the observed data, with the Nash-Sutcliffe efficiencies varying from 0.52 to 0.72. The efficiencies at the intermediate (not calibrated) gauges of the Saale are lower: only in 50% of all cases the efficiency is higher or equal 0.49 (**Table 6-5**).

The uncertainty in crop type and fertilization rates and schedule definitely influence the simulation results, and therefore it is more difficult to reproduce the observed nutrient dynamics as good as water discharge, and the calibration and validation results for water quality in terms of Nash-Sutcliffe efficiency are lower than that for water discharge. It is difficult to reproduce better the high values during extreme events for all the cases. The underestimation of the nutrient load may be due to unrealistic input data, improper setting of the model parameters or incorrect simulation of nitrogen transfer processes during the extreme events like floods. Therefore, an uncertainty analysis related to model parameters and input data is important in order to quantify these sources of uncertainty. It can help to find ways to improve the model performance.

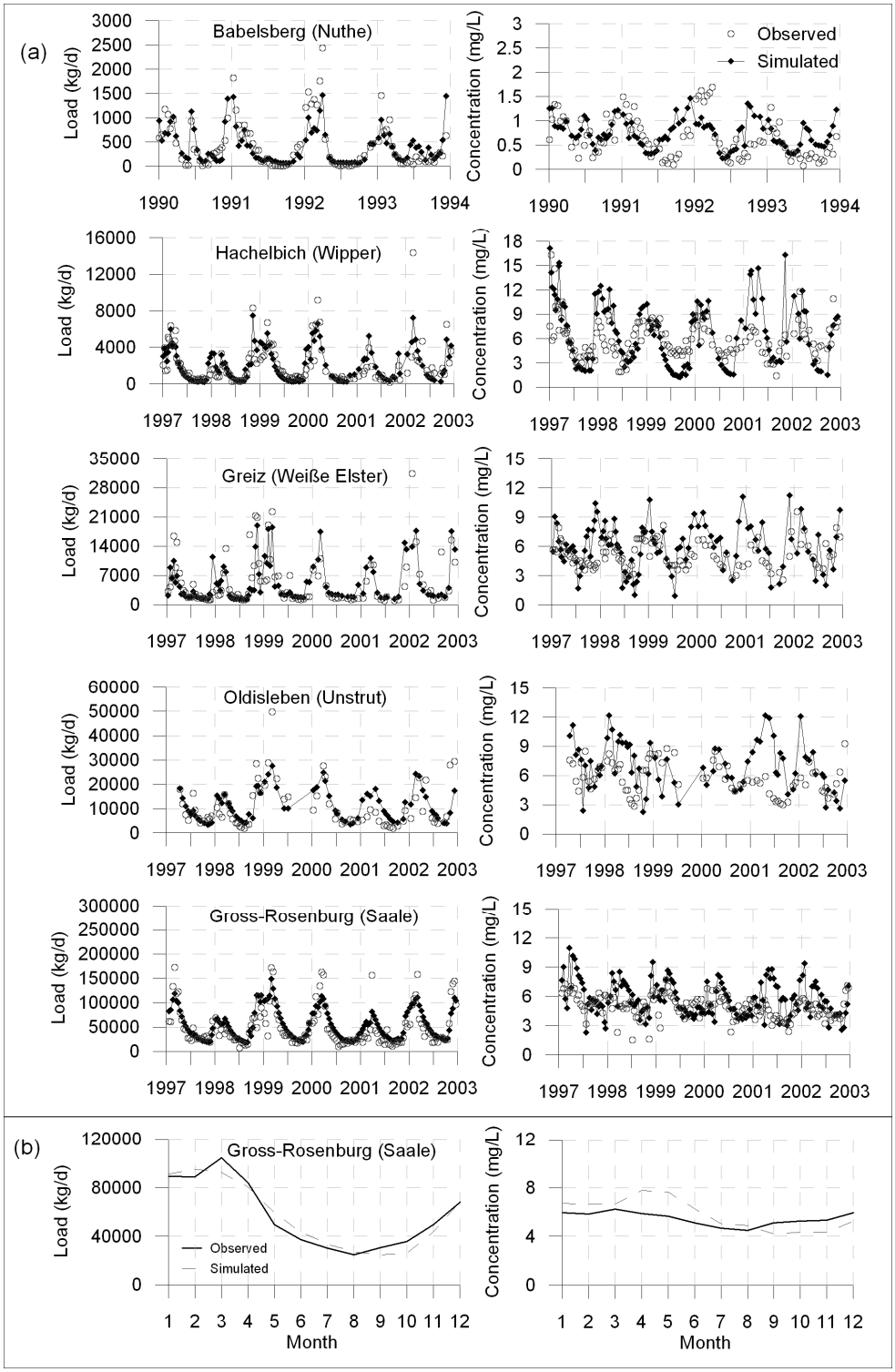

Figure 6-5: Comparison of the observed and simulated NO_3-N loads (left) and concentrations (right) at gauges Babelsberg (River Nuthe), Hachelbich (River Wipper), Greiz (River Weiße Elster), Oldisleben (River Unstrut), and Calbe-Grizehne (River Saale) (a), and comparison of the average monthly dynamics for the Calbe-Grizehne (River Saale) (b).

6.3.3. Uncertainty analysis

As mentioned above, the assumption of monoculture on arable land and the fertilization schedule as in the recommended tables can not fully represent the reality. A number of sensitive model parameters are also taken from literature, where they are often suggested as ranges. Therefore, the uncertainty analysis was performed aiming at the investigation of the separate effects of input data and model parameters on the resulting simulated nitrogen dynamics.

The uncertainty analysis was done for the Weiße Elster catchment. It considered all major crops in the region: winter barley, winter rye, winter rape, maize, summer barley and potatoes with their specific fertilization schemes. In accordance with regional data (**Table 6-3**), winter crops are fertilized twice a year, once in autumn and the second time in spring, while the summer crops are mainly fertilized shortly after plantation. The simulated results from validation (only with winter wheat) were treated as the base run for the uncertainty analysis. Then the crop type was changed to one of the major crops for each single run with all the other input data and parameter fixed. Apart from different crop types, the uncertainty related to fertilization activities is also important, as the time and the amount of fertilizer applications are recommended as ranges by the local authorities. Hence, several single runs with variation of fertilization rates 50% higher or 50% lower than the recommended ones, and time of fertilizer application two weeks earlier or later for winter wheat (all other parameters are fixed), were also included in the uncertainty analysis.

Regarding the parameters, the simulated nitrogen dynamics is most sensitive to the retention times and decomposition rates in subsurface and groundwater, therefore they are the main calibration parameters in SWIM for water quality, and uncertainty related to them was quantified by Monte-Carlo simulations. The random numbers for these four parameters were generated by triangle distributions within the pre-defined ranges (**Table 6-6**). Keeping other input data and parameters the same, the model was run 500 times with different combination of the random numbers, and the results with the Nash-Sutcliffe efficiency above 0.5 and deviation in load less than 10% were included in the resulting uncertainty boundaries. In addition, the mineralization rate (*cmn*), and soil water content as a threshold for denitrification (*deth*), which occurs under low oxygen conditions caused by high water content in soil, were also taken into account. Four single runs were carried out with changed *cmn* (50% higher or lower than the original setting) or *deth* (10% higher or lower than the original setting). The uncertainty boundaries related to parameters include all the results produced by the Monte-Carlo simulation for the four retention parameters and the single runs for the two additional parameters.

Figure 6-6 shows the uncertainty boundaries, which are formed by the maximum and minimum results of the single runs related to input data: different crops (**Fig. 6-6(a)**) and fertilization regime for winter wheat (**Fig. 6-6(b)**). The uncertainty related to crops was captured by modelling all main crops in this basin and assuming that half of the cropland is taken by one of the major crops, and the rest-by winter wheat. Most of the crops, such as potatoes, maize, winter barley, summer barley and winter rye, do not change the simulation results in terms of nitrate concentrations and load from that with winter wheat significantly. However, winter rape behaves quite different from the other crops. It can lead not only to higher NO_3-N load in the river, but also increases the number of extremely high load values. The upper boundary of the uncertainty is mostly resulted from the simulation with winter rape. It seems like the major reason of this distinct behaviour is the higher amount of fertilizers applied to this crop. The uncertainty related to the fertilization activities of winter wheat shows that the variations in fertilization rates and timing do not change the simulation results significantly, at least for the assumed changes.

Table 6-6: Parameter ranges used in the Monte-Carlo simulations for the uncertainty analysis and search for the retention parameters ranges.

Parameters	Parameter description	Parameter ranges* for random number generation	
		Minimum	Maximum
K_{sub} *(day)*	Residence time of nitrate in subsurface	1	500
K_{grw} *(day)*	Residence time of nitrate in groundwater	30	5000
λ_{sub} *(1/day)*	Decomposition rate of nitrate in subsurface	0.0001	0.5
λ_{grw} *(1/day)*	Decomposition rate of nitrate in groundwater	0.0001	0.3

*The parameters ranges were obtained from extending all the parameter settings used for the calibration and validation for the 8 basins

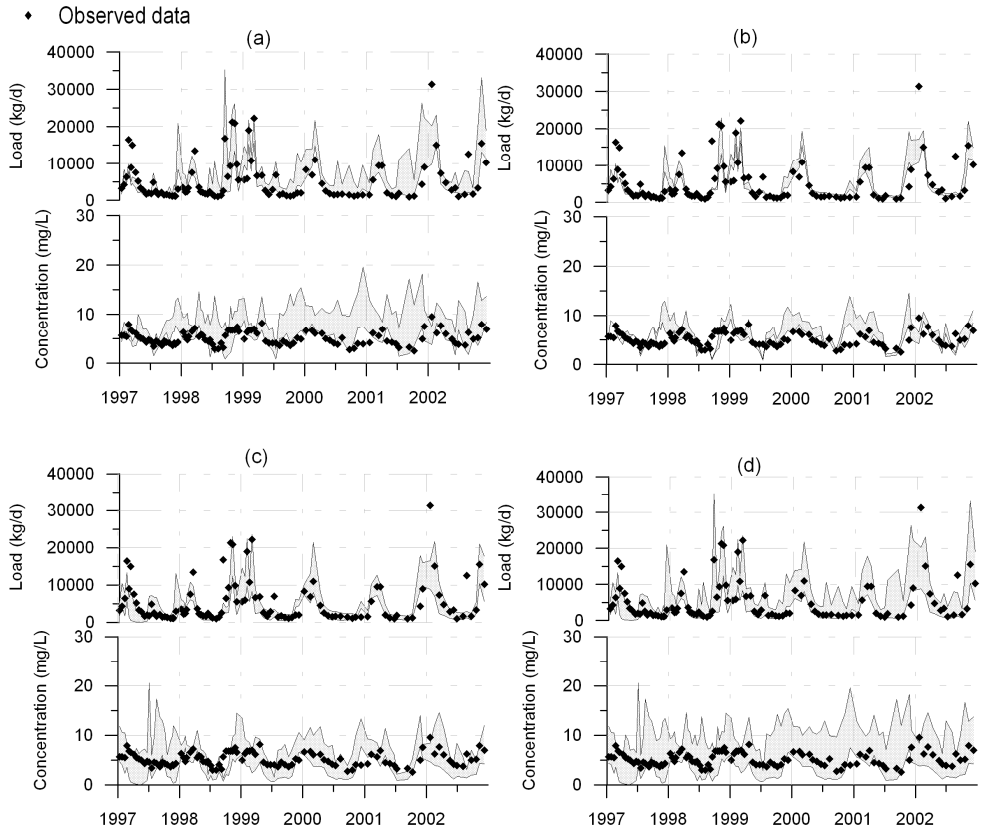

Figure 6-6: The uncertainty corridors for NO_3-N loads related to (a) input data (different crops); (b) input data (fertilization regime for winter wheat); (c) six parameters used in SWIM and (d) input data and parameters.

The uncertainty related to the model parameters is shown in **Fig. 6-6(c).** Unlike the uncertainty related to crops, the uncertainty corridor is narrower, and it includes all the low measured NO_3-N values. The simulated nitrogen dynamics is more sensitive to the retention times and decomposition rates in subsurface and groundwater, as the uncertainty corridor is mostly resulted

from the Monte-Carlo simulation. These results also show that the calibration of parameters can partly compensate the uncertainties caused by input data.

When the uncertainty of parameters and input data (fertilization and crops) are accounted together (see **Fig. 6-6(d)**), the wide boundaries contain almost all of the measured NO_3-N loads and concentrations. The results of the uncertainty analysis indicate that agricultural activities have significant influence on simulated nitrogen dynamics, especially on the extremely high loads. Hence, more realistic input data would definitely help to improve the results.

6.4. Testing the hypothesis about distributed retention parameters

It was proven that the set of global retention parameters, which are the main calibration parameters in SWIM for water quality, are sufficient to model water quality in meso-scale catchments. The results for the Saale basin show that SWIM with the global (unique for a basin) parameter settings is capable to reproduce the nitrate dynamics at the last gauge of the basin, but some improvement for intermediate gauges is still needed. Therefore, it was decided to test the hypothesis about distributed retention parameters in macro-scale basins. The idea was to apply distributed retention parameters corresponding to real denitrification conditions in soils and groundwater instead of global retention parameters, and to check how this influences simulation results in the last and intermediate gauges in a large basin. The potential improvement of results in the intermediate gauges was supposed to improve the result at the last gauge as well.

Wendland *et al.* (1993) evaluated the denitrification conditions in soils and groundwater in Germany. They analyzed different soil properties, classified soils into three denitrification conditions classes (**Table 6-7**), and estimated the residence time in groundwater based on the hydrogeological conditions. Their results indicate that in large river basins the denitrification condition in soil and groundwater can vary from very poor (*e.g.* in mountainous areas) to very good conditions (*e.g.* in lowland).

According to the classification of denitrification conditions into three classes by Wendland *et al.* (1993), the four nitrogen retention parameters in SWIM (residence times K_{sub} and K_{grw} and decomposition rates λ_{sub} and λ_{grw}) were increased to 12 to represent the denitrification process in different soil and groundwater conditions. For example, the denitrification rate in groundwater can be described by three parameters: λ_{grw1} in poor conditions, λ_{grw2} in neutral conditions and λ_{grw3} in good conditions instead of one global parameter λ_{grw}. To verify the hypothesis, the physical representation of retention parameters in SWIM should be firstly verified for each denitrification condition (plausibility test). Unfortunately, it was impossible to find three sub-catchments in the Saale belonging each to one of the three classes and having hydrological and water quality gauges. Therefore, the six meso-scale catchments with relatively homogenous or mixed denitrification characteristics were selected to test the plausibility of the retention parameters. Only when the global parameters were proved to comply with the actual conditions in six catchments, the distributed parameters could be applied for the Saale basin to test the hypothesis.

Table 6-7: Soil classification for denitrification properties according to Wendland *et al.*, 1993 ("-": poor denitrification condition; "o": neutral denitrification condition; "+": good denitrification condition).

Soil type	Soil water	Nutrients	Temperature	PH	Total evaluation
Podsol	-	-	-	-	-
Podsolige Braunerde	o	-	-	-	-
Podsolierte Parabraunerde	o	-	-	-	-
Braunerde (basenarm)	-o	o	-	-	-
Syrosem	-	-	-	-	-
Pararendzina	o	o+	o+	+	o
Rendzina	o	o+	o	+	o
Braunerde (basenreich)	o	o+	o	o+	o
Parabraunerde	o	o+	o	-o+	o
Pseudogley	+	-	o-	o-	+
Tschernosem	o+	+	+	+	+
Pseudogley	+	-o	o-	o-	+
Gley	+	+	-	o	+
Aueböden	+	+	o	+	+
Marschböden	+	+	o	o	+
Niedermoor	+	+	o	+	+
Hochmoor	+	+	o	-	+

6.4.1. Testing the plausibility of the retention parameters

Table 6-8 lists the denitrification characteristics in these subbasins based on the estimations of Wendland *et al.* (1993). The basins in the mountainous area (Mulde, upper Saale and Weiße Elster) have a high share of areas with denitrification class 1 (poor denitrificaiton conditions). The Nuthe in lowland has the best denitrification conditions, and the Stepenitz has neutral condition in both soil and groundwater. The Wipper has mixed denitrification conditions in soil, but very poor condition in groundwater. The residence time in groundwater estimated by Wendland *et al.* (1993) was available for part of the study areas, and shows an increasing trend from mountains to lowland. Generally, the decomposition conditions in soil and groundwater are consistent in the study cases, except the Wipper.

The obtained values of retention parameters for the six meso-scale catchments (see **Table 6-9**) show that parameters used in SWIM have an adequate physical representation of the actual retention conditions. For example, the parameters obtained for the Nuthe can be considered as typical values for good denitrification condition, and the lower parameters for the mountainous area represent poor denitrification conditions. This result indicates the possibility of testing the hypothesis about distributed retention parameters in large basins.

Table 6-8: Characteristics of the denitrification conditions in six meso-scale catchments (derived by overlaying maps using classification from Wendland *et al.*, 1993).

		Saale Blankenstein	Stepenitz Wolfshagen	Nuthe Babelsberg	Wipper Hachelbich	Weiße Elster Greiz	Mulde Meinsberg
Denitrification conditions in soils	Soil Class 1 (poor condition)	78%	7%	14%	29%	77%	85%
	Soil Class 2 (neutral condition)	18%	85%	49%	36%	19%	3%
	Soil Class 3 (good condition)	4%	8%	37%	35%	4%	12%
Residence time in groundwater	Min. Residence time (year)	-	1 - 5	5 - 10	0.1 - 1	-	-
	Max. Residence time (year)	-	5 - 60	30 - 400	1	-	-
Decomposition rate in groundwater		limited to negli.	unlimited to limited	unlimited	negli.	limited	limited to negli.

Table 6-9: Retention parameter values obtained for six meso-scale catchments (plausibility test).

	Saale Blankenstein	Stepenitz Wolfshagen	Nuthe Baberlsberg	Wipper Hachelbich	Weiße Elster Greiz	Mulde Meinsberg
K_{sub} *(day)*	28	10	230	4	8	14
K_{grw} *(day)*	50	141	1100	47	496	108
λ_{sub} *(1/day)*	0.0001	0.1	0.14	0.0003	0.019	0.018
λ_{grw} *(1/day)*	0.0001	0.006	0.04	0.0001	0.0012	0.0001

6.4.2. Testing the hypothesis

Instead of four global retention parameters calibrated in the previous study, 12 distributed parameters were used to indicate the three-denitrification conditions. Due to lack of more detailed information on groundwater in this study, the denitrification conditions in groundwater were assumed to be the same as in soils, since they were generally consistent in most of the meso-scale cases. The calibration process was based on the assumption that good denitrification conditions should have longer residence time and higher decomposition rates than the neutral and poor conditions, and the calibration process became much more complex due to the larger number of parameters.

After the calibration with distributed parameters, it was found that the result at the last gauge is very similar to that with the global parameters (see **Fig. 6-7**). The results in terms of Nash-Sutcliffe efficiency were improved only for one third of the intermediate gauges (see **Table 6-5** for the comparison of efficiencies), while the results for the rest were the same or even worse. The use of the distributed method did not improve the results as expected. The conclusion is that the hypothesis about the usefulness of distributed parameters for macro-scale basins was not confirmed in the Saale basin.

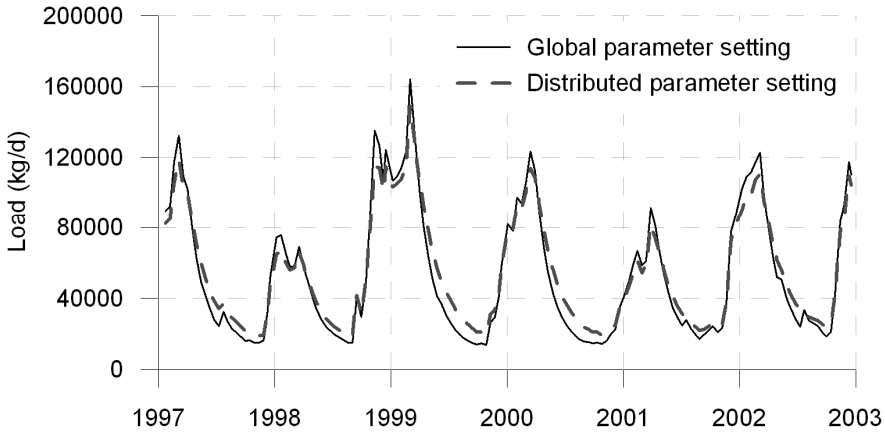

Figure 6-7: Comparison of the NO_3-N load at the gauge Calbe-Grizehne (River Saale) using global and distributed parameter settings.

One reason can be a lack of detailed information on decomposition conditions in groundwater. The assumption of the same denitrification characteristics in soils and groundwater may be not appropriate, because they are not always identical (*e.g.* in the Wipper basin). The retention time from the south mountainous areas to the north lowland areas in the Saale is hardly distinguishable only by the soil class, and elevation and other geographic characteristics may also play important roles and influence the result. Besides, SWIM is not suitable for simulating specifically hydrological processes in the karstic areas. So, the karstic areas in the northern part of the Saale basin also cause difficulties and may influence the results. Moreover, there could be uncertainties in the denitrification map (Wendland *et al.*, 1993) used for the parameter setting. Finally, a lack of management information is also a problem in this basin which includes parts of three federal states. Different agriculture policies and activities may influence actual nitrogen wash-off in parts of the basin, and affect the results.

Hence, the distributed parameter setting does not help to improve the modelling results in the macro-scale basin and its intermediate gauges. The actual denitrification condition in groundwater, which can be set for each hydrotope, may help to verify the hypothesis further in this or another basin. However, as more detailed information for groundwater is not available for the Saale, the global parameters should be still applied in SWIM, since they are sufficient to reproduce nitrogen dynamics in most parts of the basin.

6.5. Search for retention parameter ranges in meso-scale basins

Although the hypothesis of the distributed parameters in large basins was not confirmed, the different retention parameter values obtained for the meso-scale basins can still indicate some distinct characteristics in different sub-regions. Hence, a search for realistic parameter ranges could be helpful for inducting the parameter settings in the future modelling studies. As the simulated nitrogen dynamics is most sensitive to the retention times and decomposition rates in subsurface and groundwater (concluded from uncertainty analysis), only these four parameters were included in the search.

The same Monte-Carlo simulation procedure as described in the uncertainty analysis was carried out for each of six meso-scale basin: looking for the results with the Nash-Sutcliffe efficiency above 0.5 and deviation in load less than 10%. The parameter ranges used for generating random

parameter combinations are also the same as listed in **Table 6-6**. The obtained optimal parameter ranges for each basin are shown in **Fig. 6-8**.

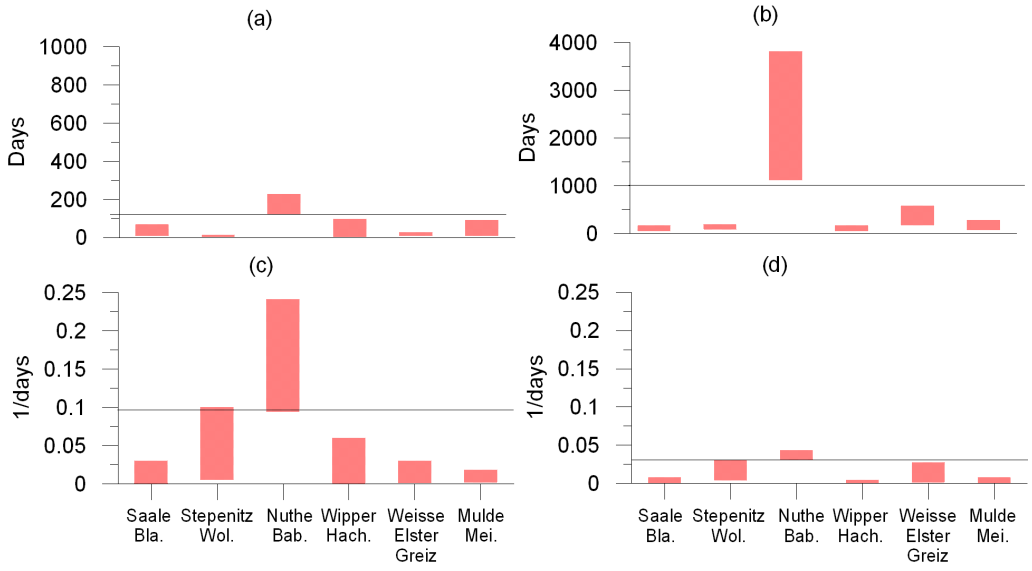

Figure 6-8: Results of the Monte-Carlo simulation: parameter ranges giving satisfactory results for each of six meso-scale basins (a) K_{sub}; (b) K_{grw}; (c) λ_{sub} and (d) λ_{grw}.

Similar results were obtained as in the plausibility test. The Nuthe catchment located in lowland area has much higher residence times and decomposition rates than the other five catchments. The ranges of residence time in soil have no clear distinctions for the catchments located in the mountainous and mixed areas. They seem to be determined not only by the relief of the basin, but also by soil properties. The ranges of residence time in groundwater comply with the minimum residence time estimated by Wendland *et al.* (1993) (compare with **Table 6-8**). The decomposition parameters have a good fit with the soil and groundwater conditions estimated by Wendland *et al.* (1993). Namely, higher decomposition values correspond to better denitrification conditions. Since the parameter ranges for mountainous and mixed catchments are similar, only two sets of optimal parameter ranges can be suggested for further studies: one for the lowland areas, and one for all others (**Table 6-10).**

Table 6-10: The suggested parameter ranges for retention parameters in mountainous and mixed areas and lowlands.

Parameters	Parameter description	Mountainous and mixed areas		Lowland areas	
		Minimum	Maximum	Minimum	Maximum
K_{sub} *(day)*	Residence time of nitrate in subsurface	1	100	100	300
K_{grw} *(day)*	Residence time of nitrate in groundwater	40	600	1000	4000
λ_{sub} *(1/day)*	Decomposition rate of nitrate in subsurface	0.0001	0.1	0.1	0.3
λ_{grw} *(1/day)*	Decomposition rate of nitrate in groundwater	0.0001	0.03	0.03	0.05

6.6. Land use / land management change

As discussed above, agricultural land use may influence the nitrate concentration and load significantly. Land use and land management scenarios were applied not to the whole Saale basin, which overlaps with three federal states with their different policies, but to two of its meso-scale subbasins. One is the Unstrut basin (gauge Oldisleben) located almost fully in Thuringia, and the second is the Weiße Elster (gauge Greiz) located almost fully in Saxony. The main objective was to estimate potential changes in NO_3-N load under the development trend and policies, and to find better management practices leading to a reduced nitrogen load.

Due to the complexity of crop rotations, only the shares of major crops were considered in the reference scenario. According to the report of the Thuringian Ministry for Agriculture, Nature Protection and Environment (Thüringer Ministerium für Landwirtschaft, Naturschutz und Umwelt, 2007), the major crops in the region are: winter wheat (42%), winter rape (21%), winter barley (12%) and summer barley (11%). The arable land in Saxony includes the following major crops: 33% of winter wheat, 19% of winter barley, 7% of summer barley, 27% of winter rape and 8% of winter rye according to the statistical data (Staatsministerium für Umwelt und Landwirtschaft, 2007). These main crops were used for the reference period considering climate data for the period from 1995 to 2002.

According to the information in regional reports, the land use change scenarios were based on the development trend of the world energy market and environmental protection targets. In the report of the Thuringian Ministry (2007) the biogas production from winter rape is highlighted, and the agricultural area for winter rape is growing since 2001. Gömann *et al.* (2007) estimated that the energy maize will occupy more than 10% of agricultural land in Saxony-Anhalt, Thuringia and Saxony by the end of 2020. Therefore, an increase of areas under maize and winter rape was included in the scenarios. On another hand, various measures are applied in the region aimed in environmental protection, namely, in reduction of nitrogen input to surface water and groundwater. These measures include ecological agriculture, optimal fertilization schemes, *etc*. Therefore, an increase and decrease of organic or mineral fertilizers were analyzed in the study. In addition, the role of cover crops and increment and reduction in agricultural land were also considered in the scenarios.

Figure 6-9 (Weiße Elster,) and **Figure 6-10** (Unstrut) show the simulated changes in nitrate nitrogen loads for each scenario compared to the reference one. According to the results, such measures as increasing areas under winter rape, higher fertilizer rates, excluding cover crops and converting pasture to agriculture land would lead to higher nitrogen loads, whereas lower fertilizer rates, set-aside of agricultural land and planting more maize instead of winter rape would reduce the nitrogen load. Mineral fertilizers have a much stronger effect on the nitrate load than organic fertilizers, so the adjustment of mineral fertilizer rates to the plant needs is essential for the control of nitrogen input into the surface waters. Cover crops, which play an important role in reduction of nitrate losses from fields, should be maintained in cropland, and the planting area of winter rape should not be enlarged significantly in areas, where environmental targets are important. As another energy plant, maize has a moderate effect on the water environment. This advantage should be accounted considering biofuel production and environmental quality plans in future. In the Unstrut basin, the changes associated with the land use scenarios are more pronounced than in the Weiße Elster basin. This is because of the larger area of cropland in the Unstrut, and the different crop types. The scenario studies revealed how important an optimal agricultural activity is. A good planning based on the modelling results can compile with the development priorities, and significantly reduce the NO_3-N loads in the future.

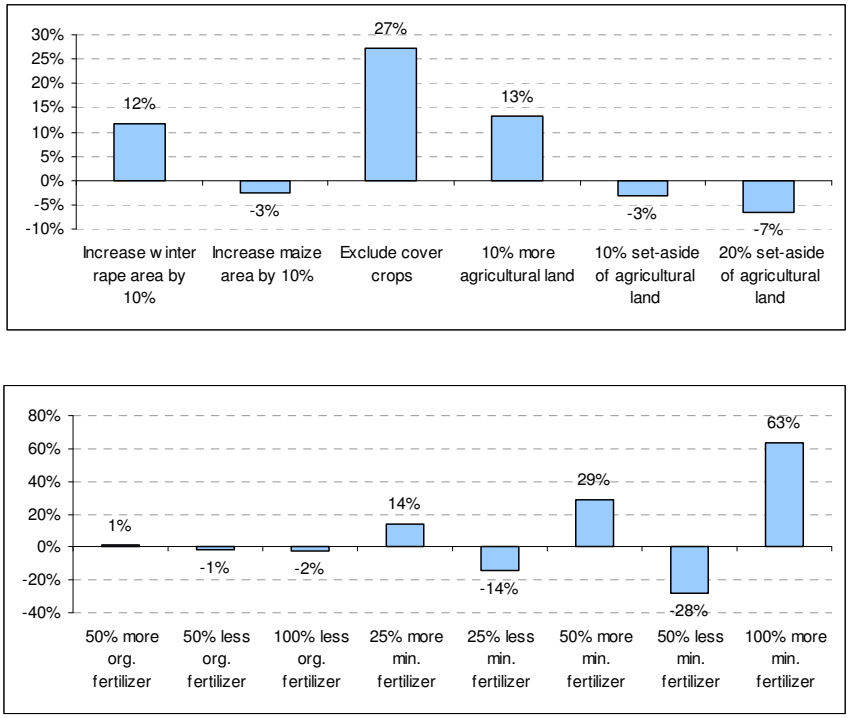

Figure 6-9: Deviations in nitrate N loads for different land use scenarios compared to the reference in the Weiße Elster (Greiz).

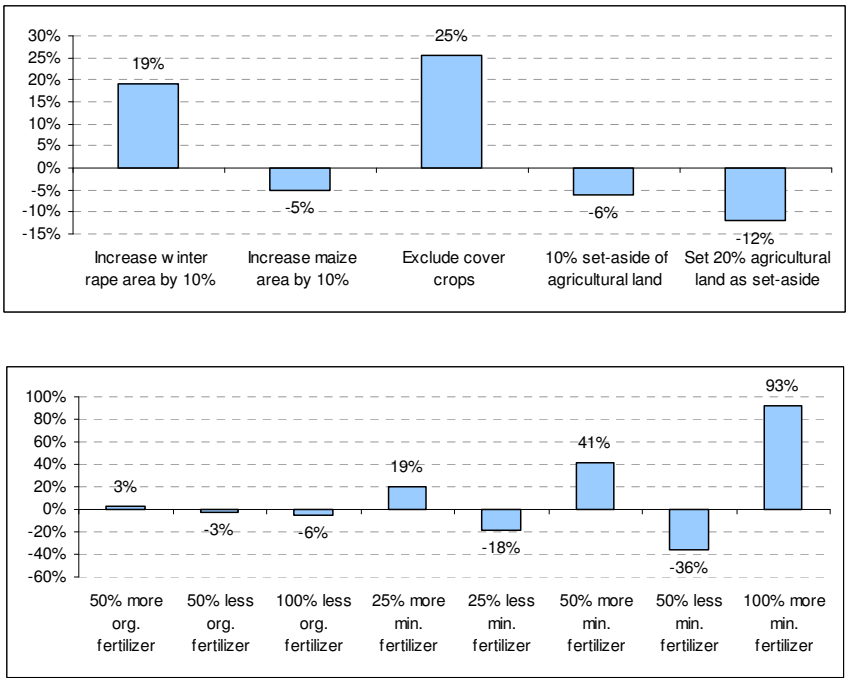

Figure 6-10: Deviations in nitrate N loads for different land use scenarios compared to the reference in the Unstrut (Oldisleben).

6.7. Conclusions

The study was focused on the upscaling of dynamical water quality modelling from meso-scale to macro-scale river basins. It included uncertainty analysis, search for retention parameter ranges depending on the catchment characteristics, and testing of the hypothesis about distributed retention parameters in macro-scale basins. The study has demonstrated that the retention parameters reflect the actual denitrification conditions in the meso-scale subbasins. The uncertainty analysis revealed that some highly fertilized crops as winter rape could be the main driver of the high nitrate loads in the river system, and that the calibration of parameters can compensate for the uncertainty in the input data to a certain extent. The results indicate the importance of the consideration of real crop rotations and parameter uncertainties in the future studies. Two sets of optimal parameter ranges for different denitrification conditions were obtained; one for the lowland areas and one for all others. These ranges have an appropriate representation of the actual conditions, and they provide suggestions on how to set and calibrate parameters for each condition.

The hypothesis about the usefulness of distributed parameters for macro-scale basins was not confirmed. This could be due to different possible reasons, like:

1. uncertainties in the denitrification maps in Wendland *et al.* (1993) used for parameter settings,
2. an assumption that denitrification conditions in soil and groundwater belong to the same class,
3. karstic areas in a part of the Saale basin notably influencing hydrological conditions, and
4. a lack of detailed information on agricultural and water management.

In any case, though the hypothesis was not confirmed, the results for the macro-scale basin of the Saale with the global retention parameters were sufficiently good, and comparable with the results for meso-scale basins. The calibration of global retention parameters should be considered as appropriate for meso-scale and macro-scale basins.

The land use change scenario study shows how important is the influence of agricultural policy on water quality in the rivers. The planting area of winter rape should not be enlarged significantly in areas, where environmental targets are important. Another energy plants, like maize, have a moderate effect on the water environment, and should be considered as an alternative of winter rape for bio-energy production. Rates of mineral fertilizers application are very important factors influencing the nitrate loads in the rivers. Hence, the optimal agricultural land use and management are essential for the reduction in nutrient loads and improvement of water quality.

Reference:

Abbaspour, K., J. Yang, I. Maximov, R. Siber, K. Bogner, J. Mieleitner, J. Zobrist, and R. Srinivasan (2007), Modelling hydrology and water quality in the pre-alpine/alpine Thur watershed using SWAT, *J. Hydrol.* **333**, 413-430.

Arheimer, B., and M. Brandt (1998), Modelling nitrogen transport and retention in the catchments of southern Sweden, *Ambio* **27**, 471-480.

Arnold, J. G., and P. M. Allen (1996), Estimating hydrologic budgets for the three Illinois watersheds, *J. Hydrol.* **176(1-4)**, 57-77.

Arnold, J. G., P. M. Allen, and G. Bernhardt (1993), A comprehensive surface-groundwater flow model, *J. Hydrol.* **142**, 47-69.

Arnold, J. G., R. Srinivasan, R. S. Muttiah, and J. R. Williams (1998), Large-area hydrologic modeling and assessment: Part I. Model development, *J. Am. Water. Works. Ass.* **34(1)**, 73-89.

Arnold, J.G., J.R. Williams, A.D. Nicks, and N.B. Sammons (1990), *SWRRB - A Basin Scale Simulation Model for Soil and Water Resources Management*, Texas A&M University Press: College Station, Texas.

Behrendt, H., M. Kornmilch, D. Opitz, O. Schmoll, and G. Scholz (2001), Flussgebietsdifferenzierte Nährstoffeinträge im Einzugsgebiet der Saale. **In:** M. Rode, K. Henle and A. Schellenberger (eds.), *Erhalt und Regenerierung der Flusslandschaft Saale*, Deutsche Akademie der Naturforscher Leopoldina, Halle (Saale), 91-105.

Bertoni, J. C. (2001), *Etude hydrologique et analyse des incertitudes sur trois bassins versants semi urbanises de la region centrale d'Argentine*, Universite Montpellier II.

Beven, K. J. (1989), Changing ideas in hydrology. The case of physically-based model, *J. Hydrol.* **105**, 157-172.

Beven, K. J. (1996), A discussion of distributed hydrological modelling. **In:** M. B. Abbott and J. Ch. Refsgaard (eds.), *Distributed Hydrological Modelling*, Kluwer Academic Publ., Dordrecht, The Netherlands.

Bicknell, B.R., J.C. Imhoff, A.S. Donigian, and R.C. Johanson (1997), *Hydrological simulation program - FORTRAM (HSPF): User's manual for release 11*, U.S. Environmental Protection Agency, EPA-600/R-97/080, Athens.

Bogena, H., B. Diekkrüger, K. Klingel, K. Jantos, and J. Thein (2003), Analysing and modelling solute and sediment transport in the catchment of the Wahnbach River, *Phys. Chem. Earth* **28**, 227-237.

Borah, D. K., M. Bera, and R. Xia (2004), Storm event flow and sediment simulations in agricultural watersheds using DWSM, *Trans. ASABE* **47(5)**, 1539-1559.

Chaplot, V., A. Saleh, D. B. Jaynes, and J. Arnold (2004), Predicting water, sediment, and NO3-N loads under scenarios of land-use and management practices in a flat watershed, *Water Air Soil Pollut.* **154(1-4)**, 271-293.

Cherry, K. A., M. Shepherd, P. J. A. Withers, and S. J. Mooney (2008), Assessing the effectiveness of actions to mitigate nutrient loss from agriculture: a review of methods, *Sci. Total Environ.* **406(1-2)**, 1-23.

De Wit, M., H. Behrendt, G. Bendoricchio, W. Bleuten, and P. van Gaans (2002), *The contribution of agriculture to nutrient pollution in three European rivers, with reference to the European Nitrates Directive*, European Water Management Online, official publication of the European Water Association (EWA).

Du, B., A. Saleh, D. B. Jaynes, and J. G. Arnold (2006), Evaluation of SWAT in simulating nitrate nitrogen and atrazine fates in a watershed with tiles and potholes, *Trans. ASABE* **49(4)**, 949-959.

EC (European Commission) (2000), Directive 2000/60/EC of the European Parliament and of the Council establishing a framework for the Community action in the field of water policy. (EU Water Framework Directive, WFD), *Off. J. Eur. Commun.* **L327**, Brussels.

Eisele, M., R. Kiese, A. Krämer, and C. Leibundgut (2001), Application of a catchment water quality model for assessment and prediction of nitrogen budgets, *Phys. Chem. Earth* **(B) 26(7-8)**, 547-551.

Even, S., G. Billen, N. Bacq, S. Thery, D. Ruelland, J. Garnier, P. Cugier, M. Poulin, S. Blanc, F. Lamy, and C. Paffoni (2007), New tools for modeling water quality of hydrosystems: an application in the Seine River basin in the frame of the Water Framework Directive, *Sci. Total Environ.* **375**, 274-291.

FGG-Elbe (2004), *Bericht über die Umsetzung der Anhänge II, III und IV der Richtlinie 2000/60/EG im Koordinierungsraum Saale (B-Bericht). Vorlage zur Elbe-Ministerkonferenz am 9. Dezember 2004*, available at http://www.fgg-elbe.de/tl_fgg_neu/fachdaten/arge_elbe.html (last asscessed: 10.10.2011).

Gömann, H., P. Kreins, and A. Richmann (2007), *Projektionen zur Änderung der regionalen landwirtschaftlichen Landnutzung, Produktion und Stickstoffüberschüsse bis 2020 im Elbeeinzugsgebiet vor dem Hintergrund sich wandelnder Rahmenbedingungen*.

Hattermann, F. F., V. Krysanova, A. Habeck, and A. Bronstert (2006), Integrating wetlands and riparian zones in river basin modeling, *Ecol. Model.* **199**, 379-392.

Hesse, C., V. Krysanova, J. Päzolt, and F.F. Hattermann (2008), Eco-hydrological modelling in a highly regulated lowland catchment to find measures for improving water quality, *Ecol. Model.* **218**, 135-148.

IKSE (Internationale Kommission zum Schutz der Elbe) (2005), *Bericht an die Europäische Kommission*, available at http://www.ikse-mkol.org/index.php?id=207&L= (last asscessed: 10.10.2011).
Krysanova, V., A. Meiner, J. Roosaare, and A. Vasilyev (1989), Simulation modelling of the coastal waters pollution from agricultural watersheds, *Ecol. Model.* **49**, 7-29.
Krysanova, V., D. Möller-Wohlfeil, and A. Becker (1998), Development and test of a spatially distributed hydrological / water quality model for mesoscale watersheds, *Ecol. Model.* **106**, 261-289.
Krysanova, V., F. Wechsung, and F.F. Hattermann (2005a), Development of the ecohydrological model SWIM for regional impact studies and vulnerability assessment, *Hydrol. Process.* **19**, 763-783.
Krysanova, V., F. Hattermann, and A. Habeck (2005b), Expected changes in water resources availability and water quality with respect to climate change in the Elbe river basin (Germany), *Nordic Hydrology* **36(4-5)**, 321-333.
Landwirtschaft und Landschaftspflege in Thüringen (2001), Düngung in Thüringen nach "Guter fachlicher Praxis", available at http://www.tll.de/ainfo/pdf/dung0108.pdf (last asscessed: 10.10.2011).
LAWA (Länderarbeitsgemeinschaft Wasser) (1998), *Beurteilung der Wasserbeschaffenheit von Fließgewässern in der Bundesrepublik Deutschland: Chemische Gewässergüteklassifikation*, first edition, Kulturbuchverlag, Berlin.
Lindenschmidt, K. (2005), *River water quality modelling for river basin and water resources management with a focus on the Saale River, Germany,* Habilitation thesis, Brandenburgische Technische Universität Cottbus.
Lunn, R., R. Adams, R. Mackay, and S. Dunn (1996), Development and applicationof a nitrogen modelling system for large catchments, *J. Hydrol.* **174**, 285-304.
Ministerium für Landwirtschaft und Umwelt in Sachsen-Anhalt (2004), *Versuchsbericht-Bodenbearbeitung und N-Düngung in der Fruchtfolge*, available at http://www.sachsen-anhalt.de/LPSA/index.php?id=28237 (last asscessed: 10.10.2011).
Ministerium für Landwirtschaft, Umweltschutz, und Raumordnung des Landes Brandenburg (2000), *Rahmenempfehlungen zur Düngung 2000 im Land Brandenburg.*
Monteith, J. L. (1965), Evaporation and the environment, *Symp. Soc. Expl. Biol.* **19**, 205-234.
Nash, J. E., and J. V. Sutcliffe (1970), River flow forecasting through conceptual models. Part I: a discussion of principles, *J. Hydrol.* **10(3)**, 282-290.
Oreskes, N., K. Shrade-Frechette, and K. Belitz (1994), Verification, Validation and Confirmation of Numerical Models in the Earth Sciences, *Science* **263**, 641-646.
Payraudeau, S., F. Cernesson, M. G. Tournoud, and K. J. Beven (2004), Modelling nitrogen loads at the catchment scale under the influence of land use, *Phys. Chem. Earth.* **29**, 811-819.
Priestley, C. H. B., and R. J. Taylor (1972), On the assessment of surface heat flux and evaporation using large scale parameters, *Mon. Weather Rev.* **100**, 81-92.
Reimann, G., and J. Seiert (2001), Das Einzugsgebiet der Saale vor dem Hintergrund der geplanten Wasserrahmenrichtlinie der EU. **In:** M. Rode, K. Henle and A. Schellenberger (eds.), *Erhalt und Regenerierung der Flußlandschaft Saale*, Deutsche Akademie der Naturforscher Leopoldina, Halle (Saale), 11-20.
Sächsische Landesanstalt für Landwirtschaft (2007), *Umsetzung der Düngeverordnung Hinweise und Richtwerte für die Praxis,* available at http://www.smul.sachsen.de/lfl/publikationen/download/3309_1.pdf (last asscessed: 10.10.2011).
Saleh, A., J. G. Arnold, P. W. Gassman, L. W. Hauck, W. D. Rosenthal, J. R. Williams, and A. M. S. McFarland (2000), Application of SWAT for the upper North Bosque River watershed, *Trans. ASAE* **43(5)**, 1077-1087.
Santhi, C., R. S. Muttiah, J. G. Arnold, and R. Srinivasan (2005), A GIS-based regional planning tool for irrigation demand assessment and saving using SWAT, *Trans. ASAE* **48(1)**, 137-147.
Staatsministerium für Umwelt und Landwirtschaft (2007), *Agrarbericht in Zahlen 2007*, available at http://www.smul.sachsen.de/smul/59.htm (last asscessed: 10.10.2011).
Stewart, G. R., C. L. Munster, D. M. Vietor, J. G. Arnold, A. M. S. McFarland, R. White, and T. Provin (2006), Simulating water quality improvements in the upper North Bosque River watershed due to phosphorus export through turfgrass sod, *Trans. ASABE* **49(2)**, 357-366.
Theile, K. (2001), Gewässergüte der Saale - Vergangenheits- und Zukunftsaspekte. **In:** M. Rode, K. Henle and A. Schellenberger (eds.), *Erhalt und Regenerierung der Flußlandschaft Saale*, Deutsche Akademie der Naturforscher Leopoldina, Halle (Saale), 117-129.

Thüringer Ministerium für Landwirtschaft, Naturschutz und Umwelt (2007), *Bericht zur Entwicklung der Landwirtschaft in Thüringen 2007 (Berichtsjahr 2006)*, available at http://www.tll.de/agb07/agb07idx.htm (last asscessed: 10.10.2011).

Volk, M., J. Hirschfeld, A. Dehnhardt, G. Schmidt, C. Bohn, S. Liersch, and P. W. Gassman (2008), Integrated ecological-economic modelling of water pollution abatement management options in the upper Ems river basin, *Ecol. Econ.* **66(1)**, 66-76.

Voss, A. (2007), *Untersuchung und Modellierung der Stickstoff und Phosphorumsatz- und Transportprozesse in mesoskaligen Einzugsgebieten des Tieflandes am Beispiel von Nuthe, Hammerfließ und Stepenitz*, Potsdam University.

Wade, A., P. Whitehead, and L.C.M. O'Shea (2002), The prediction and management of aquatic nitrogen pollution across Europe: an introduction to the Integrated Nitrogen in European Catchments project (INCA), *Hydrol. Earth. Syst. Sc.* **6(3)**, 299-313.

Wendland, F., H. Albert, M. Bach, R. Schmidt, (1993), *Atlas zum Nitratstrom in der Bundesrepublik Deutschland*, Springer Verlag, Berlin, Germany.

Whitehead, P. G., E. J. Wilson, and D. Butterfield (1998), A semi-distributed integrated flow and nitrogen model for multiple source assessment in catchments (INCA): Part I - model structure and process equations, *Sci. Total Environ.* **210**, 547-558.

Williams, J., K. Renard, and P. Dyke (1984), EPIC - a new model for assessing erosion's effect on soil productivity, *J. Soil Water Conserv.* **38(5)**, 381-383.

Zammit, C., M. Sivapalan, P. Kelsey, and N. Viney (2005), Modeling the effects of land-use modifications to control nutrient loads from an agricultural catchment in Western Australia, *Ecol. Model.* **187(1)**, 60-70.

7. Summary of the results

The present study aims to investigate the potential impacts of environmental changes (both climate change and land use) on water resources (both water quantity and quality) and hydrological extremes in Germany. Five chapters contributed to achieve this goal in different aspects:

- Chapter 2 analysed the seasonal temperature extremes in Potsdam, providing additional evidence of climate change in Germany;
- Chapter 3 evaluated temporal and spatial changes in water fluxes and water balance components under climate scenarios projected by the statistical-empirical model STAR for the whole territory of Germany;
- Chapter 4 and 5 focused on the projections of the future flood and low flow conditions respectively, using three different downscaling models (CCLM, REMO and WettReg) for the five largest river basins of Germany;
- Chapter 6 tested the applicability of SWIM to simulate nitrogen dynamics in a macro-scale basin (the Saale basin) and evaluated the impacts on NO_3-N load under potential land use changes in selected sub-regions of the Elbe basin.

Except Chapter 2, which is a pure statistical analysis on observed data, the others were constructed based on the hydrological modelling SWIM under various scenarios. The climate impacts on water quantity were analysed in different aspects using the same hydrological model setup and for the same river basins (Chapter 3, 4 and 5). The impact of land use changes on water quality was only evaluated at two meso-scale basins in eastern Germany (Chapter 6). Hence, the general description of the objectives and results of the Chapter 2 and Chapter 6 are given in section 7.1 and 7.6 separately. The summary of the other three chapters are based on the same hydrological model and study areas but driven by different climate forcing for specific purposes. It is given with regard to the following aspects: model calibration and validation (Section 7.2), performance of different downscaling models for historical and scenario periods (Section 7.3), projections of climate impacts on water resources and extremes (Section 7.4) and the uncertainty of the projections (Section 7.5). Additional results, which were not shown in Chapter 3, 4 and 5, are also completed in these sections.

7.1. Seasonal temperature extremes in Potsdam

Chapter 2 aims to demonstrate tendencies of seasonal temperature-related climate extremes for a long-term time, high-quality instrumental record. As a complementation to the large-scale climate change assessment, it examined the temperature data from the Secular Meteorological Station in Potsdam, where observation records over the last 117 years, from January 1893 to 2009 are available. Various indices for seasonal temperature-related extremes, *e.g.* mean of maximum and minimum temperatures and number of cold and warm days and nights, were selected and the significance of the tendencies was indicated by the p-value of the Mann-Kendall test. In general, all the results of this chapter illustrated a high interannual variability of temperature indices, superimposed on a warming trend. The tendencies detected are described in more detail as follows.

The first index is the mean of maximum and minimum temperatures for 1893 – 2008 for all four seasons: spring (March, April, May), summer (June, July, August), autumn (September, October, November) and winter (December, January, February). **Figure 2-2** shows seasonal warming for all seasons; on average about 1 ^{o}C / 100 years or 0.1 ^{o}C / decade. The changes in spring

minimum, summer minimum, summer maximum and autumn minimum are statistically significant at the 0.01 level, while the trend of spring maximum is significant at the 0.05 level.

The maximum diurnal amplitude (difference between maximum and minimum temperature for the same day) and seasonal amplitude (difference between maximum and minimum temperature for the same season) were also analysed for each season. However, most (five out of eight) changes illustrated in **Fig. 2-3** are not statistically significant. The most significant decreasing tendency (at the 0.01 level) was found for the maximum diurnal amplitude for autumn.

The numbers of cold and warm days and nights were determined for each season for the interval 1893 – 2008 (2009 for winter), based on a subjective definition of seasonal "cold" and "warm", because it is found more meaningful and easier to interpret by the readership. For example, the seasonal threshold for cold nights were selected as –10 ^{o}C for winter, 0 ^{o}C for spring and autumn and +10 ^{o}C for summer (**Fig. 2-4**), the seasonal threshold for cold days were selected as 0 ^{o}C for winter, +10 ^{o}C for spring and autumn and +20 ^{o}C for summer (**Fig. 2-5**), for warm nights were selected as 0 ^{o}C for winter, +10 ^{o}C for spring and autumn and +15 ^{o}C for summer (**Fig. 2-6**) and for warm days were selected as +10 ^{o}C for winter, +20 ^{o}C for spring and autumn and +30 ^{o}C for summer (**Fig. 2-7**). The warm-extreme indicators, such as the number of hot days were found to increase. In agreement with the warming of winter temperatures, the cold-extreme indicators, such as the number of frost nights (with minimum daily temperature below 0 °C) and of ice days (with maximum daily temperature below 0 °C) have been decreasing. Five indices (hot summer days, cold summer nights, cold autumn days, warm summer and spring nights) are significant at the 0.01 level and three indices (warm winter days, cold and warm autumn nights) at the 0.05 level.

Finally, the indicators related to frost and hot days are illustrated in **Fig. 2-8**, **2-9** and **2-10**. The results show that the last frost day has been occurring earlier than before in spring without statistical significance, while in autumn, frosts have been starting later (at the significance level 0.05). The frost-free interval is increasing on an average of one day per decade, also indicating a statistically significant (at the 0.05 level) warming tendency.

Chapter 2 indicates that global and general findings of ubiquitous warming are in general agreement with temperature extremes in a specific, long-term, high-quality observation record. However, it also shows the strong natural variability at a single station and that extremes in a single year may differ significantly from the dominating tendency. Hence, one has to be careful with the interpretation of warming. Rather than re-iterating the global warming statement with every exceptional warm spell and questioning it with every exceptional cold spell (*e.g.* January 2010), one needs to take a more balanced view with consideration of long-term records and natural variability.

7.2. Calibration and validation of the SWIM model in large river basins

SWIM was intensively calibrated and validated in terms of river discharges, water balance components (Chapter 3), flood (Chapter 4) and low flow (Chapter 5) conditions for the largest five German rivers. The parameter estimation routine PEST (Doherty, 2004) was applied, as auto-calibration procedure optimising discharge or logarithmic discharge (specifically for calibrating low flows) at selected gauges. The major parameters used for calibration are listed in Annex IV as well as the comparison of the parameter values used for flood and low flow modelling. Three statistical criteria, the Nash-Sutcliffe Efficiency (NSE), Logarithmic Nash-Sutcliffe Efficiency

(LNSE) and deviation in water balance, were used to evaluate the model performance for different purposes.

In Chapter 3, the calibration procedure was carried out for five main discharge gauges for each of the five river basins. 24 intermediate gauges at the main tributaries and the main rivers (mostly with the drainage areas larger than 5 000 km^2) were only included to verify the spatial performance of SWIM (**Table 3-2** and **Fig. 3-1(b)**). In the calibration period (1981 – 1990), the NSE varies from 0.80 to 0.90 for the five main gauges (Versen, Intschede, Neu-Darchau, Frankfurt-Osthafen and Hofkirchen) and the deviation in water balance is not higher than 3% (**Table 3-3**). In the validation period (1961 – 1980), the NSE and the deviation in water balance for these five gauges are ranging from 0.81 to 0.85 and from -8% to 6%, respectively. The discharge at the most of the 24 gauges was well reproduced by SWIM with NSE above 0.6 and deviation within ±10%, even without additional calibration. At the gauges Trier UP, Havelberg and Schöna, the simulated results do not comply with the observed values well enough. This is assumed to be mainly due to poorer climate data and water management interference, which was not considered in the simulation.

In Chapter 4 and Chapter 5, additional climate observations and land use data from outside Germany were used to simulate the peak discharges and low flow conditions. River discharge at 12 gauge stations (**Fig. 4-1**) that are representative of the flood conditions in the main rivers and some large tributaries were calibrated and validated based on observed climate data. Three additional gauges were included in the validation procedure. With the more intensive calibration and better input data, all daily discharges were well reproduced even for the gauges which were not specifically calibrated. NSE greater than 0.8 and the deviations in water balance of within ±3% are achieved (**Table 4-3**). In the validation period (1961 – 1980), all efficiencies are above 0.7 and the deviation in water balance is within ±7%.

Low flows were calibrated using a specific statistical criterion, Logarithmic Nash-Sutcliffe Efficiency (LNSE) to magnify the weight of the low flows in the whole hydrograph (Chapter 5). The discharge data at 24 gauges (**Fig. 5-1(b)**) was selected to calibrate and validate the model, including 20 gauges in the large rivers and their main tributaries in Germany (with drainage area > 5000 km^2) and 4 gauges from the near-natural small catchments (drainage area ≤ 500 km^2). In general, high LNSE (≥ 0.7) indicating satisfactory results are achieved for most rivers in both the calibration and validation periods (**Table 5-3**): the LNSE values are greater than 0.7 for 17 gauges, and greater than 0.8 for 11 of the 24 gauges. The LNSE values in the calibration period are slightly higher (≥ 0.7 at 21 gauges) than in the validation period (≥ 0.59 at 21 gauges).

When comparing the calibration parameter values used for flood modelling with the ones used for low flow simulations, obvious differences in the values are evident for the parameters related to percolation among soil layers and from soil layer to shallow groundwater zone. In general, a longer groundwater flow lag, smaller baseflow factors and correction factors for soil saturated conductivity are needed to better simulate the low flows (Annex IV). There are only small differences between the routing coefficients that are used to calculate the storage time constant for surface and subsurface flow. There is no general changing pattern in the other parameters, *e.g.* correction factor for potential evaporation and initial groundwater flow contribution to stream flow.

Although different number of the gauges were included in Chapter 3, 4 and 5, **Figure 7-1** shows the NSE and LNSE for the 29 gauge stations used in Chapter 3 for the period 1961 – 2000, as an overall summary of the validation results for flood and low flow simulations. Only 3 out of the 29 gauges have NSE smaller than 0.7 and 7 gauges have LNSE smaller than 0.7. One problematic

gauge is the Havelberg at the river Havel, a large tributary of the Elbe, with both NSE and LNSE less than 0.6. The discharge simulated at this gauge is much lower than the measurements. The underestimation of the river discharge is mainly due to the mining activities which heavily influenced river discharges of the Havel especially during the 1970s and 1980s. Large amounts of water were extracted from underground and discharged into the rivers producing water levels higher than natural in the Havel, which cannot be reproduced by the model. In addition, the river Havel is regulated by weirs and the lower reaches is also influenced by the Elbe River.

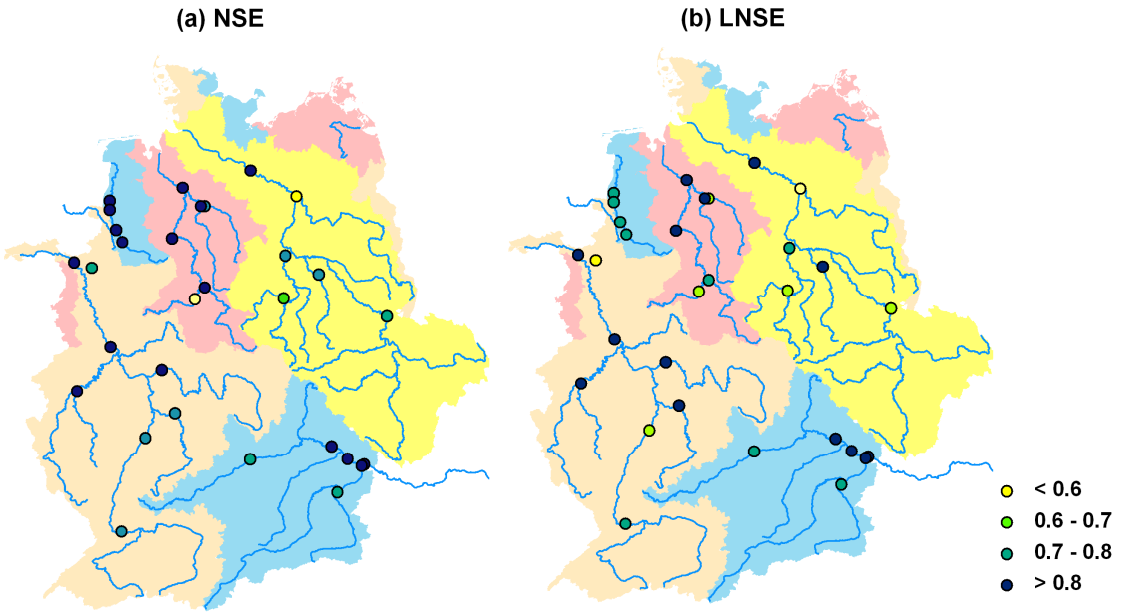

Figure 7-1: The statistical results for the 29 gauges in the period 1961 – 2000 ((a) NSE and (b) LNSE).

In addition to the statistical criteria, the results from the SWIM model were also intensively validated in terms of hydrographs (**Fig. 3-3**), water components (**Fig. 3-4**), 95 and 99 percentiles of river discharge (**Table 4-4**), and flood and low flow frequency curves (**Fig. 4-4** and **Fig. 5-6**). In general, SWIM could successfully reproduce the river discharges and extremes using observed climate data in most of the studied gauges. As the 50-year flood and low flow levels are essential for extreme analysis in this study, **Figure 7-2** summarizes the 50-year flood and low flow levels at the 29 gauges estimated for the simulation period 1961 – 2000 versus the corresponding observed values. It can be seen that the extreme flood level can be well simulated by SWIM but most of low flows are marginally underestimated. This underestimation may be partly due to river management which is not considered in the hydrological modelling.

Finally, it was possible to calibrate and validate the snow processes with the extended snow module. Long-term measured snow data is available at about 26 climate stations in Austria and the Swiss part of the Danube and Rhine basins. In general, the snow depth can be well reproduced for most of the stations: high NSE ($\geq$ 0.6) indicating satisfactory results are achieved for 16 stations during the calibration periods. **Figure 7-3** shows the simulated snow depth (figures in the left) at four selected climate stations in the calibration period 1981 – 1990 compared with the observations. The simulated dynamics of snow accumulation and melt show good agreement with observed values at 3 stations with NSE larger than 0.8 (> 0.7 without considering the snow free period). The corresponding average daily snow depths (**Fig. 7-3** right) also confirm a good model

performance with NSE larger than 0.7 (> 0.48 without considering the snow free period) for the validation period (1961 – 1980).

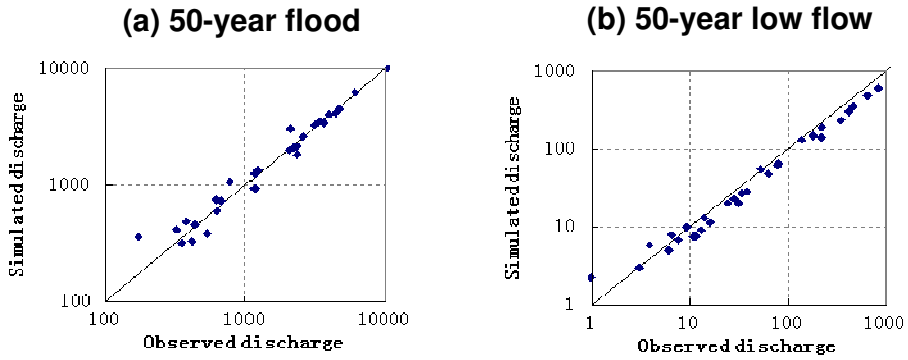

Figure 7-2: Comparison of the simulated 50-year flood and low flow levels at 29 gauges with the observed ones for the control period 1961 – 2000.

At some stations (see the example **Fig. 7-3(d)**), however, the snow depth is still reproduced by SWIM with large errors. There are several possible reasons that add difficulties to simulate the snow dynamics well for all the stations. First, the degree-day factor is not fully distributed in modelling such large basins. Only the elevation information was considered to modify the degree-day factor spatially. Other information like radiation and slope direction was not included in the model due to the insufficient climate data and semi-distributed structure of model SWIM. Second, the bias between the interpolated and actual climate condition at specific points leads to inaccuracies. Since the climate data was interpolated into the centroids of subbasins and then corrected for each hydrotope based on its elevation characteristics, errors can be generated through these processes. Third, the spatial resolution of this study (250 m) might be too coarse to precisely simulate the point processes. However, a fully distributed model at such fine resolution often requires large computational resources and data and is not suitable for large-scale hydrological modelling. Hence, the extended snow model needs to be tested for some small-scale catchments in the future, where the detailed information such as climate and river discharge at the outlet is available.

7.3. The performance of different downscaling models for the reference and scenario periods

Detailed information on the four downscaling models used in this study was presented in Section 1.3. In this section the performance of these models were assessed by cross-comparison of the climate projections and the related hydrological responses for both the reference and scenario periods.

First, the four models were divided into two groups regarding their data availability, *i.e.* STAR and the other three (REMO, CCLM and WettReg). Compared to the latter three models, which can project 100-years or longer climate scenarios, STAR was developed for medium-term (about 50 – 60 years) regional climate projections. In addition, the latter three models generated their own control run from 1961 to 2000 while STAR considers the observed historical climate data as the control run due to its statistical analogue resampling technique from observations. Hence, the performance of STAR in projecting the future scenarios was described separately and a cross comparison was applied for the other models in both the reference and scenario periods.

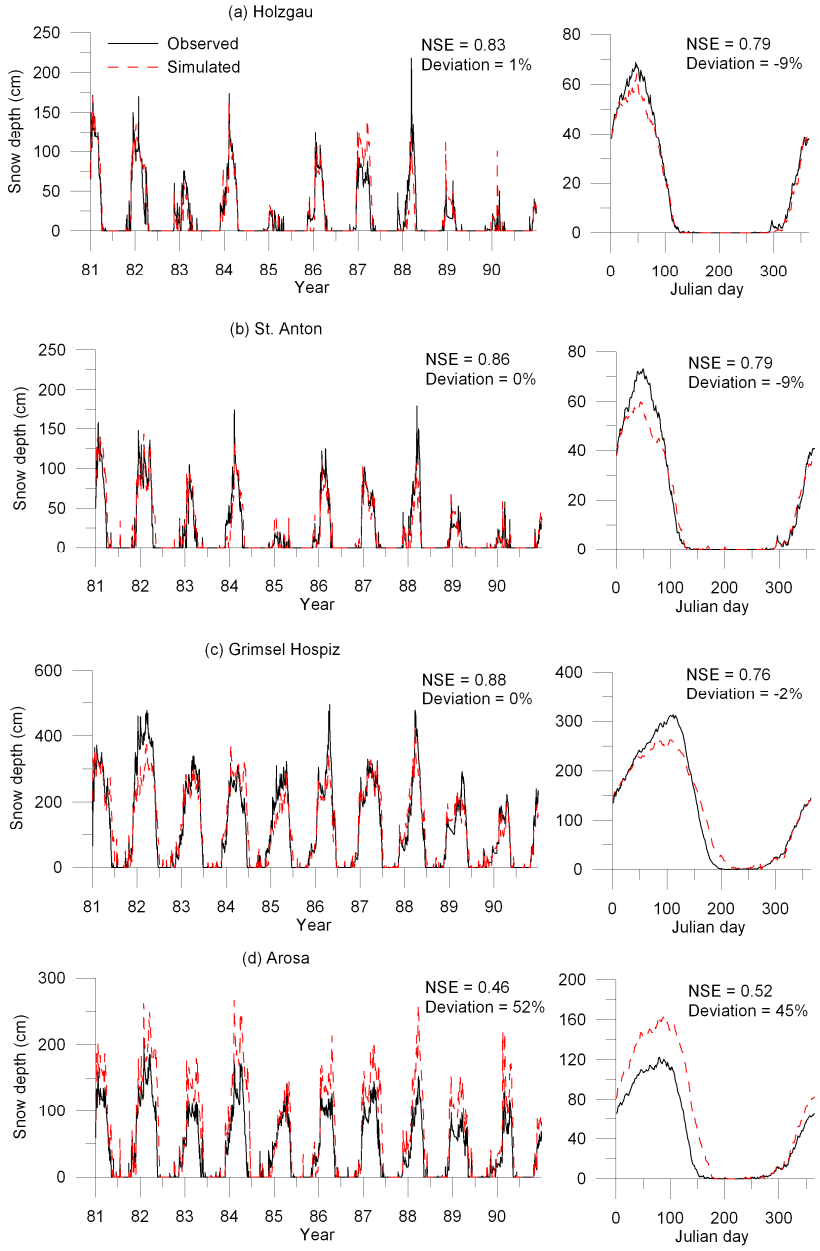

Figure 7-3: Simulated and observed snow depth (left) at four selected climate stations for the period 1981 – 1990 and the corresponding average daily snow depth (right) for the same stations during the validation period (1961 – 1980).

Since there is no control run available for STAR, the reliability of the hydrological response using the STAR realizations was tested for the coming 10 years (from 2009 to 2018), assuming that the climate is not likely to vary suddenly and significantly in the short term. The simulated seasonal dynamics, that comply with the observed ones (1961 – 1990) in all six selected rivers, show that STAR is capable to project the seasonal variability reasonably (**Fig. 3-7**).

Based on the STAR A1B scenario, the spatial changes between the projected (2051 – 2060) and observed (1961 – 1990) annual precipitation and average annual temperature were shown in **Fig. 3-5**. The annual precipitation is projected to decrease in eastern and south-eastern Germany significantly, while there may be an increase in precipitation in the north-western and western Germany. The annual average temperature is projected to rise by 2 to more than 3 °C in the country. **Figure 3-6** (left) shows the observed and projected annual dynamics of precipitation for the basins Ems, Saale and the upper Danube, indicating that STAR is able to model the year-to-year variability reasonably. In addition, slight downward trends were projected by STAR in the Saale and Danube basins. In **Fig. 3-6** (right), the seasonal changes in precipitation display an increase in winter precipitation (strongest for the Ems) and decrease in summer precipitation (strongest for the Danube) for the three rivers.

The climate driving forces generated by REMO, CCLM and WettReg were analysed in terms of annual and summer average temperature and precipitation for both the reference (1961 – 2000) and two scenario periods (2021 – 2061 and 2061 – 2100). The simulated values by each RCM realization are compared with the observed values in the reference period, and only the differences between them are plotted in **Fig. 5-7**.

Both annual and summer temperatures are projected by the physical RCMs with a bias ranging from -1.3 to 0.7 °C. CCLM projects cooler conditions (from -1.3 to -0.9 °C) in both realizations and REMO overestimates the temperature marginally (from 0.5 to 0.7 °C). The temperature generated by the medium realization of WettReg is in good agreement with the observed values both in summer time and the whole year. REMO and WettReg generate reasonable results for annual and summer precipitation, with a bias of 20 – 30 mm, while CCLM has a bias of more than 100 mm in annual precipitation. For the summer temperature and precipitation, however, the bias of all realizations becomes smaller compared to the annual values with the exception of the summer precipitation generated by REMO. The results indicate better performance of the summer climate scenarios than winter ones.

The hydrological response driven by these three RCM control runs were checked in terms of the 95, 99 percentiles of the discharge and the 10- and 50-year flood level (**Tables 4-4** and **4-5**). For both 95 and 99 percentiles, simulated results with WettReg provide the best results for most rivers in Germany compared to those with REMO and CCLM. REMO can be considered as the second best climate model in reproducing high flows, as 9 – 10 of 15 simulated results driven by REMO control runs have a bias of less than 20%. The highest differences were produced by SWIM driven by the CCLM climate, for which much higher flows were generated in practically all gauges. The 10- and 50-year flood simulated driven by the dynamical RCMs control runs (**Table 4-5** and **Fig. 4-4**) shows lower differences with observational data compared to the high flow (95 and 99 percentile discharge) simulations. The results under the REMO control runs are closer to the observed floods than those under the CCLM control runs. Considering simulations using WettReg, the agreement between the simulated flood levels and observed values is lower than that for the high flows, although the differences in most cases are still within 20% for both flood levels.

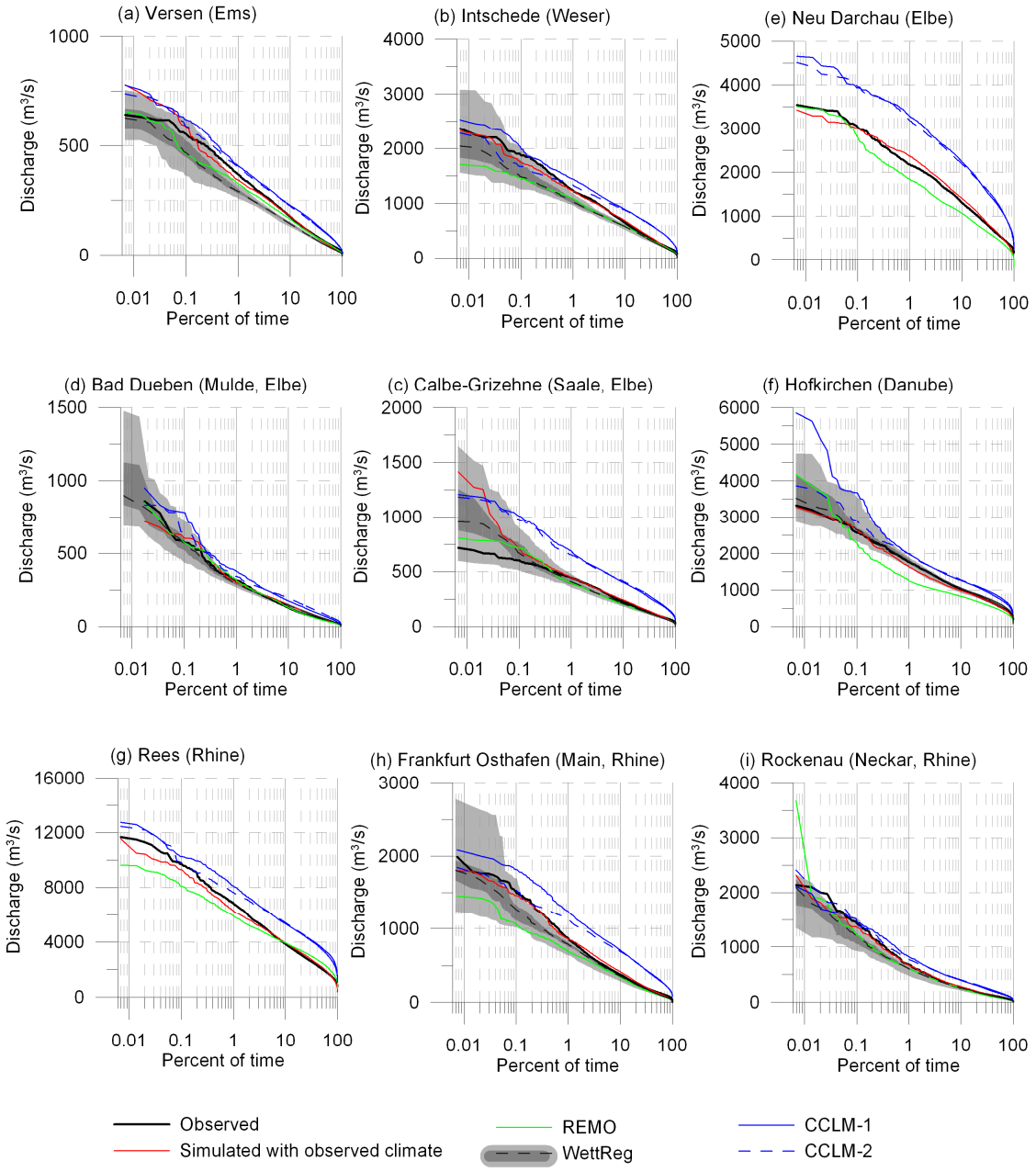

Figure 7-4: Observed and simulated flow duration curves driven by observed climate data and the three RCMs (CCLM, REMO and WettReg) during reference period at nine selected gauges (For the international rivers Elbe and Rhine, the WettReg scenarios are not available outside Germany.).

In addition to the analysis in the previous chapters, the simulated duration curves driven by different RCMs (REMO, CCLM and WettReg) were compared with the observations at nine selected gauges for the period 1961 – 2000 (**Fig. 7-4**). This comparison provides an extra validation of the simulated discharge using observed climate data and it reflects the simulated discharge characteristics at each percentile (from low to high flows) driven by different RCMs. At last, the simulated and observed average daily discharges of the same reference period were shown in **Fig. 7-5**, displaying the seasonal response of river discharges under different RCM scenarios. Both figures confirm the previous findings:

- SWIM can reproduce the daily river discharges using observed climate data successfully at most of the studied gauges,
- WettReg provides the best results during the reference period for most rivers in Germany compared to those with REMO and CCLM,
- REMO can be considered as the second best climate model in reproducing the whole duration curves as well as seasonal variability, however, it has significant biases for the southern Alpine regions outside Germany (see **Fig. 7-5(f) and (g)**);
- CCLM projects much wetter conditions than observed in most parts of Germany.

Finally, **Figure 5-7** also demonstrates the changing pattern by comparing the scenario data with their corresponding control runs for the RCMs REMO, CCLM and WettReg. Regarding the annual and summer average temperature, all RCMs project a steady increase of 2 – 3 °C in this century. However, no common trend in precipitation is projected by all models. The 60 realizations from the empirical-statistical model WettReg show a continuously downward trend in precipitation, while the two physical models (REMO and CCLM) project more dynamic changes with an increase in precipitation in the middle of this century and a marginal decrease at the end of this century. It should be noticed that all three downcaling models project similar summer precipitations in the last 40 years of this century. Hence a more robust projection of low flow conditions was to be expected due to more robust climate input in summer. The large difference of the projected annual precipitation partly reveals the reason why it was more difficult to obtain similar change pattern of flood (occurring mostly in winter) simulated by SWIM driven by different downcaling models (Chapter 4).

In summary, the simulated river discharges driven by the dynamic climate models REMO and CCLM have a greater bias compared to the observations while the ones driven by the empirical-statistical models have better agreement with the observed discharges. Because of the large bias from the dynamic RCMs, different approaches to "correct" the climate output (termed "bias correction") were conducted in various climate impact studies instead of applying the outputs from RCMs directly (see the review of regional climate models for hydrological impact studies by Teutschbein and Seibert, 2010). However, the credibility of such a "correction" is currently under extensive discussion, particularly concerning the extreme events. Graham *et al.* (2007) stated that the use of the delta approach (Hay *et al.*, 2000), which adds the change in projected climate to an observational database, offers a robust method to compare average outcomes from different climate models, but not hydrological extremes. Kay *et al.* (2006) found that direct use of the RCM data could result in relatively good estimates of flood frequency, even though there might be a systematic bias in the overall hydrological budget. Lenderink *et al.* (2007) claimed that the direct use of RCM data might be preferred when other discharge characteristics than the mean (such as extremes) are of interest. Recently, Johnson and Sharma (2011) compared the performance of six scaling and bias correction methods for constructing scenarios from 38 GCMs across Australia. They found that there is significant uncertainty associated with the bias correction estimates for the future projections. Taking into account the uncertainty of the bias correction methods, especially for extreme events, no bias corrections was applied in this study. Instead, the downcaling models were carefully selected according to their usefulness for hydrological impact simulations (Bronstert, 2007b) and for each sub-study individually. For example, we selected the scenarios generated by empirical-statistic model STAR, which can be directly applied without bias correction, to study the average seasonal dynamics and average annual water flow components (Chapter 3). For the projection of extreme events like flood and low flows, we used the other three downcaling models directly for both the control and scenario period assuming that the RCM biases in the future are approximately the same as in the control climate (Chapter 4 and 5).

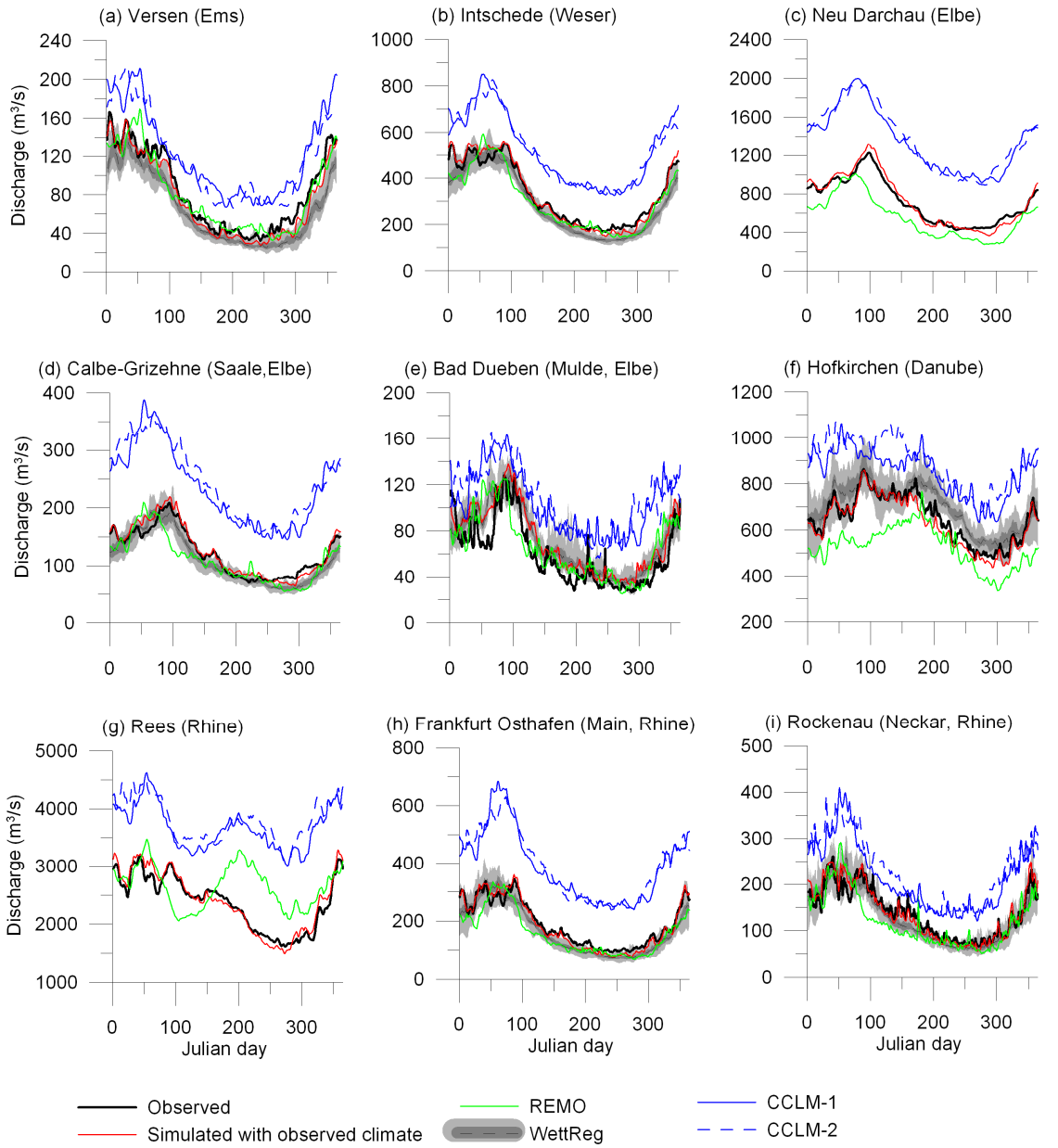

Figure 7-5: Observed and simulated average daily discharges driven by observed climate data and the three RCMs (CCLM, REMO and WettReg) during reference period at nine selected gauges. (For the international rivers Elbe and Rhine, the WettReg scenarios are not available outside Germany.).

7.4. The impact of climate change on water fluxes and hydrological extremes in Germany

The first German-wide impact assessment of water fluxes dynamics under climate change was performed using statistical-empirical model STAR as the input climate forcing. The scenario results for the period 2051 – 2060 show that the reduction of water discharge in summer and autumn is likely to be a considerable problem in Germany compared to the reference period 1961 – 1990, especially in the southeastern part of Germany (**Fig. 3-7**). All the six rivers (Ems, Weser, Saale, Danube, Main and Neckar) show a decline in water discharge (about 8% – 30%) in summer and autumn months (**Table 3-5**). In the winter months, all the rivers tend to have more

stream flow (about 5% - 18%), especially the Ems river basin in the north-western coastal region (**Table 3-5**). Regarding the major water flow components for the same scenario period, evapotranspiration could increase by about 25 mm on average in Germany, mainly due to higher temperature (**Fig. 3-8(a)**). The changes in groundwater recharge and runoff generation are spatially different (**Fig. 3-8(b)** and **(c)**). Southern Germany and large parts of the Elbe basin have a negative tendency in both groundwater recharge and total runoff, while more water is expected in northwestern Germany. The climate impact assessment demonstrates potential shortage of water resources in the Elbe, upper Danube and the upper part of the Rhine Valley.

The 50-year flood and low flows estimated for the two scenario periods (2021 – 2060 and 2061 – 2100) were compared to the ones derived from the control period (1961 – 2000) using the same climate models. Here only the results for the second scenario period are summarized. The two dynamical models (REMO and CCLM) and the statistical-empirical model (WettReg) projected different characteristics of the flood conditions for the future. In general, the two dynamic models projected wetter conditions and higher floods than the statistical-empirical model and resulted in a variety of temporal and spatial changes in both directions (**Fig. 4-9** and **Fig. 4-10**). In contrast, the medium results obtained using WettReg normally show a steady and simple trend in temporal flood generation and rather small changes in spatial distribution (**Fig. 4-11**). More than half of the realizations generated by the two dynamical models suggest an increase of about 10 – 20% in the 50-year flood levels in the rivers Weser, Rhine, Main, Saale and Elbe. The Ems and the German part of the Danube do not have a clear trend, whereas there is a likelihood of 20% decrease in the flood level for the Neckar (**Fig. 4-12**). In contrast, the model WettReg projects a downward trend for the northern basins Ems and Weser (10%), and Saale (20%), and no distinct trend can be found for the Main, Danube, and Neckar (**Fig. 4-13**). The dynamic models also imply an extension of flood season in winter, so that the extreme flood events may also occur frequently in spring and summer in the Saale River (**Fig. 4-14**). However, there was no shift in flood seasons in the results driven by WettReg. In conclusion, no strong change pattern could be detected driven by all three downscaling models. There are more significantly increasing trends in high flow and flood levels simulated using REMO, whereas most of the changes under CCLM scenarios are moderate and most of the significantly decreasing trends in floods were found in simulations driven by WettReg.

Compared with flood projections, the signal of severer low flow is much stronger (**Fig. 5-8**, **5-9**, and **5-10**). The current 50-year extreme low flows are likely to occur more frequently in western and southern Germany towards the end of this century as suggested by 80% of all realizations (**Fig. 5-11**). Central Germany may also become a more critical region as suggested by all CCLM realizations and the medium WettReg realization with more frequent extreme low flows. The rivers originating in the alpine regions outside of Germany will probably have greater low flows as more rain falls instead of snow in winter and spring. August and September, which are already the dry months in most German rivers, are likely to experience low river discharges more frequent. In addition, the low flow season tends to expand into late autumn, increasing further the risk of water stress in water-related sectors (**Fig. 5-12**).

The strong signal of severe low flow conditions also comply with the decline in water discharge in summer and autumn months driven by STAR scenarios. The main reasons are higher evapotranspiration due to higher temperatures, and lower or practically the same precipitation in summer. The higher temperature increases the potential evapotranspiration and can lead to a reduction in river flows even when the precipitation remains unchanged. In addition, the earlier harvest of winter crops and the following faster growth of cover crop aggravate the loss of soil water and decrease of runoff in these months. During the warmer and drier times, the deficit of

precipitation accompanied by higher evapotranspiration demand is thus the major threat reducing the water availability and triggering the extreme low flows.

7.5. The uncertainty of climate impact studies

Kay *et al.* (2009) investigated the sources of uncertainty for climate change impact studies especially on flood frequency. They suggested that the largest uncertainty comes from the GCM structures. However, this is due to the extremely large increases in winter rainfall predicted by one of the five GCMs they used. If the results from this GCM are omitted, the uncertainty relating to modeling of future climate (*e.g.* RCMs) is still larger than emission scenarios or hydrological modelling. Therefore one of the main objectives of this study is to investigate different sources of uncertainty such as structure of climate models, emission scenarios and the multi-realizations generated by each model.

The source of uncertainty in STAR comes from the 100 realizations generated for the A1B scenario. In general, the uncertainty for high water discharge is much larger than that for low flows, and the uncertainty in winter time is much larger than that in summer (**Fig. 3-7**). Regarding the water components, the mean changes in actual evapotranspiration are relatively certain compared to runoff and groundwater recharge (**Fig. 3-8**). The reason is that temperature is the main driver of potential evapotranspiration and the trend of it is consistent in all 100 realizations. Hence, the actual evapotranspiration is increasing as long as water supply (precipitation) is sufficient. In some regions, *e.g.* the Elbe basin and the upper Rhine valley, where the water resources are very vulnerable to a changing climate, the uncertainty is more substantial. In contrast, the drier areas have lower uncertainty in projected runoff and groundwater recharge. The regions with high water productions have higher uncertainty in runoff and groundwater recharge.

With regard to flood projections, the major uncertainty is assumed to be the use of RCMs with different structures. In many cases, two dynamic models yield different temporal and spatial patterns from the statistical-empirical model, and the unbalanced number of realizations from each model makes it difficult to summarize all model results. Besides, there are major sources of uncertainty in the scenarios generated by each RCM. For the WettReg model, the major source of uncertainty is assumed to be the multiple realizations for every emission scenario. Although only the medium result was taken into the final evaluation, the large deviations from the medium result should not be ignored, especially for floods in some basins such as the Elbe and Rhine (**Fig. 4-13**). In simulations driven by CCLM, the important source of uncertainty is represented by two realizations from GCM that were used as the forcing data for the control runs and the initial boundary conditions for the scenario runs. As a result, the two CCLM realizations lead to two opposite directions of the hydrological response under each emission scenario (**Fig. 4-10**). In the simulations driven by REMO, the "external" uncertainty originates from different emission scenarios: only the results in some basins agree in all three scenarios (**Fig. 4-9**).

In contrast, the impacts of different sources of uncertainty are relatively smaller in low flow projections, so that a strong signal of severe low flow conditions can be detected in 80% of the scenarios used. This is partly due to the robust climate projections in the summer half year and partly due to the closer link between low flow and temperature, which is usually a robust variable in climate models. Moreover, the lower temporal variability of low flows (in the order of weeks) is more in accordance with the temporal resolution of the climate scenarios (Middelkoop *et al.*, 2001; Bronstert *et al.*, 2007b).

7.6. From meso- to macro-scale dynamic water quality modelling for the assessment of land use change scenario

The implementation of the European Water Framework Directive requires reliable tools to predict the water quality situations in streams caused by planned land use changes at the large-scale regional river basins. However, process-based models, which can better represent the distributed processes than the simplified conceptual models, were rarely applied to assess water quality for the macro-scale river basins. The main objectives of this study are 1) to test the applicability of the process-based ecohydrological model SWIM for simulating nitrogen dynamics in a macro-scale basin, 2) to estimate changes in NO_3-N load under potential land use changes. To achieve these goals, the uncertainties related to input data and parameterisation in SWIM were intensively investigated. The usefulness of distributed retention parameters was tested aiming to improve the spatial representation of the model for a large catchment.

The main study area is the Saale river basin, the second largest tributary of the Elbe River in regards to length and discharge (after Vlatava, Czech Republic). In addition, seven meso-scale catchments located in the Elbe basin (the Stepenitz, gauge Wolfshagen; the Nuthe, gauge Babelsberg; the Wipper, gauge Hachelbich; the Unstrut, gauge Oldisleben; the upper Saale, gauge Blankenstein; the Weiße Elster, gauge Greiz; and the Mulde, gauge Meinsberg) were also included in the modelling study, partly to investigate the model uncertainties and the physical representation of retention parameters in SWIM, and partly to simulate land use change scenarios (see **Fig. 6-2** and **Table 6-1**).

First, the calibration and validation of SWIM for all eight catchments was performed for water discharge and then for concentrations and loads of nitrogen. **Table 6-4** includes the NSE (from 0.7 to 0.84) and the deviations in water discharge (within ±3%) for each of the eight basins for the validation period. Generally, the efficiencies are satisfactory and the deviations in water discharge are low for all catchments. The calibration and validation of SWIM for nitrogen dynamics was done for the Saale basin, checking also several intermediate gauges. In addition, a calibration and validation was done separately for seven meso-scale catchments with the "global" (unique for the basin) retention parameters: residence times in subsurface and groundwater (K_{sub} and K_{grw}) and the decomposition rates in subsurface and groundwater (λ_{sub} and λ_{grw}). The efficiencies and the deviations in NO_3-N load for all basins are listed in **Table 6-4** and **6-5**. In general, the seasonal dynamics of NO_3-N load were reproduced well by SWIM. The efficiency at the last gauge of the Saale basin is 0.70, indicating a good simulation result for this macro-scale basin. The simulated NO_3-N loads in seven meso-scale catchments (**Table 6-4**) are in a good agreement with the observed data, with the Nash-Sutcliffe efficiencies varying between 0.52 and 0.72. The efficiencies for the simulated NO_3-N load at the intermediate (not calibrated) gauges of the Saale are lower: only in 50% of all cases the efficiency is higher or equal 0.49 (**Table 6-5**).

The meso-scale Weiße Elster catchment was used for the uncertainty analysis, aiming to investigate the separate effects of input data and model parameters on the resulting simulated nitrogen dynamics (**Fig. 6-6**). It is found that winter rape behaves different from other crops, and can lead not only to higher NO_3-N load in the river, but also increase the number of extremely high load values. Unlike the uncertainty related to crops, the uncertainty corridor of retention parameters is narrower. It includes all the low measured NO_3-N values. The results of the uncertainty analysis indicate that agricultural activities have significant influence on simulated nitrogen dynamics, especially on the extremely high loads.

The next step was to test the plausibility of the retention parameters in SWIM and to search for the parameter ranges for six meso-scale catchments with relatively homogenous or mixed

denitrification characteristics. The calibrated/validated values of the retention parameters for the six meso-scale catchments (**Table 6-9**) show that parameters used in SWIM have an adequate physical representation of the actual retention conditions. For example, the Nuthe catchment located in a lowland area has much higher residence times and decomposition rates than the other five catchments.

As the retention parameters were proved to comply with the actual conditions in six catchments, 12 distributed parameters indicating the three denitrification conditions were applied. It aimed to improve the simulation results at the intermediate gauges and the outlet for the macro-scale Saale basin. However the use of the distributed method did not improve the results as expected. The result at the last gauge is very similar to the one with the global parameters (**Fig. 6-7**). The results in terms of Nash-Sutcliffe efficiency were improved only for one third of the intermediate gauges, while the results for the rest were the same or even worse. Hence, the usefulness of distributed parameters for macro-scale basins was not confirmed in the Saale basin. The possible reasons are: a lack of detailed information on decomposition conditions in groundwater, a lack of management information in different federal states, poor simulation of hydrological processes in the karstic areas and the uncertainties in the denitrification map of Germany (Wendland *et al.*, 1993).

Although the hypothesis testing the usefulness of distributed parameters for macro-scale basins was not confirmed in the Saale basin, the Monte-Carlo simulation procedure was carried out for each of six meso-scale basins with the aim of finding optimal parameter ranges for future studies. The parameters value resulting in Nash-Sutcliffe efficiencies above 0.5 and deviations in load less than 10% were taken into account. The obtained optimal parameter ranges also confirmed the results in the plausibility test (**Fig. 6-8**). That is, higher decomposition values correspond to better denitrification conditions. Two sets of optimal parameter ranges were suggested in this study: one for the lowland areas and one for other geographical conditions (**Table 6-10**).

Finally, land use and land management scenarios were applied to two meso-scale subbasins: the Unstrut basin (gauge Oldisleben) almost entirely located in the federal state of Thuringia, and the Weiße Elster (gauge Greiz) almost entirely located in the federal state of Saxony. According to **Fig. 6-9** and **6-10**, increasing areas under winter rape, higher fertilizer rates, excluding cover crops and converting pasture to agriculture land would lead to higher NO_3-N loads, whereas lower fertilizer rates, set-aside of agricultural land and planting more maize instead of winter rape would reduce the NO_3-N load. Mineral fertilizers have a much stronger effect on the NO_3-N load (50% more mineral fertilizer can cause 29 – 41% more NO_3-N load) than organic fertilizers (only 1% more load). Thus, adjusting the mineral fertilizer rates to the plant needs is essential for the control of nitrogen input into surface water. Cover crops, which play an important role in the reduction of nitrate losses from fields, should be maintained on cropland. The planting area of winter rape should not be increased significantly in areas, where environmental targets are important. As another energy plant, maize has a moderate effect on the water environment (3 – 5% less NO_3-N loads with an increase of 10% in the maize area). The scenario studies revealed how important an optimal agricultural strategy is. Good planning based on the modelling results can compile with the development priorities, and helps to reduce the NO_3-N loads in the future.

8. Conclusions and outlooks

In conclusion, the main part of the presented study analysed the environmental impacts on water resources and hydrological extremes by applying the hydrological model SWIM under various climate and land use change scenarios. Both the hydrological model and the environmental change scenarios were carefully selected considering the study purposes, the characteristics of the climatic and hydrological models and their capability for large-scale studies. Instead of applying the original hydrological model directly, a new glacier module was developed and the snow module of SWIM was extended to better simulate the hydrological processes for the basins in the cold alpine regions. Crop rotation was also adapted for the warmer conditions projected by climate scenarios. It took about two years to collect the various input data for SWIM for Germany and also for the neighbouring countries. SWIM was then extensively applied for various river basins (from meso- to macro-scale basins and from pluvial to nival-pluvial regimes) and for different study purposes (both water quantity and quality). All the modeling results show that SWIM is reasonably able to simulate water resources and extremes using observed climate data at a daily time step and it is able to analyse the impacts of climate and land use changes in Germany reliably. Along with the quantification of environmental change impacts, the uncertainty inherent in hydrological and climatic models was taken into account, indicating the robust projection results. Besides the modelling exercises, the observed temperature data at a local scale was analysed, which gives additional evidence of the necessity for the climate impact studies in Germany.

As the final conclusion of the entire study, only the essential findings corresponding to the main objectives are stated as follows.

1 . *Projection of changes in the seasonal dynamics of water fluxes, spatial changes in water balance components and the flood and low flow conditions under climate change for the five largest river basins in Germany (Chapter 2, 3, 4 and 5):* Germany has already experienced climate change with an increase of ca. 1°C in annual average temperature and a moderate increase (9%) in annual precipitation between 1901 and 2000 (Schönwiese *et al.*, 2006). The simple statistical analysis of the long-term observed temperature extremes at Potsam also shows a warming trend at the local scale in Germany. This result indicates a general agreement with the global and general findings of ubiquitous warming. In addition, it shows the strong natural variability at a single station, which is superimposed on the general warming trend. Hence, a more balanced view with consideration of old records and natural variability is needed when interpreting the warming trend.

The climate scenarios for Germany suggest a continuous increase in temperature and various change patterns in precipitation within this century. Driven by the statistical-empirical model STAR, the results for the scenario period 2051 – 2060 show that water discharge in all six rivers would be 8% - 30% lower in summer and autumn compared to the reference period (1961 – 1990), with the strongest decline expected for the Saale, Danube and Neckar. Higher winter flow is expected in all of these rivers and the increase is most significant for the Ems (about 18%). The actual evapotransipration that is simulated is likely to increase by 25 mm on average in Germany, while total runoff generation may decrease in southern and eastern Germany.

For the flood projections, no consistent and robust change direction was suggested under all applied scenarios generated by REMO, CCLM and WettReg. For the scenario period 2061 –

2100, more than half of realizations generated by the two dynamical models suggest an increase of about 10 – 20% in the 50-year flood levels in the rivers Weser, Rhine, Main, Saale and Elbe. The Ems and the German part of the Danube do not have a clear trend, while there is a likelihood of decrease in the flood level by 20% for the Neckar. In contrast, the WettReg model projects a downward trend for the northern basins of the Ems and Weser (10% lower flood level), and Saale (20% lower). No distinct trend could be found for the Main, Danube, and Neckar. The dynamic models also imply an extension of flood season in winter, so that the extreme flood events may also occur frequently in spring and summer in the Saale River, but there was no shift in flood seasons in the results driven by WettReg.

The 50-year low flow is likely to occur more frequently in western, southern and parts of central Germany in the period of 2061 – 2100 as suggested by more than 80% of the model runs driven by the same three RCMs. The current low flow period (from August to September) may be extended until the late autumn by the end of this century.

2 . *Impacts on NO_3-N load under the potential land use changes in selected sub-regions of the Elbe basin (Chapter 6)*: the Saale River, a large tributary of the Elbe River, was a polluted water body due to the heavy nutrients loads from the high proportion of agricultural land in the basin. According to the scenario results, increasing areas under winter rape, higher fertilizer rates, excluding cover crops and converting pasture to agriculture land would lead to higher NO_3-N loads, whereas lower fertilizer rates, set-aside of agricultural land and planting more maize instead of winter rape would reduce the NO_3-N load. Mineral fertilizers have a much stronger effect on the NO_3-N load than organic fertilizers. Cover crops, which play an important role in the reduction of nitrate losses from fields, should be maintained on cropland. The planting area of winter rape should not be increased significantly in areas, where environmental targets are important. As another energy plant, maize has a moderate effect on the water environment.

3 . *Investigation into the various sources of uncertainty (Chapter 3, 4, 5, and 6):* in climate impact projections, the major uncertainty lies in climate projections, namely different RCM structures, emission scenarios and multiple realizations. In general, the uncertainty of high flow in winter as well as extreme floods remains high, so that no distinct directions of change in flood levels were suggested by all the scenarios used. In contrast, the projected changes in low flows appear more consistent and certain. This is due to the more robust climate projections in the summer months (both temperature and precipitation), the closer relationship between low flow and temperature and the lower temporal variability of low flows. In the water quality modeling for NO_3-N load, large uncertainties originate from the input data of agricultural activities, which especially influence the extremely high loads. The calibration of the retention parameters in the hydrological model SWIM, however, can compensate for the uncertainty of the input data to a certain extent.

The robust conclusion of this study is that most part of Germany is likely to experience lower water availability in summer and autumn under a warmer climate. The low flow season may extend to late autumn with more severe low flow conditions in western, southern and parts of central Germany at the end of this century. The NO_3-N load in rivers is significantly influenced by the agriculture management, especially crop types and mineral fertilizers applications. Hence, an optimal agricultural land use and management are essential for the improvement of water quality in the context of the regional development plans for future.

An extensive overview of the environmental impacts on water resources was presented in this paper. However, there is still much effort to be done for a further comprehensive study in Germany on this topic. Chapter 6 was only focused on the impact of land use changes on the NO_3-N load, while Chapter 3, 4 and 5 were devoted to the climate impact assessment on river discharges without consideration of changes in land use patterns, except the adaptation of crop rotations. Thus, neither the climate impacts on water quality nor the land use impacts on water availability were investigated so far. As stated previously, the environmental factors jointly affect water resources, either exacerbating or alleviating the undesirable changes in water resources. For example, sustainable water and land-use management are helpful to alleviate the water stress caused by climate factors. Hence, a more comprehensive environmental impact research is still required to support a sustainable water management in the future.

Future work should also address the sources of uncertainty from different GCMs for climate impact studies, as all the RCM runs in this study are based on one GCM ECHAM5 projection.

Finally, it should mention that there are also some limitations in the methods of investigation. Firstly, the daily simulation time step restricted the model SWIM to reproduce the flash floods in the small or meso-scale catchments. Secondly, some important flood generation processes in SWIM (*e.g.* surface flow generation) are represented by conceptual formulations, which also restrain the application of SWIM for reproducing flash floods. Hence, only the plain floods in large river basins were considered in this study. Thirdly, to better simulate the low flow and NO_3-N conditions, especially for meso-scale catchments, more detailed soil and groundwater information are required.

Therefore, the future tasks in regard to environmental impacts are planned as follows:

1. *Climate impacts on water quality:* As complementation to Chapter 6, the 100 realizations from model STAR will be applied to analyse the climate impacts on water quality for the meso- and large-scale basins. Prior to the application of climate scenarios, the parameters related to decomposition of the nutrients in SWIM might need to be represented by temperature dependent expressions. Driven by the large number of realizations, both the projected water temperature and the nutrient load will be compared with the ones under current conditions. This study will be aimed at finding the potential changes caused by a warming climate and analyse which environmental factor (climate or land use) plays a bigger role on the river water quality.

2. *Environmental impacts (both climate and land use changes) on hydrological extremes:* As stated in Chapter 5, the low flow conditions are heavily controlled by the management strategies in the basins or along the rivers. For the meso-scale basins (area < 500 km^2), the changes in land use can also be a considerable factors for the regional flood risk assessment, as the influence of land use on storm runoff generation in the meso-scale can be of higher relevance than in the macro-scale basins (Bronstert *et al.*, 2007a). Hence, the regional land use change scenarios will also need to be integrated into the available RCM scenarios to reveal the potential changes on river discharges in a more sophisticated context. In addition, such studies require improvements to SWIM or another specific hydrological model to simulate the river discharges in a higher temporal resolution, *e.g.* in hourly time steps.

3. *Uncertainty of flood projections:* Chapter 4 reveals the large uncertainty in flood projections due to different RCM structures, emission scenarios and realizations even without considering the difference among GCMs. Hence, with the availability of

additional 12 RCM scenarios driven by different GCMs, it is possible to obtain a "complete range" of simulation results for the five largest river basins. This evaluation will not only yield a general directions of change in flood levels as expressed by the ensemble means, but also help assess the uncertainty bounds due to GCM and RCM structures separately and both together.

4. *Reduction of the uncertainty in flood projections:* As it suggested in Chapter 4, it may be more meaningful to use and further develop specific tools or models "specialised" in flood conditions. The tailored scenario methods for regional flood conditions have been proposed in recent years, *e.g.* by considering observed trends and correlations of flood prone circulation patterns and flood events of specific catchments (Samaniego and Bárdossy, 2007), or by empirical-statistical downscaling optimised for flood events, *e.g.* by Bürger (2009). Other future work, which complements the extreme value statistics, is to take additional information besides the annual maximum discharges into account and provide more robust estimation on the trends of the extremes. For example, changes in the whole shape of the river duration curve may also reveal some clue of the changing trend in flood conditions.

5. *Validation of the extended snow and glacier module applied for small-scale basins.* The extended snow and glacier modules are important products of this study and help reproduce river discharges in large basins reasonably. However, detailed snow and glacier processes could not be validated due to the lack of the necessary information at the local level. Hence, it would be helpful to test these modules for some small glacier covered basins, where both the SWIM input data, the long-term information on the discharge at basin outlet and the snow and glacier data are available.

Reference

Arheimer, B., and M. Brandt (1998), Modelling nitrogen transport and retention in the catchments of southern Sweden, *Ambio* **27**, 471-480.

Arnold, J. G., P. M. Allen, and G. Bernhardt (1993), A comprehensive surface-groundwater flow model, *J. Hydrol.* **142**, 47-69.

Arnold, J. G., R. Srinivasan, R. S. Muttiah, and J. R. Williams (1998), Large-area hydrologic modeling and assessment: Part I. Model development, *J. Am. Water. Works. Ass.* **34(1)**, 73-89.

Arnold, J.G., J.R. Williams, A.D. Nicks, and N.B. Sammons (1990), *SWRRB - A Basin Scale Simulation Model for Soil and Water Resources Management*, Texas A&M University Press: College Station, Texas.

Baker, A. (2003), Land use and water quality, *Hydrol. Process.* **17(12)**, 2499-2501.

Bates, B.C., Z.W. Kundzewicz, S. Wu, J.P. Palutikof (eds.) (2008), *Climate Change and Water - IPCC Technical Paper VI*, IPCC Secretariat, Geneva, IPCC Secretariat, Geneva.

Bergstrom, S., and B. Carlsson (1993), Hydrology of the Baltic Basin, *Swedish Meteorological and Hydrological Institute Reports: Hydrology* **7**, 21.

Beven, K. J. (1989), Changing ideas in hydrology. The case of physically-based model, *J. Hydrol.* **105**, 157-172.

Beven, K. J. (1996), A discussion of distributed hydrological modelling. **In:** M. B. Abbott and J. Ch. Refsgaard (eds.), *Distributed Hydrological Modelling*, Kluwer Academic Publ., Dordrecht, The Netherlands.

Bicknell, B.R., J.C. Imhoff, A.S. Donigian, and R.C. Johanson (1997), *Hydrological simulation program - FORTRAM (HSPF): User's manual for release 11*, U.S. Environmental Protection Agency, EPA-600/R-97/080, Athens.

Borah, D. K., M. Bera, and R. Xia (2004), Storm event flow and sediment simulations in agricultural watersheds using DWSM, *Trans. ASABE* **47(5)**, 1539-1559.

Bormann, H. (2010), Rrunoff regime changes in german rivers due to climate change, *Erdkunde* **64(3)**, 357-279.

Braithwaite, R. J., and Y. Zhang (1999), Modelling changes in glacier mass balance that may occur as a result of climate changes, *Geogr. Ann.* **81A(4)**, 489-496.

Braithwaite, R. J., and Y. Zhang (2000), Sensitivity of mass balance of five Swiss glaciers to temperature changes assessed by tuning a degree-day model, *J. Glaciol.* **46(152)**, 7-14.

Bronstert, A. (2003), Floods and climate change: Interactions and impacts, *Risk Anal.* **23(3)**, 545-557.

Bronstert, A., D. Niehoff, and G. Bürger (2002), Effects of climate and land-use change on storm runoff generation: present knowledge and modelling capabilities, *Hydrol. Process.* **16**, 509-529.

Bronstert, A., A. Bárdossy, C. Bismuth, H. Buiteveld, M. Disse, H. Engel, U. Fritsch, Y. Hundecha, R. Lammersen, D. Niehoff, and N. Ritter (2007a), Multi-scale modelling of land-use change and river training effects on floods in the Rhine basin, *River Res. Appl.* **23(10)**, 1102-1125.

Bronstert, A., V. Kolokotronis, D. Schwandt, and H. Straub (2007b), Comparison and evaluation of regional climate scenarios for hydrological impact analysis: General scheme and application example, *Int. J. Climatol.* **27**, 1579-1594.

Buck, W., K. Ferkel, H. Gerhard, H. Kalwelt, J. van Malde, K. Niffes, B. Ploeger, and W. Schmitz (1993), *Der Rhein unter Einwirkung des Menschen - Ausbau, Shifffahrt, Wasserwirtschaft*, KHR-Report I-11, Lelystad.

Busch, D., M. Shirmer, B. Schuchardt, and P. Ullrich (1989), Historical changes of the River Weser. **In:** G.E. Petts (eds.), *Historical change of large alluvial rivers: Western Europe*, J. Wiley & Sons, Chichester, 297-321.

Böhm, U., K. Keuler, H. Österle, M. Kücken, and D. Hauffe (2008), Quality of a Climate Reconstruction for the CADSES region, *MetZ special issue Regional climate modeling with COSMO-CLM (CCLM)* **17(8)**, 477-485.

Bürger, G. (2009), Dynamically vs. empirically downscaled medium-range precipitation forecasts, *Hydrol. Earth. Syst. Sci.* **13**, 1649-1658.

Connolley, W. M., and T. J. Bracegirdle (2007), An Antarctic assessment of IPCC AR4 couple models, *Geophys. Res. Lett.* **34(L22505)**, 6.

DESTATIS, (2010), *Umweltnutzung und Wirtschaft. Tabellen zu den Umweltökonomischen Gesamtrechnungen – Ausgabe 2010*, Statistisches Bundesamt, Wiesbaden, Germany.

Dettinger, M., and D. Cayan (1995), Large-scale forcing of recent trends toward early smowmelt runoff in California, *J. Clim.* **8**, 606-623.
Doherty, J. (2004), *PEST: Model Independent Parameter Estimation. Fifth edition of user manual*, Watermark Numerical Computing, Brisbane, Australia.
Dore, M. (2005), Climate change and changes in global precipitation patterns: What do we know?, *Environ. Int.* **31**, 1167-1181.
Dyurgerov, M., and M. Meier (2005), *Glaciers and the Changing Earth System: A 2004 Snapshot*, Institute of Arctic and Alpine Research, Colorado.
Easterling, D., C. Meehl, C. Parmesan, S. Changnon, T. Karl, and L. Mearns (2000), Climate extremes: Observations, Modelling, and Impacts, *Science* **289(5487)**, 2068-2074.
Enke, W., T. Deutschlaender, F. Schneider, and W. Kuechler (2005a), Results of five regional climate studies applying a weather pattern based downscaling method to ECHAM4 climate simulations, *Meteorologische Zeitschrift* **14(2)**, 247-257.
Enke, W., F. Schneider, and T. Deutschlaender (2005b), A novel scheme to derive optimized circulation pattern classifications for downscaling and forecast purposes, *Theor. Appl. Climatol.* **82**, 51-63.
Fontaine, T. A., T. S. Cruickshank, J. G. Arnold, and R. H. Hotchkiss (2002), Development of a snowfall-snowmelt routine for mountainous terrain for the soil water assessment tool (SWAT), *J. Hydrol.* **262**, 209-223.
Fowler, H. J., S. Blenkinsop, and C. Tebaldi (2007), Linking climate change modelling to impacts studies: recent advances in downscaling techniques for hydrological modelling, *Int. J. Clim.* **27(12)**, 1547-1578.
Gelfan, A., J. Pomeroy, and L. Kuchment (2004), Modelling Forest Cover Influences on Snow Accumulation, Sublimation, and Melt, *J. Hydrometeorology* **5(5)**, 785-803.
Georgiyevsky, V., and I. Shiklomanov (2003), Climate change and water resources. **In:** I.A. Shiklomanov and J.C. Rodda (eds.), *World Water Resources at the Beginning of the 21st Century*, UNESCO, Cambridge, United Kingdom.
Gerstengarbe, F., M. Kücken, and P. Werner (2009), *Modellvergleich der regionalen Klimamodelle REMO, CCLM, WETTREG und STAR II*, PIK (Potsdam Institute for Climate Impact Research) internal report, Potsdam.
Giorgetta, M. A., G. P. Brasseur, E. Roeckner, and J. Marotzke (2006), Preface to Special Section on Climate Models at the Max Planck Institute for Meteorology, *J. Clim.* **19**, 3769-3770.
Goldewijk, K. (2001), Estimating global land use change over the past 300 years: the HYDE database, *Global Biogeochemical Cycles* **15(2)**, 417-433.
Graham, L., J. Andreasson, and B. Carlsson (2007), Assessing climate change impacts on hydrology from an ensemble of regional climate models, model scales and linking methods - a case study on the Lule River basin, *Clim. Change* **81**, 293-307.
HAD (Hydrologischer Atlas von Deutschland) (2000), Bundesministerium für Umwelt, Naturschutz und Reaktorsicherheit, ISBN 3-00-005624-6.
Hattermann, F., V. Krysanova, F. Wechsung, and M. Wattenbach (2005), Runoff simulations on the macroscale with the ecohydrological model SWIM in the Elbe catchment - validation and uncertainty analysis, *Hydrol. Process.* **19**, 693-714.
Hattermann, F. F., V. Krysanova, A. Habeck, and A. Bronstert (2006), Integrating wetlands and riparian zones in river basin modeling, *Ecol. Model.* **199**, 379-392.
Hay, L., R. Wilby, and G. Leavesley (2000), A comparison of delta change and downscaled GCM scenarios for three mountainous basins in the United States, *J. Am. Water Resour. Assoc.* **36**, 387-398.
Haylock, M. R., G. Cawley, C. Harpham, R. Wilby, and C. M. Goodess (2006), Downscaling heavy precipitation over the United Kingdom: a comparison of dynamical and statistical methods and their future scenarios, *Int. J. Clim.* **26(10)**, 1397-1415.
Hesse, C., V. Krysanova, J. Päzolt, and F.F. Hattermann (2008), Eco-hydrological modelling in a highly regulated lowland catchment to find measures for improving water quality, *Ecol. Model.* **218**, 135-148.
Hock, R. (2003), Temperature index melt modeling in mountain areas, *J. Hydrol.* **282**, 104-115.
Hock, R. (2005), Glacier melt: a review of processes and their modeling, *Progress in Physical Geography* **29(3)**, 362-391.

Honisch, M., C. Hellmeier, and K. Weiss (2002), Response of surface and subsurface water quality to land use changes, *Geoderma* **105(3-4)**, 277-298.
Hooghoudt, S. (1940), Bijdrage tot de kennis van enige natuurkundige grootheden van de grond, *Versl. Landbouwkd. Onderz.* **46(14)**, 515-707.
Hörmann, G., A. Horn, and N. Fohrer (2005), The evaluation of land-use options in mesoscale catchments: Prospects and limitations of eco-hydrological models, *Ecol. Model.* **187(1)**, 3-14.
Ierodiaconou, D., L. Laurenson, M. Leblanc, F. Stagnitti, G. Duff, S. Salzman, and V. Versace (2005), The consequences of land use change on nutrient exports: a regional scale assessment in south-west Victoria, Australia, *J. of Env. Manag.* **74(4)**, 305-316.
IPCC (2007a), *Climate Change 2007: Impacts, Adaptation and Vulnerability - Summary for Policymakers. Working Group II Contribution to the Fourth Assessment Report of the Intergovernmental Panel on Climate Change*, Cambridge University Press.United Kingdom and New York, NY, USA.
IPCC (2007b) *Climate Change 2007: The Physical Science Basis. Contribution of Working Group I to the Fourth Assessment Report of the Intergovernmental Panel on Climate Change*, Cambridge University Press, United Kingdom and New York, NY, USA.
Jacob, D. (2001), A note on the simulation of the annual and inter-annual variability of the water budget over the Baltic Sea drainige basin, *Meteorol. Atmos. Phys.* **77**, 61-73.
Johnson, F., and A. Sharma (2011), Accounting for interannual variability: A comparison of options for water resources climate change impact assessments, *Water Resour. Res.* **47(W04508)**, 20.
Kay, A., H. Davies, V. Bell, and R. Jones (2009), Comparison of uncertainty sources for climate change impacts: flood frequency in England, *Climatic Change* **92**, 41-63.
Kay, A., R. Jones, and N. Reynard (2006), RCM rainfall for UK flood frequency estimation. II. Climate change results, *J. Hydrol.* **318**, 163-172.
Krysanova, V., A. Meiner, J. Roosaare, and A. Vasilyev (1989), Simulation modelling of the coastal waters pollution from agricultural watersheds, *Ecol. Model.* **49**, 7-29.
Krysanova, V., D. Möller-Wohlfeil, and A. Becker (1998), Development and test of a spatially distributed hydrological / water quality model for mesoscale watersheds, *Ecol. Model.* **106**, 261-289.
Krysanova, V., F. Wechsung, and F.F. Hattermann (2005), Development of the ecohydrological model SWIM for regional impact studies and vulnerability assessment, *Hydrol. Process.* **19**, 763-783.
Krysanova, V., F. Hattermann, and F. Wechsung (2007), Implications of complexity and uncertainty for integrated modelling and impact assessment in river basins, *Environ. Modell. Softw.* **22**, 701-709.
Lenderink, G., A. Buishand, and W. van Deursen (2007), Estimates of future discharges of the river Rhine using two scenario methodologies: direct versus delta approach, *Hydrol. Earth Syst. Sci.* **11(3)**, 1145-1159.
Lin, S. J. and R. B. Rood (1996), Multidimensional flux-form semi-Lagrangian transport schemes, *Mon. Wea. Rev.* **124**, 2046–2070.
Lins, H., and J. Slack (1999), Streamflow trends in the United States, *Geophys. Res. Lett.* **26(2)**, 227-230.
Lunn, R., R. Adams, R. Mackay, and S. Dunn (1996), Development and applicationof a nitrogen modelling system for large catchments, *J. Hydrol.* **174**, 285-304.
Majewski, D. (1991), The Europa Modell of the Deutscher Wetterdienst, *ECMWF Seminar on numerical methods in atmospheric models* **2**, 147-191.
Mattikalli, N., and K. Richards (1996), Estimation of surface water quality changes in response to land use change: application of the export coefficient model using remote sensing and geographical information system, *J. Env. Manag.* **48(3)**, 263-282.
McCarthy, J., O. Canziani, N. Leary, Dokken, D.J., and K. White (2001), *IPCC: Climate Change 2001: Impacts, Adaptation and Vulnerability*, Cambridge University Press, Cambridge.
Middelkoop, H., K. Daamen, D. Gelllens, W. Grabs, J. Kwadijk, H. Lang, Parmet, B.W.A.H, B. Schädler, J. Schulla, and K. Wilke (2001), Impact of climate change on hydrological regimes and water resources management in the Rhine basin, *Climatic Change* **49**, 105-128.
Monteith, J. L. (1965), Evaporation and the environment, *Symp. Soc. Expl. Biol.* **19**, 205-234.
Orlowsky, B., F. Gerstengarbe, and P. Werner (2008), A resampling scheme for regional climate simulations and its performance compared to a dynamical RCM, *Theor. Appl. Climatol.* **92**, 209-223.
Pardé, M. (1933), *Fleuves et rivieres*, Librairie Armand Colin.
Paterson, W. (1994), *The physics of glaciers (3rd Ed.)*, Pergamon, Oxford.

Petrow, T., and B. Merz (2009), Trends in flood magnitude, frequency and seasonality in Germany in the period 1951 - 2002, *J. Hydrol.* **371**, 129-141.
Porporato, A., E. Daly, and I. Rodriguez-Iturbe (2004), Soil water balance and ecosystem response to climate change, *Am. Nat.* **164(5)**, 625-632.
Priestley, C. H. B., and R. J. Taylor (1972), On the assessment of surface heat flux and evaporation using large scale parameters, *Mon. Weather Rev.* **100**, 81-92.
Rangwala, I., J. Miller, G. Russell, and M. Xu (2010), Using a global climate model to evaluate the influences of water vapor, snow cover and atmospheric aerosol on warming in the Tibetan Plateau during the twenty-first century, *Clim. Dyn.* **34(6)**, 859-872.
Rockel, B., A. Will, and A. Hense (2008), The regional climate model COSMO-CLM (CCLM), *Meteorologische Zeitschrift* **17(4)**, 347-348.
Roeckner, E., G. Bäuml, L. Bonaventura, R. Brokopf, M. Esch, M. Giorgetta, S. Hagemann, I. Kirchner, L. Kornblueh, E. Manzini, A. Rhodin, U. Schlese, U. Schulzweida, and A. Tompkins (2003), *The atmospheric general circulation model ECHAM5. Part I: Model description*, Max Planck Institute for Meteorology, MPI for Meteorology, Bundesstr. 53, 20146 Hamburg, Germany.
Samaniego, L., and A. Bárdossy (2007), Relating macroclimatic circulation patterns with characteristics of floods and droughts at the mesoscale, *J. Hydrol.* **335**, 109-123.
Sangrey, D., K. Harrop-Williams, and J. Kaliber (1984), Predicting ground-water response to precipitation, *ASCE J. Geotech. Eng.* **110(7)**, 957-975.
Schmidli, J., C. Frei, and P. Vidale (2006), Downscaling from GCM precipitation: a benchmark for dynamical and statistical downscaling methods, *Int. J. Clim.* **26(5)**, 679-689.
Schönwiese, C., T. Staeger, and S. Trömel (2006), Klimawandel und Extremereignisse in Deutschland. **In:** *Klimawandel und Extremereignisse in Deutschland - Klimastatusbericht 2005*, Deutscher Wetterdienst, Offenbach, 7-17.
Sircoulon, J. (1990), *Impact Possible des Changements Climatiques a Venir sur les Ressources en eau des Regions Arides et Semi-Arides. Comportement des Cours d'eau Tropicaux, des Rivieres et des Lacs en Zone Sahelienne*, World Meteorological Organisation, Geneva, Switzerland.
Smedema, L., and D. Rycroft (1983), *Land Drainage - Planning and Design of Agricultural Drainage Systems*, Cornell University Press, Ithaca, NY.
Stahl, K., H. Hisdal, J. Hannaford, L. Tallaksen, H. van Lanen, E. Sauquet, S. Demuth, M. Fendekova, and J. Jodar (2010), Streamflow trends in Europe: evidence from a dataset of near-natural catchments, *Hydrol. Earth Syst. Sci.* **14**, 2367–2382.
Statistisches Bundesamt Deutschland (2008), *Statistical Yearbook 2008, a*vailable in German (http://www.destatis.de/jetspeed/portal/cms/Sites/destatis/Internet/DE/Content/Publikationen/Querschnittsveroeffentlichungen/StatistischesJahrbuch/Jahrbuch2008,property=file.pdf), (last asscessed: 13.09.2011).
Steppeler, J., G. Doms, U. Schaettler, H. Bitzer, A. Gassmann, U. Damrath, and G. Gregoric (2003), Meso-gamma scale forecasts using the nonhydrostatic model LM, *Meteorol. Atmos. Phys.* **82**, 75-96.
Stier, P., J. Feichter, S. Kinne, S. Kloster, E. Vignati, J. Wilson, L. Ganzeveld, I. Tegen, M. Werner, Y. Balkanski, M. Schulz, O. Boucher, A. Minikin, and A. Petzold (2005), The aerosol climate model ECHAM5-HAM, *Atmos. Chem. Phys.*, **5**, 1125–1156.
Suklitsch, M., A. Gobiet, H. Truhetz, N. Awan, H. Göttel, and D. Jacob (2010), Error characteristics of high resolution regional climate models over Alpine area, *Clim. Dyn.* **37(1-2)**, 377-390.
Tarend, D. (1998), Changing flow regimes in the Baltic States. **In:** *Proceedings of the Second International Conference on Climate and Water, Espoo, Finland, August 1998*, Helsinki University of Technology, Helsinki, Finland.
Teutschbein, C., and J. Seibert (2010), Regional climate models for hydrological impact studies at the catchment scale: A review of recent modeling strategies, *Geography Compass* **4(7)**, 834-860.
Thomas, I., and B. Bates (1997), Responses to the variability and increasing uncertainty of climate in Australia. **In:** *The Third IHP/IAHS G. Covach Colloquium: Risk, Reliability, Uncertainty and Robustness of Water Resources Systems, 19–21 September, 1996*, UNESCO, Paris, France.
UBA (Umweltbundesamt) (2001), *Environmental Policy: Water Resources Management in Germany*, Umweltbundesamt, Dessau, 67 pp.
UBA (Umweltbundesamt) (2007), *Neue Ergebnisse zu regionalen Klimaänderungen - Das statistische Regionalisierungsmodell WETTREG - Hintergrundpapier*, Umweltbundesamt, Dessau, 27 pp.

Van Ulden, A., and G. van Oldenborgh (2006), Large-scale atmospheric circulation biases and changes in global climate model simulations and their importance for climate change in Central Europe, *Atmos. Chem. Phys.* **6**, 863-881.

Voss, A. (2007), *Untersuchung und Modellierung der Stickstoff und Phosphorumsatz- und Transportprozesse in mesoskaligen Einzugsgebieten des Tieflandes am Beispiel von Nuthe, Hammerfließ und Stepenitz*, Potsdam University.

Waylen, P., R. Compagnucci, and M. Caffea (2000), Inter-annual and inter-decadal variability in stream flow from the Argentine Andes, *Phys. Geogr.* **21(5)**, 452-465.

Wechsung, F., A. Hanspach, F. Hattermann, P. Werner, and F. Gerstengarbe (2006), *Klima- und anthropogene Wirkungen auf den Niedrigwasserabfluss der mittleren Elbe: Konsequenzen für Unterhaltungsziele und Ausbaunutzen*, Potsdam Institut für Klimafolgenforschung, Potsdam.

Wendland, F., H. Albert, M. Bach, R. Schmidt, (1993), *Atlas zum Nitratstrom in der Bundesrepublik Deutschland*, Springer Verlag, Berlin, Germany.

Westmacott, J., and D. Burn (1997), Climate change effects on the hydrologic regime within the Churchill-Nelson River Basin, *J. Hydrol.* **202(1-4)**, 263-279.

Whitehead, P. G., and M. Robinson (1993), Experimental basin studies - an international and historical perspective of forest impacts, *J. Hydrol.* **145(3-4)**, 217-230.

Whitehead, P. G., E. J. Wilson, and D. Butterfield (1998), A semi-distributed integrated flow and nitrogen model for multiple source assessment in catchments (INCA): Part I - model structure and process equations, *Sci. Total Environ.* **210**, 547-558.

Wilby, R., and T. Wigley (1997), Downscaling general circulation model output: a review of methods and limitations, *Progress in Physical Geography* **21(4)**, 530-548.

Williams, J., K. Renard, and P. Dyke (1984), EPIC - a new model for assessing erosion's effect on soil productivity, *J. Soil Water Conserv.* **38(5)**, 381-383.

Woods, A. (2006), *Medium-Range Weather Prediction: The European Approach. The Story of the European Centre for Medium-Range Weather Forecasts*, Springer, New York.

Ye, B., Y. Ding, E. Kang, G. Li, and T. Han (1999), Response of the snowmelt and glacier runoff to the climate warming up in the last 40 years in the Xinjiang Autonomous Region, *China. Sci. China* **42(1)**, 41-45.

Zebisch, M., T. Grothmann, D. Schröter, C. Haße, U. Fritsch, and W. Cramer (2005), *Climate Change in Germany – Vulnerability and Adaptation of climate sensitive Sectors (Klimawandel in Deutschland – Vulnerabilität und Anpassungsstrategien klimasensitiver Systeme). Report commissioned by the Federal Environmental Agency, Germany (UFOPLAN 201 41 253)*, Potsdam Institute of Climate Impact Research, Germany.

List of Figures

List of Tables

List of Units

Unit	Description
%	percentage
°C	degree celsius
cm	centimeter
d	day
g cm^{-3}	gram per cubic centimeter
ha	hectare
kg	kilogram
km	kilometer
km^2	square kilometer
m	meter
m a. s. l.	meters above see level
m^3	cubic meter
m^3/s	cubic meter per second
mg/L	milligram per liter
mm	millimeter

List of Symbols

Symbol	Description	Unit
7Q50	The annual 7-day minimum flow with a 50-year recurrence interval	$m^3 s^{-1}$
b_i	Annual glacier mass balance at a given glacier hydrotope	mm $year^{-1}$
cmn	Mineralization rate	-
DDF_{ice}	Degree-day factor for glacier	mm °C day^{-1}
DDF_{snow}	Degree-day factor for snow	mm °C day^{-1}
deth	Soil water content as a threshold for denitrification	-
$Elev_{centroid}$	Elevation of the centroid in a subbasin	m
$Elev_{hydrotop}$	Mean elevation of the hydrotope	m
E_s	Rate of snow sublimation	mm day^{-1}
H	Snow depth	cm
i	Volumetric content of ice	-
K_{grw}	Residence times (the time period subject to denitrification) in groundwater	days
K_{sub}	Residence times (the time period subject to denitrification) in subsurface	days
M_{ice}	Ice melt rate	mm day^{-1}
M_{snow}	Snowmelt rate	mm day^{-1}
MQ_{month}	Mean monthly runoff	$m^3 s^{-1}$
MQ_{year}	Mean annual runoff	$m^3 s^{-1}$
N	Nitrogen	-
NO_3-*N*	Nitrate nitrogen	-
$N_{o\text{-}ac}$	Active organic N	-
$N_{o\text{-}st}$	Stable organic N	-
N_{res}	Fresh organic N	-
$N_{t,in}$	Nitrogen input at time t	kg ha^{-1} d^{-1}
$N_{t,out}$	Nitrogen output	kg ha^{-1} d^{-1}
P	Phosphous	-
p	Significance level	-
P_{lab}	Labile P	-
$P_{m\text{-}ac}$	Active mineral P	-
$P_{m\text{-}st}$	Stable mineral P	-
P_{org}	Organic P	-
P_{res}	Fresh organic P	-
P_{snow}	Snow accumulation	mm day^{-1}
Q_{obs}	Observed discharge	$m^3 s^{-1}$
Q_{sim}	Simulated discharge	$m^3 s^{-1}$
$\overline{Q}_{obs}$	The mean value of the observed data	$m^3 s^{-1}$
$\overline{Q}_{sim}$	The mean value of the simulated data	$m^3 s^{-1}$
r^2	Correlation coefficient	-
S	Snowmelt rate	mm day^{-1}
SNO	Water content of snow	mm
SO_2	Sulfur dioxide	-
T	Taily mean temperature	°C

t0	1st October	-
t1	30th September	-
T_{grad}	Correction coefficient	°C m^{-1}
$T_{hydrotope}$	Corrected temperature for hydrotopes	°C
T_{max}	Daily maximum temperature	°C
T_{min}	Daily minimum temperature	°C
TN	Air temperature at hour N	°C
T_s	Snow pack temperature	°C
$T_{subbasin}$	Temperature interpolated into the centroids of subbasins	°C
ULMAX	Water holding capacity of the snow pack	-
V	Snow pack compression rate	cm day^{-1}
VSN	Water outflow from the snowpack	cm
w	Volumetric content of liquid water	-
X_s	Snowfall rate	mm day^{-1}
Δt	Time step	day
λ_{grw}	Decomposition rates in groundwater	day^{-1}
λ_{sub}	Decomposition rates in subsurface	day^{-1}
μ	Location parameter	-
ξ	Shape parameter	-
ρ_i	Density of ice	g cm^{-3}
ρ_o	Density of fresh fallen snow	g cm^{-3}
ρ_s	Density of snow pack	g cm^{-3}
ρ_w	Density of water	g cm^{-3}
σ	Scale parameter	-

List of Abbreviations

Abbreviation	Description
A1B	Emission scenarios with an assumption of balanced across energy sources
A2	Emission scenario with an assumption of a very heterogeneous world with continuously increasing global population and regionally oriented economic growth
AM7	Annual Minimum 7-day mean flows
AR4	Fourth Assessment Report
B1	Emission scenario with an assumption of a convergent world with the same global population but with rapid changes in economic structures toward a service and information economy, with reductions in material intensity, and the introduction of clean and resource-efficient technologies.
BAGLUVA	Method of BAGROV und GLUGLA to estimate the long-term average actual evaporation and runoff
BGR	Bundesanstalt für Geowissenschaften und Rohstoffe
BÜK 1000	Bodenübersichtskarte Maßstab 1:1000000
CAP	Common Agricultural Policy
CCLM	Cosmo-Climate Local Model
CEC	Commission of the European Communities
CEC	Climate & Environment Consulting Potsdam GmbH
CORINE	Coordination of Information on the Environment
DB	relative Deviation in water or load Balance
DEM	Digital Elevation Model
DESTATIS	Statistisches Bundesamt Deutschland
DTR	Diurnal Temperature Range
DWD	Deutscher Wetterdienst (German Meteorological Service)
DWSM	Dynamic Watershed Simulation Model
EC	European Commission
ECHAM5	5th generation of the ECHAM (from ECMWF und Hamburg) general circulation model
ECMWF	European Centre for Medium-Range Weather Forecasts
EPIC	Erosion Productivity Impact Calculator
EWA	European Water Archive
FGG-Elbe	Flussgebietsgemeinschaft Elbe
GCM	General Circulation Model
GEOSTAT	Geodaten der Bundesstatistik
GEV	Generalized Extreme Value distributions
GIS	Geographic Information System
GLOWA	Globaler Wandel des Wasserkreislaufes (Global Change and the Hydrological Cycle)
GRDC	The Global Runoff Data Centre
HAD	Hydrologischer Atlas von Deutschland (Hydrological Atlas of Germany)
HadRM	The Hadley Regional climate Model
HIRHAM	Regional Climate Model (HIRLAM dynamics + the Hamburg physics package)
HSPF	Hydrological Simulation Program - FORTRAN

IKSE	International Kommission zum Schutz der Elbe
IPCC	International Panel for Climate Change
LAI	Leaf Area Index
LAWA	Bund/Länder-Arbeitsgemeinschaft Wasser
LISFLOOD	a GIS-based distributed model for river basin scale water balance and *flood* simulation
LM	Lokal-Modell
LNSE	Logarithmic Nash-Sutcliffe Efficiency
MM5	Das Mesoscale Meteorology Model 5
MM7	Monthly Minimum 7-day discharges
MPI-OM	Max-Planck-Institut Ocean Model
NASA	National Aeronautics and Space Administration
NSE	Nash-Sutcliffe Efficiency
PAR	Photosynthetic Active Radiation
PC	Pardé Coefficient
PEST	Parameter ESTimation routine
PIK	Potsdam Institut für Klimafolgenforschung (Potsdam Institute for Climate Impact Research)
PWM	Probability-Weighted Moments
RCM	Regional Climate Models
REMO	REgional MOdel
SCS	Soil Conservation Service
SRES	Special Report on Emissions Scenarios
SRTM	Shuttle Radar Topographic Mission
STAR	STAtistical Regional model
SWAT	Soil and Water Assessment Tool
SWIM	Soil and Water Integrated Model
UBA	Das Umweltbundesamt
UKHI	UK Meteorological Office High Resolution model
UNESCO	United Nations Educational, Scientific and Cultural Organization
WettReg	Wetterlagenbasierte Regionalisierungsmethode (weather-type based regionalization method)
WFD	Water Framework Directive
WMO	World Meteorological Organization
XCCC	Canadian Climate Centre model

Annex

I: Monthly pardé coefficients at three selected gauges in each river basin, indicating the river regimes at different stretches of the rivers.

Pardé coefficient (PC) describes the mean monthly distribution of runoff over the year by the relation between the mean monthly (MQ_{month}) and mean annual (MQ_{year}) runoff (Pardé, 1933). (**Equation I-1**)

$$PC_{month} = \frac{MQ_{month}}{MQ_{year}} \qquad \text{(I-1)}$$

The detailed river network and the location of the selected discharge gauges are shown in **Fig. I-1** and the monthly Pardé coefficient at selected gauges are shown in **Fig. I-2**.

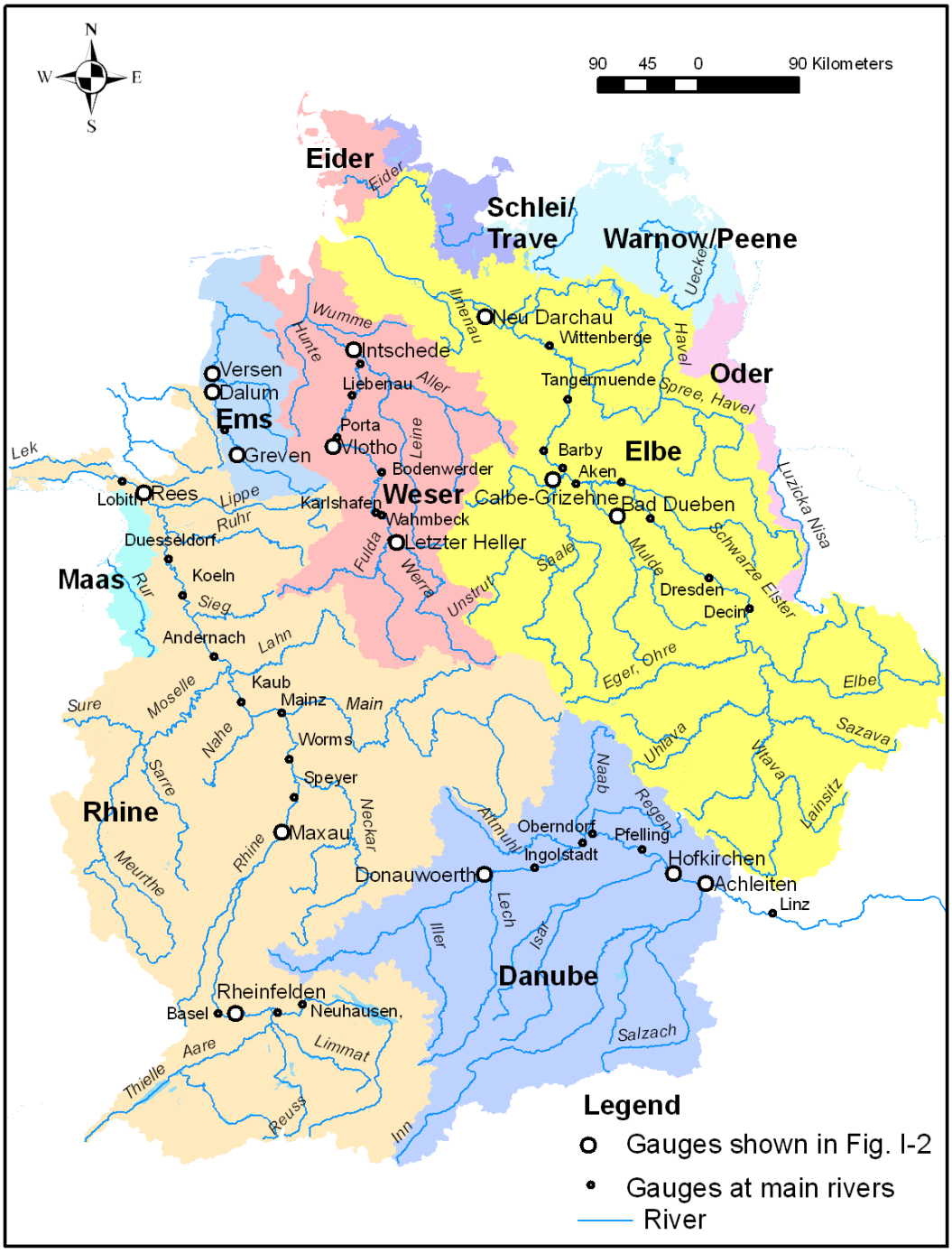

Figure I-1: River network and the location of the selected discharge gauges at the main rivers.

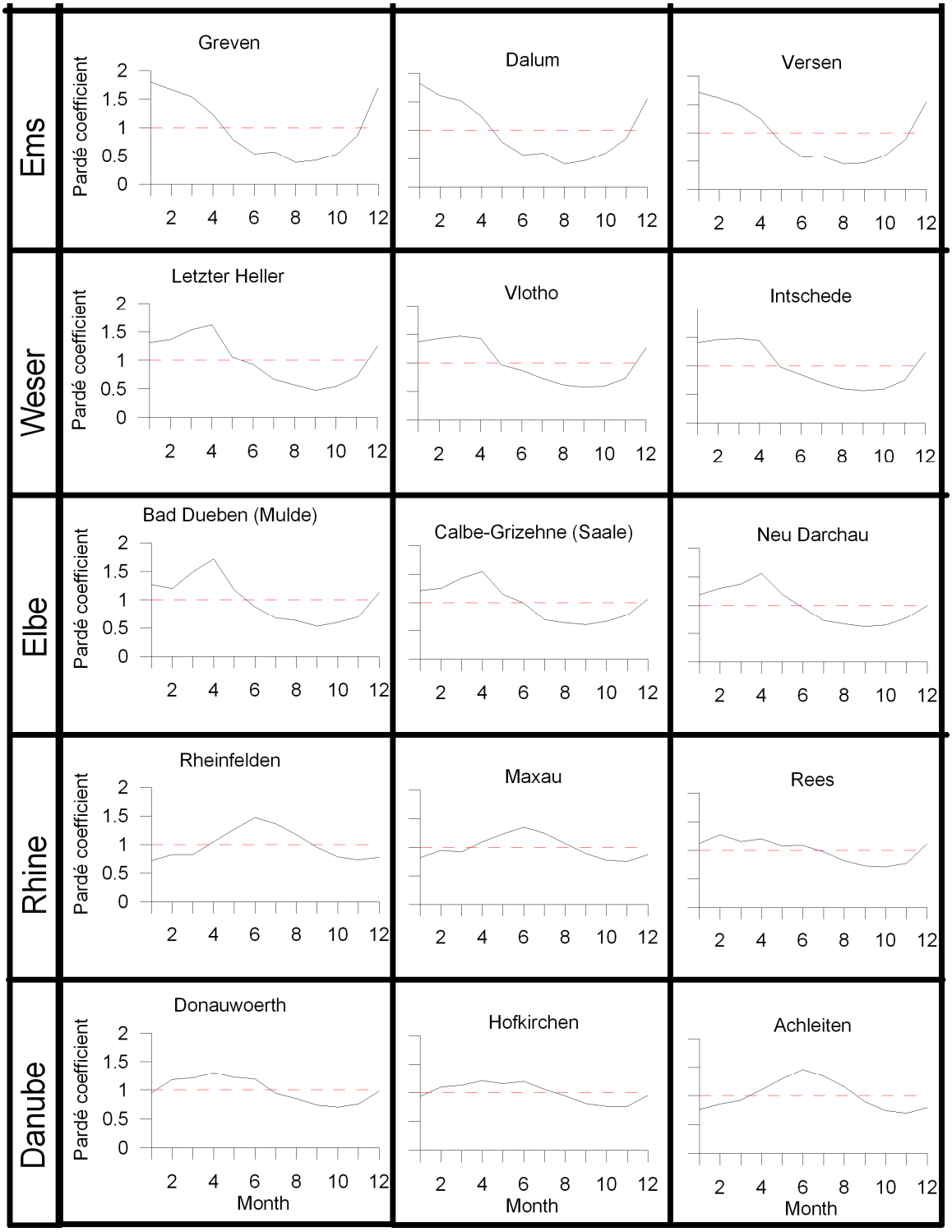

Figure I-2: The monthly Pardé coefficients at the selected gauges.

II Land use changes between 1990 and 2000 (data source: CORINE 1990 and CORINE 2000 land cover data set of the European Environment Agency)

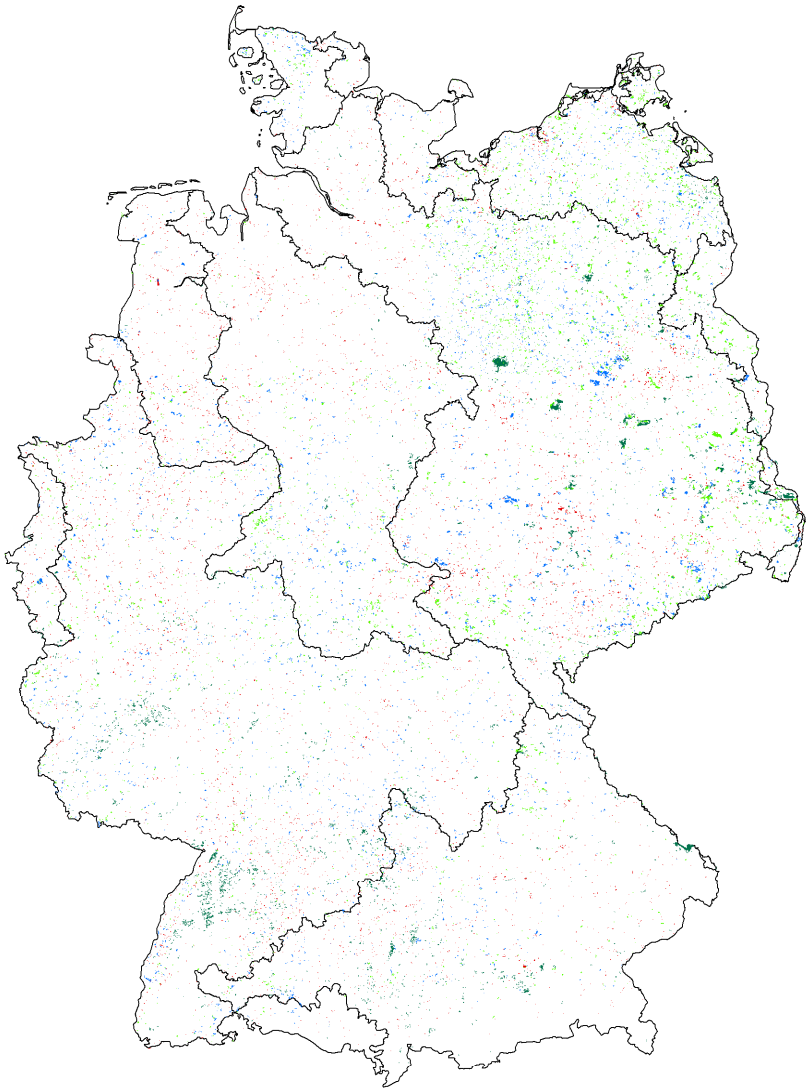

changed to urban area
changed to grassland
changed to arable land
changed to forest

III: List of the 2-sided p-value and the relative changes in annual average, maximum and minimum 7-day mean discharge for the 117 selected gauges

Gauge Nr.	River	Name	Beginning year	Ending year	Drainage area (km^2)	Annual average discharge 2-sided p-value*	Annual average discharge Relative change (%)**	Annual maximum discharge 2-sided p-value*	Annual maximum discharge Relative change (%)**	Annual minimum 7-day mean flow 2-sided p-value*	Annual minimum 7-day mean flow Relative change (%)**
6335020	Rhine River	Rees	1951	2006	159300	0.805	3	0.238	18	0.069	18
6335050	Rhine River	Duesseldorf	1951	2006	147680	0.761	5	0.125	21	0.043	18
6335060	Rhine River	Koeln	1951	2006	144232	0.697	5	0.087	24	0.138	14
6335070	Rhine River	Andernach	1951	2006	139549	0.467	9	0.120	22	0.020	25
6335100	Rhine River	Kaub	1951	2006	103488	0.355	10	0.040	26	0.032	23
6335150	Rhine River	Mainz	1951	2006	98206	0.433	9	0.093	21	0.012	25
6335170	Rhine River	Speyer	1951	2006	53131	0.983	2	0.241	16	0.143	16
6335180	Rhine River	Worms	1951	2006	68827	0.596	6	0.208	16	0.047	22
6335200	Rhine River	Maxau	1951	2006	50196	0.805	-1	0.358	11	0.132	15
6335304	Main	Frankfurt A. M. (Osthafen)	1963	2006	24764	0.818	6	0.187	22	0.028	40
6335350	Lahn	Leun (Neu)	1951	2006	3571	0.666	4	0.000	50	0.216	11
6335400	Rhine River	Rheinfelden	1951	2006	34550	0.783	2	0.098	17	0.283	10
6335600	Neckar	Rockenau-Ska	1951	2006	12710	0.216	17	0.860	-15	0.025	31
6335601	Neckar	Lauffen	1951	2006	7916	0.467	10	0.708	2	0.118	20
6335602	Neckar	Plochingen	1951	2006	3995	0.299	15	0.821	10	0.001	49
6336050	Moselle River	Cochem	1951	2006	27088	0.312	16	0.053	34	0.529	12
6336800	Moselle River	Perl	1974	2006	11522	0.236	-23	0.408	10	0.067	-24
6336900	Saar River	Fremersdorf	1952	2006	6983	0.057	13	0.387	85	0.105	-16
6337100	Weser	Vlotho	1951	2006	17618	0.656	5	0.036	32	0.484	6
6337200	Weser	Intschede	1951	2006	37720	0.475	-6	0.252	9	0.719	2
6337250	Aller	Rethem	1951	2006	14730	0.567	-10	0.631	18	0.136	-22
6337400	Weser	Hann.-Muenden	1951	2006	12442	0.656	4	0.009	41	0.221	14
6337501	Aller	Marklendorf	1951	2006	7209	0.091	-26	0.626	0	0.355	-17
6337502	Aller	Celle	1951	2006	4374	0.740	4	0.932	-1	0.646	1
6337503	Diemel	Helminghausen	1951	2006	103	0.656	-3	0.219	-2	0.319	18
6337504	Eder	Schmittlotheim	1951	2006	1202	0.567	-6	0.017	37	0.113	-47
6337505	Eder	Affoldern	1951	2006	1452	0.666	-4	0.095	21	0.009	42
6337506	Fulda	Grebenau	1951	2006	2975	0.994	-1	0.056	38	0.646	14
6337507	Fulda	Guntershausen	1951	2006	6366	0.904	-2	0.063	30	0.462	9

Gauge Nr.	River	Name	Beginning year	Ending year	Drainage area (km^2)	Annual average 2-sided p-value*	Annual average Relative change (%)**	Annual maximum 2-sided p-value*	Annual maximum Relative change (%)**	Annual minimum 7- 2-sided p-value*	Annual minimum 7- Relative change (%)**
6337508	Fulda	Rotenburg	1951	2006	2523	0.849	3	0.040	40	0.489	-5
6337509	Leine	Herrenhausen	1951	2006	5304	0.606	4	0.404	35	0.292	-15
6337510	Leine	Schwarmstedt	1951	2006	6443	0.882	-4	0.601	19	0.893	-2
6337511	Werra	Allendorf	1951	2006	5166	0.805	-7	0.132	22	0.312	8
6337512	Werra	Heldra	1951	2006	4302	0.994	-2	0.198	20	0.070	26
6337513	Werra	Letzter Heller	1951	2006	5487	0.983	-1	0.134	26	0.326	10
6337514	Weser	Bodenwerder	1951	2006	15924	0.860	2	0.147	23	0.416	8
6337515	Weser	Doerverden	1953	2006	22110	0.742	-7	0.443	10	0.800	-7
6337516	Weser	Karlshafen	1951	2006	14794	0.794	2	0.085	27	0.416	9
6337517	Weser	Liebenau	1953	2006	19910	0.684	-8	0.259	15	0.848	-6
6337518	Weser	Porta	1951	2006	19162	0.994	-1	0.063	23	0.641	1
6337519	Weser	Wahmbeck	1951	2006	12996	0.539	6	0.052	30	0.369	12
6338100	Ems	Versen	1951	2006	8369	0.433	8	0.899	7	0.003	41
6338110	Ems	Dalum	1964	2006	4981	0.845	-8	0.879	1	0.879	3
6338130	Ems	Rheine Unterschleuse Up	1951	2006	3740	0.596	11	0.238	14	0.944	2
6340050	Ilmenau	Bienenbuettel	1955	2006	1434	0.346	114	0.845	156	0.104	34
6340110	Elbe River	Neu-Darchau	1951	2006	131950	0.750	-5	0.232	27	0.489	-9
6340120	Elbe River	Dresden	1951	2006	53096	0.232	16	0.340	35	0.147	27
6340130	Elbe River	Wittenberg	1951	2006	61879	0.186	19	0.157	38	0.408	13
6340140	Elbe River	Barby	1951	2006	94060	0.816	-2	0.772	6	0.666	7
6340150	Elbe River	Wittenberge	1951	2006	123532	0.740	-5	0.429	19	0.400	-8
6340160	Elbe River	Tangermuende	1960	2006	97780	0.791	-4	0.063	47	0.339	-9
6340170	Elbe River	Aken	1951	2006	70093	0.511	9	0.484	17	0.577	9
6340180	Elbe River	Magdeburg-Strombruecke	1951	2006	94942	0.916	2	0.184	38	0.989	4
6340190	Elbe River	Torgau 1	1951	2006	55211	0.249	16	0.179	40	0.273	19
6340300	Saale	Calbe-Grizehne	1951	2006	23719	0.805	-4	0.636	11	0.441	-6
6340301	Saale	Halle Trotha	1954	2006	17979	0.210	-16	0.575	12	0.030	-20
6340501	Havel	Rathenow Hauptschleuse Up	1951	2006	19288	0.004	-31	0.989	-1	0.000	-121
6340510	Havel	Ketzin	1951	2006	16173	0.000	-51	0.035	-20	0.000	-162
6342200	Iller	Kempten	1951	2006	955	0.347	-5	1.000	26	0.816	-1
6342520	Altmuehl	Eichstaett	1951	2006	1400	0.061	28	0.596	-13	0.000	54
6342600	Danube River	Regensburg/Schwabelweis	1951	2006	35399	0.238	13	0.036	25	0.130	15
6342800	Danube River	Hofkirchen	1951	2006	47496	0.355	10	0.013	27	0.173	12
6342900	Danube River	Achleiten	1951	2006	76653	0.567	5	0.340	5	0.006	22

Gauge Nr.	River	Name	Beginning year	Ending year	Drainage area (km^2)	Annual average 2-sided p-value*	Annual average Relative change (%)**	Annual maximum 2-sided p-value*	Annual maximum Relative change (%)**	Annual minimum 7- 2-sided p-value*	Annual minimum 7- Relative change (%)**
6342910	Danube River	Oberndorf	1951	2006	26448	0.280	11	0.042	25	0.191	12
6342920	Danube River	Pfelling	1951	2006	37687	0.249	13	0.023	28	0.155	13
6342926	Isar	Lenggries	1951	2006	1403	0.286	12	0.832	-12	0.000	64
6357500	Oder River	Eisenhuettenstadt	1951	2006	52033	0.750	-5	0.316	-12	0.799	-7
9305003	Isar	Mittenwald - Karwendelsteg	1951	2006	400	0.616	-4	0.621	21	0.489	4
9305020	Chamb	Furth Im Wald	1951	2006	276	0.097	27	0.061	51	0.175	21
9305022	Mitternacher Ohe	Eberhardsreuth	1951	2006	113	0.286	18	0.157	22	0.003	35
9305024	Ilz	Kalteneck	1951	2006	762	0.029	27	0.004	55	0.027	19
9305028	Weisser Regen	Koetzing	1951	2006	226.5	0.347	13	0.810	-5	0.055	-19
9305035	Grosser Regen	Zwiesel	1951	2006	177	0.069	23	0.011	63	0.013	28
9305036	Osterbach	Roehrnbach	1951	2006	120	0.067	26	0.027	46	0.059	22
9305062	Schmutter	Fischach	1951	2006	133	0.074	13	0.067	49	0.312	-4
9305065	Mindel	Offingen	1951	2006	951	0.110	18	0.551	20	0.486	10
9305068	Osterach	Reckenberg	1951	2006	126	0.548	-3	0.059	58	0.020	26
9305069	Breitach	Breitachklamm	1951	2006	117	0.041	23	0.000	88	0.007	58
9305077	Baierzer Rot	Achstetten	1951	2006	264	0.027	18	0.046	-35	0.002	31
9305086	Grosse Vils	Vilsbiburg	1951	2006	318	0.028	24	0.072	32	0.002	34
9305091	Glonn	Hohenkammer	1951	2006	392	0.475	6	0.972	-29	0.392	6
9305094	Ammer	Weilheim	1951	2006	601	0.729	0	0.977	43	0.412	12
9305095	Ammer	Oberammergau	1951	2006	114	0.994	1	0.718	32	0.548	9
9305103	Leutasch	Mittenwald	1951	2006	109	0.697	1	0.938	21	0.849	-1
9305111	Traun	Stein Bei Altenmarkt	1951	2006	378	0.949	-1	0.529	6	0.106	10
9305113	Tiroler Achen	Staudach	1951	2006	944	0.794	0	0.362	9	0.591	4
9305116	Attel	Anger	1951	2006	244	0.160	12	0.270	18	0.631	0
9305125	Vils	Pfronten Ried	1951	2006	110	0.816	2	0.047	48	0.246	11
9305128	Weisse Traun	Siegsdorf	1951	2006	183	0.761	1	0.100	32	0.059	22
9305131	Aitrach	Lauben	1951	2006	308.1	0.636	6	0.433	12	0.425	-13
9305134	Breg	Hammereisenbach	1951	2006	158	0.567	8	0.047	47	0.255	15
9305142	Lobach	Leuterschach	1951	2006	109	0.860	2	0.577	20	0.340	-24
9305145	Wertach	Biessenhofen	1951	2006	450	0.425	10	0.893	9	0.893	2
9305146	Saalach	Unterjettenberg Rechtes Ufer	1951	2006	940	0.539	-7	0.899	0	0.591	6
9316013	Gutach	Gutach	1951	2006	145	0.520	11	0.548	18	0.972	0
9316018	Murg	Rotenfels	1951	2006	468.8	0.708	7	0.177	33	0.052	-23
9316025	Kinzig	Schwaibach	1951	2006	957	0.255	16	0.729	6	0.007	41

Gauge Nr.	River	Name	Beginning year	Ending year	Drainage area (km^2)	Annual average 2-sided p-value*	Annual average Relative change (%)**	Annual maximum 2-sided p-value*	Annual maximum Relative change (%)**	Annual minimum 7- 2-sided p-value*	Annual minimum 7- Relative change (%)**
9316052	Wutach	Oberlauchringen	1951	2006	617	0.529	7	0.224	22	0.280	20
9316092	Rotach	Friedrichshafen	1951	2006	129	0.041	22	0.577	15	0.458	13
9316093	Untere Argen	Beutelsau	1951	2006	261	0.450	-7	0.989	7	0.408	-10
9316094	Seefelder Aach	Uhldingen	1951	2006	271.5	0.666	6	0.511	-13	0.392	10
9316095	Schussen	Gerbertshaus	1951	2006	790	0.211	12	0.366	7	0.682	-4
9316097	Argen	Giessen	1951	2006	652	0.362	12	0.871	1	0.063	20
9316175	Speyerbach	Neustadt A.D.W	1951	2006	311	0.170	-19	0.849	-16	0.101	-13
9316342	Lahn	Biedenkopf	1951	2006	304.2	0.626	-3	0.085	30	0.081	-47
9316380	Enz	Hoefen	1951	2006	218.18	0.182	17	0.057	53	0.520	-9
9316383	Fichtenberger Rot	Mittelrot	1951	2006	125.9	0.299	16	0.489	-9	0.076	23
9316418	Sinn	Mittelsinn	1951	2006	457	0.261	17	0.001	74	0.713	-7
9316420	Elsava	Rueck	1951	2006	142	0.983	-1	0.916	4	0.865	0
9316426	Roter Main	Bayreuth	1951	2006	333	0.100	25	0.053	31	0.871	-5
9316436	Baunach	Leucherhof	1951	2006	383	0.072	29	0.020	52	0.026	45
9316471	Glatt	Hopfau	1951	2006	202	0.708	4	0.232	22	0.450	-22
9316492	Elz	Mosbach	1951	2006	155	0.677	9	0.319	8	0.385	13
9316497	Eyach	Bad Imnau	1951	2006	330.54	0.493	9	0.572	14	0.012	44
9316501	Nagold	Altensteig	1951	2006	134.4	0.677	12	0.734	17	0.362	12
9316503	Brettach	Neuenstadt	1951	2006	141.4	0.961	4	0.761	-3	0.160	31
9316505	Lein	Abtsgmuend	1951	2006	245.7	0.377	-11	0.005	-110	0.186	19

*2-sided p-value was calculated using Mann-Kendall test

**Relative changes ΔX_R were calculated using equation III-1 (Petrew and Merz, 2009):

$$\Delta X_R = \frac{X^*_{2006} - X^*_{1951}}{\overline{X}} * 100\% \qquad \text{(III-1)}$$

Where X^*_{2006} and X^*_{1951} are the value of the estimated trend line at the end and at the start of the analyzed time period. $\overline{X}$ is the mean value of the time series of the studied time period.

IV: List of major parameters used for calibration and their values for different modelling purposes

Parameter	Explanation	Ranges
abf	Alpha factor for groundwater, which characterizes the groundwater recession (the rate at which groundwater flow is returned to the stream).	0.01 - 6
bff	Baseflow factor for basin, which calculates percolation in soil from layer to layer.	0.2 - 1.0
del	Groundwater delay (days): The time it takes for water leaving the bottom of the root zone until it reaches the shallow aquifer.	10 - 200
gwq0	Initial groundwater flow contribution to streamflow (mm/day)	0.01 - 6
roc2	Routing coefficient to calculate the storage time constant for the reach for the surface flow.	1 - 100
roc4	Routing coefficient to calculate the storage time constant for the reach for the subsurface flow.	1 - 100
sccor	Correction factor for saturated conductivity (applied for all soils).	0.01 - 10
thc	Correction factor for potential evapotranspiration on sky emissivity.	0.3 - 1.5

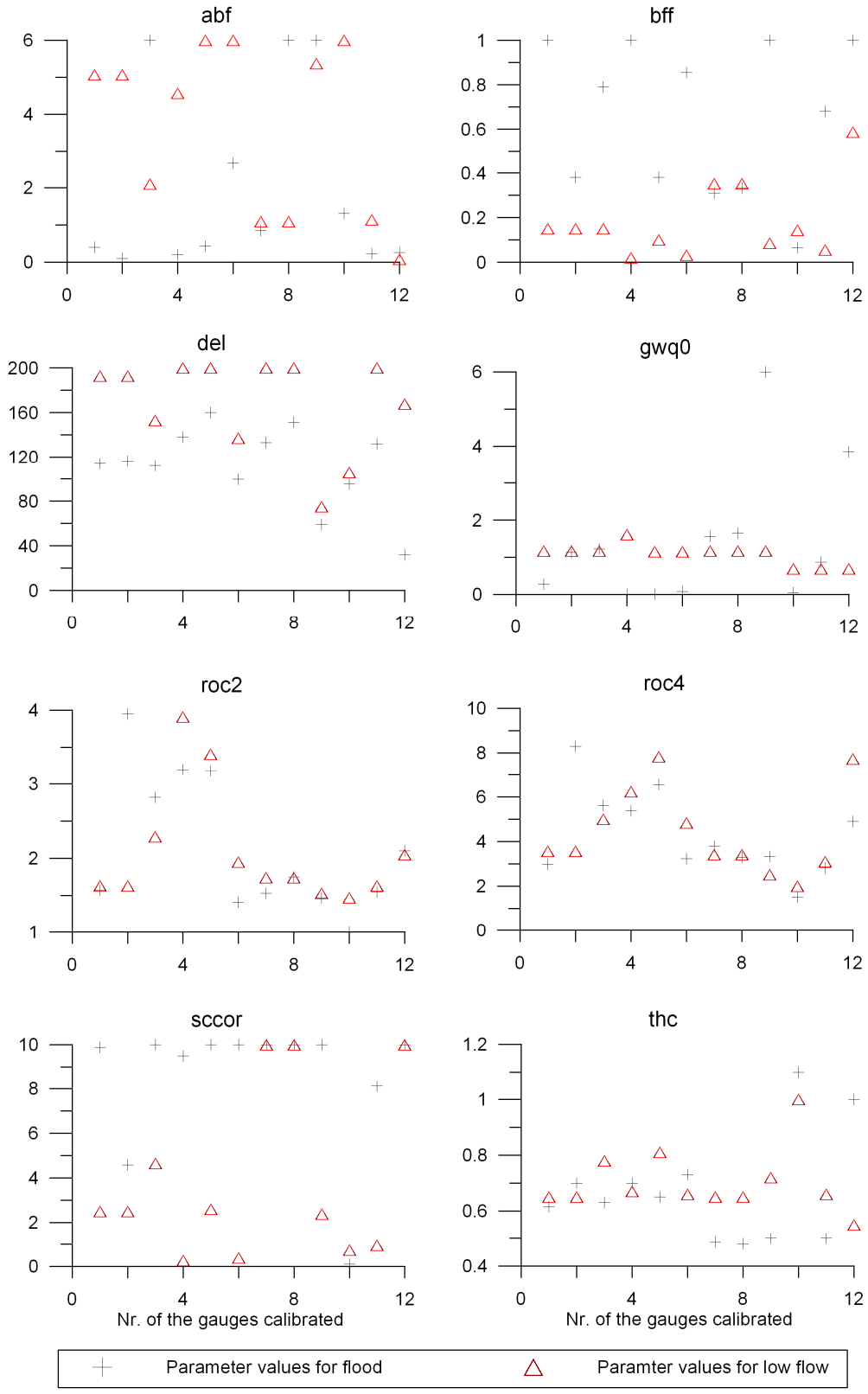

Figure IV-1: Calibration parameter values for modelling floods and low flows separately at 12 discharge gauges, which are listed in Table 4-3.